THE EXPRESSION PROFILE OF CYTOGLOBIN IN HUMAN FIBROTIC LUNG, AND THE PROTECTIVE ROLE OF CYTOGLOBIN IN HYPOXIA AND OXIDATIVE STRESS IN *VITRO*.

By

MELINDA CARPENTER

A thesis submitted to the

The University of Birmingham

for the degree of

DOCTOR OF PHILOSOPHY

School of Bioscience

University of Birmingham

September 2009

Abstract

Cytoglobin (CYGB), a novel member of the globin family, has been shown to be upregulated in response to hypoxia, oxidative stress and fibrogenesis. Presented here is evidence of CYGB expression within cells of fibrotic lesions taken from patients with Idiopathic Pulmonary Fibrosis (IPF) and Chronic Obstructive Pulmonary Disease (COPD). CYGB staining was observed in fibroblasts, endothelial cells, type II pneumocytes, type I pneumocytes, haematopoietic stem cells and inflammatory cells, which were identified using cell specific markers. Cell types which express other members of the globin family, including smooth muscle and red blood cells were negative for CYGB. Fibroblasts were consistently positive for CYGB. CYGB expression was consistently positive within the lesion, and more variable at the edge. This study also provides evidence of an increase in CYGB expression in response to hypoxic and oxidative stress in *vitro;* however there was no evidence of cytoprotection with over expression of CYGB in response to these insults. There is evidence presented here that the increase in CYGB expression with fibrosis previously reported in the literature, is likely to relate to the hypoxic environment of the lesion and the influx of fibroblasts which are consistently CYGB positive. CYGB is likely to have a role in oxygen and redox homeostasis.

Acknowledgments

First and foremost I would like to thank my supervisors, Nik Hodges and Kevin Chipman from the University of Birmingham and Martyn Foster and Mark Graham from AstraZeneca for their guidance and support over the last 4 years. Thanks also go to my fellow PhD students at the University of Birmingham, and Kate Pinnion from AstraZeneca for always being there to have a brew, offer advice, and discuss scientific, technical, and personal issues.

Thanks go to AstraZeneca for the financial support, and use of laboratories and tissue samples without which this project could not have progressed. Thanks go to everyone in Safety Assessment at AstraZeneca for all their help in the labs, and for making me so welcome.

A special mention must go to my Fiance, Richard Goodall, for supporting me throughout my PhD and always having such faith in me. A massive thank you also to my family, to my parents for putting me up for the last 6 months, and my siblings and siblings-in-law for all their advice, support, and ability to make me laugh! Finally, thanks to all of my friends who have offered great comic relief and emotional support.

Table of Contents

List of Figures

List of Tables

Abbreviations

A+	anti-CYGB siRNA 1
A-	siRNA negative control 1
ABC	StreptABComplex/HRP kit
AP-1	Activator Protein 1
AP-2	Activator Protein 2
APS	Ammonium Persulfate
ARDS	Acute Respiratory Distress Syndrome
ARE	Antioxidant Response Element
AUF	Antigen Unmasking Fluid
αSMA	Alpha Smooth Muscle Actin
ATP	Adenosine triphosphate
AZ	Acellular Zone
B+	anti-CYGB siRNA 2
B-	siRNA negative control 2
BioGaM	Biotinylated Goat anti Mouse Secondary Antibody
BioGaR	Biotinylated Goat anti Rabbit Secondary Antibody
BioHaM	Biotinylated Horse anti Mouse Secondary Antibody
BioSaR	Biotinylated Swine anti Rabbit Secondary Antibody
BSA	Bovine Serum Albumin
C+	anti-CYGB siRNA 3
CAIX	Carbonic Anhydrase IX
CCR7	Chemokine (C-C motif) receptor 7
CD	Cluster of Differentiation
cDNA	Complimentary DNA
cis-PnA	cis Parinaric acid

CK	Cytokeratin
CMPC	Circulating Mesenchymal Proginator Cells
CMV	Cytomegalovirus
COPD	Chronic Obstructive Pulmonary Disease
COX-2	Cyclooxygase-2
C_T	Threshold cycle number
CTGF	Connective Tissue Growth Factor
CXCR4	CXC cytokine receptor 4
CYGB	Cytoglobin (human)
Cygb-	Negative CYGB Expression
Cygb+	Positive CYGB Expression
CYGB+	Cytoglobin over expressing HEK293 cells
D+	siRNA negative control 4
DAB	3,3'-diaminobenzidine
DCF	1,2-dichlorofluoroescein
DCFH	2,7-dichlorofluoroescein
DCFH-DA	2,7-dichlorofluoroescein acetate
DMSO	dimethly sulfoxide
DNA	Deoxyribonucleic acid
dNTP	Deoxyribonucleotide triphosphate
DTT	Dithiotheritol
E	Endothelial cells
ECACC	European Collection of Cell Cultures
ECM	Extracellular Matrix
EMT	Epithelial Mesenchymal Transition
EPO	Erythropoietin
EpRE	Electrophile Response Element
ET-1	Endothelin-1

F	Fibroblast
FB	Fibrosing Border
FBLoV	Fibrosing border with a Significant Loss of Vasculature
FBS	Fetal Bovine Serum
Fe	Iron
FGF-1	Fibroblast Growth Factor-1
FPG	Formamidopyrimidine DNA glycosylase
GAPDH	Glyceraldehyde 3-phosphate dehydrogenase
GbX	Globin X
GFP	Green Fluorescing Protein
GOLD	Global Initiative for COPD
H&E	Haematoxylin and Eosin
H_2O_2	Hydrogen Peroxide
Hb	Haemoglobin
HEK 293	Human Embryonic Kidney 293 cells
HIF-1	Hypoxia Inducible Factor 1
HIPBS	Hypoxia Inducible Protein Binding Sites
His	Histidine
HNSCC	Head and Neck Squamous Cell Carcinoma
HO•	Hydroxly Radical
HRP	Horse Radish Peroxidase
HRE	Hypoxia Response Element
HSC	Haematopoietic Stem Cell
HxHb	Hexa-haemoglobin
I	Type I pneumocyte
Ig	Immunoglobulin
IHC	Immunohistochemistry
II	Type II pneumocyte

II-I	Differentiating type II pneumocyte
IL-1β	Interleukin 1β
ILD	Interstitial Lung Disease
IPF	Idiopathic Pulmonary Fibrosis
IR	Immunoreactivity
LMPA	Low Melting Point Agarose
LPS	Lipopolysaccharide
Luc-2	Luciferase-2
LVRS	Lung Volume Reduction Surgery
Mb	Myoglobin
MF	Myofibroblast
MMP	Matrix Metalloproteinase
mRNA	messenger RNA
MTT	3-[4,5-dimthylthiazol-2-yl]-2,5-diphenyl Tetrazolium Bromide
NADPH	Nicotinamide adenine dinucleotide phosphate
NF-1	Nuclear Factor 1
NFAT	Nuclear factor of activated T-cells
NFkB	Nuclear factor kappa-light-chain-enhancer of activated B cells
Ngb	Neuroglobin
NGS	Normal Goat Serum
NHS	Normal Horse Serum
NMPA	Normal Melting Point Agarose
NO	Nitric Oxide
NrF-2	Nuclear Factor-2
NSS	Normal Swine Serum
$O2^{\bullet-}$	Super Oxide Anion
ODD	Oxygen Dependant Degredation
PBS	Phosphate Buffered Saline

PCNA	Proliferating Cell Nuclear Antigen
PCR	Polymerase Chain Reaction
PDGF	Platelet Derived Growth Factor
PECAM-1	Platelet Endothelial Cell Adhesion Molecule-1
PGE	Prostaglandin E_2
PHD	Prolyl hydroxylase domain protein
PMA	Phorbol 12-myristate 13-acetate
Pro-Coll I	Pro-collagen I
PSG	Penicillin, Streptomycin and Glutamine
RISC	RNA-induced silencing complex
RNA	Ribonucleic acid
RNAi	interfering RNA
ROS	Reactive Oxygen Species
RT	Reverse Transcriptase
RT-PCR	Reverse Transcriptase-PCR
SDS	Sodium Dodecyl Sulfate
shRNA	Short hairpin RNA
siRNA	short interfering RNA
SM	Smooth Muscle
SOD	Superoxide Dismutase
S-S	Disulphide Bond
ssDNA	Single Stranded DNA
STAP	Stellate cell activation associated protein
STAT	Signal Transduction and Transcription Proteins
T_{25}	$25cm^2$ Cell Culture Flask
T_{75}	$75cm^2$ Cell Culture Flask
TAA	Thioacetamide
TAK-1	TGFβ activated kinase-1

TGF-β1	Tumour Growth Factor-β1
TIMP-1	Tissue Inhibitor of Metalloproteinases
TNFα	Tumour Necrosis Factor α
TSA	Tyramide Signal Amplification Kit
Tx	Thromboxane
UIP	Usual Interstitial Pneumonia
UTR	Untranslated Region
VEGF	Vascular Endothelial Growth Factor
VFB	Vascular Fibrosing Border
pVHL	Von Hippel-Lindau Protein
WGA	Wheat Germ Agglutinin

CHAPTER 1: GENERAL INTRODUCTION

1.1 Cytoglobin

1.1.1 Identification of Cytoglobin

Cytoglobin (CYGB) was initially reported in rat tissue in 2001 following a study investigating proteomic differences between quiescent and activated rat hepatic stellate cells both *in vitro* and *in vivo*. Marked upregulation of, a then unknown protein, was observed in activated cells, and temporarily termed STAP (stellate cell activation-associated protein) (Kawada *et al.*, 2001). The protein and cDNA sequence were isolated, identifying a heme protein which was found to be a homogenic dimer, with 40% homology to myoglobin and predicted to have cytoplasmic localisation (Kawada *et al.*, 2001).

Human CYGB was reported later in 2002 (Burmester *et al.*, 2002). It was initially identified on chromosome 17q25 following sequence searching for potential globins (Burmester *et al.*, 2002). A novel sequence was found, cloned and expressed. The sequence coded for a protein 190 amino acids in length, and contained the typical helix structure of a globin fold. Northern hybridization using mRNA from numerous different human tissues and developmental stages showed expression in all tissue samples, and thus the term ‘Cytoglobin’ was coined (Burmester *et al.*, 2002). The identification of Human CYGB on chromosome 17q25 was further substantiated in 2002 (Trent and Hargrove, 2002) again through searching available human genomic sequence data for predictive globin domains. Expression was observed to be ubiquitous and the alias ‘histoglobin’ was conceived and used. (Trent and Hargrove, 2002)

The term Cytoglobin was later used in preference to histoglobin and STAP. Cytoglobin was concluded to be a novel member of the globin protein family, and the 4th identified in humans.

1.1.2 Structure of Cytoglobin

Akin to the other members of the human globin family (haemoglobin (Hb), myoglobin (Mb) and more recently identified neuroglobin (Pesce *et al.*, 2002) (Ngb), CYGB is a heme protein (de Sanctis *et al.*, 2003; de Sanctis *et al.*, 2004a; Fago *et al.*, 2004a; Makino *et al.*, 2006; Sawai *et al.*, 2003; Sugimoto *et al.*, 2004; Trent and Hargrove, 2002; Vinck *et al.*, 2004). Crystallisation of the CYGB protein confirmed a homodimeric structure (de Sanctis *et al.*, 2003; Fago *et al.*, 2004a; Sugimoto *et al.*, 2004) which dimerises via 2 intramolecular disulphide bonds (Sugimoto *et al.*, 2004). Each CYGB chain is composed of a core 150 residues, in which the heavily conserved three-over-three α-helical sandwich fold of a 'classic' globin resides (de Sanctis *et al.*, 2003; Makino *et al.*, 2006; Sugimoto *et al.*, 2004). Additional segments of approximately 20 residues, which are not common to Hb or Mb, were observed at the N and C termini (Burmester *et al.*, 2002; de Sanctis *et al.*, 2003; Makino *et al.*, 2006). A large apolar cavity was evident adjacent to the heme (de Sanctis *et al.*, 2003; de Sanctis *et al.*, 2004a), which despite being structurally different to those observed in Hb and Ngb (de Sanctis *et al.*, 2004a), could have a role in ligand storage, enzymatic reactions, ligand transport (de Sanctis *et al.*, 2003; de Sanctis *et al.*, 2004a) or as a transient ligand docking site (de Sanctis *et al.*, 2004a).

1.1.2.1 Heme Structure

CYGB, and Ngb are hexacoordinated hemoglobins (HxHb) (de Sanctis *et al.*, 2003; de Sanctis *et al.*, 2004b; Sawai *et al.*, 2003; Trent and Hargrove, 2002; Vinck *et al.*, 2004), whilst Mb and Hb are pentacoordinated hemoglobins. Heme is comprised of a porphorin ring with 4 nitrogen atoms at the centre, bound to an iron (Fe) atom, forming a flat plane. Fe has 6 binding coordinates, of which 4 are bound via nitrogen atoms to the porphorin ring, and the fifth binds a His residue (His113 in CYGB) (Sawai *et al.*, 2003) within the heme vicinity (see Figure 1.1). The remaining coordinate remains unbound in pentacoordinate heme, thus can be readily bound by ligands. The 6th coordinate of the hexacoordinate heme is bound to another His residue, in CYGB His81 ((Sawai *et al.*, 2003).

Figure 1.1 Heme Structure

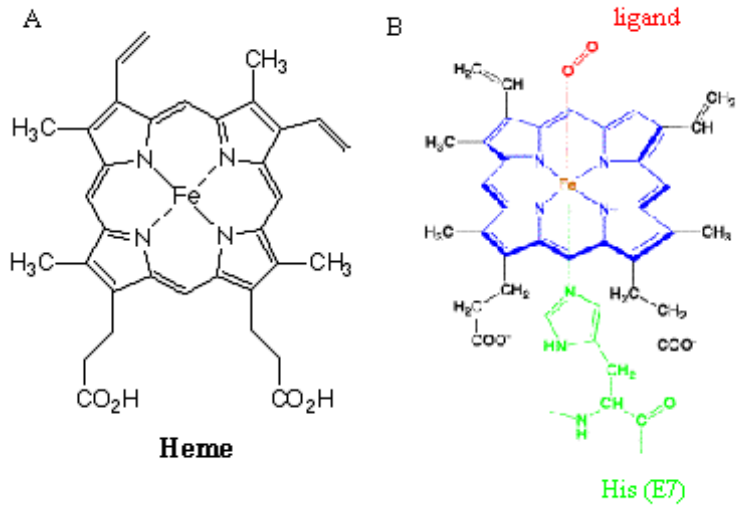

(A) The atomic structure of heme (B) The atomic structure of penta-coordinated Heme.

Hexacoordinated hemoglobins are found in numerous taxa including animals, protests, cynaebacteria and all plants (Smagghe *et al.*, 2006; Weber and Fago, 2004), however the presence of HxHbs in vertebrates has only recently being discovered (Pesce *et al.*, 2002). The roles of HxHbs remain elusive, however they are frequently associated with cellular roles such as scavaging of NO and reactive oxygen species (ROS) (see section 1.4 for details about ROS), oxygen signaling, enzymatic catalysis, and oxygen transport and storage. Several studies have investigated peroxidise activity of CYGB, however the data is conflicting with 2 reports giving evidence to support this theory (Asahina *et al.*, 2002; Kawada *et al.*, 2001) and one refuting it (Trandafir *et al.*, 2007), further research is required to clarify the capacity of CYGB for enzymatic reactions.

1.1.2.2 Ligand Binding

Hexacoordinated heme generally have a lower ligand affinity than pentacoordinated heme, as dissociation of the 6th coordinate must occur prior to ligand binding (Hamdane *et al.*, 2003; Smagghe *et al.*, 2006; Stryer, 1995; Weber and Fago, 2004). Despite these kinetic requirements HxHbs can bind oxygen and other ligands reversibly. CYGB has been shown to have an affinity for oxygen comparable to Mb (Sawai *et al.*, 2003; Trent and Hargrove, 2002). The oxy-CYGB complex is stable (Sawai *et al.*, 2003), yet oxygen binding is reversible (Trent and Hargrove, 2002), enabling a putative role in oxygen transport and storage (Sawai *et al.*, 2003; Trent and Hargrove, 2002). Of note although the coordination of the heme is distinct between CYGB and Mb, the primary structure of the CYGB heme pocket most closely resembles that of Mb than the other human globins (Trent and Hargrove, 2002). The influence of other factors on ligand binding has been investigated. It has been reported that binding of O_2 with CYGB is pH independent, and exothermic (Fago *et al.*, 2004a), which

draws further parallels with Mb. The two CYGB heme interact in a positive and negative manner, as binding at one heme can encourage or impede binding at the other (Fago *et al.*, 2004a).

CYGB contains 2 conserved cysteine residues, which are close enough to form a disulphide bond (Hamdane *et al.*, 2003). Disruption of this bond by mutating either cysteine, or the use of chemical reducing agents such as dithiothreitol (DTT), resulted in a reduced affinity for oxygen (Hamdane *et al.*, 2003), due to minor changes in the structure of the heme pocket (Vinck *et al.*, 2004). It has subsequently been hypothesised that there is a direct link between the redox state of the cell and the affinity of CYGB for oxygen (Hamdane *et al.*, 2003), as the presence of an electron donor would initiate release of oxygen by reducing breaking the S-S bond (Hamdane *et al.*, 2003). This bond could be fundamental in the role of CYGB, enabling CYGB to act as an oxygen reservoir, releasing oxygen under hypoxia. It should be noted that although intramolecular disulphide bonds are present in numerous proteins, none have yet been found within the globin family. Intermolecular disulphide bonds are fundamental to the role of invertebrate extracellular Hbs, but have not been observed in vertebrate Mbs or Hbs (Hamdane *et al.*, 2003).

1.1.3 The Globin Family

Globin proteins are widespread if not ubiquitous throughout the kingdoms of living organisms (Fago *et al.*, 2004b). CYGB analogues have been reported in an all the vertebrate classes: fish (Fuchs *et al.*, 2005); reptiles (Xi *et al.*, 2007); amphibians (Fuchs *et al.*, 2006; Xi *et al.*, 2007); birds (Kugelstadt *et al.*, 2004) and mammals. The most prominent variation between species is the presence or absence of the C-terminus extension ((Fuchs *et al.*, 2005; Kugelstadt *et al.*,

2004; Patel *et al.*, 2008). The primary and quaternary structural diversity of the globin family is vast. However, the characteristic globin fold of the tertiary structure is common throughout the globin family, suggesting evolution of all globin proteins from one ancesteral gene (Weber and Fago, 2004).

The first globin gene is thought to have originated approximately 1.8 billion years ago, corresponding with the accumulation of toxic oxygen in the atmosphere. Consequently the original function of globins has been proposed as being a scavenger of toxic gases, including oxygen, carbon monoxide and nitric oxide (Fago *et al.*, 2004b; Weber and Fago, 2004).

As yet only 5 globins have been found within vertebrates: Mb, Hb, Ngb, CYGB and the novel GlobinX (GbX) (Roesner *et al.*, 2005), which has recently been observed in fish and amphibians but appears absent within higher vertebrates. In contrast to the vertebrates, there are 3 classes of globins in micro-organisms, and numerous forms in the plant, and invertebrate kingdoms. Despite the vast diversity of globins they all occupy one or more of a selection of functional niches, including: transport and storage of oxygen, oxygen homeostasis, enzymatic activities and scavenging of reactive oxygen and nitrogen species (Weber and Fago, 2004). As summarised in section 1.1.2.1, the human globins, Hb, Mb, Ngb and CYGB, fall into two classes based on heme structure. It appears the hexa-coordinate globins are of a more ancient origin than the penta-coordinate globin, which are thought to have arisen for specific roles (Weiland *et al.*, 2004). The ligand affinity of hexa-coordinate hemes typically prevents a role in oxygen transport and storage, whilst penta-coordinate hemes are thought to have evolved to deal with the demand for oxygen transport as the size of organisms increased through time.

Figure 1.2 The Human Globins

	Myoglobin	**Haemoglobin**	**Cytoglobin**	**Neuroglobin**
Localisation	Muscle	Red blood cells	Ubiquitous	Neurons
Heme Structure	Penta coordinated	Penta coordinated	Hexa coordinated	Hexa coordinated
Protein structure	Monomer	4 subunits	2 subunits	monomer
Role	Transport oxygen in muscle	Transport oxygen via the blood	Unknown	Unknown
Oxygen Affinity	Highest	Lowest	Comparable to myoglobin	Higher than hemoglobin

A figure to show the fundamental differences between the 4 human globins

1.1.4 Phylogeny of Cytoglobin

The Human CYGB gene is located on chromosome 17q25, and consists of 4 exons and 3 introns (Trent and Hargrove, 2002), the most 3' of which is found in mammals but not chicken or fish. The addition of this exon is thought to have arisen during early mammalian evolution (Burmester *et al.*, 2004). The translated human protein is 190 amino acids in size, (Burmester *et al.*, 2002) considerably larger than known vertebrate Mbs and Hbs, due to N and C terminal extensions. The C-terminal extension is thought to be due to the addition of the exon, whereas the N-terminal extension is thought to have arisen following a duplication event. Similar extensions have previously been observed in several invertebrate and primitive

vertebrate globins, although the functional properties remain unknown (Burmester *et al.*, 2002; Pesce *et al.*, 2002)

Figure 1.3 Globin Family Phylogeny

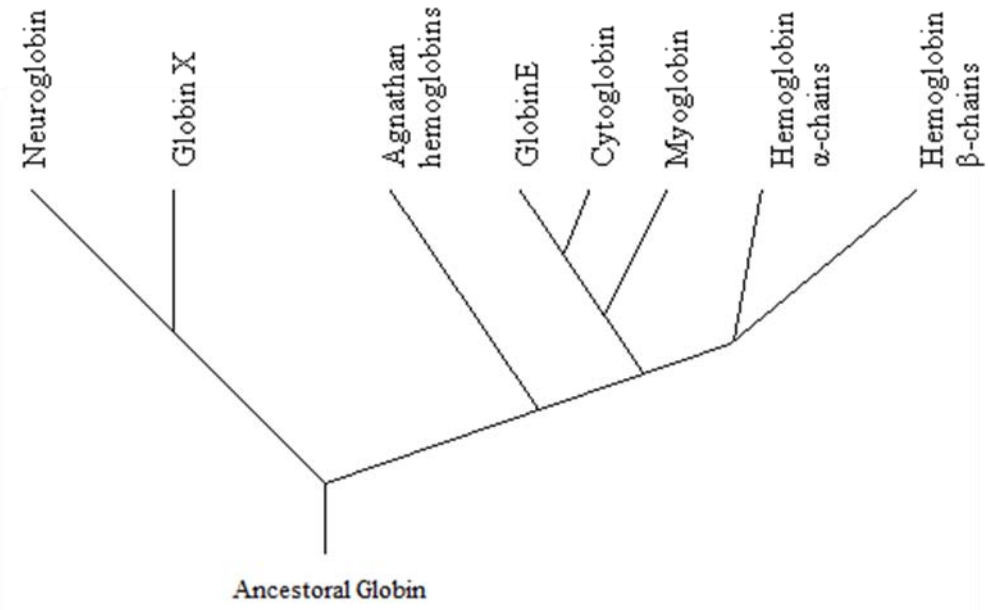

A diagrammatic representation of the globin family phylogenetic tree. Adapted from Burmester *et al* 2004.

The structure of CYGB is highly conserved: mouse and human CYGB share over 90% identity (Pesce *et al.*, 2002; Trent and Hargrove, 2002), the residue substitution rate is estimated to be $0.3x10^{-9}$ amino acid replacements per year (Burmester *et al.*, 2004; Fago *et al.*, 2004b), implying the structure of CYGB to be fundamental to an ancient essential biological function. CYGB shares less that 30% primary sequence identity with human globins (Trent and Hargrove, 2002), which could be a result of the sequence variation and substitution rates of Hb and Mb being considerably higher than that of CYGB. The protein

with which it shares the highest sequence identity is Lamphreys Hb (Sugimoto *et al.*, 2004), possibly due to a common hexa-coordinate structure.

There is evidence that HxHbs, including CYGB, are more ancient that penta coordinated hemoglobins (Sugimoto *et al.*, 2004; Trent and Hargrove, 2002) implying the role of Hxhbs to be evolutionarily fundamental. Hb evolved from Mb and CYGB approx. 600 million years ago (See Figure 1.3) (Sugimoto *et al.*, 2004), coordinating with the development of the circulatory system. CYGB shares a clade with vertebrate Mb (Burmester *et al.*, 2002; Burmester *et al.*, 2004; Sugimoto *et al.*, 2004), and the eye-specific globin in birds (GbE) (Burmester *et al.*, 2004; Kugelstadt *et al.*, 2004), indicating CYGB to have a role similar to Mb, potentially in oxygen transport (Burmester *et al.*, 2004; Kawada *et al.*, 2001). The chromosomal regions in which Mb and CYGB are located are believed to have formed from an ancient duplication event (Burmester *et al.*, 2002). CYGB separated from Mb approximately 550 million years ago. The close genetic relationship between Mb and CYGB implies that of all the globins, the role of CYGB is likely to be most closely related to Mb. Potentially Mb and Ngb could be specialised forms of CYGB evolved for oxygen transport in muscle and neuronal tissue respectively.

1.1.5 Localisation of Cytoglobin Expression

1.1.5.1 Tissue and Cell Specific Cytoglobin expression

CYGB expression was first reported to be ubiquitously expressed following a study by Hargrove and Trent. The human tissues investigated in this study were extensive and included heart, brain, kidney, lung, breast, skeletal muscle, gastrointestinal tract and pancreas. The ubiquitous expression of CYGB has been further substantiated in human studies (Schmidt *et*

al., 2004), as well as in chicken (Kugelstadt *et al.*, 2004), *Xenopus laevis* (Xi *et al.*, 2007), dog (Ostojic *et al.*, 2006), mice (Singh *et al.*, 2009) and rat (Geuens *et al.*, 2003; Nakatani *et al.*, 2004) tissues.

There is evidence that CYGB is absent from heart and skeletal muscle in the reptile Iguana, and that these organs do not express Mb (Xi *et al.*, 2007). The study compared this to the expression of CYGB within the same tissues of *X.laevis*, in which CYGB and not Mb is present, and concluded that expression of CYGB could be compensatory for the absence of Mb (Xi *et al.*, 2007) It could also be argued that the opposite is true, with expression of Mb in *X.laevis* tissues compensating for the lack of CYGB. If CYGB is more evolutionarily ancient one could argue that the later model is more likely than the former proposed by Xi *et al.*

CYGB expression has been observed in an array of cell types. There is evidence of CYGB expression in fibroblasts of various organs including liver (Nakatani *et al.*, 2004; Schmidt *et al.*, 2004) heart, muscle, colon, kidney, tendon, skin (Schmidt *et al.*, 2004), hepatic stellate cells (Asahina *et al.*, 2002; Schmidt *et al.*, 2004), myofibroblasts (Kawada *et al.*, 2001), chondrocytes, osteoblasts and osteoclasts in rats (Schmidt *et al.*, 2004). Models using mice have shown CYGB expression in hepatic stellate cells (Man *et al.*, 2008) and fibroblasts of the heart, lung, kidney, thigh muscle and stomach (Man *et al.*, 2008). CYGB expression in human fibroblasts (Halligan *et al.*, 2009) and epithelial cells (Shigematsu *et al.*, 2008) has also been confirmed in *vivo.*

Cells which have been shown to be CYGB negative include endothelial cells (Kawada *et al.*, 2001; Nakatani *et al.*, 2004; Schmidt *et al.*, 2004), kupffer cells (Kawada *et al.*, 2001),

hepatocytes (Kawada *et al.*, 2001; Schmidt *et al.*, 2004), epithelial cells (Nakatani *et al.*, 2004), red blood cells (Nakatani *et al.*, 2004; Schmidt *et al.*, 2004), macrophages (Nakatani *et al.*, 2004), dermal fibroblasts (Nakatani *et al.*, 2004), skeletal muscle cells (Nakatani *et al.*, 2004; Schmidt *et al.*, 2004), mature chondrocytes (Schmidt *et al.*, 2004), goblet cells (Schmidt *et al.*, 2004) and heart muscle cells (Schmidt *et al.*, 2004) in rats. Mice have presented with negative staining in endothelial cells, hepatocytes and red blood cells.

Studies into the neuronal expression of CYGB support a model in which CYGB is expressed in a sub population of neurons, in both the central and peripheral nervous systems but absent from the surrounding glia (Geuens *et al.*, 2003; Ostojic *et al.*, 2006; Ostojic *et al.*, 2008; Schmidt *et al.*, 2005), predominantly however, neurons are negative for CYGB.

Although CYGB appears to be expressed is all tissues, there is considerable evidence that CYGB is expressed mainly in fibroblasts and cells of the fibroblast lineage, although CYGB expression does not appear to be limited to this cell population. It is interesting that CYGB has been shown in several studies to be negative in red blood cells, muscle cells and the majority of nerve cells, which is notable as each of these cells express a cell specific globin which could compensate for the lack of CYGB expression.

1.1.5.2 Subcellular Localisation of Cytoglobin

There are conflicting reports in the literature regarding the subcellular localisation of CYGB in non neuronal cells. An in *vitro* study presents evidence of exclusive nuclear (Geuens *et al.*, 2003) localisation of CYGB, whilst several in *vivo* and in *vitro* studies show exclusively cytoplasmic localisation (Hodges *et al.*, 2008; Huang *et al.*, 2006; Kawada *et al.*, 2001;

Nakatani *et al.*, 2004; Schmidt *et al.*, 2004; Xi *et al.*, 2007). There is some evidence to support expression of CYGB with the nuclei and cytoplasm of a sub population of mouse liver fibroblasts, and hepatic stellate cells (Man *et al.*, 2008). Where CYGB is observed within neurons expression has been shown to be both nuclear and cytoplasmic by both in *vivo* and in *vitro* studies (Hodges *et al.*, 2008; Li *et al.*, 2006; Schmidt *et al.*, 2004). There is however no evidence of specific nuclear import of CYGB arguing against nuclear localisation (Schmidt *et al.*, 2004). CYGB was not detected in extracellular matrix in *vivo* (Schmidt *et al.*, 2004), or cell culturing media in *vitro* (Kawada *et al.*, 2001) implying CYGB is unlikely to be excreted. CYGB was found to be absent from membrane and mitochondrial cell fractions (Li *et al.*, 2006).

It is now widely believed that CYGB is an intracellular protein which is likely to localise exclusively to the cytoplasm in non neuronal cells, and to both the cytoplasm and nuclei in neurons. The regulation and role of CYGB is thus likely to differ between these 2 cells types.

1.1.6 Genetic Regulation of Cytoglobin Expression

Sequence searching to find putative CYGB gene regulatory elements highlighted binding regions for the following transcription factors: AP-1 (Singh *et al.*, 2009; Wystub *et al.*, 2004), AP-2, NF-1, NFκB, STAT (Wystub *et al.*, 2004), C-Ets-1, SP1 (Guo *et al.*, 2006), NFAT (Singh *et al.*, 2009), erythropoietin. (EPO) (Guo *et al.*, 2006; Guo *et al.*, 2007; Guo *et al.*, 2007) and Hypoxia Inducible Factor-1 (HIF-1) (Guo *et al.*, 2007; Singh *et al.*, 2009; Wystub *et al.*, 2004). In addition binding of HIF-1 to putative binding sites has also been reported (Guo *et al.*, 2007). These transcription factors are known to have role in regulation of housekeeping genes and or, protection against oxidative stress, and or the cellular hypoxic

response (See section 1.3 for more details about hypoxia). CYGB mRNA contains conserved hypoxia inducible stabilisation sites in the 3' untranslated region (Wystub *et al.*, 2004). Collectively this implies a role for hypoxia in regulation of CYGB expression.

Site directed mutagenesis of the c-Ets-1 and SP-1 sites resulted in a significant reduction in CYGB promoter activity (Guo *et al.*, 2007). This study concluded that c-Ets-1 and SP-1 had a fundamental role in normoxic CYGB expression, and potentially work synergistically. Subsequently activity of the CYGB promoter was shown to increase in response to hypoxia, potentially via the 3 hypoxia response elements (HRE) in the CYGB promoter, 2 of which bind HIF-1, and the other EPO. Mutations to each HRE site individually reduced the hypoxic response, whilst mutations to all 3 sites simultaneously blocked the hypoxic response completely (Guo *et al.*, 2007). Mutations to HRE's however did not affect basal transcription (Guo *et al.*, 2007), and mutation of the c-Ets-1 and Sp-1 sites did not affect the hypoxic response. In addition, HIF-1 has been shown to increase activity of the CYGB promoter (Singh *et al.*, 2009).

There is sufficient evidence of an increase in CYGB promoter activity in response to hypoxia, via the HIF-1 pathway. The regulatory mechanisms of basal transcription, and hypoxia response appear to be distinct.

1.1.7 Hypoxia and Cytoglobin

Vertebrate CYGB expression at the mRNA and protein level has been shown to increase in response to hypoxia in both in *vivo* ((Fordel *et al.*, 2004; Fordel *et al.*, 2007b; Mammen *et al.*, 2006; Schmidt *et al.*, 2004) and in *vitro* models ((Guo *et al.*, 2007; Huang *et al.*, 2006)(Singh

et al., 2009) (Fordel *et al.*, 2004; Fordel *et al.*, 2007a).The in *vivo* models used rodents and have shown hypoxic induction of CYGB in a range of organs, including eyes, brain, heart, liver and skeletal muscle. Fordel *et al* (Fordel *et al.*, 2007a) showed reoxygenation following hypoxic treatment in *vivo* and in *vitro* decreased CYGB expression back to basal levels (Guo *et al.*, 2007). The localisation of the CYGB signal in the brain has been shown to remain constant with hypoxia (Mammen *et al.*, 2006).

The hypoxic response of CYGB expression was shown to be linked to HIF-1, as hypoxia induced CYGB mRNA upregulation was absent in muscle, liver and heart of HIF-1 knockout mice (Fordel *et al.*, 2004).

CYGB may have a cytoprotective role against hypoxic stress. Over expression of CYGB in islets of langerhanns has been shown to increase cell viability following transplantation, a process associated with prolonged ischemic conditions (Stagner *et al.*, 2005). It was proposed that CYGB over expression could enable cells to bind and use oxygen under lower oxygen tensions than cells without excessive CYGB. An in *vitro* study however presented conflicting data showing that CYGB over expression did not increase cell viability in response to hypoxic insult, and neither did inhibition of CYGB expression reduce cell viability (Fordel *et al.*, 2007a), unless hypoxic insult was accompanied with glucose deprivation.

CYGB has also been associated with regulation of cellular respiration (Halligan *et al.*, 2009). Nitric oxide (NO) inhibits mitochondrial respiration. Over expression of CYGB inhibits this action of NO, most probably as CYGB can bind NO and convert it into nitrate (Halligan *et al.*, 2009). Inhibition of CYGB expression using shRNA reduced nitrate production, increased

nitrosylation of proteins and heme, and made cells more sensitive to NO induced inhibition of cell respiration (Halligan *et al.*, 2009). CYGB over expression has also been shown to increase cell respiration and proliferation (Halligan *et al.*, 2009)

CYGB expression is increased in response to hypoxia, and may have a cytoprotective role however current understanding is limited. CYGB may also have a role in regulation of respiration.

1.1.8 Oxidative Stress and Cytoglobin

Oxidative stress is the accumulation of reactive oxygen species (See section 1.4 for more details about oxidative stress) CYGB expression in rat brain localised to regions which are responsive to oxidative stress (Mammen *et al.*, 2006). CYGB was shown to be upregulated in hereditary ferritinopathy neurones, a condition characterised by iron induced oxidative stress (Powers, 2006). Additionally an in *vitro* study showed an increase in CYGB mRNA with H_2O_2 treatment (Li *et al.*, 2007). Oxidative stress could therefore have a role in regulation of CYGB.

A cytoprotective role of CYGB against oxidative stress has been speculated in the literature and supported by studies which have shown a reduction in oxidative stress induced cell death (Fordel *et al.*, 2006) lipid peroxidation (Hodges *et al.*, 2008; Xu *et al.*, 2006) and DNA damage (Hodges *et al.*, 2008) with CYGB over expression in *vitro.* In addition knocking out CYGB expression reduced cell viability following H_2O_2 treatment (Li *et al.*, 2007). CYGB offer cytoprotection against oxidative stress by oxyradical scavenging. CYGB overexpressing

cells were shown to have an increased rate of oxyradical scavenging, supporting this theory (Xu *et al.*, 2006).

CYGB expression is increased in response to oxidative stress, an insult to which CYGB appears to offer cytoprotection, potentially through scavenging of ROS.

1.1.9 Cytoglobin and Cancer

The CYGB gene localises at 17q25, a region associated with cancers (McRonald *et al.*, 2006; Xinarianos *et al.*, 2006). The CYGB promoter has been shown to be frequently hypermethylated, in a range of tumours, which correlates with a reduction or loss of CYGB expression (McRonald *et al.*, 2006; Shaw *et al.*, 2006; Shaw *et al.*, 2009; Shivapurkar *et al.*, 2008; Xinarianos *et al.*, 2006). Demethlyation of the CYGB promoters with 5'-aza-2'-deoxycytidine induced CYGB expression (Shaw *et al.*, 2009; Shivapurkar *et al.*, 2008), indicating methylation is related to gene silencing.

Tumour development is associated with the onset of hypoxia, as is CYGB expression (See section 1.1.7). Using HNSCC (Head and neck squamous cell carcinoma) cells the effects of promoter methylation and HIF-1α activity upon CYGB expression were investigated. It was shown that at a high level of promoter methylation, indicating methylation of both alleles, the CYGB levels were low despite hypoxic treatment and induction of HIF-1α. At lower methylation levels, indicating methylation of one allele, CYGB expression increased in response to hypoxia. This study supports further a model of CYGB expression in response to hypoxia, but indicated that regulation of the CYGB promoter via methylation dominates over hypoxia.

Although CYGB expression is absent in several cancers, there is evidence of CYGB expression in others (Genin *et al.*, 2008; Shivapurkar *et al.*, 2008). RNAi was used to reduce CYGB expression in a non small cell lung cancer line, which resulted in an increase in colony formation, whilst forced over expression reduced cell growth and colony formation. In contradiction another study showed a correlation between a reduction of CYGB expression and reduced tumour development, however this study did not specifically target CYGB (Sheffer *et al.*, 2007)

The available evidence suggests that CYGB is a putative tumour suppressor.

1.1.10 Cytoglobin and Fibrosis

The CYGB promoter is regulated in part by c-Ets-1 (Guo *et al.*, 2006), a transcription factor associated with airway remodelling, a fibrogenic process. Additionally the original identification of CYGB was in a fibrotic study. There has thus been much speculation about the relationship between CYGB and fibrosis (See section 1.2 for overview of fibrosis).

Rodent studies have shown an increase in CYGB expression at the mRNA and protein level in fibrotic compared to non fibrotic tissues (Kawada *et al.*, 2001; Kida *et al.*, 2007; Man *et al.*, 2008; Nakatani *et al.*, 2004; Tateaki *et al.*, 2004). CYGB induction was shown to be via PKC signalling (Nakatani *et al.*, 2004). The localisation of the CYGB signal appears to remain constant (Man *et al.*, 2008). The source of this increase remains elusive and could be due to an increase in the number of cells expressing CYGB in the area, or an increase in subcellular expression. An increase in CYGB expression in response to fibrotic stimuli has also been

reported in *vitro* (Gnainsky *et al.*, 2007; Kawada *et al.*, 2001; Nakatani *et al.*, 2004; Zion *et al.*, 2009). Thioacetamide (TAA), which initiates a fibrogenic response, increases CYGB expression in *vivo* and in *vitro* (Gnainsky *et al.*, 2007; Zion *et al.*, 2009). The activity of TAA can be inhibited by halofuginone, which also inhibited CYGB upregulation in *vivo* and in *vitro* (Gnainsky *et al.*, 2007; Zion *et al.*, 2009).

The role of CYGB may be pro-fibrogenic, and or anti-fibrogenic. Reduction in CYGB expression in *vitro* correlated with reduced activation of myofibroblasts, indicating CYGB expression to be fibrogenic, however reduction of CYGB expression in this study was not targeted independently. CYGB was shown to have a role in regulating fibroblast proliferation (Halligan *et al.*, 2009), and over expression of CYGB has also been shown to reduce cell migration (Nakatani *et al.*, 2004) and increase collagen production (Nakatani *et al.*, 2004) adding further support to a pro-fibrotic role for CYGB.

There is also evidence of an anti-fibrotic role for CYGB. Over expression of CYGB in hepatic stellate cells in *vivo* reduced fibrotic progression and associated necrosis significantly, and inhibited the increase in pro-coll 1, TGF-β1 and TIMP-1 transcripts associated with fibrogenesis (Xu *et al.*, 2006). Transfection of CYGB after the onset of fibrosis in rats induced marked remodelling of the extracellular matrix and reduced fibrosis and necrosis (Xu *et al.*, 2006). Additionally in *vitro*, CYGB over expression prevented oxidative stress induced differentiation of hepatic stellate cells into the activated phenotype (Xu *et al.*, 2006).

There is evidently a relationship between CYGB and fibrosis, however the source of CYGB expression, regulation, and role CYGB in fibrosis remains elusive

1.2 Pulmonary Fibrotic Disease

1.2.1 The Respiratory tract

1.2.1.1 Structure

The respiratory tract is separated into the upper and lower respiratory tracts, which meet at the bifurcation of the trachea The lower respiratory tract refers to the lungs and can be further segregated into the conducting and respiratory zones. The conducting zone transports air to the respiratory zone where gaseous exchange takes place. The conducting zone comprises of bronchi which split repeatedly into the terminal bronchioles. The terminal bronchi are the smallest non respiratory bronchioles of the lung, due to the absence of alveoli. The terminal bronchi feed into the respiratory zone which is comprised of further divisions of bronchioles to alveolar ducts, finally leading to the alveoli.

1.2.1.2 Bronchioles

Bronchioles are fundamentally comprised of an epithelial layer, smooth muscle and mesenchyme (see Figure 1.4). Higher order bronchioles and bronchi may also contain cartilage and glands within the structure. The epithelium is predominantly composed of ciliated columnar epithelial cells, however an array of other cell types can also be observed. The cell type composition of the epithelium varies in accordance with localisation within the respiratory tract. Cell types which contribute towards the bronchial epithelial layer include Goblet cells, Clara cells, Brush cells and Basal cells to name a few (Breeze and Turk, 1984).

Figure 1.4 Lung Structure

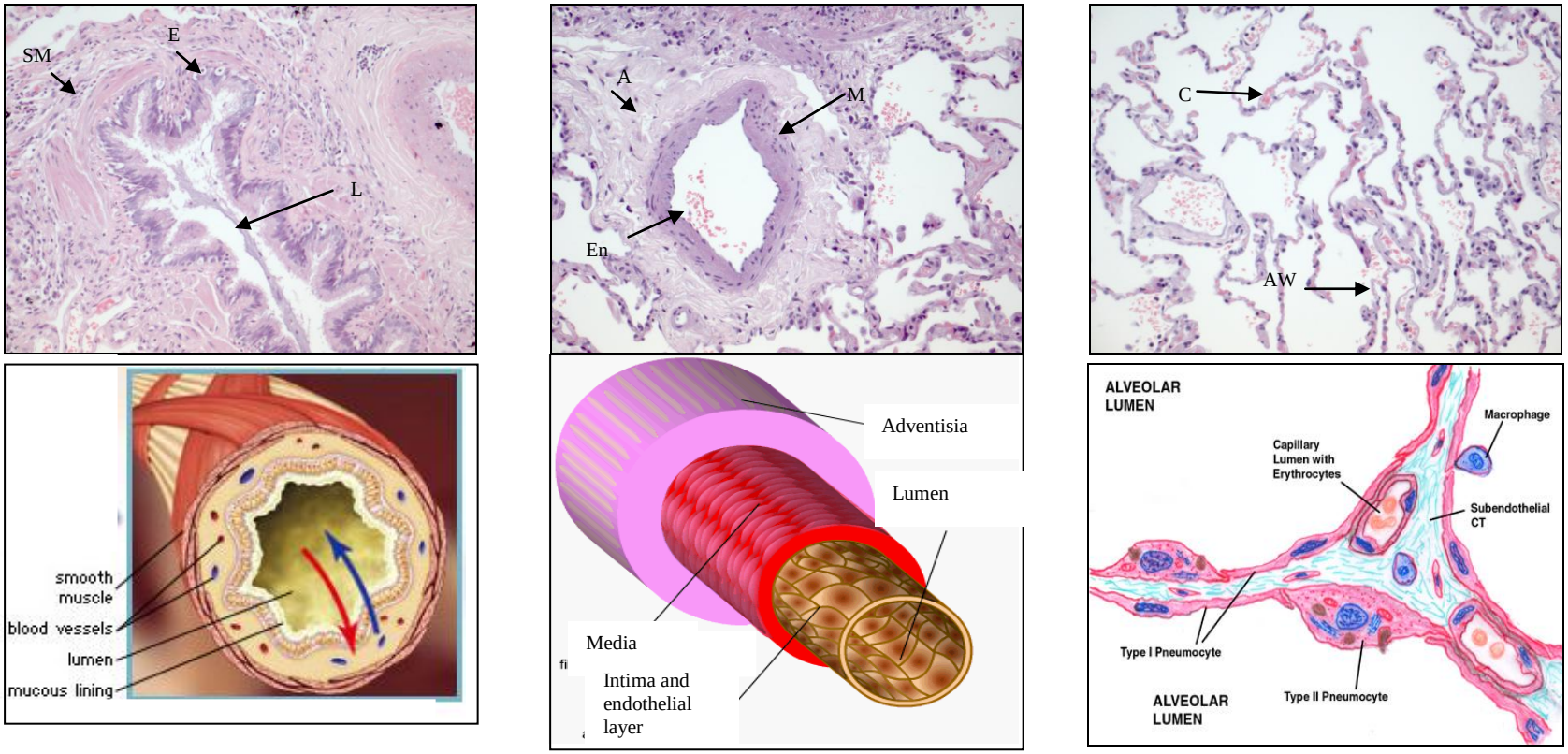

Pictures and diagrams to show the structure of bronchioles (left), vasculature (middle) and parenchyma (right). The diagrams were sourced and adapted from the following internet sites. Bronchioles (left) http://media-2.web.britannica.com/eb-mdeia/28/69628-004-BA27EB34.jpg , Artery (middle) http://images.google.co.uk/ imgres? imgurl=http ://www.s-cool.co.uk/assets/learn_its/alevel/biology/transport/transport-in-mammals/2008-01-22_102617.gif&imgrefurl=http://www.s-cool.co.uk/alevel/biology/transport/ transport-in-mammals.html, Parenchyma (right) education.vetmed.vt.edu/.../labs/Lab25/lab25.htm.KEY: SM: Smooth Muscle. E: Epithelial cells. L: Lumen. A: Adventisia, M: Media. En: Endothelial cells. C: Capillarie. AW: Alveolar Wall. All pictures were taken at x20 and are 30% of original size.

1.2.1.3 Vasculature

Artery walls are comprised of 3 layers (See Figure 1.4), the intima, the media and the adventisia. The intima encompasses a layer of endothelial cells, connective tissue and internal elastic lamina. The major component of the media is smooth muscle and elastic fibres. The adventisia is comprised of connective tissue, predominantly collagen.

The capillary walls of the pulmonary microvasculature are comprised of a layer of squamous endothelial cells joined by tight junctions surrounded by extracellular matrix termed the basal lamina. (See Figure 1.4)

1.2.1.4 Parenchyma

Lung parenchyma, or the alveoli bed, is essentially comprised of epithelial cells layered upon connective tissue and capillaries (see Figure 1.4). There are two alveolar epithelial cell types, termed type I and type II pneumocytes. Type I pneumocytes are thin squamous epithelial cells, which overlay the capillaries lining the alveolar bed. Type I pneumocytes cover the majority of the alveolar wall and have a primary role in gaseous exchange. Type I pneumocytes can be identified using Wheat Germ Agglutinin (WGA). WGA is lectin which has been reported to bind N-acetylglucosamine on the surface of type I pneumocytes universally (Barkhordari *et al.*, 2004).

Type II pneumocytes are large, round epithelial cells of the alveolar bed (See Figure 1.4). The population of type II cells far exceeds that of type I cells, however they occupy only 7% of the alveolar surface. Type II cells were first established as ‘defenders’ of the alveolus in 1977 (Mason and Williams, 1977), since which the roles of the type II pneumocytes have become

well known, and include synthesis and secretion of surfactant (which reduces surface tension in the lung) (Buckingham *et al.*, 1966), and progenitors of type I pneumocytes in response to damage. The role of type II pneumocytes in surfactant synthesis enables the use of surfactant A as a cell specific marker. Cytokeratin immunoreactivity can be used as a marker of differentiation of Type II cells into Type I cells (Hinata *et al.*, 2003). Fibroblasts and inflammatory cells are also observed within the lung parenchyma.

1.2.2 Fibrosis in the Context of Pulmonary Disease

Fibrosis can be defined as excessive deposition of extracellular matrix which can impede normal organ function. Fibrosis is frequently associated with pulmonary diseases. Pulmonary diseases can be categorised as restrictive or obstructive (Green, 2002). Patients diagnosed with obstructive lung diseases present with difficulties in exhaling air, due to conditions such as Chronic Obstructive Pulmonary Disease (COPD), asthma, and emphysema. COPD is an inflammatory disease (Chung and Adcock, 2008; Gadgil and Duncan, 2008), with elements of fibrosis in the upper cartilaginous airways and parenchyma (Green, 2002). In contrast restrictive lung diseases such as interstitial lung diseases (ILDs) create difficulties in the inhalation of air. ILDs are chronic inflammatory diseases with progressive fibrosis of the alveolar walls and peribronchiolar and perivascular connective tissue. ILDs can be further categorised into three groups, ILDs with known etiology including occupational or environmental factors, drugs or infections, ILDs associated with systemic disorders such as collagen vascular disorders or sarciodosis, and ILDs with no known cause, the idiopathic interstitial pneumonias of which idiopathic pulmonary fibrosis (IPF) is the most common (Green, 2002)

1.2.2.1 Chronic Obstructive Pulmonary Disease (COPD)

COPD is a leading cause of morbidity and mortality in both the developed and developing world. It was reported in 2003 that COPD affects approximately 1% of the UK population as a whole, and the prevalence increases with age to approximately 10% in males over 75 (Britton, 2003). It is well established that the most significant risk factor is tobacco smoking, however only 15-20% of smokers present clinically with COPD (Kim *et al.*, 2008).

COPD is a disorder characterised by irreversible airflow limitation and airway inflammation. Airflow limitation is a consequence of a lack of elastic recoil of the lung, and an increase in airflow resistance (Szilasi *et al.*, 2006). Emphysema, chronic bronchitis and obstructive bronciolitis all contribute to COPD, to varying extents, and as such the range of pathologies observed in COPD is vast. COPD is graded according to severity, using a GOLD (Global initiative for chronic Obstructive Lung Disease) standard. The GOLD standard takes into account the 'forced expiratory volume in one second' and 'forced vital capacity' to determine the classification from stage I, mild to stage IV, very severe (GOLD website www.goldcopd.com).

Emphysema is the development of permanent air space enlargement in the terminal bronchioles, respiratory bronchioles and alveoli. Emphysema is thought to be the result of a protease/antiprotease imbalance caused by repetitive inflammation and episodes of fibrosis (Szilasi *et al.*, 2006), which accelerates epithelial and endothelial apoptosis. The emphysematous process remains incompletely understood.

Chronic bronchitis can be defined pathologically as presenting with increased mucous production, goblet cell hyperplasia, epithelial changes, airway inflammation, smooth muscle hypertrophy and submucosal bronchial gland enlargement (Szilasi *et al.*, 2006) in the airways. The predominant feature is mucous hypersecretion, which doesn't necessarily result in obstruction of the airways. In smaller airways epithelial atrophy and metaplasia is also observed. Of note a difference in the pathology of COPD and asthma is the thickness of the basement membrane, which in COPD remains within the normal range, and is thickened in asthma (Szilasi *et al.*, 2006).

Obstructive bronchiolitis is inflammation of the small and peripheral airways (<2cm in diameter). The typical inflammatory insult involves macrophages and CD8+ T lymphocytes predominantly (Szilasi *et al.*, 2006). An increase in fibroblast numbers is also observed with obstructive bronchiolitis, and an associated increase in extracellular matrix deposition, and fibrosis.

The fibrosis observed in COPD is heterogenic both between different patients and sections of lung from the same patient. A range of fibrosis is thus observed making COPD a good model to investigate the fibrogenic process.

1.2.2.2 Idiopathic Pulmonary Fibrosis (IPF)

IPF is characterised as fibrosis of the lung in the absence of a known causative agent. The overall incident rate of IPF in the UK was reported to be 4.6 in 100 000 in 2003 (Gribbin *et al.*, 2006), and the mean survival is approximately 3 years post diagnosis (Meltzer and Noble, 2008). IPF patients present with Usual Intersitial Pneumonia (UIP), the pathology of which

includes dense fibrotic lesions interspersed with normal lung architecture (Meltzer and Noble, 2008). This increase in scar tissue, and disruption of architecture result in a reduced level of gaseous exchange and compliance of the lung.

The pathogenesis of IPF remains elusive, however the literature favours a model of alveolar epithelial injury and consequent release of pro-fibroproliferative and pro-inflammatory mediators, initiating defective repair pathways. Fibrosis supersedes repair, there is deficient resolution of the tissue and subsequently fibrosis progresses (Meltzer and Noble, 2008).

The fibrosis observed in IPF is dynamic and homogenic (Gomperts and Strieter, 2007) and non self limiting. IPF is appropriate as a positive control model for fibrosis.

1.2.3 Pulmonary Fibrosis at a Cellular Level

1.2.3.1 Fibrosis and Repair

Fibrosis is, in essence, excessive deposition of extracellular matrix (ECM), stimulated through injury, infection or inflammation. Fibrosis is therefore readily associated with repair pathways. In normal wound repair there are typically 2 distinct phases, a regenerative phase and fiboplasia. Injured cells are replaced by cells of the same cell type during the regenerative phase, whilst in fibroplasias, connective tissue supports the region of damage, replacing normal cell structure (Wynn, 2008). Fibrosis is thus an essential aspect of wound healing, however a lack of balance between fibrogenesis and fibrolysis leads to the formation of deleterious fibrotic lesions. The production of fibrotic lesions can be both permanent and reversible, such as in idiopathic pulmonary fibrosis (IPF) and acute respiratory distress syndrome (ARDS) respectively. The latter can be reversed upon administration of oxygen,

however in the absence of oxygen, the point at which the fibrotic lesions transform from a reversible to a permanent state is unknown.

The process of fibrogenesis is not uniform throughout pulmonary diseases which present with fibrosis, although there are common aspects. Interstitial pulmonary fibrosis typically involves injury to alveolar epithelial cells resulting in an inflammatory response which initiates migration of fibroblasts to the site of the injury, within the alveolar septum and/or lumen where they proliferate and secrete extracellular matrix (Fireman *et al.*, 2001)

1.2.3.1.1 Alveolar Epithelial Cell Injury

Injury to alveolar epithelial and endothelial cells initiates the release inflammatory mediators from endothelial and epithelial cells which, through increased blood vessel permeability and basement membrane disruption, enable easy recruitment of inflammatory cells the site of injury (Wynn, 2008)

Alveolar epithelial cells could also be directly involved in mediation of pulmonary fibrosis. In response to injury or pro-fibrotic factors, alveolar epithelial cells can modify cell morphology and gene expression, subsequently producing pro-fibrotic factors which can regulate the function and differentiation of fibroblasts (Willis and Borok, 2007). It has also been suggested that bidirectional signalling could occur between epithelial cells and fibroblasts, with each cell mediating the function, proliferation and survival of the other (Rennard, 2001; Willis and Borok, 2007). It has been observed in mice that the presence of an intact epithelium suppresses fibroblast proliferation and ECM deposition (Willis and Borok, 2007). This could be due to the suggested production of Transforming Growth Factor-β1 (TGF-β1) by healthy

alveolar epithelial cells which can inhibit the proliferation of fibroblasts (Hostettler *et al.*, 2008). Further evidence of the direct involvement of epithelial cells in pulmonary fibrosis is Endothelin-1 (ET-1). ET-1 is a vasoconstrictor which is commonly associated with fibrosis. ET-1 expression was observed in type I and type II pneumocytes of rats treated with bleomycin to induce fibrosis, whilst it was limited to the airways in healthy rats, implying a pro fibrotic role of alveolar epithelial cells in fibrosis via the production of ET-1 (Mutsaers *et al.*, 1998). Of note ET-1 was also observed in macrophages and peribronchiolar, perivascular and alveolar septa connective tissue, and the media and intima of vessels, thus alveolar epithelial cells are not the exclusive source of ET-1 during fibrosis (Mutsaers *et al.*, 1998).

Alveolar epithelial cells observed in IPF are morphologically abnormal, frequently hyperplasic and hypertrophic, presenting alterations in cytokeratin (CK) expression and increased apoptosis especially in regions adjacent to fibrotic foci (Selman and Pardo, 2006; Willis and Borok, 2007). The alveolar epithelial cells of IPF patients have been shown to express a range of pro-fibrotic chemokines including TGF-β, Tumour Necrosis Factor-α (TNF-α), ET-1, Platelet Derived Growth Factor (PDGF) (Willis and Borok, 2007) and Connective Tissue Growth Factor (CTGF) (Pan *et al.*, 2001). In contrast, there is evidence of the expression of Matrix Metalloproteinases (MMP) by alveolar epithelial cells of IPF patients, which degrade ECM, however the expression of MMPs may also contribute to remodelling. Chronic inflammation is observed in IPF, and considered to instigate progressive fibrosis, there is increasing evidence however that instead IPF results from repeated cycles of epithelial injury and activation (Selman and Pardo, 2006).

There is a higher abundance of apoptotic alveolar epithelial and endothelial cells, and bronchiolar epithelial cells in COPD patients than observed in healthy subjects. This could result from an increase in apoptosis or a decrease in clearance of apoptotic cells by macrophages (Henson *et al.*, 2006). This persists after ceasation of smoking making it unlikely to be an acute response to smoke specific injury. Apoptotic cells produce pro-fibrotic chemokines such as TGF-β1, which could contribute to the fibrosis observed in COPD (Henson *et al.*, 2006). Smoking is known to kill precursors of epithelial and endothelial cells, inhibit airway cell chemotaxis and prolilferation and induce senescence upon epithelial cells, preventing efficient repair in response to smoke specific injury, which is likely to augment the potentiality of a fibrogenic response (Chung and Adcock, 2008). COPD patients have also shown an increase in expression of genes involved in ECM production, degradation and apoptosis following microarray analysis of bronchiole epithelial cells and alveolar macrophages. An increase in both proliferation and apoptosis of alveolar epithelial cells is observed with emphysema, which contributes to COPD (Chung and Adcock, 2008).

1.2.3.1.2 Inflammation

Inflammation is readily associated with fibrosis however inflammatory cells may have an anti-fibrotic, pro-fibrotic and no fibrotic role in pulmonary fibrosis (Luzina *et al.*, 2008). Although inflammation typically precedes fibrosis (Fries *et al.*, 1994) there is evidence that fibrosis can occur in response to epithelial injury without an inflammatory aspect (Willis and Borok, 2007). This has been observed in models of IPF (Selman and Pardo, 2006). Where inflammation has a fibrogenic role, the key role is the expression of fibrogenic factors and recruitment of fibroblasts.

T-lymphocytes, which can be identified immunohistochemically using CD3 as a marker, are known to synthesise an array of cytokines which modulate proliferation, recruitment and ECM production of fibroblasts, and mediate ECM turnover (Luzina *et al.*, 2008). It has long be speculated that inflammation contributes to fibrotic disease progression, however of the cytokines released by T-lymphocytes some have anti-fibrotic roles, so potentially T cell infiltration could also reduce disease progression (Luzina *et al.*, 2008).

COPD is an inflammatory disease, and subsequently there has been much focus on the inflammatory aspects of COPD (Rennard, 2001). The parenchyma has been shown to contribute to the activation and recruitment of inflammation (Fries *et al.*, 1994), and conversely, inflammatory cells modulate the activity of parenchymal cells (Rennard, 2001). There is evidence that inflammation in response to infection is likely to contribute to the pathogenesis of COPD (Sethi and Murphy, 2008), and that inflammation in COPD is inextricably linked to fibrogenic processes (Hogg, 2008). One direct relationship between inflammatory cells and COPD pathogenesis is the enhanced COX-2 expression (See section 1.2.3.3.3 for more details) observed in alveolar macrophages of COPD patients (Barnes, 2004). This results in elevated Prostaglandin-2 (PGE) production (see for more details), which increases mucous secretion, and coughing (Barnes, 2004). A reduction in mucous secretion has been observed with Cox inhibitors. Mediators of inflammation are fundamental to COPD and are secreted by inflammatory cells, epithelial cells, endothelial cells and fibroblasts (Barnes, 2004).

The influence of inflammation on the fibrotic lesion remains elusive, however an influx of inflammatory cells is frequently observed prior and during fibrosis.

1.2.3.1.3 Fibroblast migration and activation

Fibroblasts are known to migrate to the region of injury, where they become activated, proliferate, and secrete extracellular matrix components. Fibroblasts are not a homogenous population, there are a diverse range of fibroblast phenotypes characterised by cell surface markers, receptor expression, cytoskeletal structure and cytokine production (Ramos *et al.*, 2001). Fibroblast subtypes differ in growth rates, collagen expression levels and responses to cytokines (Uhal *et al.*, 1998). It has subsequently been suggested that each fibroblast subpopulation could be responsible for specific functions, such as mediating inflammatory and epithelial responses, regulating recruitment, activation and proliferation of other fibroblasts, and extracellular matrix deposition (Fries *et al.*, 1994).

Myofibroblasts

Expression of αSMA (alpha smooth muscle actin) by fibroblasts was first identified in 1971 (Gabbiani *et al.*, 1971), and this subset of fibroblasts was termed myofibroblasts (Fireman *et al.*, 2001; Shahar *et al.*, 1999; Uhal *et al.*, 1998). Myofibroblasts are larger (Uhal *et al.*, 1998), more proliferative, more contractile and have an increased level of ECM production than normal fibroblasts (Darby and Hewitson, 2007), which are typically senescent. Under normal repair myofibroblast are lost via apoptotic pathways, enabling resolution of injury. In fibrosis myofibroblasts are not lost and instead contribute to fibrotic progression. There is evidence of apoptosis resistant myofibroblasts in IPF (Garneau-Tsodikova and Thannickal, 2008; Laurent *et al.*, 2008). There was subsequently speculation that differentiation to myofibroblastic phenotype could be an initial step in apoptosis in normal repair, however apoptotic fibroblasts have been shown to have αSMA+ and αSMA– phenotypes (Uhal *et al.*, 1998), implying no correlation between αSMA expression and apoptosis.

The bronchoalveolar lavage of IPF patients has more myofibroblast (Fireman *et al.*, 2001; Ramos *et al.*, 2001; Shahar *et al.*, 1999), which express higher levels of pro fibrotic chemokines (Ramos *et al.,* 2001) than those from healthy subjects. Immunohistochemistry of IPF tissue has shown individual αSMA+ cells in the parenchyma dissociated from airways and blood vessels considered to be myofibroblasts, and bundles of loosely associated αSMA+ cells (Ohta *et al.*, 1995), believed to be smooth muscle. Proliferation of smooth muscle in IPF is a key pathological feature, which results in the formation of ectopic bundles of smooth muscle within the parenchyma (Kanematsu *et al.*, 1994).

COX-2 Expression

COX-2 is an enzyme which produces PGE (prostaglandin E_2) from arachidonic acid. COX-2 expression is controlled primarily at the transcriptional level (Park and Christman, 2006), which is induced by TNF-α and IL-1b, in response to TGF-β1. PGE has a short half life (Diaz *et al.*, 1998), and so is only locally active and often acts upon the cells from which it was produced offing a feedback mechanism. PGE has been shown to decrease fibroblast proliferation, inhibit collagen synthesis and promote collagen degradation, indicating PGE to be anti-fibrotic (Park and Christman, 2006). TGF-β1 is the most potent pro fibrotic factor yet identified, however this pathway offers an anti-fibrotic role for TGF-β1 (Laurent *et al.*, 2008).

The expression of cyclooxygense-2 (COX-2) by fibroblasts is differentially expressed by fibroblasts from IPF, COPD and non fibrotic controls subjects. COPD shows an enhanced COX-2 mRNA basal level compared to controls and IPF subjects (Xaubet *et al.*, 2004). Stimulation of COX-2 expression by interleukin-1b (IL-1b) increased expression in COPD

and control fibroblasts but not those from IPF (Xaubet *et al.*, 2004). This loss of induction in IPF derived fibroblasts has also been observed following stimulation with PMA, LPS and IL-1 (Wilborn *et al.*, 1995). Fibroblasts from IPF show a 2 fold decrease in COX-2 expression than normal fibroblasts (Wilborn *et al.*, 1995). The fibroblasts from IPF and COPD are thus distinct in their COX-2 expression, with excessive expression in COPD and a lack of COX-2 expression and induction in IPF (Xaubet *et al.*, 2004).

This lack of basal and induced COX-2 in fibroblasts from IPF patients resulting in reduced PGE levels (Keerthisingam *et al.*, 2001) could be a fundamental in the onset of fibrotic rather than repair pathways. IPF models using bleomycin treated mice have shown that COX-2 inhibition, or deficiency in expression correlate with a decrease in PGE secretion and subsequent increase in fibrotic response and collagen content (Hodges *et al.*, 2004; Keerthisingam *et al.*, 2001). Additionally one study showed equal levels of COX-2 expression, and subsequent PGE in IPF and normal fibroblasts, however these fibroblasts produced more thromboxane (Tx), a profibrotic chemokine which increases proliferation of fibroblasts and DNA and RNA synthesis (Cruz-Gervis *et al.*, 2002). Despite the equivalent levels of PGE between normal and IPF fibroblasts, the IPF fibroblasts were more pro-fibrotic due to an increased Tx:PGE ratio (Cruz-Gervis *et al.*, 2002). IPF derived fibroblasts have also been shown to express higher levels of CTGF (Pan *et al.*, 2001) and ET-1 (Shahar *et al.*, 1999) which each stimulate proliferation of fibroblasts. IPF derived fibroblasts also respond differently to growth factors than normal fibroblasts including TNF-α, TGF-β1 and PDGF in response to which normal fibroblasts increase in prolilferation, whilst IPF derived fibroblasts increased synthetic activity (Hetzel *et al.*, 2005). There is sufficient evidence of a pro-fibrotic

fibroblasts phenotype in IPF, which is likely to contribute significantly to the fibrotic pathogenesis.

The levels of PGE are increased in COPD (Barnes, 2004), potentially through an increase in COX-2 expression in both fibroblasts and alveolar macrophages (Barnes, 2004). This induction in expression is thought to be due to chemokines originating from inflammation (Barnes, 2004), in addition to an increased rate of basal expression (Xaubet *et al.*, 2004). Cigarette smoke has also been shown to increase COX-2 expression and subsequent PGE production (Martey *et al.*, 2004), and is known to decrease fibroblast proliferation and induce fibroblast senescence (Chung and Adcock, 2008). The onset of a senescent fibroblast phenotype in COPD has been speculated to contribute to abnormal wound healing and ineffective repair (Chung and Adcock, 2008). The high levels of the anti-inflammatory and anti-fibrotic PGE are somewhat contradictory to the fibrotic element observed in COPD, however several pro-fibrotic chemokines are upregulated in COPD which could compensate for the effects of PGE, these include Tx, ET-1, TNF-α, TGF-β1, IL-1b and MMP. These chemokines have roles in regulating the activation, proliferation, migration and section of ECM by fibroblasts, and ECM destruction (Barnes, 2004).

Source of fibroblasts

The source of fibroblasts recruited to fibrosing lesions offers differences in fibroblasts phenotypes. There are 3 suggested origins of fibroblasts: proliferation of resident fibroblast; circulating fibroblast precursors; and epithelial-mesenchymal transition (EMT).

Circulating fibroblast precursors express lymphocyte markers including CD34, CD45, CD13, mesenchymal markers such as Pro-collagen I and III, Vimentin and Fibronectin, and chemokine receptors CXCR4 and CCR7 which are important in migration from vascular to extravascular regions (Gomperts and Strieter, 2007). These are bone marrow derived and have the capacity to differentiate into a range of mesenchymal cells, including adipocytes, osteoblasts, chondrocytes and fibroblasts, and so have been termed circulating mesenchymal progenitor cells (CMPC) (Gomperts and Strieter, 2007). There is evidence that fibroblasts of this source could contribute to IPF (Andersson-Sjoland *et al.*, 2008).

EMT can be induced in response to an array of chemokines including TGF-β1, CTGF, IL-1 and Fibroblast Growth Factor-1 (FGF-1), and can be enhanced by proteolytic degradation of the basement membrane (Willis and Borok, 2007). Consequently over expression of MMP can disrupt the basement membrane and induce EMT (Willis and Borok, 2007). Characteristics of EMT have been observed in IPF (Selman and Pardo, 2006).

1.2.3.2 Microvascular changes

The extensive remodelling of the alveolar bed in fibrosis, and destruction of lung architecture has, unsurprisingly, an effect on the resident microvasculature. There have been conflicting reports in the literature as to whether there is an increase in microvasculature loss, or neovasculatisation with fibrosis (Tzouvelekis *et al.*, 2006). There is increasing evidence of a role in the balance of angiostatic and angiogenic factors in vascular remodelling in fibrotic disorders, thus is appears vasculature changes are significant in the pathogenesis of fibrosis. It is likely that microvasculature loss, and neovascularisation occur in different regions of the same fibrotic lesion, with loss being observed in fibrosed, highly acellular foci, and

angiogenesis being focused in the associated fibrosing, cellular tissue. It remains unclear whether angiogenesis drives fibrosis through neovasculagenesis supplying fibrogenic factors, or acts to compensate the fibrotic insult through supplying anti-fibrotic agents ((Tzouvelekis *et al.*, 2006; Voelkel *et al.*, 2007). There is a relationship between hypoxia and fibrogenesis, as such one could speculate that excessive ECM deposition causes fibrosis and loss of microvasculature, and subsequently the onset of hypoxia. Angiogenesis occurs in response to hypoxia, to increase oxygen supply to the region.

The alterations in microvasculature of COPD and IPF remain elusive. IPF is associated mainly with angiogenesis, which is thought to contribute to fibrosis (Keane *et al.*, 1997; Keane *et al.*, 2001). VEGF is a highly potent angiogenic factor which is differentially expressed with different COPD pathologies. There is evidence of increased VEGF in chronic bronchitis (Orihara and Matsuda, 2008), however an associated increase in microvessel number has yet to be established. Emphysema is associated with a decrease in VEGF, which may contribute to the destruction of the alveolar septa via endothelial apoptosis (Orihara and Matsuda, 2008; Siafakas *et al.*, 2007). As mentioned earlier within COPD there could be both pro and anti-angiogenic events occurring simultaneously in different regions of the lung.

1.2.3.3 Vascular remodelling

Vascular remodelling of pulmonary arteries is frequently observed in COPD (Vaughan *et al.*, *2006*). Endothelial cells have impaired function, which subsequently results in an increased thrombogenic capacity of the arteries (Voelkel *et al.*, 2007). Pulmonary hypertension is often associated with COPD, and believed to initiate intimal thickening, arteriole muscularisation and remodelling of the vessel wall. (Jeffery, 2001) In addition endothelial dysfunction and

subsequent loss of the moderation of vasculature tone and cell growth may initiate vascular wall remodelling (Santos *et al.*, 2002).

Remodelling can be defined as 'an alteration in size, mass or number of tissue structural components that occurs during growth or in response to injury and/or inflammation.' (Jeffery, 2001). There are several contributing factors to vascular remodelling in COPD: Intimal and medial hyperplasia and/or hypertrophy, intimal and medial fibrosis, elastic lamina changes, infiltration of mesenchymal cells and T-lymphocytes (Jeffery, 2004), re-orientation of medial smooth muscle fibres (radial alignment from longitudinal), apoptosis, activation and loss of endothelial cells, and development of thrombi (Jeffery, 2004; Santos *et al.*, 2002; Vaughan *et al., 2006*).

Unpublished data generated at AstraZeneca by G.Sirico (2006) has shown a correlation in desmin and vimentin immunoreactivity with vascular remodelling. There is evidence of an increase in disorganised Vimentin staining within the media and intima of severely remodelled vessels. High levels of ordered vimentin positive staining was observed in mild lesions, the signal of which was lost with moderate remodelling. There was an increase in desmin negative zones in the media with increased severity of remodelling, which infiltrated into intimal regions in severely remodelled vessels. The loss of a desmin positive population, and gain in vimentin indicates a mesenchymal origin of cells involved in vascular remodelling.

1.2.4 Pulmonary Fibrosis and Associated Hypoxia

Airflow obstruction and microvasculature loss observed in pulmonary fibrosis may lead to decreased oxygen transport and alveolar hypoxia. Sub-cellular hypoxic events are summarised in 3.3.1. Hypoxia initiates cellular and structural changes within the lung, and effects the pathogenesis of fibrosis.

1.2.4.1 Hypoxia and Fibrotic Pathogenesis

Hypoxia is involved in regulating numerous cellular processes including collagen synthesis, angiogenesis, apoptosis and proliferation, all of which contribute to fibrogenesis (Higgins *et al.*, 2008). Hypoxia has been shown to trigger recruitment of inflammatory cells, and increase expression of inflammatory mediators, which could initiate and perpetuate fibrosis (Jain and Sznajder, 2005).

There is evidence that hypoxia has detrimental effects on alveolar epithelial cells, affecting expression of VEGF and surfactant, initiating apoptosis, and disrupting cytoskeletal integrity. Epithelial damage could act as an initial insult stimulating the onset of fibrosis, or in a model in which a hypoxic environment originates from fibrogenesis, the repeated epithelial damage could contribute to the pathogenesis of the disease (Jain and Sznajder, 2005).

Additionally, hypoxia can stimulate epithelial to mesenchymal transition, and inhibition of the hypoxic response has been shown to reduce fibrogenesis (Higgins *et al.*, 2007). It is evident that hypoxia has a key role in fibrotic pathogenesis, progressing the disease.

1.2.4.2 Vascular Remodelling in Response to Hypoxia

There is evidence of a role for hypoxia in vascular remodelling. Acute hypoxia has been shown to increase proliferation of pulmonary fibroblasts, however many in *vitro* studies have found that hypoxia does not have a direct effect upon smooth muscle and endothelial cell proliferation (Pak *et al.*, 2007). Proliferation of adventisial fibroblasts is observed within hours of hypoxic insult, however medial and intimal remodelling is only observed after days of hypoxia. (Pak *et al.*, 2007)(Stenmark *et al.*, 2002) There are many fibroblast subtypes within the vessel wall and adventisia (Stenmark *et al.*, 2002). It is plausible that these fibroblasts respond to hypoxic insult through proliferation, ECM deposition, secretion of mutagenic factors, and differentiation in to a myofibroblast phenotype, and potentially further differentiation into smooth muscle cells. These reports in the literature support data generated by G.Sirico at AstraZeneca (2006) which showed that a mesenchymal component was key in vascular remodelling.

1.2.5 Pulmonary Fibrosis and Oxidative Stress

Oxidative stress results from an imbalance in the generation of reactive oxygen species (ROS), and the antioxidant response. The result is accumulation of harmful oxygen species, and subsequent damage to DNA, proteins and lipids (See section 1.4). There is evidence, however for an important role of ROS in intracellular signalling. There is mounting evidence of oxidative stress in pulmonary fibrosis, potentially originating from an increase ROS generated from inflammatory insult, and a decrease in the antioxidant response due to defects in endogenous antioxidants (Chung and Adcock, 2008)

The primary contributors and perpetuators of pulmonary fibrosis are epithelial and/or endothelial cell damage and apoptosis; inflammation; and recruitment, proliferation and differentiation of fibroblasts. ROS has been shown to be involved in mediating the inflammatory response; inflammatory cells release ROS to recruit further inflammatory cells to an area of damage (Chung and Adcock, 2008). ROS initiate activation of growth regulatory cytokines, including TGF-β, which is involved in fibroblast recruitment, proliferation, and differentiation into the myofibroblast phenotype (Kinnula and Myllarniemi, 2008). Additionally redox modulators and antioxidants have been shown to attenuate progression of fibrosis (Kinnula and Myllarniemi, 2008).

Although the mechanistic details by which ROS contribute to fibrogenesis remain elusive, there is increasing evidence that oxidative stress contributes to fibrotic disease progression.

1.3 Hypoxia

Oxygen deprivation (hypoxia), even transient, can produce irreversible cellular damage to cells, which depend on aerobic respiration. Oxygen homeostasis is subsequently fundamental to cellular function (Stroka *et al.*, 2001).

1.3.1 Hypoxia Inducible Factor 1 (HIF-1)

The Hypoxia Inducible Factor 1 (HIF-1) is the principal factor in mediating cellular adaption to hypoxia. HIF-1 is a transcription factor, which regulates the expression of numerous genes during hypoxia through the binding of conserved HREs (hypoxia response elements) in the promoters of target genes, and recruitment of co activators (Stroka *et al.*, 2001). HIF-1 is known to regulate the expression of genes involved in angiogenesis, glucose metabolism, vasodilation, respiration, erythropoiesis, oxygen sensing, pH homeostasis and autophagy (Brahimi-Horn and Pouyssegur, 2009). To achieve these functions, at the subcellular level HIF-1 is known to mediate mobility, differentiation, proliferation, cell death and cell survival (Berra *et al.*, 2006; Koh and Powis, 2009; Wenger, 2002).

HIF-1 is heterodimeric, comprised of two subunits, HIF-1α and HIF-1β. There are three isoforms of the α-subunit (HIF-1α. HIF-2α and HIF-3α) and two isoforms of the β-subunit. (Brahimi-Horn and Pouyssegur, 2009). The function and regulation of HIF-1α has been studied intently, however HIF-2α and HIF-3α have only recently been identified and so knowledge in this field remains limited. Each of the isoforms of the α subunit have been associated with oxygen sensing, however the β-subunit is constitutively expressed, and not regulated in response to oxygen tension.

1.3.2 Hypoxic regulation of HIF-1α Activity

HIF-1 activity is modulated via post-translational modification of the α-subunit under normoxic conditions. Each of the isoforms of the α-subunit are regulated in a similar manner (Brahimi-Horn and Pouyssegur, 2009). Under normoxic conditions prolyl hydroxylation, by prolyl hydroxylase domain proteins (PHDs), of the ODD (oxygen dependant degradation domain) region of the HIF-1α protein occurs. The activity of PHDs is dependent on molecular oxygen and Fe^{2+}, and subsequently only occurs under normoxic conditions. Hydroxylation encourages interaction with pVHL (von Hippel Lindau tumour suppressor protein), which is part of a multi-protein ubiquitin ligase complex (VHL/Elongin B/Elongin C), and covalently binds ubiquitin to the HIF-1α protein. Ubiquitin signals HIF-1α for degradation, as it enables the docking of the HIF-1α protein into a multi-subunit proteolytic proteasomal complex, which specifically degrades ubiquitinated proteins (Brahimi-Horn and Pouyssegur, 2009). In addition to signalling HIF-1α for degradation, PHDs also hydroxylase the C-terminal of HIF-1α, inhibiting binding of transcriptional co-factors (Berra *et al.*, 2006; Brahimi-Horn and Pouyssegur, 2009; Wenger, 2002)

Under hypoxic conditions the lack of oxygen inhibits the function of prolyl hydroxylases, thus preventing binding of HIF-1α with pVHL. The consequential stabilisation of HIF-1α enables translocation to the nucleus, dimerisation with HIF-1β, recruitment of transcription co-factors, and subsequent regulation of gene expression.

1.3.3 Non-Hypoxia regulation of HIF-1α

HIF-1 regulation is not limited to oxygen tension changes. The subunit, HIF-1α is known to respond to non hypoxic stimuli including mechanical stress, growth factors, cytokines, and

metal ions (Kietzmann and Gorlach, 2005a). There is evidence that ROS which are summarised in 2.4, are involved in both hypoxic, and non-hypoxic regulation of HIF-1α (Kietzmann and Gorlach, 2005a). Physiologically, an association in the regulation of ROS and HIF-1 is logical, as the formation of ROS requires molecular oxygen, and thus the pathways involved in ROS generation and oxygen homeostasis are inextricably linked.

ROS signalling is involved in several of the pathways, which stimulate non-hypoxic activation of HIF-1α, and as such a role for ROS in non-hypoxic regulation of HIF-1α has been studied. Non-hypoxic stimulators of HIF-1α include thrombin, PDGF (Platelet Derived Growth Factor) and TGF-β (Transforming Growth Factor-β). Several studies have shown that treatment with antioxidants such as ascorbic acid (vitamin C) and vitamin E, inhibit activation of HIF-1α by these non hypoxic stimulators, suggesting a role for ROS in signalling HIF-1α activation (Kietzmann and Gorlach, 2005a). Hydrogen peroxide has been shown to induce HIF-1α activation at low concentrations (0-50μM), but inhibit accumulation of HIF-1α at higher concentrations (Kietzmann and Gorlach, 2005a). This supports a model of a sensitive redox switch in modulation of HIF-1α activity, enabling rapid cellular response to stimuli.

The mechanism by which ROS mediates HIF-1α activity remains elusive, however there is evidence to suggest a role for NADPH oxidases, which are known to generate ROS, mainly superoxides. NADPH oxidases are involved in pathways which link stimulation by thrombin, PDGF, angiotensin II, and mechanical stress to HIF-1α activation. Inhibition of NADPH oxidases have been shown to inhibit activation of the HIF pathway in response to non hypoxic stimuli, and over-expression of a NADPH oxidase subunit resulted in an increase in HIF-1α

levels (Kietzmann and Gorlach, 2005a)(Kietzmann and Gorlach, 2005b) ROS derived from NADPH oxidases may have a significant role in HIF-1 regulation to non hypoxic stimuli.

1.3.4 Hypoxic regulation of HIF-1α by Reactive Oxygen Species (ROS)

ROS have been reported to act as signalling molecules in the upregulation of HIF-1α in response to hypoxia (Kietzmann and Gorlach, 2005a). The mechanism of ROS mediation remains elusive. There is evidence that the heme containing enzymes, such as NADPH oxidases, and the mitochondria are involved in hypoxic signalling via ROS generation (Kietzmann and Gorlach, 2005a). It could be assumed, based on the relationship between ROS and oxygen, that an increase in oxygen levels results in an increase in ROS, and as such, increased levels of ROS would inhibit the HIF pathway. In support of this assumption, H_2O_2 has been shown to reduce the DNA binding capacity of HIF-1 and destabilise HIF-1α, a reduced redox state has been shown to enhance DNA binding and cofactor recruitment, and increased levels of the super oxide ion have been shown to decrease HIF-1α levels (Kietzmann and Gorlach, 2005a). Studies researching mitochondria ROS generation and hypoxia presented evidence to both support and refute this assumption. Numerous studies showed that a decrease in mitochondrial ROS initiated a hypoxic response, substantiating the above assumption (Kietzmann and Gorlach, 2005a). In contradiction, several studies have shown an increase in mitochondrial ROS in hypoxic treated cells, and that inhibition of mitochondrial function did not initiate a hypoxic response. (Kietzmann and Gorlach, 2005a)(Kaluz *et al.*, 2009). It is evident that ROS play a critical role in regulating the HIF pathway however the means of this regulation remains unresolved, at present.

1.3.5 Carbonic Anhydrase 9 (CAIX) as a Marker of Hypoxia

Carbonic Anhydrase IX (CAIX), a transmembrane protein with an extracellular CA domain, is one of 15 human isoforms of CA (Kaluz *et al.*, 2009). The *CAIX* gene is readily inducible but there is no evidence for a basal level of transcription. Six cis-acting elements have shown to function upon the CAIX gene promoter, 5 in a positive, and 1 in a repressive manner. The activation elements have been shown to bind SP1, AP1 and HIF-1α to activate the promoter. The HIF-1α binding site is key to CAIX expression. Mutations to this region, or an absence of HIF-1α, inhibited activation of CAIX expression completely. Binding of factors to the additional sites, were shown to enhance or reduce expression in response to HIF-1α.

HIF-1α is rapidly turned over by the cell, reports have stated a half-life in the order of 30 seconds up to 2 minutes. Detecting HIF-1α protein is therefore problematic, and as the regulation emphasis is at a post-translation rather than transcription level, detection of the protein activity, in oppose to mRNA levels is key in determining HIF-1α activity. The expression of CAIX has been shown to reflect the transcriptional activity of HIF-1α, rather than the level of HIF-1α protein, and subsequently has been presented as a marker for HIF-1α activity. CAIX can therefore be used as marker for hypoxia, however only in the same manner as HIF-1α. It is important to appreciate that CAIX upregulation is also observed following non-hypoxic activation of HIF-1 (Kaluz *et al.*, 2009; Valko *et al.*, 2007)

1.4 Oxidative Stress

1.4.1 Oxidative Stress

Oxidative stress results from an imbalance in the generation and neutralisation of reactive oxygen species (ROS). ROS have crucial physiological roles, however as ROS readily oxidise DNA, lipids and proteins, accumulation of ROS causes extensive cellular and systemic damage. ROS are subsequently associated with numerous human diseases and the process of aging (Droge, 2002; Macdonald *et al.*, 2003).

1.4.2 Generation of Reactive Oxygen Species

ROS are oxygen species, which are more reactive than molecular oxygen, including non-radicals such as hydrogen peroxide, and radicals such as the super oxide anion ($O_2^{\bullet -}$) and the hydroxyl radical ($HO^{\bullet}$). The electron transport chain phase of aerobic respiration is the primary source of ROS; of all oxygen respired, 1-3% is leaked as $O_2^{\bullet -}$ (Valko *et al.*, 2007). ROS are also generated by enzymes, such as NADPH oxidases (see section 1.3.3).

Iron has a role in modulating oxidative stress. For example, under oxidative stress $O_2^{\bullet -}$ can release Fe^{2+} from iron containing molecules. Fe^{2+} is then readily available to react with H_2O_2 resulting in the following reaction:

$$Fe^{2+} + H_2O_2 \rightarrow {}^{\bullet}HO + OH^- + Fe^{3+}.$$

The $HO^{\bullet}$ radical is very reactive, as it has a half life of ~10^{-9}s it reacts close to its formation. This demonstrates the damaging cascade of ROS as although H_2O_2 has relatively low reactivity (see 1.4.5), it has the potential to react further, generating highly reactive oxygen radicals (Valko *et al.*, 2007).

1.4.3 Antioxidants in the Detoxification of ROS,

There are numerous factors involved preventing ROS accumulation and maintaining ROS homeostasis, these are referred to as antioxidants. Antioxidants are both enzymatic and non-enzymatic factors, which neutralise ROS to produce non-reactive oxygen species. For example, catalase is an antioxidant enzyme, which converts hydrogen peroxide to oxygen and water. Other mechanisms of detoxification include vitamins E and C, glutathione (GSH) and superoxide dismutase (SOD) (Macdonald *et al.*, 2003; Scandalios, 2005). Antioxidant enzymes, such as SOD and catalase, are transcriptionally upregulated under conditions of oxidative stress through the binding of the transcription factor NrF-2 (nuclear factor E2-related factor 2) to enhancer regions, ARE (antioxidant response element) and EpRE (Electrophile response element) within their gene promoter sequences (Numazawa and Yoshida, 2004)

1.4.4 Roles and Consequences of Reactive Oxygen Species

At low concentrations ROS have essential physiological roles, of which a few examples are summarised here. The arteries of carotid bodies utilise ROS to regulate ventilation. A reduction in arterial oxygen reduces cellular respiration, thus decreasing the quantity of ROS produced through the electron transport chain. The concentration of ROS acts as a sensor of arterial oxygen pressure, and effects signalling to control ventilation (Droge *et al* 2002). ROS also have an immunological role, as the production of free radicals by macrophages acts as a broad-spectrum antibiotic, destroying numerous pathogens as the first line of defence. In

addition to this ROS activate fibroblasts to synthesise collagen in the process of wound healing (Droge, 2002).

In contrast however, at high levels ROS can also be pathogenic. Examples include; the excessive production of ROS by macrophages causes chronic inflammation and rheumatoid arthritis (Droge, 2002). ROS cause damage to lipids and subsequently membranes. Disruption of the mitochondrial membrane ultimately leads to the release of cytochrome c, and the initiation of apoptotic pathways (Macdonald *et al.,* 2003). The DNA damage resulting from ROS is thought to be involved in the cellular aging process and the formation of cancerous cells (Droge, 2002).

1.5 Project Aims

The overall aim of this project was to characterise the CYGB expression profile in fibrotic lesions, and use IHC markers of hypoxia, proliferation, angiogenesis and fibrotic severity to determine a mechanistic relationship between the fibrotic lesion and CYGB expression. Additionally in vitro models were used to investigate 2 insults associated with fibrosis, oxidative stress and hypoxia, and determine whether CYGB offered cytoprotection in response to these.

2. MATERIALS AND METHODS

2.1 Materials

All materials were of the highest quality available and the majority were supplied by Sigma-Aldrich Company Ltd, Poole, UK. The suppliers of other materials are summarised in appendix.

2.2 Cell Culture

2.2.1 Culturing Cells

Cell culture was carried out under sterile conditions maintained by a class II tissue culture hood (Aura 4, Bio Air, Italy). All reagents were autoclaved and exposed solely to sterile conditions. Human Embryonic Kidney 293 cells (HEK Cells) and Cytoglobin over expressing HEK293 cells (CYGB+ cells) (both cell lines were donated by AstraZeneca) were maintained with DMEM media (Dulbecco's Modified Eagles Medium (1000 mg/L glucose), 10 % (v/v) Fetal bovine serum (FBS), 2 mM L-Glutamine, 100 units/ml penicillin, 100 µg/ml streptomycin).

The cell lines were cultured in 25 cm^2 (T_{25}) and 75 cm^2 (T_{75}) flasks in a humidified chamber (AirAura 4, Bio Air, Italy. 5 % CO_2, 95 % Air.) at 37˚C. Every other day the cells were either reseeded or the media was replaced with fresh media, depending upon the confluency of the cells. Cells were re-seeded or frozen once they reached 70-80 % confluency.

2.2.2 Seeding and freezing cells

The media was aspirated off, and cells washed with phosphate buffered saline **(**PBS, 2.7 mM KCl, 137 mM NaCl, and 10 mM Phosphate Buffer, pH7.4). Trypsin-EDTA (0.25 % Trypsin, 0.02 % EDTA) was added to detach the cells from the flask surface. Following a 10 minute incubation of the cells in a humidified chamber (37˚C, 5 % CO_2, 95 % Air.), DMEM media was added, inhibiting the trypsin. The suspension was centrifuged at 1000 rpm for 3 minutes using a Sanyo MSE falcon 6/300. The supernatant was removed and the pellet resusupended in fresh media, or freezing media (FBS with 10 % (v/v) dimethylsulphoxide (DMSO)).

Cells re-suspended in freezing media were placed into cryovial's (Nalgene, New York) and stored, in a polystyrene box overnight at -80˚C before being moved to liquid nitrogen for long-term storage. Cells re-suspended in fresh media were counted using a haemocytometer (a minimum total count of 100 cells, over 4 or more quadrants), and seeded at an appropriate density into relevant cellware.

2.3 Protein Analysis

2.3.1 Protein Extraction

Cells were cultured in T_{25} flasks, or 6 well plates. The media was aspirated and cells washed with 5 ml of warm PBS. The cells were scraped into RIPA buffer (50 mM Tris pH 7.6, 150 mM NaCl, 1% (v/v) NP-40, 1 mM EDTA, 1% (w/v) Sodium-deoxycholate, 1 mM NaF) and transferred to an eppendorf tube. Cell lysis was achieved by vigorous pipetting with a Gilson P1000, followed by 30 minutes incubation on ice, with vortexing at 10 minute intervals. The cells were then centrifuged at 13, 000rpm, 4˚C for 10 minutes in a bench top centrifuge (Sanyo Hawk MSE 15/05). Following centrifugation the supernatant was aspirated from the

pellet and transferred to an eppendorf. This was used immediately or placed in liquid nitrogen (snap freezing) and stored at -80˚C. The pellet was discarded.

2.3.2 Protein Quantification

2.3.2.1 Bradford Assay

The Bradford assay was used when quantifying proteins at The University of Birmingham. Protein quantification was determined using the protocol described by Bradford (Bradford, 1976). The reagent was prepared by diluting 1:5 in UHQ water and filtered using a syringe and a 0.45µm filter. The absorbance of the samples was measured by a spectrophotometer at wavelength 595nm. A standard curve (1-10 µg/ml Bovine serum albumin (BSA)) was used to estimate the protein concentration within the samples.

2.3.2.2 BCA Protein Assay

The BCA Protein Assay Kit was the standard method for quantifying proteins at AstraZeneca, Loughborough. This was used to quantify protein samples extracted from HEK 293 and CYGB+ following treatment with hypoxia (Chapter 5) and hydrogen peroxide (Chapter 6) prior to western blotting. The principle of the kit is similar to that of the Bradford assay, in that a colour change occurs upon the addition of protein, and a standard curve is created which is used to estimate the concentration of the unknown samples. The kit was used following the manufacturer's instructions.

2.3.3 Concentrating Protein Samples

A centrifugal filter unit (Millipore) was used to concentrate the protein samples, according to the manufacturer's instructions. Protein samples from HEK cells and CYGB+ cells were centifuged at 14,000g and 4^{o}C for 10 minutes.

2.3.4 Western Blotting

Unless otherwise stated, 20 µg of protein was loaded onto either a 12% polyacrylamide gel obtained from BioRad, or 12.5 % polyacrylamide gel made in house (*Stacking gel (4 %)*: 4 % Acrylamide, 125 mM Tris-HCl pH6.8, 0.1 % SDS, 10 µl/10 ml TEMED, 10 % (w/v) APS. *Resolving gel (12.5 %)*: 12.5 % Acrylamide, 375 mM Tris-HCl pH8.8, 0.1 % SDS, 15 µl/10 ml TEMED, 10 % (w/v) APS). At least one molecular weight marker was loaded along-side the samples. The gel was electrophorised in running buffer (25 mM Tris base, 192 mM glycine, 0.1 % SDS), using BioRad power Pac 200, for 90 minutes at 100 volts.

Following electrophoresis the gel was removed and incubated for 15 minutes at 4˚C in transfer buffer (20 mM Tris base, 150 mM glycine, 20 % (v/v) methanol). The stacking gel was removed and covered with a nitrocellulose membrane, which had been pre-soaked in transfer buffer. This was sandwiched between scotch brite pads and 2 layers of filter paper on either side, and placed in the transfer cassette. This was placed, alongside an ice block (for cooling), into an electrophoresis tank, filled with transfer buffer, and electrophorised for 120 minutes at 100 volts. Following transfer the membrane was incubated on a shaker in blocking buffer (0.1 M Tris base, 0.15 M NaCl, 0.05 % (v/v) Tween 20, 5 % (w/v) low fat powdered milk, pH8) either at 4˚C overnight, or at room temperature for 1 hour.

The blocking buffer was removed and the membrane washed with wash buffer (0.1 M Tris base, 0.15 M NaCl, 0.05 % (v/v) Tween 20, pH 8). If samples were being probed with 2 antibodies the molecular weight (MW) marker was used to guide cutting of the membrane in half horizontally, so that each half contained the correct area of the membrane. The membrane was than incubated with the appropriate dilution of primary antibody (details in legend of relevant figure) in blocking buffer, either at 4˚C overnight, or at room temperature for 1 hour, on a shaker.

The membrane was then washed 6 x 5 minutes with wash buffer, prior to a 1-hour incubation with the secondary antibody (unless stated otherwise a goat anti mouse secondary was used (diluted 1:10,000)) diluted in blocking buffer, at room temperature on a shaker. The membrane was washed 6 times over 30 minutes with wash buffer.

The membrane was then incubated with chemiluminescence reagents (following manufacturer's instructions) for 1 minute. In the absence of light, hyperfilm was laid onto the membrane for a maximum of 5 minutes and then developed using an x-o-graph machine.

2.3.5 Fluorescence Microscopy

HEK and CYGB+ cells were seeded at 50,000 cells per well on Lab-Tek II chamber slides (previously coated with 10 % fibronectin) and incubated overnight in a humidified chamber (5 % CO_2, 95 % Air) at 37˚C.

The cells were fixed in 10 % formalin for 15 minutes at room temperature, followed by 3 washes with PBS. The permeability of half the wells of each cell line was increased by the

addition of 0.1 % triton-x-100/PBS followed by 3 washes with PBS. The cells were then blocked with 3 % BSA/PBS for an hour. The BSA was aspirated and the cells were incubated with either an anti-cytoglobin (monoclonal, at 0.125, 0.17, 0.25, 0.5, 1, 2 or 10 µg/ml) or anti-α-tubulin (5 µg/ml) antibody diluted in 3 % BSA/PBS for 90 minutes. An anti-α-tubulin antibody was used as a positive control. Two controls of background staining were used, Mouse IgG1 was used as an isotype control (10 µg/ml) to measure non specific antibody staining and the primary antibody was replaced with buffer to determine levels of non specific binding of the secondary antibody and endogenous fluorescence.

The cells were washed 3 times with PBS and a rabbit anti mouse Alexa-488-labelled secondary antibody (diluted 1:300) was added for 40 minutes. Following this the cells were washed three times with PBS. The chamber was removed and vectashield mounting medium containing propidium iodide and a coverslip added. These could then be kept in the dark at 4˚C for several weeks and analysed using a confocal microscope (AxioPlan 2 Imaging, Zeiss,).

Fluorescence microscopy (AxioPlan 2 Imaging, Zeiss,) was used to visualise the cells, and photos were taken digitally (AxioVision 3.1).

2.4 Histology

Human tissue was fixed for 48 hours in 10 % buffered formalin processed through alcohols and embedded in paraffin. Four micron sections were cut by the histology team at AstraZeneca, Loughborough, on a microtome and dried overnight at 37^{o}C. Sections were

dewaxed in xylene, ethanol, and industrial methylated spirit and placed in water prior to staining.

2.4.1 Haematoxylin and Eosin Staining

The histology team at AstraZeneca (Charnwood) stained the sections with Gills II Haematoxylin (Pioneer Research Chemicals Ltd, Colchester, Essex, UK), and Eosin Y (Acros Organics, Fisher Scientific, Loughborough, Leicestershire, UK) on a Leica ST5020 Autostainer (Leica Microsystems, Milton Keynes, Buckinghamshire, UK) using standard procedures (Bancroft and Stevens 1990).

2.4.2 Immunohistochemistry (IHC)

The antibodies used to determine cell types immunohistochemically, and the appropriate protocols are summarised in Table 3.1 The cell types the antibodies were used to identify are summarised in section 3.3.

Standard Procedure

Antigen retrieval of the sections, where required was achieved by using either trypsin digestion or heat treatment through microwaving or pressure cooking. (Table 3.1). Trypsin digestion involved the incubation of the slides with 0.1 % trypsin, 0.1 % calcium chloride pH7.8 at 37°C for 30 minutes. Microwaving involved submergence of the slides in the appropriate retrieval solution (Table 3.1) and microwaving at 98°C, 1 minute using a RHS-2 rapid microwave histoprocessor (Milestone Srl, Sorisole, Italy). Pressure cooking involved incubation of the slides in the appropriate retrieval solution (Table 3.1), and cooking at 15 lb pressure for 2 minutes. The subsequent steps were carried out by hand or using a LabVision

Autostainer, depending on the slide number, and availability of equipment. The specific concentrations and reagents used for each antibody are summarised in Table 3.1.

The slides were washed for 3x2 minutes with wash buffer (PBS, 0.05 % Tween, pH7.4), before incubating for 10 minutes with H_2O_2, (diluted in methanol, see Table 3.1 for concentration) to quench endogenous peroxides. The slides were washed in wash buffer for 3x2 minutes. Slides were then blocked with 20 % (v/v) protein block, to reduce non specific binding of the secondary antibody, (see Table 3.1) for 20 minutes prior to incubation with the appropriate primary antibody (see Table 3.1, diluted in 0.1 %BSA in PBS with 0.05 % Tween, except the anti-cytoglobin antibody (which was diluted in normal horse serum see Table 3.2) for 60 minutes at room temperature (or overnight at 4^{o}C). Appropriate isotope controls (see Table 3.1), applied at the same concentration as the primary antibody of interest were used to differentiate between true signal and background. The sections were then incubated with the appropriate secondary antibody (see Table 3.1), diluted in 0.1 %BSA in PBS with 0.05 % Tween, for 20 minutes at room temperature. Amplification of the signal was achieved by incubating with an amplification kit (see Table 3.1 for when each of the kits was used) after washing with wash buffer for 3x2 minutes. The amplification kits used were StreptABComplex/HRP kit (ABC), Tyramide Signal Amplification^{TM} kit (TSA), and EnVision$^{®}$ FLEX (see below for details). All the kits were used following manufacturers instructions. When the EnVision$^{®}$ kit was used the wash buffer supplied in the kit was used for the IHC protocol instead of the PBS with 0.05 % Tween, the incubation time with the primary antibody was reduced to 30 minutes and the block and secondary antibody steps were eliminated from the protocol.

3,3'-diaminobenzidine (DAB) was used as the chromagen, the incubation time with DAB varied depending upon the primary antibody being used. A positive control was used to determine the DAB time every time the antibody was used, which was replicated for all other sections. The sections were counterstained with haematoxylin and dehydrated by grading through the alcohols to xylene, before mounting in mounting medium (Merck, Lutterworth, Leicestershire, UK).

Principles of the StreptABComplex/HRP kit (ABC)

The ABC kit is used after incubation with a biotinylated secondary antibody. A Streptavidin/Horseradish Peroxidase (HRP) conjugate from the ABC kit binds to the secondary antibody through avidin-biotin binding (See figure 2.1). The HRP then oxidises DAB producing a brown colour.

Principles of the Tyramide Signal Amplification^{TM} kit (TSA)

The TSA kit works on similar principles to the ABC kit, but there is an additional step. The TSA kit is used after incubation with a biotinylated secondary antibody. A Streptavidin/Horseradish Peroxidase (HRP) conjugate from the TSA kit binds to the secondary antibody through avidin-biotin binding (See Figure 2.2). An additional reagent is then added, which is oxidised by the HRP and biotin labelled tyramide is produced. The biotin labelled tyramide deposits around the site of the antigen. The Steptavidin/HRP conjugate is then added again, and binds through avidin-biotin binding, to the deposited biotin, thus increasing the number of HRP molecules available in the region The HRP then oxidises DAB producing a brown colour.

Figure 2.1 Principles of the ABC and EnVision®FLEX IHC Amplification Kits

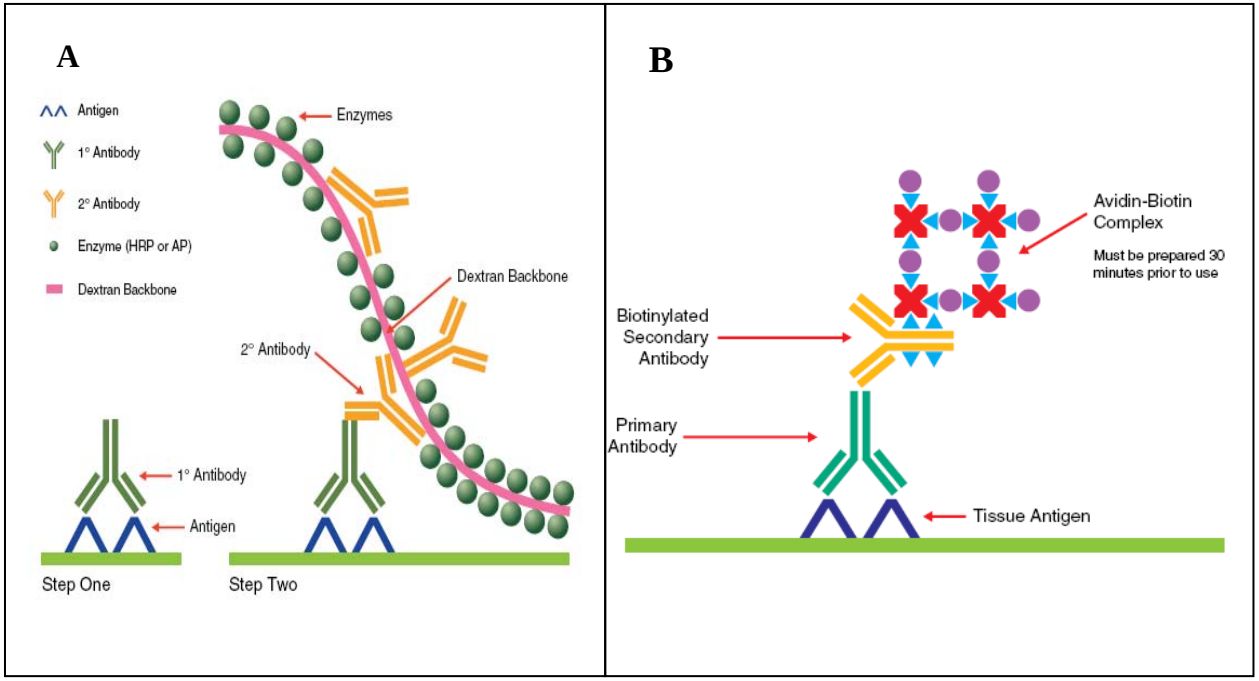

A diagrammatic representation of the principles behind the A) EnVision®FLEX IHC amplification kits *(Dako EnVision®FLEX kit Brochure)* **and B) StreptABComplex/HRP** (*Dako StreptABComplex/HRP kit brochure*).

Figure 2.2 Principles of the Tyramide Signal Amplification kit (TSA) Kit

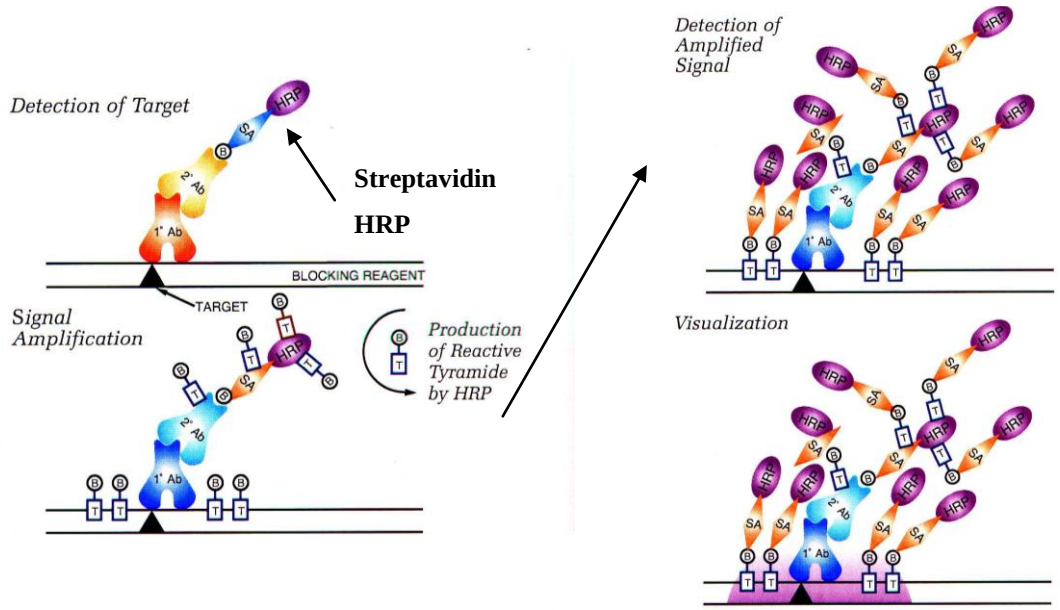

A diagrammatic representation of the Tyramide Signal Amplification kit (TSA) (*PerkinElmer® TSA Signal Amplification brochure)* used for immunohistochemistry.

Principles of the EnVision®FLEX kit

The main element of the EnVision® FLEX kit is EnVision®FLEX Peroxidase. This is a polymer with a dextran backbone, to which secondary antibody molecules and HRP are bound (See Figure 2.1). This is added to the slides for 30 minutes at room temperature after incubation with the primary antibody, which must have been raised in either rabbit or mouse. The EnVision®FLEX Peroxidase binds to the primary antibody through the secondary antibody molecules. The HRP on the polymer then reacts with DAB to give a signal. This kit doesn't involve biotin: avidin interactions eliminating any background of a biotin origin.

The signal from the EnVision®FLEX kit can be amplified using EnVision®FLEX+, where a linker is added after incubation with the polymer. The linker increases the amount of HRP available for DAB to interact with, increasing the signal.

2.5 The MTT Assay

The 3-[4,5-dimthylthiazol-2-yl]-2,5-diphenyl Tetrazolium Bromide (MTT) assay is commonly used within the literature to measure cell viability, and was originally described by Mosmann (Mosmann, 1983). The MTT assay is a colorimetric assay. Water soluble yellow MTT readily diffuses across membranes, once within the cell, mitochondrial reductase enzymes react with MTT to produce formazan, a purple precipitate. The formazan is solubilised by adding DMSO, and the absorbance measured at 570 nm. The presence of formazan is thus representative of mitochondrial function, and cell viability.

CYGB+ and HEK293 cells were seeded onto collagen coated 96 well plates, and grown to confluence before incubation with treatments. There were at least 3 sample replicates within each experiment. Following treatment MTT was added to a final concentration of 0.5 mg/ml

and incubated for 4 hours at 37˚C. DMSO was added directly to the media to a final concentration of 50 % (v/v), and incubated for 24 hours at room temperature. The absorbance of each sample was measured using a spectrophotometer at 570nm, comparing each sample to a blank (equal quantities DMSO and DMEM). The experiment was repeated 3 times, and the mean relative absorbance used for analysis.

2.6 RNA Extraction and Quantification

2.6.1 RNA Extraction

RNA extraction was carried out using one of 3 kits, the RNAqueaous-4 PCR kit (Ambion), RNeasy 96 (Qiagen) or the RNeasy mini kit (Qiagen) following manufacturer's instructions. The kits all work similar principles. Cells were lysed in lysis buffer, and then frozen (in lysis buffer) for future RNA extraction or processed immediately. The samples were centrifuged onto a filter, which was washed repeatedly before the sample was eluted into RNase free water or elution buffer. The RNA samples were stored at -80^{o}C.

2.6.2 DNase Treatment of RNA Samples

Where DNase treatment was necessary RNA was incubated with DNase I in DNase buffer (0.2U/µl) in a ratio of 1:1 for 45 minutes at 37^{o}C. DNase Inactivation Reagent was added to each sample to a final concentration of 5% (v/v), the sample was mixed and incubated at room temperature for 1 minute. The sample was then centrifuged at 1000rpm for 10 minutes to pellet the DNase Inactivation Reagent.

2.6.3 RNA Quantification

The RNA samples were quantified using one of the 2 following systems, Agilent RNA 6000 Nano kit or Ribogreen® RNA Quantification kit (molecular probes), following manufacturer's instructions.

2.6.3.1 Agilent

The Agilent RNA 6000 Nano kit is Lab-on-a-chip technology. RNA samples are loaded onto the chip alongside a molecular ladder and read by the 2100 Bioanalyzer. The amount and integrity of RNA is determined.

2.6.3.2 RiboGreen

The RiboGreen® RNA Quantification kit uses fluorescence to measure the RNA concentration within a sample. A RNA standard was used to create both standard curves recommended in the kit. The curve covering most closely the range of the sample values was used in interpretation of the data. The standard curve and samples were incubated with RiboGreen reagent, which reacts with RNA to produce fluorescence, measured at 485nm excitation, 585nm emission using a Wallac EnVision™ (Perkin Elmer).

CHAPTER 3: THE CYTOGLOBIN EXPRESSION PROFILE OBSERVED IN COPD AND IPF TISSUE.

3.1 Introduction

The expression of CYGB has been shown to be induced in response to fibrotic stimuli in *vivo* and in *vitro* (see general introduction for further details) (Nakatani *et al.*, 2004; Xu *et al.*, 2006). It has been observed that cytoglobin expression is induced during fibrosis of the lung, liver, pancreas and kidney (Nakatani *et al.*, 2004). In *vitro* over expression of CYGB has been shown to offer protection against oxidative stress induced fibrogenesis (Xu *et al.*, 2006), and over expression of CYGB in *vivo* increased recovery prospects of fibrosing tissue (Xu *et al.*, 2006). Contradictory, over expression of CYGB has also been shown to increase collagen I mRNA expression in *vitro* (Nakatani *et al.*, 2004).

Cytoglobin expression has been observed within fibroblasts in a variety of tissues in man, rats and mice. The fibroblast is a key player in fibrogenesis, and a substantial increase in cell number is observed. The literature presents evidence of 3 origins of fibroblasts during fibrosis: Proliferation of resident fibroblasts; Epithelial mesenchymal transition; and migration of circulating mesenchymal precursors. Potentially the cytoglobin expression profile of fibroblasts could relate to their origin.

The profile of CYGB expression within and around the fibrotic lesion remains elusive, as does the characterisation of the cell types which present with cytoglobin expression in fibrotic tissue, and the changes with fibrotic disease progression, all of which would aid in determining the role of CYGB in the fibrosis.

3.2 Aim

The aim of this study was to characterise the cell types which express CYGB in normal and fibrosed human lung, determine the changes in cell type distribution with fibrotic disease progression and the subsequent changes in the CYGB expression profile. Lung resections taken from COPD and IPF patient were used as models of fibrosis.

The specific objectives were:

- To identify the cell types within IPF, COPD and non fibrosed control tissue which presented with CYGB immunoreactivity.
- To ascertain the changes in the cell type distribution with fibrosis, and determine any correlation with CYGB expression.
- Determine if the CYGB expression is related to the origin of fibroblasts.

3.3 Methods

3.3.1 Immunohistochemistry

3.3.1.1 Panel Selection

The COPD sections used in this study were from Lung Volume Reduction Surgery (LVRS) of COPD GOLD Class IV patients and were ethically acquired (see appendix for an example ethical form completed by each patient). Tissue sections of 4μm were stained with Haematoxylin and Eosin (H&E) in order to determine the morphology of the sections. The pathology of the sections was interpreted and the sections were grouped, according to the predominant phenotype, into the following classifications: sclerosis, fibrosis, consolidated fibroplasia, diffuse fibroplasia and pneumonitis, with the intention of selecting a minimum of 5 sections to represent each category. Sections with processing related tissue damage, or surgical bleeding were eliminated. A panel of 22 sections from 14 patients was selected, representing 1 sclerotic section, 6 fibrosis and 5 of each of the remaining categories. In addition to the COPD panel, 9 sections taken from patients with IPF were used as a positive control for fibrosis. Sections taken from the periphery of lung tumour tissue were used as fibrosis-negative control tissue. From the selection of the control sections available, 5 were suitable for use as negative controls, as the others presented with fibrosis.

3.3.1.2 Method Development

The IHC protocol is summarised in chapter 2. In order to obtain optimal staining, each stage of the protocol was adapted specifically for each antibody. All of the antibodies, with the exception of those raised against Cytoglobin, had been previously optimised by the histology team at AstraZeneca, Charnwood (See below for details of optimisation). The optimised

method was tested and developed further, if required. The final protocols used for each stain are summarised in Table 3.1

Optimisation of the IHC Protocol

The initial approach in optimising the IHC method was to determine the necessity of antigen retrieval, and most efficient method. The antigen retrieval methods investigated included treatment with either trypsin, or heat. Heat treatments were performed in Antigen Unmasking Fluid (Vector Labs: H-3300), using a microwave (98ºC 1 min) or pressure cooker (15lb, 2 minutes).

The initial protocol optimisation experiment used the following protocol. The sections were de-waxed using xylene, ethanol and industrial methylated spirit and placed in water prior to antigen retrieval. Endogenous peroxides were quenched with 0.5% hydrogen peroxide, before incubating with the appropriate primary antibody, for 1 hour at room temperature. The concentration of the primary antibody used was ascertained using manufacturer's instructions and, or previously optimised methods. The sections were then incubated with an appropriate secondary antibody, followed by the reagents of the TSA kit. DAB was applied to the sections for a maximum of 20 minutes or until a signal was observed. Appropriate isotope controls, applied at the same concentration as the primary antibody, were used to differentiate between true signal and background (see Table 3.1).

Should staining prove unsuccessful, further antigen retrieval methods were investigated, including incubating the slides in Boric Acid (0.2M) at 60^{o}C overnight, and using an EDTA based buffer, (pH 9) with heat treatment.

Table 3.1 Immunohistochemistry Protocol Details for each Antibody

Antigen Recognised	[Primary Antibody] (µg/ml)	Antigen Retrieval Method	[H_2O_2] (%)	Protein Block (20%)	Negative Control	Secondary Antibody	[Secondary Antibody] (µg/ml)	Signal Amplification System
αSMA	0.7	None	0.5	NGS	Mouse IgG2a kappa	BioGaM	4.5	TSA
CD3	4	PC AUF	0.5	NSS	Rabbit Ig	BioSaR	1.8	ABC
CD31 (PECAM-1)	3.75	None	3	NGS	Mouse IgG1	BioGaM	4.5	TSA
CD34 Class II	1.6	MW-AUF	6	NGS	Mouse IgG1	BioGaM	4.5	ABC
C-Kit	150	PC-AUF	3	NGS	Rabbit Ig	BioGaR	0.5	ABC
Collagen I	5.5	PC-AUF	0.5	NGS	Mouse IgG1	BioGaM	4.5	ABC
Cytoglobin	5	MW-AUF	3	NHS	Mouse IgG1	BioHaM	5	TSA
Cytokeratin	1.7	MW - EDTA	0.5	NGS	Mouse IgG1	BioGaM	4.5	ABC
Desmin	2.3	None	0.5	NGS	Mouse IgG1	BioGaM	4.5	ABC
MAC 387	3.3	MW-AUF	0.5	-	Mouse IgG1	-	-	EnVision
PCNA	0.45	PC-AUF	3	NGS	Mouse IgG2a	BioGaM	4.5	ABC
Surfactant	5	MW-AUF	0.5	NHS	Mouse IgG2b	BioHaM	5	ABC
Vimentin	3.6	MW-AUF	0.5	NGS	Mouse IgG1	BioGaM	4.5	ABC
Wheat Germ Agglutinin	5	None	0.5	NHS	Acetylglucosasmine Sugar	-	-	ABC

A table to summarise the details of immunohistochemical protocols used for specific antibodies. KEY AUF: Antigen Unmasking Fluid (Vector Labs). H: High pH Retrieval Solution (Dako). EDTA: 1mM EDTA based buffer pH9 MW: Microwave. PC: Pressure cook. NGS: Normal Goat Serum. NHS: Normal Horse Serum. BioGaM: Biotinylated Goat anti Mouse. BioGaR: Biotinylated Goat anti Rabbit. BioSaR: Biotinylated Swine anti Rabbit. BioHaM: Biotinylated Horse anti Mouse. TSA: Tryamide Signal Amplification Kit. ABC: Streptavidin AB/HRP kit. αSMA: α smooth muscle actin, PCNA: proliferating cell nucleur antigen

Once a retrieval method had been established, further optimisation, if required was used to enhance the signal and reduce background staining. Different amplification kits were investigated, such as ABC, EnVision FLEX® and EnVision FLEX+® (See chapter 2 for more details). The concentration of the antibody was increased or decreased, and overnight (4ºC) incubation was investigated. The concentration of hydrogen peroxide was increased to 3% or 6%. Secondary antibodies raised in horse were investigated, as was diluting the antibodies in serum rather than diluent.

3.3.1.3 Dual Staining

Dual staining of S100A4 and CD3 was used to as a marker of fibroblasts. The sections were de-waxed using xylene, ethanol and industrial methylated spirit and placed in water prior to staining. The sections were pressure cooked in Antigen Unmasking Fluid for 2mins at 15lb pressure for antigen retrieval. Endogenous peroxides were quenched with 3% hydrogen peroxide for 10minutes at room temperature. Sections were blocked with normal swine serum (20%) before incubation with a rabbit anti human anti-CD3 primary antibody (8µg/ml) for 1 hour at room temperature. The isotype control used was rabbit Ig (Dako). A biotinylated swine anti rabbit (5µg/ml) secondary antibody was then added to the sections followed by the reagents of the ABC kit. Staining used a nickel DAB chromogen. The sections were stored in water during the staining process. A rabbit anti human S100A4 primary antibody (0.9µg/ml) was then added for 1 hour at room temperature, followed by the EnVision kit. The isotype control was Rabbit Ig (Serotec). The sections were stained using a red chromogen (NovaRED), before dehydration by grading through the alcohols to xylene, and mounting in DPX mounting medium (Merck, Lutterworth, Leicestershire, UK)

3.3.1.4 Sirius Red Staining

The slides were dewaxed using xylene, ethanol and industrial methylated spirit and placed in water prior to staining with Gills Haematoxylin for 10 minutes. The sections were then washed in running tap water, before incubating with picro-sirius red (0.1% (w/v) sirius red in saturated aqueous solution of picric acid) for 1 hour. The slides were washed twice in acidified water (31.25% (v/v) glacial acetic acid) before dehydration in ethanol and xylene, and mounting in DPX mounting medium (Merck, Lutterworth, Leicestershire, UK).

3.3.1.5 Microscopy and Photography

The slides were analysed using an Axioskop 2 plus microscope (Zeiss) with a polarised lens. Pictures were taken using a Kodak Imaging programme.

3.3.1.6 Determining Cytoglobin Positive Cell Types

The panel was stained with an array of cell specific markers which are summarised in the table 3.2. Serial sections were stained to enable comparison between one slide and the next. Every 5^{th} section was stained for CYGB. Where more than one marker was needed to identify a specific cell type, unless stated otherwise, parallel sections were stained with appropriate markers and the relative staining of cell populations was compared to identify if a cell population was staining with one of the markers or both. The same approach was used to identify CYGB positive cell populations: The positive staining cell population observed on one slide (representing a specific cell type) was compared to that which stained with CYGB on another slide to identify Cygb+ cell populations. Each section selected in the panel was examined for the presence of each of the cell types summarised below. The cell types which were observed to be Cygb+ on each section were noted. Using serial sections has limitations,

Table 3.2 Summary of Cell Specific Markers

Cell Type	Markers used	
	Positive	**Negative**
Fibroblast	Vimentin S100A4	CD34 α Smooth Muscle Actin CD3
Haematopoietic Fibroblast	Vimentin S100A4 CD34	α Smooth Muscle Actin CD3
Myofibroblast	Vimentin S100A4 α Smooth Muscle Actin	CD34 CD3
Haematopoietic Myofibroblast	Vimentin S100A4 CD34 α Smooth Muscle Actin	CD3
Smooth Muscle	α Smooth Muscle Actin Desmin	
Haematopoietic Stem Cell	c-kit CD34	Vimentin
T cells	CD3	
Endothelium	CD31	
Type II Pneumocytes	Surfactant A	Cytokeratin
Differentiating Type II Pneumocytes	Surfactant A Cytokeratin	
Type I pneumocytes	Lectin	
Macrophages	MAC387	

A table to summarise the markers used to identify specific cell types using immunohistochemistry. Positive refers to the cell type showing expression of the marker, negative refers to the absence of the marker

Of particular note one cannot be definite about co-localisation of a stain within a particular cell as though present on one slide a cell may be absent from the next. Notably therefore populations of cells were compared between serial sections rather than individual cells.

3.3.1.6.1 Identifying Fibroblasts

Several markers were used to identify fibroblasts, and the sub populations of fibroblasts. Vimentin, a mesenchymal marker reacts with fibroblasts cells. S100A4 reacts with fibroblasts and CD3+ lymphocytes. Dual staining for S100A4 and CD3 was used to identify fibroblasts, however there was some steric hindrance in the dual staining, and as such CD3 did not stain all the CD3+ cells in the sections. Parallel staining for vimentin was also used to verify that cell populations were of a mesenchymal origin, and therefore fibroblasts.

Myofibroblasts were identified from the fibroblasts population using an antibody against αSMA. The fibroblasts were categorised further, by examining cross reactivity with CD34, a marker of former haematopoietic origin.

The 4 categories:

Haematopoietic Fibroblasts	Vimentin+ S100A4+ CD3- CD34+ αSMA-
Fibroblasts	Vimentin+ S100A4+ CD3- CD34- αSMA-
Haematopoietic Myofibroblasts	Vimentin+ S100A4+ CD3- CD34+ αSMA+
Myofibroblasts	Vimentin+ S100A4+ CD3- CD34- αSMA+

Of note, where the S100A4+, Vimentin+, CD3- population was more abundant than the staining for both αSMA and CD34, and there was a presence of both αSMA and CD34 markers, it was assumed CD34+ and CD34-, myofibroblasts and fibroblasts were present (the relative amounts of CD34 and αSMA staining were used to determine the assumed ratio of

fibroblast phenotypes). Without dual staining it was not possible to ascertain if the CD34+ population belonged solely to the αSMA+ or – population, or vice versa.

3.3.1.6.2 Identifying Smooth Muscle Blocks

It is widely known that actins are proteins which contribute to the microfilament structure of the cytoskeleton, and have a role in cellular contraction. There are several different isoforms of actin, of which α-smooth muscle actin (α-SMA) is found in smooth muscle cells. This was therefore used as a marker of smooth muscle cells, however other cells type are also positive for this marker, including myofibroblasts and myoepithelial cells.

Desmin is another component of the cytoskeleton, and is specific to muscle cells. Staining for desmin and α-SMA (on parallel sections) was used to differentiate smooth muscle cells from myofibroblast and myoepithelial populations.

3.3.1.6.3 Identifying Stem Cells of a Hematopoietic Origin

Immunoreactivity with CD34 and c-kit (CD117) was used to identify stem cells of a hematopoietic origin.

3.3.1.6.4 Identifying microvasculature

CD31 was used to identify the microvasculature. The CD34 phenotype of the microvasculature was also noted.

3.3.1.6.5 Identifying pneumocytes

Type II pneumocytes were identified using surfactant A. In addition pan cytokeratin was used to identify the subpopulation of type II pneumocytes which were differentiating into type I pneumocytes. Wheat Germ Agglutinin (WGA) was used to identify type I pneumocytes

3.3.1.6.6 Identifying inflammatory cells

CD3 was used to identify T-lymphocytes and MAC387 was used as a marker of macrophages. Of note CD3 is present on the majority of T-lymphocytes but can be lost with maturity.

3.3.1.7 Characterising the Cytoglobin Expression Profile of Fibrotic Lesions

Each of the COPD, IPF and normal sections were examined and a fibrotic lesion, or a region of parenchyma, was selected for analysis on each section. There were 3 criteria which had to be met for the region to be selected for analysis, the first was that it was one of the most fibrosed regions on the section, the second, that the pathology of the region was constant throughout all of the slides being used in analysis, and finally that the region could confidently be navigated to on subsequent sections, ensuring comparison of equivalent areas. There were 20 lesions interpreted from COPD tissue, 9 from IPF tissue and 5 from controls.

3.3.1.7.1 Applying a Fibrosis Score to each Lesion

Each selected region was first given an overall grade for fibrosis. A fibrotic score was applied using the scoring system described by (Ashcroft *et al.*, 1988). Additionally a Sirius red grading system was applied. Sirius red stains small and large collagen fibres green and orange respectively, the relative amount of green to orange staining was used for scoring. Collagen I,

which increases with fibrosis, forms classic large collagen fibres, and thus can be typically identified by yellow orange staining. Collagen III, which decreases with fibrosis, typically forms small reticular fibres which stain green with Sirius red. Of note the size and arrangement of the fibre determines the colour observed rather than any other characteristic, as the colour generated is due to bifurcation of light via a polarised lens (Montes and Junqueira, 1991). Collagen II for example can show weak staining of either colour.

Grade 1: 25% > Orange
Grade 2: 45% > Orange >26%
Grade 3: 54% > Orange >46%
Grade 4: 74% > Orange >55%
Grade 5: 75% < Orange

The fibrosis scores of the lesion were compared to the scores representing the density of specific cell types and the CYGB expression profile observed (see 3.3.1.7.2 for details) to determine if there was a relationship between the extent of fibrosis and the cell type and CYGB characteristics of the lesion.

3.3.1.7.2 Characterising the Cell type Distribution and Associated Cytoglobin Profile of the Fibrotic Lesion

Where fibrotic lesions were selected for analysis, the lesion was segregated into zones, the 'Acellular Zone', 'Fibrotic border' and 'Edge' (See figure 3.1), and each region was interpreted independently. For every zone of every lesion the following interpretation was done.

1. To determine the cytoglobin expression across the lesion a cytoglobin expression profile was assigned to each region. This took into account the expression of CYGB in cells which had previously shown CYGB expression in the panel, as such negative

staining observed in smooth muscle cells, red blood cells, tumour cells and nerve cells did not contribute to the classification. If all cells (other than smooth muscle, red blood cells, nerves and tumour cells) in the region were positive it was assigned a Cygb+ profile, if all were negative a Cygb- profile. If there was a mix of Cygb+ and Cygb- cells it was classified as showing a mixed profile.

2. Cell type markers were used to determine the presence or absence of the cell types summarised previously (see table 3.2 for details about identifying specific cell types).
3. Each cell type graded to represent the relative density of the cell type, 0: No staining. 1: sparse 2: midway and 3: abundant
4. For each cell type observed within each zone of the fibrotic lesion the CYGB expression profile was determined.

   Negative: There was no evidence of CYGB staining in the cell population

   Mixed: There was evidence of CYGB staining in the cell population, but not the entire cell population

   Positive: The cell population was all CYGB positive

For example, CD3 was used to identify lymphocytes in a lesion. The AZ and edge were negative for CD3 but the fibrosing border demonstrated sparse CD3 immunoreactivity. The density of the CD3 cell population was noted to be grade 1 in the fibrosing border and grade 0 in the AZ and edge. The CD3 population in this region showed both positive and negative immunoreactivity for CYGB so was assigned a mixed CYGB profile.

Figure 3.1 Zones of the Fibrotic Lesion

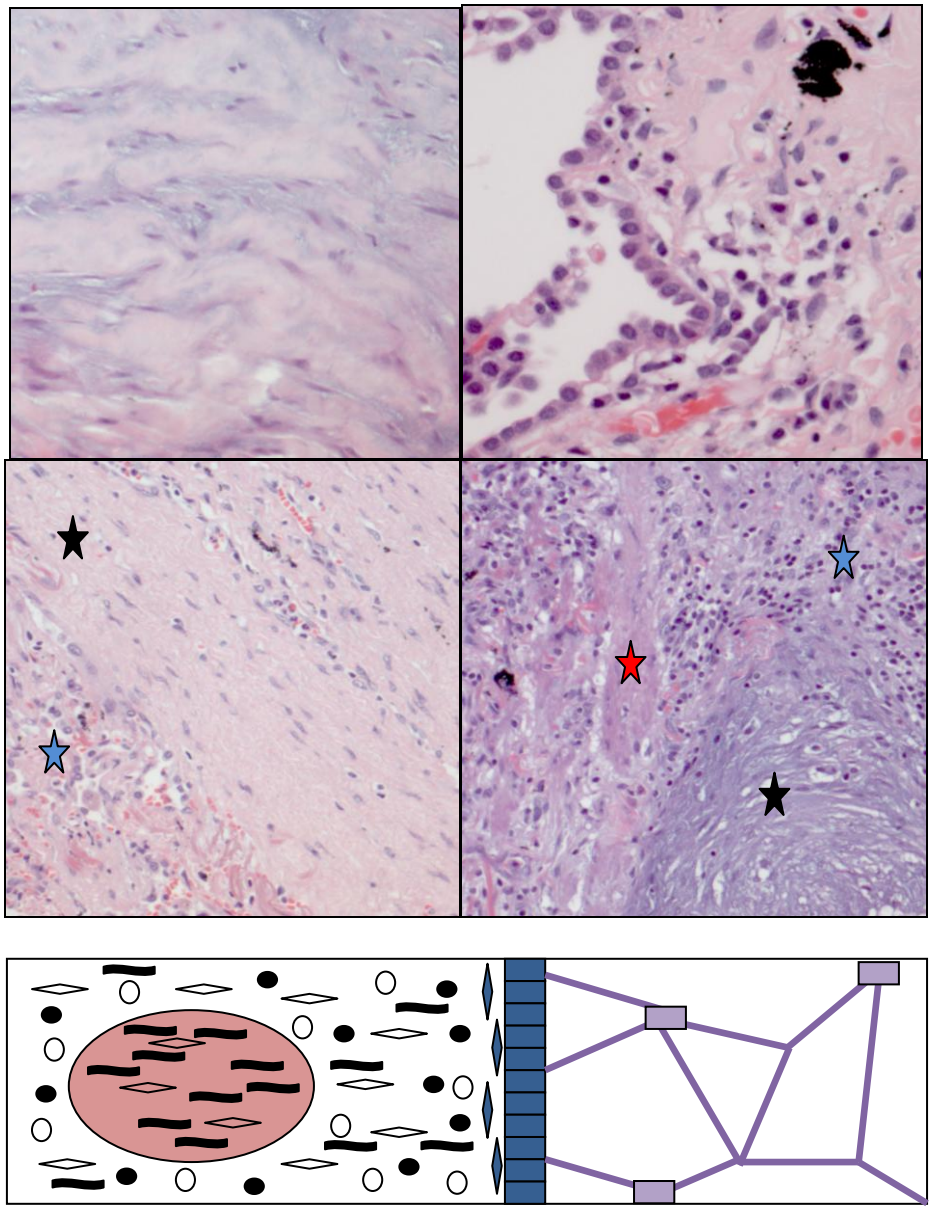

Pictures of H&E staining to show different regions observed in a fibrotic lesion, and a diagrammatic representation. Top left picture: an acellular zone observed in COPD (x20). Top right picture: An edge lesion observed in COPD (X20). Bottom left picture: An acellular zone and fibrotic border observed in COPD (x10). Bottom right picture: an acellular zone and fibrotic border observed in IPF (x10). Black stars highlight acellular regions, blue stars highlight the fibrosing border and red stars highlight ectopic smooth muscle bundles observed in IPF. The key cell types are presented in the diagrammatic representation of a fibrotic lesion Purple region: normal parenchyma. Blue region: Edge. Red region: Acellular zone. Fibroblasts Endothelial cells Inflammatory cells Type II pneumocytes collagen and elastins Alveolar wall

3.3.1.8 Analysing the cell density data

The data was collated, and each disease state and lesion zone were analysed independently, forming 7 categories: COPD AZ, COPD Fibrosing border, COPD edge, IPF AZ, IPF fibrosing border, IPF edge and control tissue. For each category the number of lesions which presented with each cell type was calculated. For example, the frequency of lesions in which CD3 staining was observed in each category:

	Frequency
COPD AZ	0
COPD Fibrosing border	14
COPD edge	3
IPF AZ	0
IPF fibrosing border	9
IPF edge	1
Control tissue	4

The number of lesions which presented with each cell type at each density was then calculated for each category. For example the frequency with which CD3 was observed at each density level:

Density Score:	**0**	**1**	**2**	**3**
COPD AZ	18	-	-	-
COPD Fibrosing border	6	6	2	6
COPD edge	16	3	-	-
IPF AZ	9	-	-	-
IPF fibrosing border	-	1	2	6
IPF edge	8	1	-	-
Control tissue	1	4	-	-

This data was presented graphically, where the total size of the bar of the graph represented the number of lesions which present with each cell type, and the formats within the bar represented the frequency of each of the density scores for the relevant cell type.

Graphical representation of each category enabled comparative analysis of cell type densities between both disease and fibrotic area.

3.3.1.9 Analysing the Cytoglobin Expression Data

CYGB staining data was collected and analysed in the same manner as the cell density data. Each region of the lesion was interpreted individually, and a CYGB profile grade was applied to each cell type present. For each cell type, the number of lesions which presented with each CYGB grade was calculated. This data was presented graphically, where the total size of the bar of the graph represented the number of lesions which present with each cell type, and the formats within the bar represented the frequency of each of the CYGB scores for the relevant cell type.

3.4 Results

3.4.1 Cytoglobin Expression in a Range of Cell Types Within the Human Lung

The CYGB expression profile of human lung cells was identified immunohistochemically in formalin fixed paraffin embedded tissue sections, ethically acquired from patients with COPD (COPD GOLD Class IV) and IPF. Sections from peripheral tumour tissue were used as non fibrosed controls. Cell type markers, summarised in the table 3.2, were used to determine the specific cell types. In order to determine the CYGB staining profile for each cell type, serial sections were stained using anti-CYGB and the relevant cell specific antibody and the positive cell populations were compared.

Parenchymal cells which stained positively for cytoglobin in IPF, COPD and control tissue included fibroblasts, myofibroblasts (see figure 3.2), lymphocytes, macrophages (see figure 3.3) endothelial cells (see figure 3.4), type I pneumocytes and type II pneumocytes (see figure 3.5). Bronchiolar epithelium and peri-bronchiolar chondrocytes stained positively for cytoglobin in IPF, COPD and control tissue (see figure 3.6). Peri-bronchiolar smooth muscle was consistently negative (see figure 3.6). Within the vasculature, endothelial cells showed immunoreactivity for cytoglobin, as did vimentin positive cells within the intima and media, and fibroblasts and myofibroblasts within the adventisia (see figure 3.4). Red blood cells were consistently negative. Of note, tumour and nerve cells had a cytoglobin negative profile whilst glial cells stained positively for cytoglobin (see figure 3.7), however the frequency of these observations was too small (n=1) to draw solid conclusions.

Figure 3.2 Cytoglobin Staining in Fibroblasts

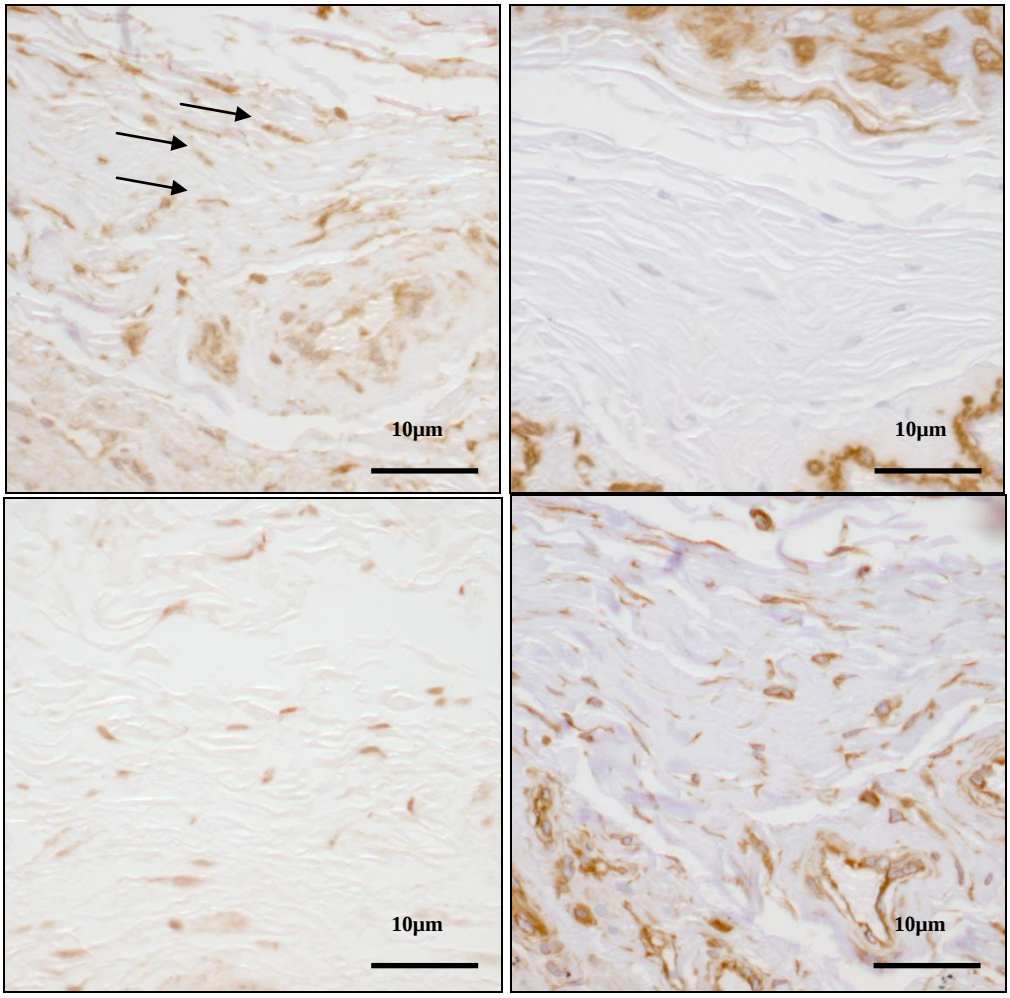

Photographs to show cytoglobin staining (top left, highlighted by arrows) in αSMA (top right) negative fibroblasts in connective tissue of an IPF section. Vimentin (bottom right) and S100A4 (bottom left) were used as markers of fibroblasts. All pictures are x20. It is evident that the Vimentin and S100A4 positive cell populations are also CYGB positive. Pictures are 40% of original size.

Figure 3.3 Cytoglobin Staining in Inflammatory cells

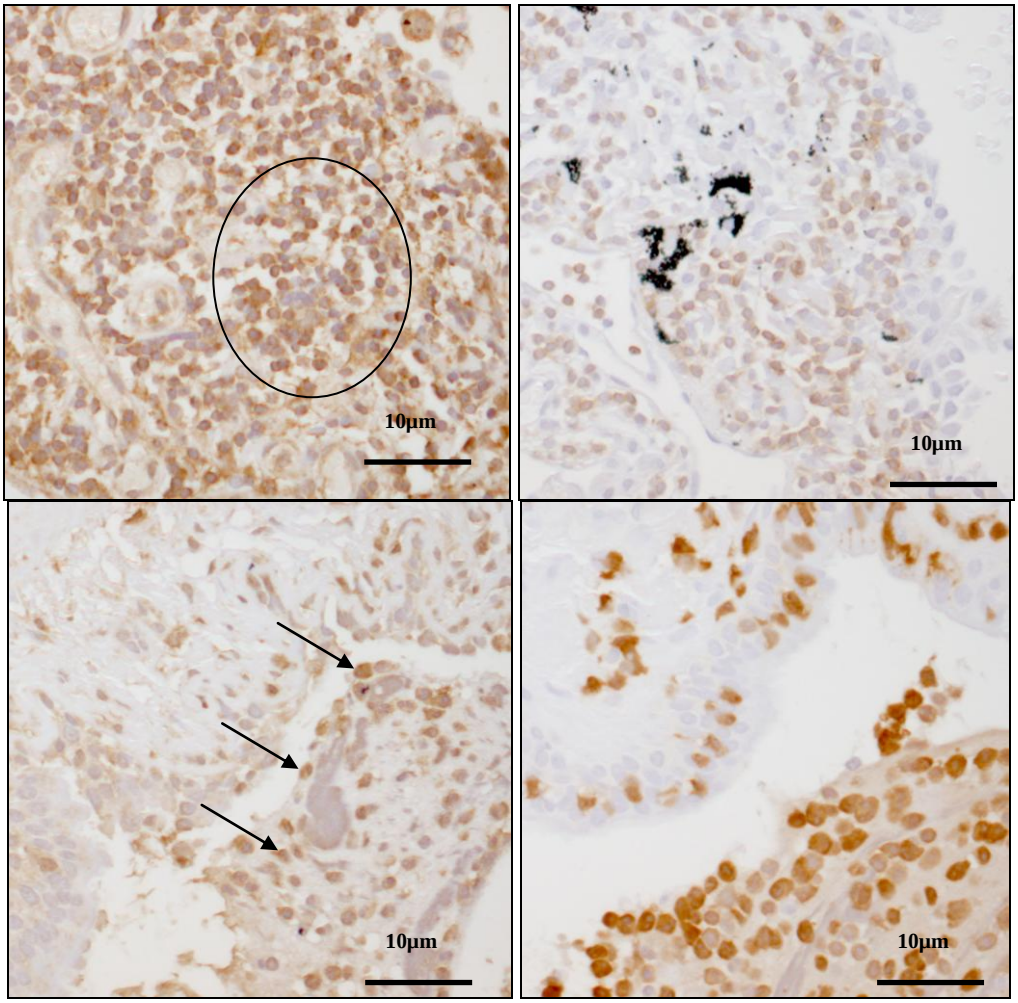

Photographs to show cytoglobin staining (top and bottom left) in inflammatory cells. CD3 staining (top right) was used as a marker or lymphocytes and MAC387 (bottom right) was used as a marker of macrophages. The top 2 pictures are of an inflammatory foci in COPD tissue, and the bottom, a mucous filled bronchiole. All pictures are x20. It is evident that the CD3 and MAC387 positive cell populations are also CYGB positive. Pictures are 40% of original size. Arrows highlight MAC387 positive cells and circle highlights CD3 positive cells.

Figure 3.4 Cytoglobin Staining in the Vasculature

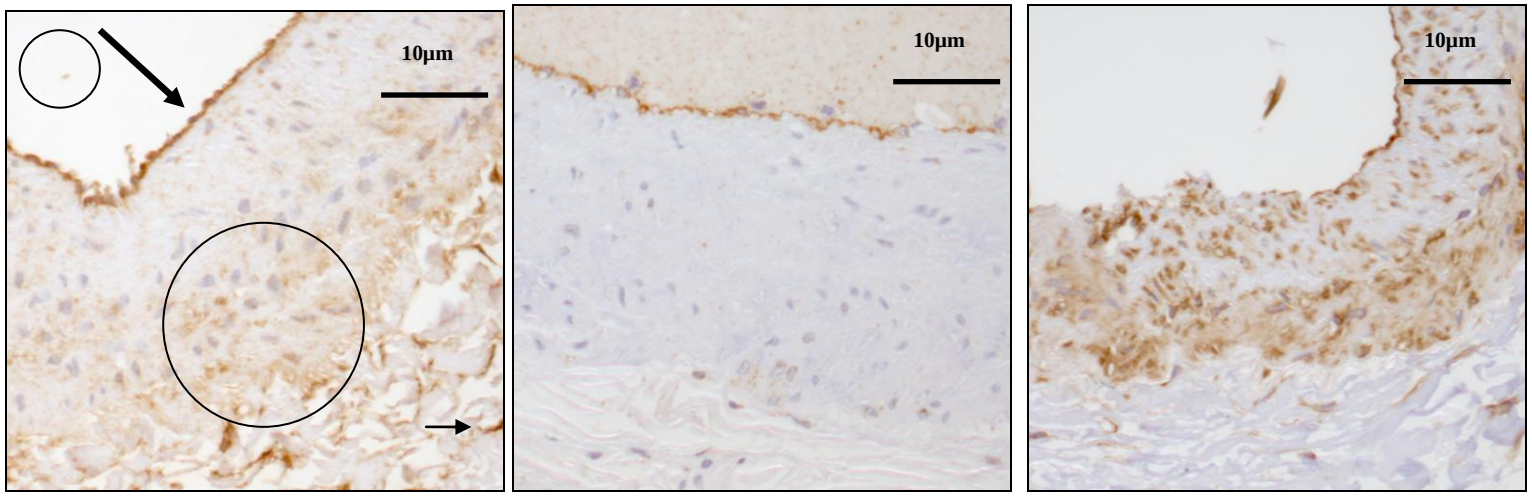

Photographs to show CYGB staining in the vasculature. Cytoglobin staining (left) was evident in adventisia fibroblasts (small arrow), the endothelium (large arrow) and vimentin positive cells in the intima and media (large circle). Negatively staining red blood cells are circled (small circle). The middle picture shows CD31 staining which is an endothelial marker to show the endothelium of this vessel is intact and corresponds to the CYGB staining. The picture on the right hand side is vimentin staining to show that the vimentin positive cell populations were also CYGB positive in the intima, media and adventisia. All pictures were taken at x20, and are at 40% of the original size. The vessel was from a COPD section.

Figure 3.5 Cytoglobin Staining in Pneumocytes

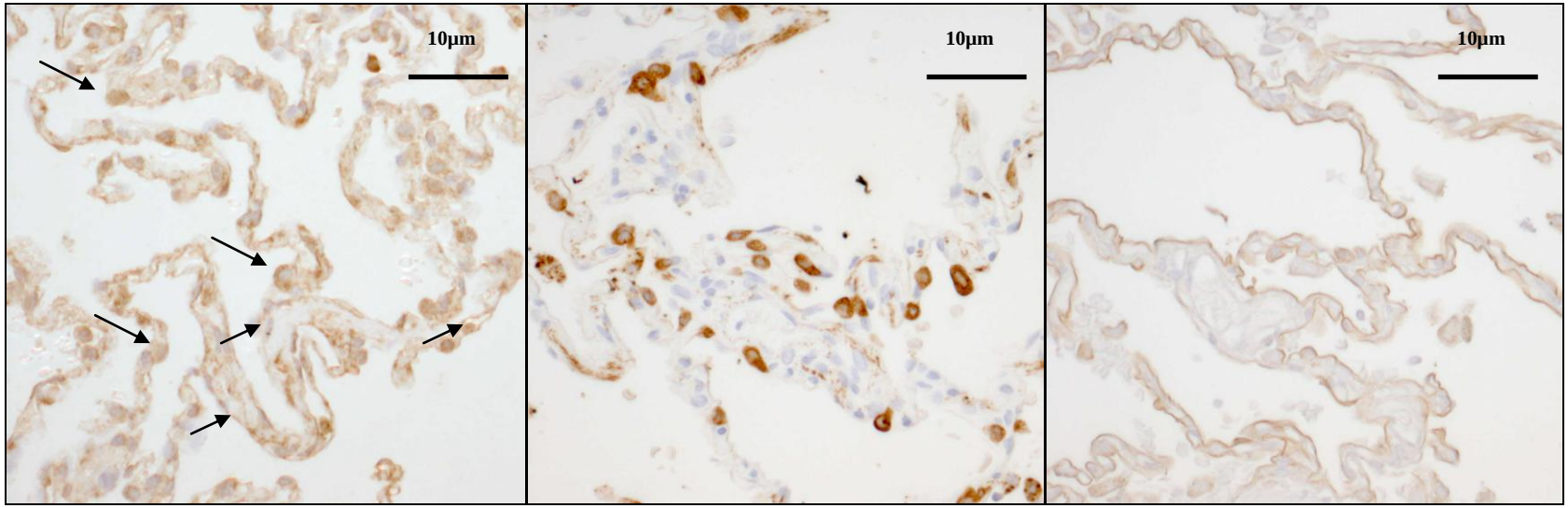

Photographs to show CYGB staining in pneumocytes. Cytoglobin staining (left) was evident in type II pneumocytes (arrows pointing downwards) and type I pneumocytes (arrows pointing upwards). The middle picture shows surfactant A staining which is a type II pneumocytes marker to show that the surfactant A positive cell population corresponds to those cells highlighted by downward arrows in the left hand picture. The right hand picture shows staining of wheat germ agglutinin (WGA) which is a type I pneumocyte marker. This picture shows that the WGA positive cell population corresponds to those cells highlighted by upward arrows in the left hand picture. All pictures were taken at x20 using a COPD section, and are at 40% of the original size.

Figure 3.6 Cytoglobin Staining in Bronchioles

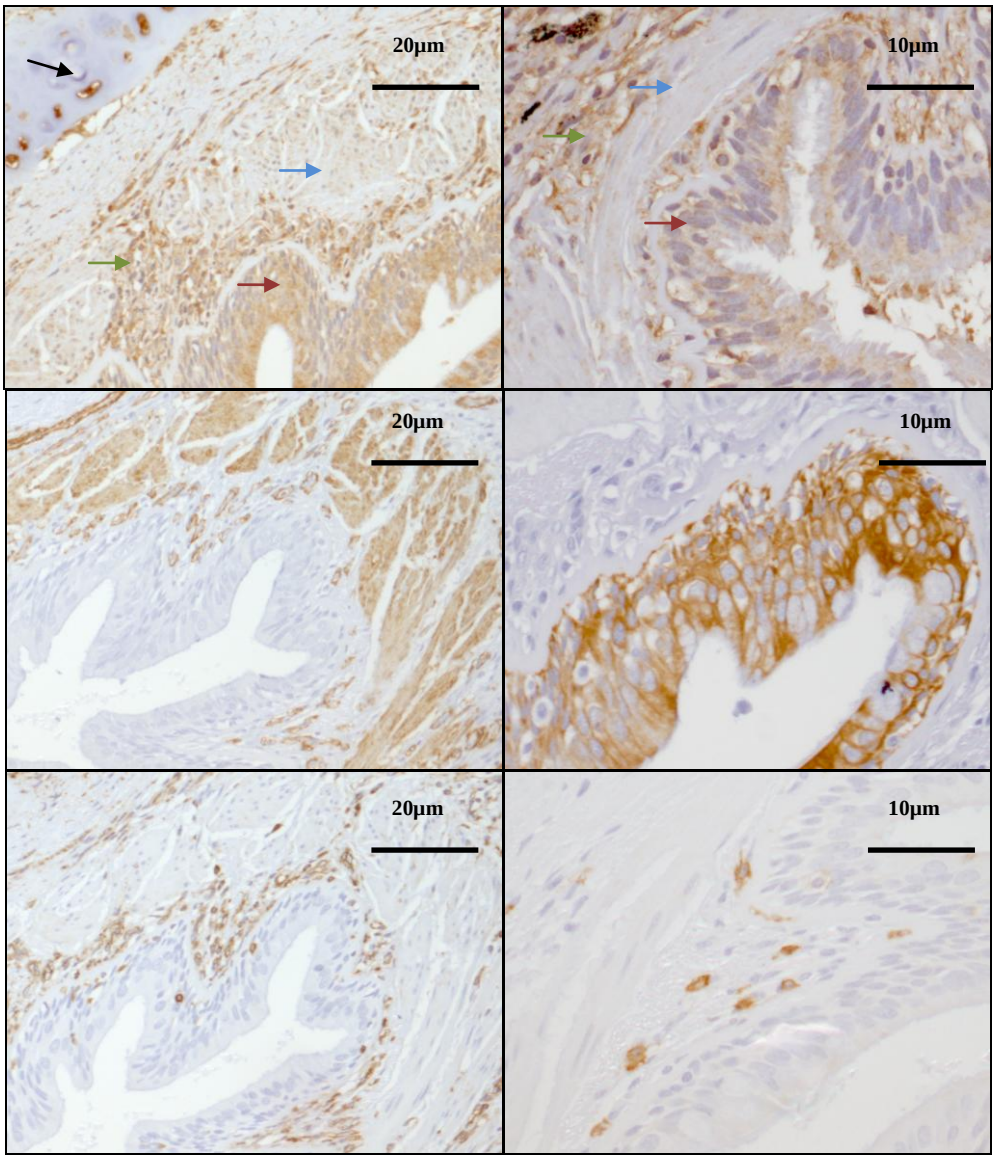

Photographs to show cytoglobin positive staining in the epithelium, mesenchyme and chrondrocytes of a COPD bronchiole, and negative staining in smooth muscle blocks. The top 2 pictures show CYGB staining at x10 and x20 on the left and right respectively. Chondrocytes are highlighted by the black arrow, mesenchyme by the green arrow, epithelium by the red arrow and smooth muscle by the blue arrow. The middle two pictures show staining of the same region with α smooth muscle (muscle marker at x10) and cytokeratin (epithelium marker at x20) on the left and right respectively. This validates that the regions labelled in the top pictures are muscle and epithelium. The bottom 2 pictures are show vimentin and c-kit staining on the left and right respectively. This shows that the region labelled with the green arrows in the top 2 pictures contain mesenchymal cells and stem cells with a haematopoietic origin. Pictures are 40% of original size.

Figure 3.7 Cytoglobin Staining in Tumour and Nerve cells

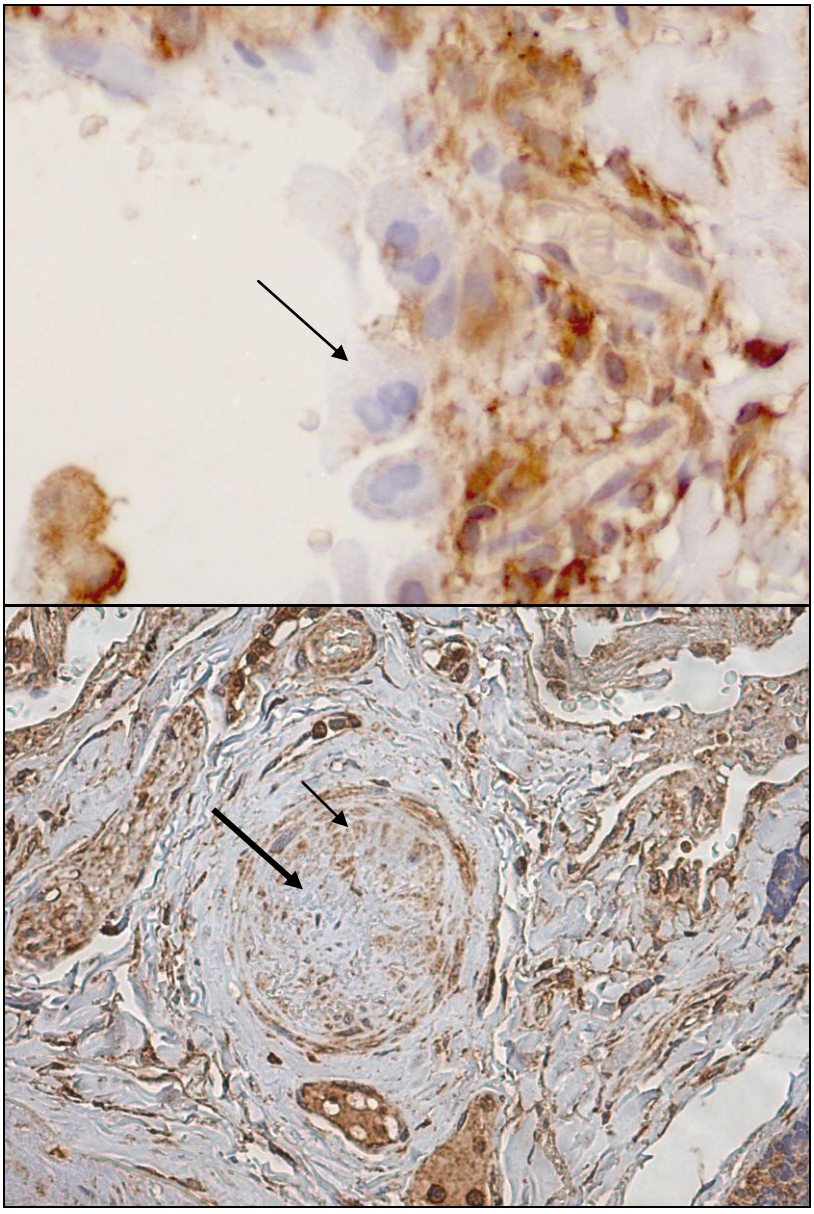

The top pictures shows negative CYGB staining in cells characteristic of tumour cells (x40) observed in COPD. The bottom picture shows a nerve bundle with CYGB positive glial cells (small arrow) and negative nerve cells (large arrow) observed in COPD (x20). Pictures are 40% of original size.

3.4.2 Distribution of Cytoglobin Expression Across the Fibrotic Lesion

The fibrotic lesions observed in COPD and IPF tissue were segregated into 3 distinct regions, the 'acellular zone' (AZ), the 'fibrotic border (FB)', and the 'edge' (see figure 3.1). The fibrotic borders observed in COPD tissue presented with 2 different phenotypes with respect to vascularity, and were grouped accordingly: the vascular fibrosing border (VFB); and the fibrotic border with a significant loss of vascularity (FBLoV). Significant loss of vascularity was characterised as presenting with either a low density (grade 1, see appendix for photographic representation) or complete absence of CD31 staining.

For each lesion analysed an overall CYGB profile was assigned to each area (see section 3.3 for details). The CYGB profiles assigned were thus: all cells CYGB positive, all cells CYGB negative or a mixed profile. As summarised in table 3.3, the cells in the AZ region consistently showed a positive CYGB profile in IPF and COPD lesions. The FBLoV of COPD lesions were also consistently positive for CYGB staining. The vascular fibrosing border of COPD and IPF lesion frequently displayed a mixed CYGB profile (60 and 40% of the lesions respectively). A mixed CYGB profile was ever present in the control tissue and the predominant profile at the edge. The overall CYGB expression profile of the IPF and COPD lesions was an all positive profile in the AZ, with an increasing bias towards a mixed CYGB profile across the fibrosing border towards the edge. In order to determine whether this was a characteristic of the lesion itself, or the cell types which localised to the different areas of the lesion, the density of each cell type within each area of the lesion, and the relating CYGB profile was determined.

Table 3.3 Cytoglobin Expression Observed in Different Areas of the Fibrotic Lesion

		Edge	**VFB**	**FBLoV**	**AZ**
All positive CYGB profile	COPD	35% (17)	40% (14)	100% (6)	100% (20)
	IPF	44% (9)	60% (9)	-	100% (9)
	Control	0% (5)	-	-	-
Mixed Cygb+/- profile	COPD	65% (17)	60% (14)	0% (6)	0% (20)
	IPF	56% (9)	40% (9)	-	0% (9)
	Control	100% (5)	-	-	-

A table to show the overall CYGB expression observed in different regions of the fibrotic lesion, or normal parenchyma. An 'all positive' CYGB profile was assigned when all cells which have shown reactivity with CYGB were positive in the region. (The CYGB expression in cells such as smooth muscle, nerve, tumour and red blood cells was not taken into account as these were consistently negative). A 'mixed' CYGB profile was assigned when the cells (not including muscle, nerve, red blood or tumour) in the region showed both CYGB negative and positive expression. Represented in the table is the % of lesions interpreted which showed each CYGB expression profile. In brackets is the number of lesions interpreted for each category.

3.4.3 Distribution of Cell Types, and the Relating CYGB Expression across the Fibrotic Lesion

Each region of each lesion was interpreted independently, creating 8 ‘categories’ for analysis: COPD AZ, COPD FBLoV, COPD VFB, COPD Edge, IPF AZ, IPF FB, IPF Edge and Control. For each category, the cell types present, and relative level of density were noted (See section 3.3 for details). The markers used to identify each of the cell types are summarised in table 3.2. The density of each cell type within each category was scored as follows: 0 non present, 1 low density, 2 midway, 3 high density (See appendix for a photographic representation of these classifications for each cell type). In addition a CYGB expression profile was assigned. For each cell type it was determined whether the population was all positive for CYGB, all negative or showed a mixed profile. The frequency at which each cell type presented with each level of density and each CYGB profile was calculated (See section 3.3 for more details), and plotted (see figures 3.8-3.11 and 3.13-3.16).

The Ashcroft and Sirius red scores were used to determine if particular cell type profiles in the lesion related to either fibrotic score of the lesion.

Figure 3.8 COPD Acellular Zone

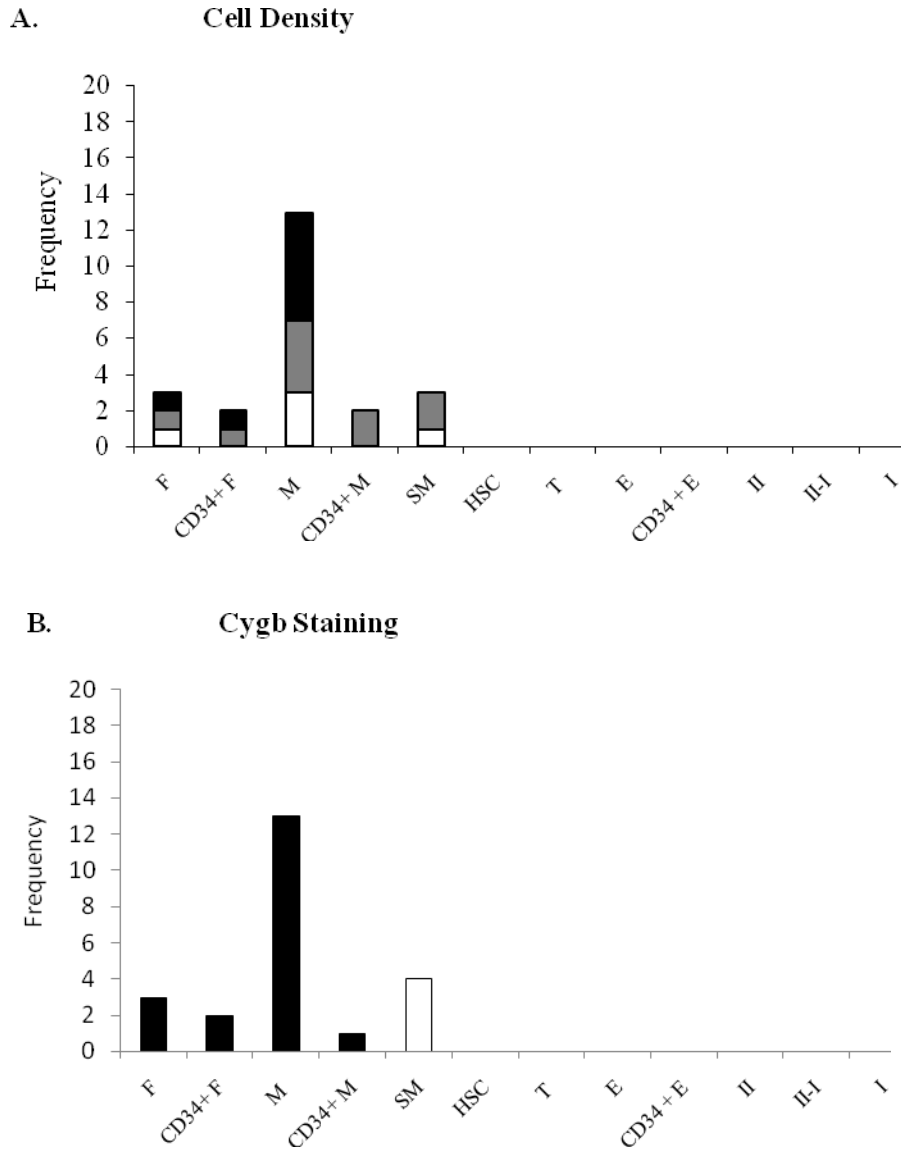

Graphs to show the cell types which localised to the acellular zone of COPD fibrotic lesions and their density and CYGB expression profile (n=20). Graph A shows the cell density of each cell type within the region. The size of the bar represents the frequency of lesions in which each cell type was present, and the formats represent the number of lesions in which each cell type was at a particular density. White represents sparse, Black abundant and grey neither sparse nor abundant (see M&M and appendix for more details). Graph B shows the CYGB profile of each cell type within the region. The size of the bar represents the frequency of lesions in which each cell type was present, and the formats represent the number of lesions in which each CYGB profile was observed. White represents all negative CYGB expression, Black represents an all positive profile. F: Fibroblasts, M: Myofibroblasts, SM: Smooth Muscle, HSC: Haematopoietic stem cells, T: T lymphocytes, E: Endothelium, II: Type II pneumocytes, II-I: Differentiating type II pneumocytes, I: Type I pneumocytes

Figure 3.9 COPD Fibrosing Border with a Significant Loss in Vascularity

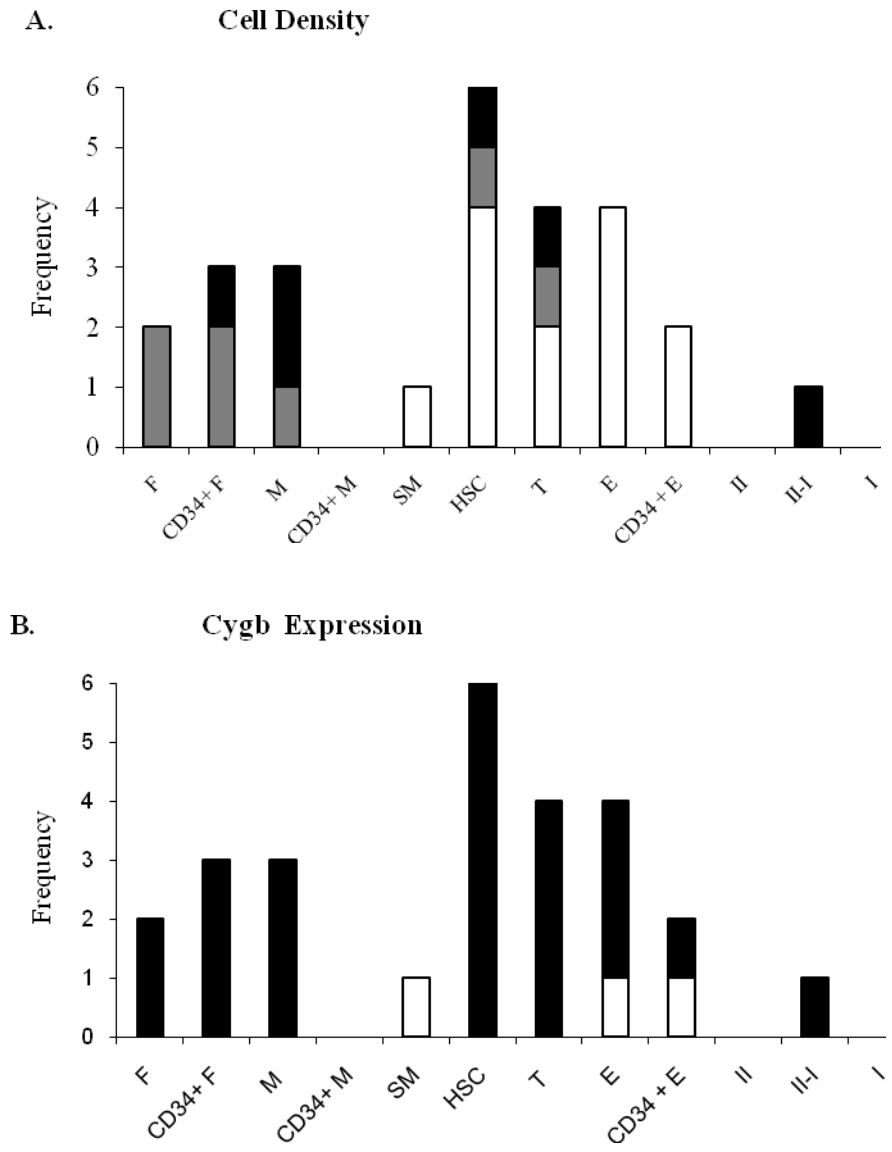

Graphs to show the cell types which localised to the fibrosing border with a significant loss of vascularity in COPD fibrotic lesions (n=6) and their density and CYGB expression profile. Graph A shows the cell density of each cell type within the region. The size of the bar represents the frequency of lesions in which each cell type was present, and the formats represent the number of lesions in which each cell type was at a particular density. White represents sparse, Black abundant and grey neither sparse nor abundant (see M&M and appendix for more details). Graph B shows the CYGB profile of each cell type within the region. The size of the bar represents the frequency of lesions in which each cell type was present, and the formats represent the number of lesions in which each CYGB profile was observed. White represents all negative CYGB expression, Black represents an all positive profile. F: Fibroblasts, M: Myofibroblasts, SM: Smooth Muscle, HSC: Haematopoietic stem cells, T: T lymphocytes, E: Endothelium, II: Type II pneumocytes, II-I: Differentiating type II pneumocytes, I: Type I pneumocytes

Figure 3.10 COPD Vascular Fibrosing Border

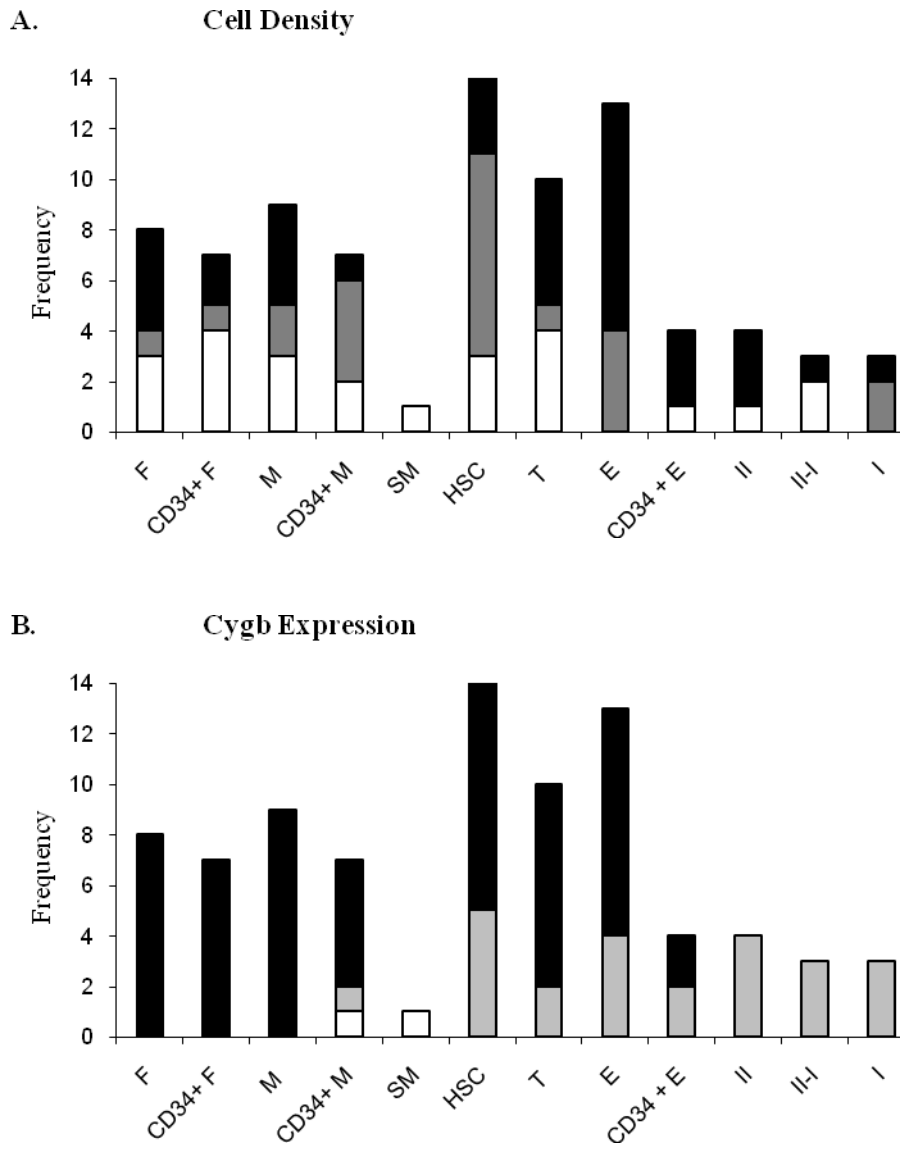

Graphs to show the cell types which localised to the vascular fibrosing border in COPD fibrotic lesions (n=14) and their density and CYGB expression profile. Graph A shows the cell density of each cell type within the region. The size of the bar represents the frequency of lesions in which each cell type was present, and the formats represent the number of lesions in which each cell type was at a particular density. White represents sparse, Black abundant and grey neither sparse nor abundant (see M&M and appendix for more details). Graph B shows the CYGB profile of each cell type within the region. The size of the bar represents the frequency of lesions in which each cell type was present, and the formats represent the number of lesions in which each CYGB profile was observed. White represents all negative CYGB expression, Black represents an all positive profile, Grey represents a mixed profile. F: Fibroblasts, M: Myofibroblasts, SM: Smooth Muscle, HSC: Haematopoietic stem cells, T: T lymphocytes, E: Endothelium, II: Type II pneumocytes, II-I: Differentiating type II pneumocytes, I: Type I pneumocytes

Figure 3.11 COPD Edge Lesion

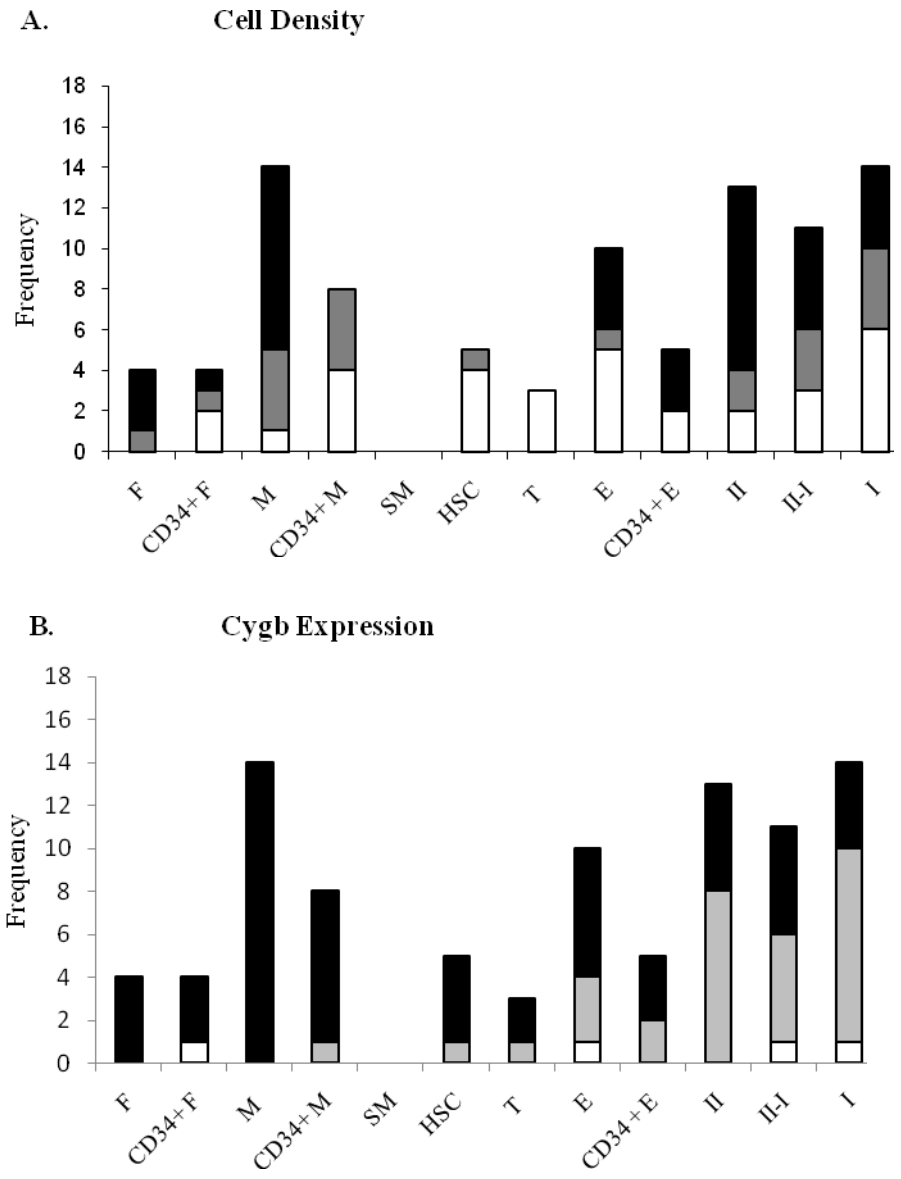

Graphs to show the cell types which localised to the edge of COPD fibrotic lesions (n=17) and their density and CYGB expression profile. Graph A shows the cell density of each cell type within the region. The size of the bar represents the frequency of lesions in which each cell type was present, and the formats represent the number of lesions in which each cell type was at a particular density. White represents sparse, Black abundant and grey neither sparse nor abundant (see M&M and appendix for more details). Graph B shows the CYGB profile of each cell type within the region. The size of the bar represents the frequency of lesions in which each cell type was present, and the formats represent the number of lesions in which each CYGB profile was observed. White represents all negative CYGB expression, Black represents an all positive profile, Grey represents a mixed profile. F: Fibroblasts, M: Myofibroblasts, SM: Smooth Muscle, HSC: Haematopoietic stem cells, T: T lymphocytes, E: Endothelium, II: Type II pneumocytes, II-I: Differentiating type II pneumocytes, I: Type I pneumocytes

Figure 3.12 Cytoglobin Staining in Cells of the COPD Lesion

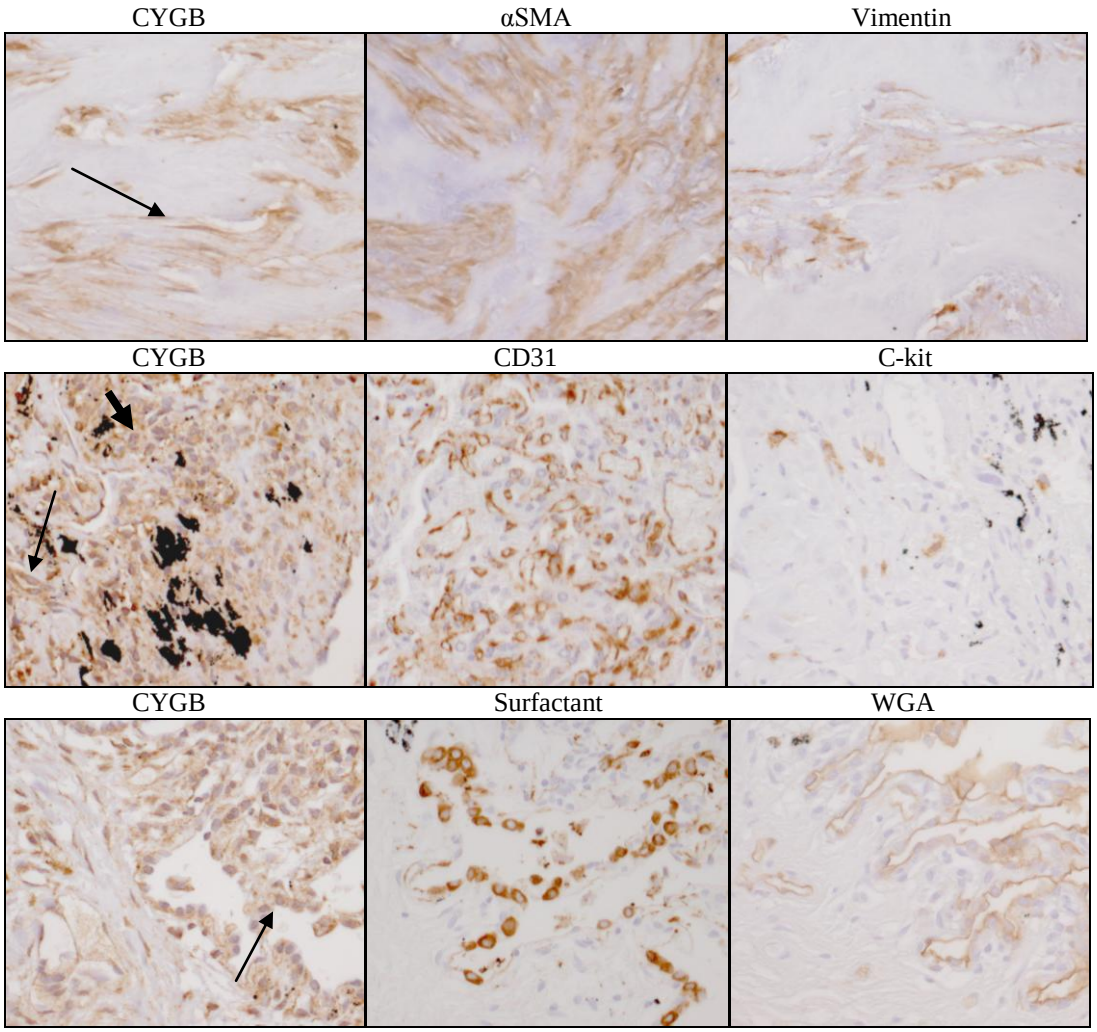

Pictures to show CYGB staining within different areas of COPD fibrotic lesions. Top row is the AZ (x20), the middle row VFB (x10), and the bottom shows the edge (x20). Cell type markers are shown to demonstrate which cell type typically reside in the region. In the top row, the arrow highlights CYGB staining in cells which are also immunoreactive for αSMA and vimentin. In the middle row the thick arrow highlights CYGB staining in a cell which is morphalogically similar to one which stained for c-kit on a serial section. The thin arrow highlights CYGB staining in an endothelial cell. In the bottom row, the arrow highlights CYGB staining in type I and II pneumocytes at the lesion edge. Pictures are 30% of original.

3.4.3.1 COPD

3.4.3.1.1 Acellular Zone

The AZ was comprised primarily of collagen and matrix, with little or no immunoreactivity (IR) for any cell type marker, indicating a predominantly acellular phenotype (see figure 3.8). The predominant cell type was CD34- myofibroblasts, which were present in all lesions with some cellularity (see figures 3.8 and 3.12). Small blocks of smooth muscle were observed in a subset of lesions.

In the AZ all cells present were positive for CYGB, with the exception of smooth muscle, which was consistently negative (See figure 3.8).

3.4.3.1.2 Fibrosing Border with a Significant Loss of Vascularity

The fibroblasts observed in FBLoV were exclusively either a fibroblast or myofibroblast population, and were present in all FBLoV, at a moderate to high density. These were subsequently the predominant cell type (see figure 3.9 and 3.12). All myofibroblasts were CD34-. The fibroblast population was mixed in terms of CD34 staining.

Hematopoietic stem cells (HSC) were observed in all FBLoV (see figure 3.9), mostly however at a low density. Lymphocytes were mainly either absent or at low levels in FBLoV. Smooth muscle was rarely seen in the FBLoV. By definition endothelial cells were absent or sparse in the FBLoV regions. Staining of the endothelial marker, CD31 was observed in 5 of the FBLoV lesions, of which 1 showed co-localisation with CD34 in all CD31 positive cells, 3 showed co-localisation with CD34 in subsets of the CD31+ cells and 1 was CD34-.

In the FBLoV cells were predominantly CYGB positive, with the exception of smooth muscle which was negative. Cells of a fibroblast lineage, HSCs and T lymphocytes were exclusively positive for CYGB staining (see figure 3.9 and 3.12).

3.4.3.1.3 Vascular Fibrosing Border

T lymphocytes, HSCs and endothelial cells were observed consistently in VFB at a moderate to high cell density (see figure 3.10 and Figure 3.12). Co-localisation of the endothelial marker CD31 with CD34 in the VFB was observed in all lesions with the exception of 1 (see figure 3.10). Pneumocytes and smooth muscle were rarely present in the VFB. Cells of a fibroblast lineage were present in all VFB. Myofibroblasts and fibroblasts co-localised in 29% of VFB lesions, an exclusively myofibroblast phenotype was observed in 42% of lesions, and an exclusively αSMA negative fibroblast phenotype in 29% of VFB lesions. The density of myofibroblasts and fibroblast varied across the lesions. A CD34+ fibroblast phenotype was observed in 80% of the VFB lesions, in both myofibroblasts and fibroblasts.

Myofibroblasts and fibroblasts were consistently CYGB positive within the VFB. Smooth muscle was consistently CYGB negative, and pneumocytes consistently presented a mixed CYGB profile. T lymophocytes, HSCs and endothelial cells predominantly stained positive for CYGB, however some mixed CYGB profiles were observed (see figure 3.10). The lesions with a mixed CYGB profile for HSCs also presented with a mixed profile for endothelial cells. The lesions with a mixed CYGB profile in T-lymphocytes were not the same as those in which a mixed CYGB profile was observed in HSCs and endothelial cells. Individual T-lymphocytes in the parenchyma were consistently positive, however foci of T-lymphocytes regularly presented with both Cygb+ and Cygb- staining within different cells of the foci.

There was a shift towards a mixed CYGB profile in the VFB, although most cell types presented with an all positive CYGB profile. (See figure 3.10 and 3.12).

3.4.3.1.4 Edge Lesions

The predominant cell types at the edge lesion were type I, type II and differentiating type II pneumocytes (see figure 3.11 and 3.12). The density of the different pneumocytes varied throughout the lesions. Cells of a fibroblast lineage were observed underneath pneumocytes at the fibrotic edge in 16 of the 17 edge lesions investigated, frequently at high densities (see figure 3.11 and 3.12). The predominant phenotype was a CD34- myofibroblast, however of the 16 lesions in which cells of a fibroblast lineage were observed, 9 lesions showed some co-localisation with CD34 (56% of lesions). Positive CD31 staining was observed in only 58% of the edge lesions, notably of those lesions without endothelial staining, the majority (63%) presented with a significant loss of vascularity in the fibrosing border (FBLoV). CD34 staining co-localised with CD31 staining in all but one lesion. A minority of lesions (3) showed a mixed CD34+ and CD34- endothelium population. T-Lymphocytes and HSCs were rarely observed at the edge.

Cells of a fibroblast linage were consistently positive for CYGB at the edge (See figure 3.11 and 3.12) HSC, T-lymphocytes, and endothelial cells were predominantly CYGB positive at the edge. Type II pneumocytes had either an all Cygb+ or mixed a CYGB profile. Type I pneumocytes presented with a Cygb-, Cygb+ and mixed profile. A Cygb- profile was rare, observed in only 1 of 17 edge lesions.

At the edge, the predominant CYGB expression profile was a mixed or Cygb+ profile for all cell types, with the exceptions of fibroblasts and myofibroblasts, which were exclusively Cygb+ (see figure 3.11 and 3.12).

3.4.3.2 IPF

3.4.3.2.1 Acellular Zone

The AZ of IPF lesions was mostly acellular, comprised of matrix and collagen. Immunoreactivity with any of the cell specific markers was observed in only 40% of lesions. Where the AZ presented with some cellularity, it consistently contained cells of a fibroblast lineage (See figure 3.13 and 3.16). Of the cellular lesions, 80% presented with myofibroblasts. CD34 staining co-localised with myofibroblasts in only 40% of lesions (n=5). All of the cells in the AZ were exclusively positive for CYGB expression.

3.4.3.2.2 Fibrosing Border

CD34- fibroblasts, HSCs, lymphocytes and smooth muscle cells were the predominant cell types in the fibrosing border of IPF lesions, and observed in all lesions, predominantly at a moderate or high cell density (See figure 3.14 and 3.16). Other fibroblastic phenotypes of cells such as CD34+ fibroblasts and myofibroblasts (CD34+ and CD34-) were observed in a subset of lesions (See figure 3.14). The endothelium was CD34+ in 7 of the 9 lesions. All lesions had a moderate to high density of endothelial cells, however the amount of CD34 positive staining in the endothelial cells was variable throughout the IPF lesions. Pneumocytes were absent from the FB in IPF (See figure 3.14).

All fibroblast phenotypes, HSCs and endothelial cells consistently presented with Cygb+ staining, and smooth muscle was consistently negative for CYGB (See figure 3.14). T-lymphocytes presented with both an all positive and mixed CYGB population (See figure 3.14). Where a mixed population was observed it was localised to inflammatory foci where not all cells were Cygb+, individual T-lymphocytes in the parenchyma were consistently positive.

3.4.3.2.3 Edge Lesions

Differentiating type II pneumocytes (CK+) were the predominant cell type at the edge of IPF lesions (See figure 3.15 and 3.16). Type I pneumocytes were mostly sparse or absent See figure 3.15. Fibroblasts were observed under the pneumocytes in all lesions, although the phenotypes varied See figure 3.15. Endothelial cells were also observed in all lesions (See figure 3.15). A mix of CD34+ and CD34- endothelial cells was observed in 6 of the 9 lesions, CD34 staining was absent from one lesion, and in 2 lesions endothelial cells were exclusively CD34+. HSC and T-lymphocytes were rarely observed at the edge of IPF lesions, and smooth muscle was absent.

All of the fibroblast phenotypes, HSCs, T-lymphocytes and endothelial cells were consistently positive for CYGB. Type II pneumocytes were exclusively Cygb+ in approximately half of the lesions, and had a mixed CYGB profile in the other half of the lesions. Type I pneumocytes predominantly had a mixed CYGB profile (See figure 3.15).

Figure 3.13 IPF Acellular Zone

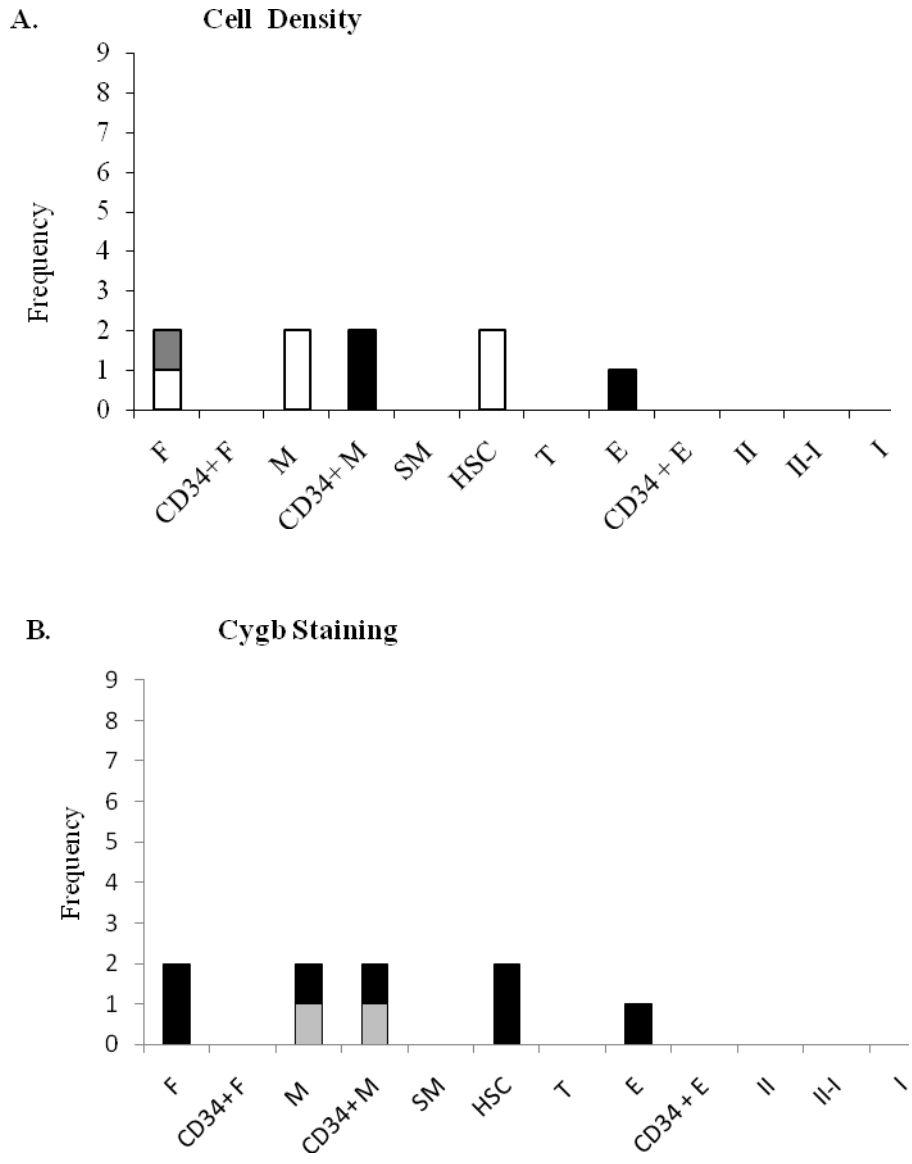

Graphs to show the cell types which localised to the acellular zone of IPF fibrotic lesions and their density and CYGB expression profile (n=9). Graph A shows the cell density of each cell type within the region. The size of the bar represents the frequency of lesions in which each cell type was present, and the formats represent the number of lesions in which each cell type was at a particular density. White represents sparse, Black abundant and grey neither sparse nor abundant (see M&M and appendix for more details). Graph B shows the CYGB profile of each cell type within the region. The size of the bar represents the frequency of lesions in which each cell type was present, and the formats represent the number of lesions in which each CYGB profile was observed. White represents all negative CYGB expression, Black represents an all positive profile. F: Fibroblasts, M: Myofibroblasts, SM: Smooth Muscle, HSC: Haematopoietic stem cells, T: T lymphocytes, E: Endothelium, II: Type II pneumocytes, II-I: Differentiating type II pneumocytes, I: Type I pneumocytes

Figure 3.14 IPF Fibrosing Border

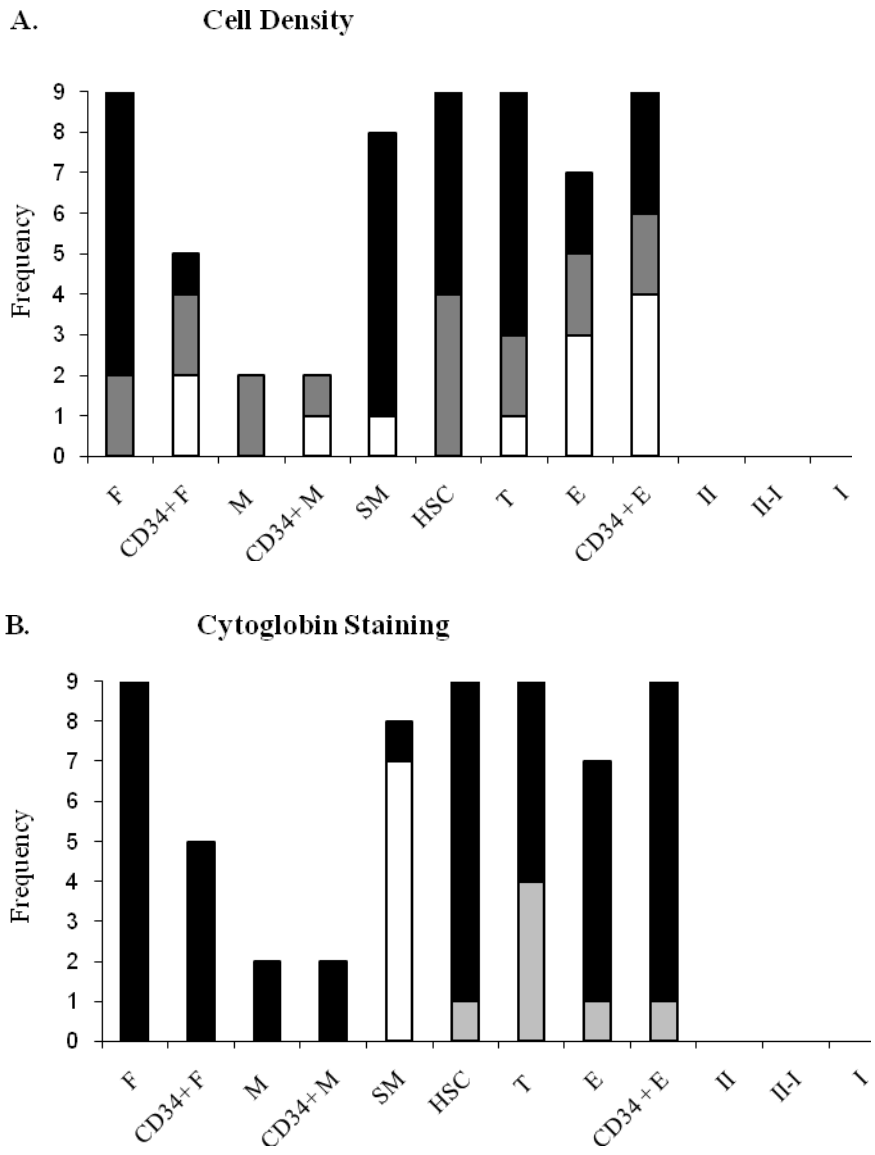

Graphs to show the cell types which localised to the fibrosing border of IPF fibrotic lesions and their density and CYGB expression profile (n=9). Graph A shows the cell density of each cell type within the region. The size of the bar represents the frequency of lesions in which each cell type was present, and the formats represent the number of lesions in which each cell type was at a particular density. White represents sparse, Black abundant and grey neither sparse nor abundant (see M&M and appendix for more details). Graph B shows the CYGB profile of each cell type within the region. The size of the bar represents the frequency of lesions in which each cell type was present, and the formats represent the number of lesions in which each CYGB profile was observed. White represents all negative CYGB expression, Black represents an all positive profile. F: Fibroblasts, M: Myofibroblasts, SM: Smooth Muscle, HSC: Haematopoietic stem cells, T: T lymphocytes, E: Endothelium, II: Type II pneumocytes, II-I: Differentiating type II pneumocytes, I: Type I pneumocytes

Figure 3.15 IPF Edge Lesion

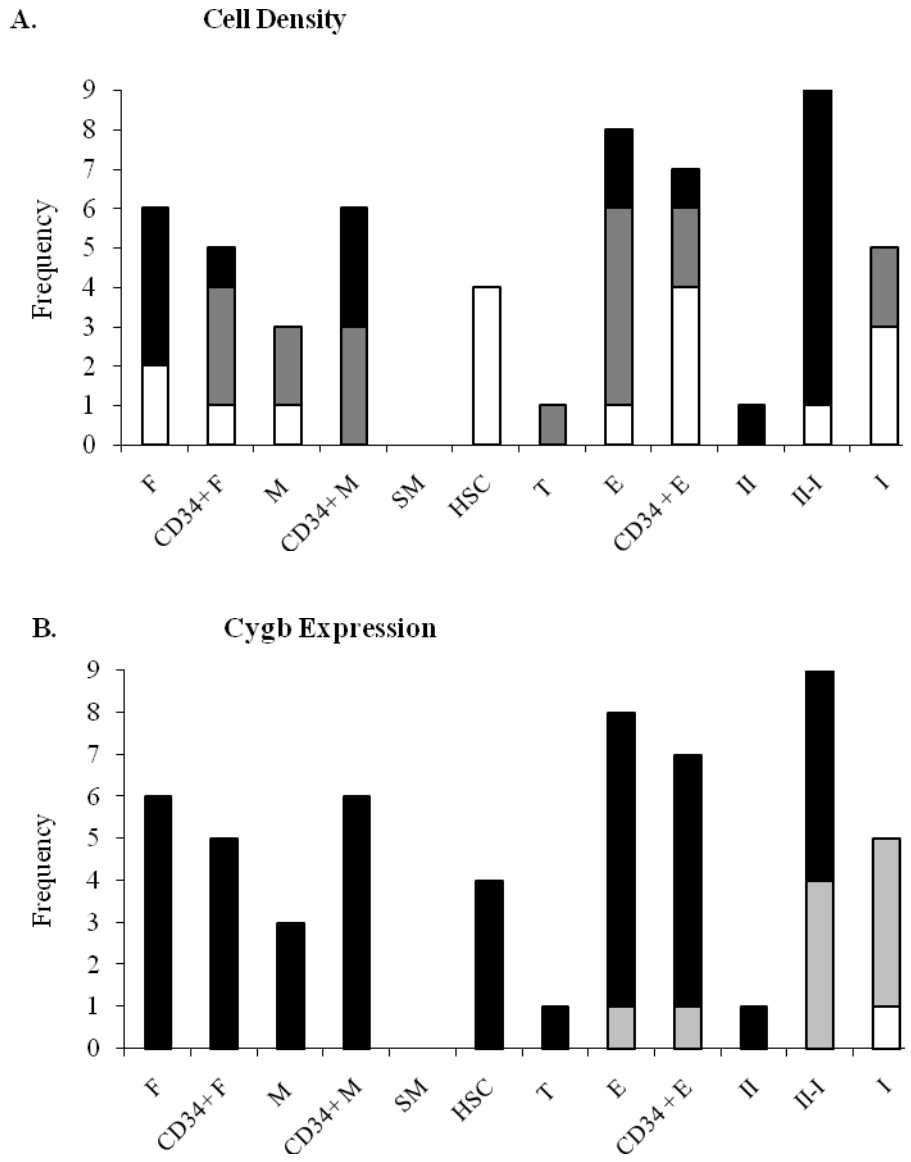

Graphs to show the cell types which localised to the edge of IPF fibrotic lesions and their density and CYGB expression profile (n=9). Graph A shows the cell density of each cell type within the region. The size of the bar represents the frequency of lesions in which each cell type was present, and the formats represent the number of lesions in which each cell type was at a particular density. White represents sparse, Black abundant and grey neither sparse nor abundant (see M&M and appendix for more details). Graph B shows the CYGB profile of each cell type within the region. The size of the bar represents the frequency of lesions in which each cell type was present, and the formats represent the number of lesions in which each CYGB profile was observed. White represents all negative CYGB expression, Black represents an all positive profile. F: Fibroblasts, M: Myofibroblasts, SM: Smooth Muscle, HSC: Haematopoietic stem cells, T: T lymphocytes, E: Endothelium, II: Type II pneumocytes, II-I: Differentiating type II pneumocytes, I: Type I pneumocytes

Figure 3.16 Cytoglobin Staining in Cells of the IPF Lesion

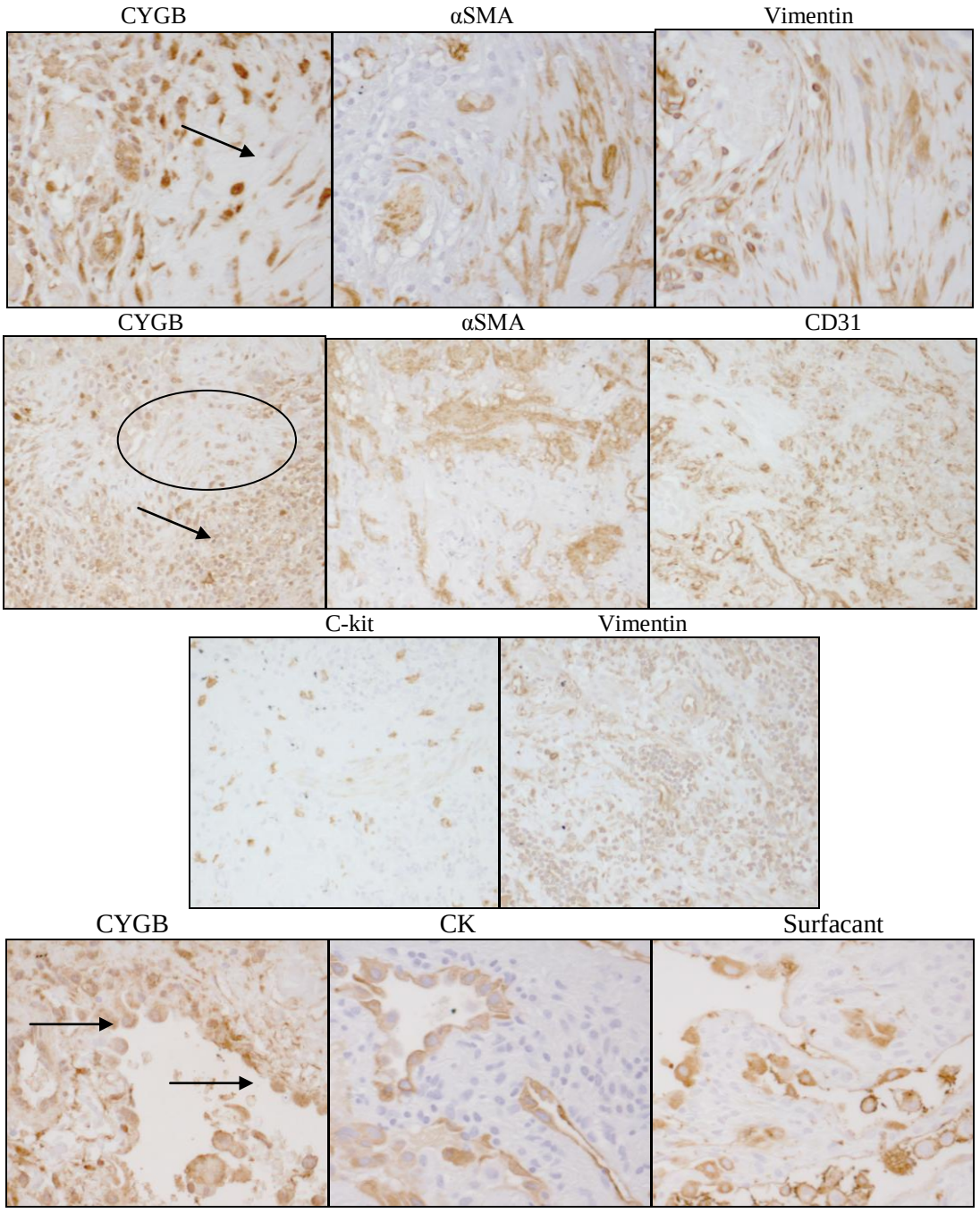

Pictures to show CYGB staining within different areas of an IPF fibrotic lesions. Top row is the AZ (x20), the middle 2 rows show the fibrotic border (x10), and the bottom shows the edge (x20). Cell type markers are shown to demonstrate which cell types typically reside in the region. In the top row, the arrow highlights CYGB staining in cells which are also immunoreactive for αSMA and vimentin. In the middle rows the arrow highlights CYGB staining in all cells in a region which shows immunoreactivity for CD31, c-kit and vimentin. The circle highlights negative staining in αSMA positive muscle. In the bottom row, the arrow highlights CYGB staining in CK+ type II pneumocytes at the lesion edge. Pictures are 30% of original.

Figure 3.17 Control Tissue

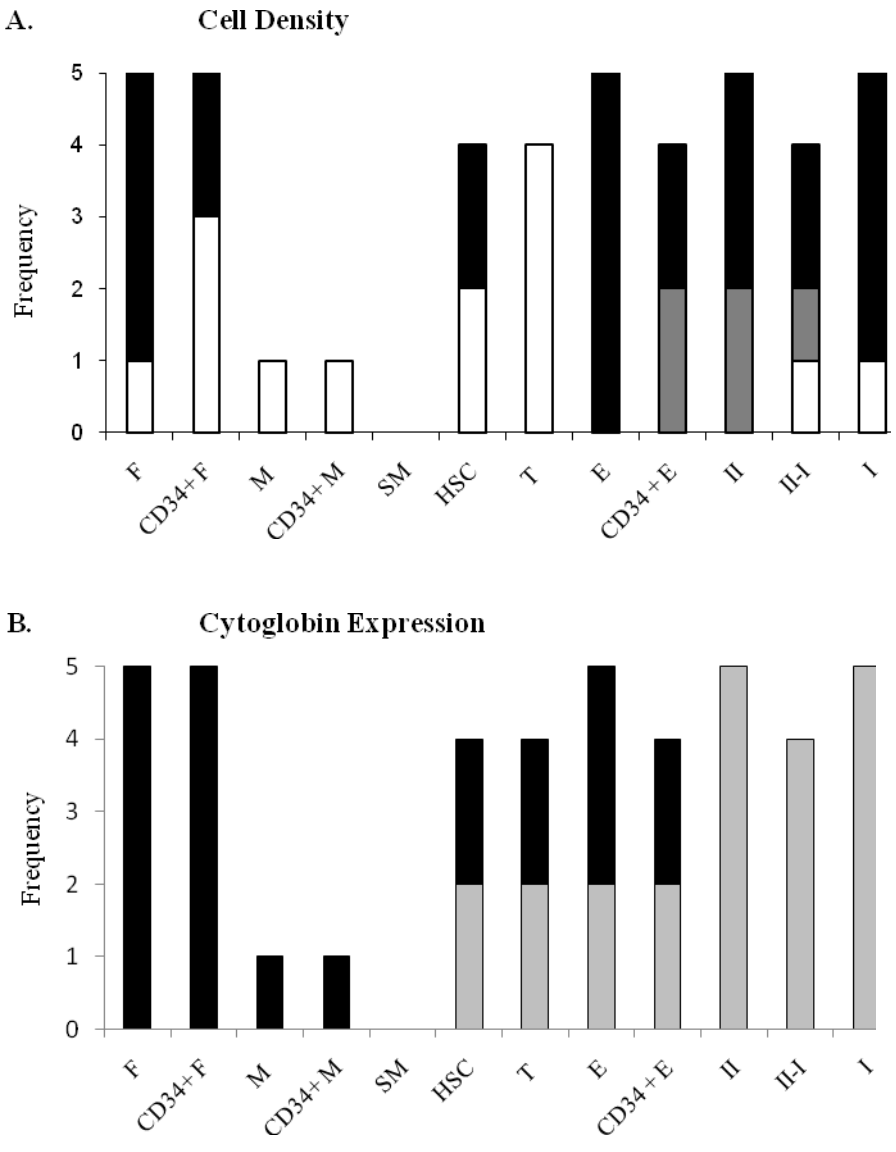

Graphs to show the cell types which localised in non fibrosed lung parenchyma and their density and CYGB expression profile (n=5). Graph A shows the cell density of each cell type within the region. The size of the bar represents the frequency of lesions in which each cell type was present, and the formats represent the number of lesions in which each cell type was at a particular density. White represents sparse, Black abundant and grey neither sparse nor abundant (see M&M and appendix for more details). Graph B shows the CYGB profile of each cell type within the region. The size of the bar represents the frequency of lesions in which each cell type was present, and the formats represent the number of lesions in which each CYGB profile was observed. White represents all negative CYGB expression, Black represents an all positive profile. F: Fibroblasts, M: Myofibroblasts, SM: Smooth Muscle, HSC: Haematopoietic stem cells, T: T lymphocytes, E: Endothelium, II: Type II pneumocytes, II-I: Differentiating type II pneumocytes, I: Type I pneumocytes

3.4.4 Cytoglobin Expression Within Specific Cell Types In Non Fibrosed Control Tissue

An array of cell types were observed in the control tissue at a high or moderate density (see figure 3.17), including endothelial cells, type I pneumocytes, type II pneumocytes, and fibroblasts (αSMA-). Myofibroblasts and T cells were sparse or absent (see figure 3.17). HSC's were present in 80% of the sections, half of the lesions in which they were present, HSCs were at a high density and the other half they were sparse. CD34 staining co-localised with fibroblasts in all control tissue, there was a mix of CD34+ and CD34- fibroblasts on all sections, with an approximately equal ratio in 3 of the 5 sections, and in 2 of the 5 sections there was substantially more CD34- than CD34+ fibroblasts. CD34 was observed in all endothelial cells of control sections, however in 80% of sections, populations of CD34- endothelial cells were also observed. In 50% of the sections which presented with both CD34+ and CD34- staining in endothelial cells, the CD34+ and CD34- populations were at approximately equal densities, whilst in the other 50% the predominance was a CD34+ phenotype.

Pneumocytes constantly had a mixed CYGB expression profile. Fibroblasts of all phenotypes were constantly all CYGB positive. Of the 5 control lesions, 2 presented a mixed CYGB profile in HSC's, T-Lymphocytes and endothelial cells, whilst of the other 3 lesions, where these cell types were present they were all Cygb+.

3.4.5 Correlating Cell Type Distribution to Fibrotic Severity

The density of several cell types showed heterogeneity between lesions in IPF and COPD. The data was ordered according to the Ashcroft and Sirius red scores for each lesion and the scores for each heterogenic cell type were analysed to determine whether there was a correlation between the fibrosis of the lesion and the cell type distribution.

The AZ of COPD lesions differed in the presence or absence of smooth muscle. The presence of smooth muscle in the AZ correlated to lesions with high Ashcroft scores. The FBLoV, VFB and edge of COPD lesions showed heterogeneity in fibroblast phenotypes. There was no correlation in the cross reactivity of CD34 with fibroblasts at the edge, or in the fibrosing border of COPD lesions, with the Ashcroft or Sirius red scores. However when ordered according to Ashcroft score there was a trend for an increase in myofibroblasts cell density with increasing Ashcroft score, and a decrease in the density of αSMA- fibroblasts (See figure 3.18). Similar observations were made at the edge. Fibroblast were observed at the edge of COPD lesions with low Ashcroft and Sirius red grades but absent from those with higher scores. An extended study would be required to draw any solid conclusions.

Variations in the density of different pneumocytes at the edge, and CD34 staining of endothelial cells in the fibrotic border of COPD lesions were not associated with the Ashcroft or Sirius red scores of the lesion.

There was more homogeneity in the cell types which localised to the IPF lesions. There were variations in the CD34 staining of endothelium in the fibrosing border, and fibroblast phenotypes at the edge but these did not show any correlation with the Ashcroft or Sirius red

Figure 3.18 Fibroblast Phenotype and Severity of the Fibrotic Lesion

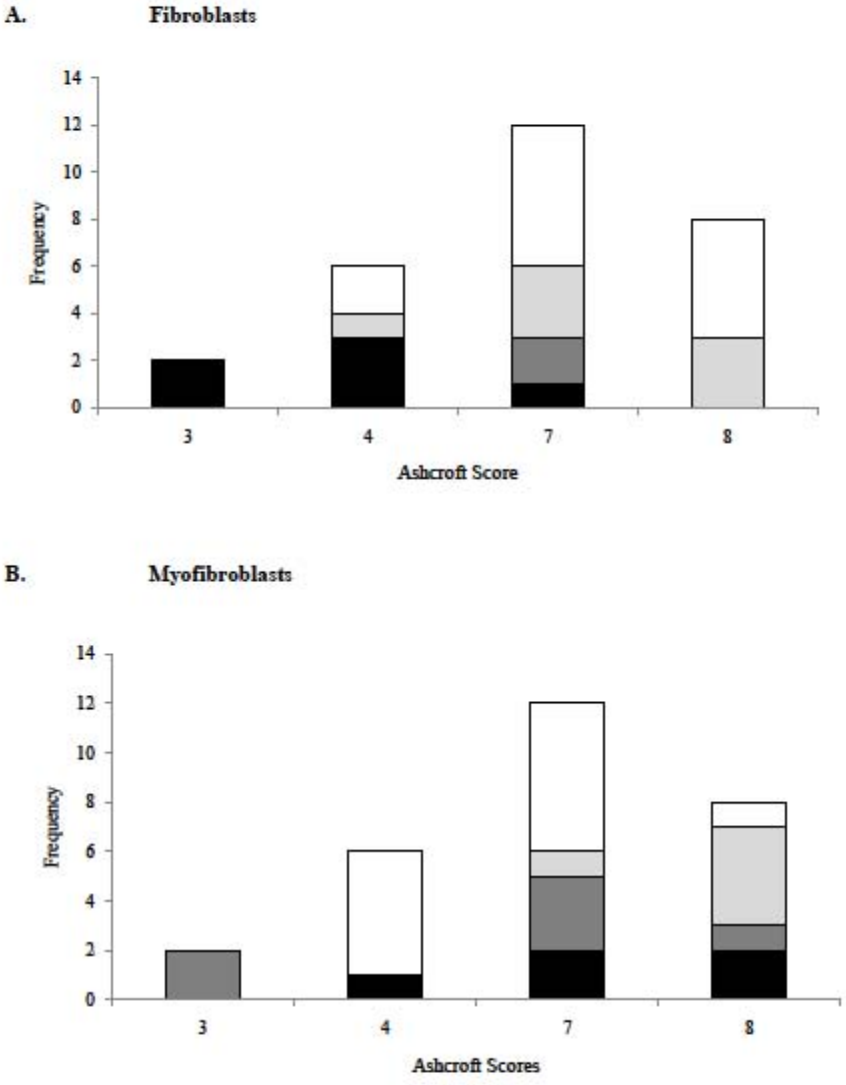

Graphs to show the relationship between the Ashcroft score of the COPD lesions, and the density of myofibroblasts and fibroblasts in the vascular fibrosing border. Graph A shows the density of fibroblasts and graph B the density of myofibroblasts. The total size of the bar represents the number of COPD lesions with each Ashcroft score. The format of each bar represents the density of myofibroblasts or fibroblasts. White: Cells absent. Light Grey: Cells sparse. Dark Grey: Density score 2 (between sparse and abundant). Black: Cells abundant.

scores of the lesion. The presence of type I pneumocytes at the lesion edge varied between lesions. Lesion with type I pneumocytes tended to have lower Sirius red scores than those without type I pneumocytes. Again an extended study would be required to form solid conclusions.

3.4.6 Comparing the Cell Types which Localise to IPF and COPD Lesions

The distribution of cell types varied between the IPF and COPD lesions. Overall there was a higher density of HSCs and CK+, differentiating type II pneumocytes in IPF lesions than COPD lesions, and a lower density of endothelial cell (See chapter 4 for more details). The predominance of COPD lesions showed co-localisation of CD34 with endothelial cells, where as a CD34- endothelial phenotype was also observed in the majority of IPF lesions. The density of T lymphocytes showed little variation between the diseases. The most varied cell type between the diseases was fibroblasts.

Fibroblasts were observed in the AZ of IPF and COPD lesions, with the myofibroblast phenotype being the most prevalent for both diseases. The co-localisation of CD34 with fibroblasts varied slightly between COPD and IPF, with CD34 staining being more frequently observed in IPF lesions. 25% (n=16) and 40% (n=5) of cellular AZ lesions presented CD34+ reactivity with fibroblast and or myofibroblasts in COPD and IPF respectively.

In the fibrotic borders of COPD and IPF (both vascular and avascular), fibroblasts were again one of the predominant cell types for both diseases, however the phenotypes differed. The fibroblasts phenotypes in COPD lesions were heterogenic (see 3.4.5), whilst those observed in IPF fibroblast were predominantly CD34- fibroblasts (αSMA-). Also of note a key difference

between the IPF and COPD fibrotic border was the presence of ectopic muscle blocks in IPF lesions.

At the edge of IPF lesions the fibroblast phenotypes were heterogenic with all lesions showing some CD34 reactivity in myofibroblasts or fibroblasts. Whilst approximately half (8 of 17 lesions) of the COPD lesions showed no CD34 co-localisation with fibroblast cells. The predominant fibroblasts phenotype was CD34- myofibroblasts in the COPD edge lesion.

3.4.7 Comparison of the Cytoglobin Expression Profile in COPD and IPF Lesions

With the exception of smooth muscle, all cells expressed CYGB within the AZ of IPF and COPD lesions. All fibroblast phenotypes showed CYGB expression in all regions of the COPD and IPF lesions and in non fibrosed control tissue. Endothelial cells, HSCs and T cells showed variability in CYGB expression. The fibrotic borders and edge of the IPF and COPD lesions were similar in that they showed some variability in CYGB expression in these cell types but predominantly an all Cygb+ profile was observed. Pneumocytes had a variable expression profile. A similar CYGB profile was observed in type II pneumocytes at the edges of both IPF and COPD lesions with an approximately 50:50 split in lesions which had an all Cygb+ profile and those which had a mixed CYGB profile for both COPD and IPF lesions. The CYGB profile of type I pneumocytes differed between COPD and IPF, with no IPF lesions having an all Cygb+ profile.

The CYGB expression profile of the COPD and IPF lesions differed to that observed in the same cell types in non fibrosed tissue. In non fibrosed tissue, HSCs, T cells, and endothelium

presented as frequently with a mixed CYGB profile as a Cygb+ profile, however within the lesions these cell types predominantly presented with a Cygb+ profile. The pneumocytes of non-fibrosed tissue consistently had a mixed CYGB profile, whereas at the lesion edge a Cygb+ profile was also observed.

The characteristics of the lesion may have an effect upon the CYGB expression profile in the cells which showed variation in expression. This is investigated in chapter 4.

3.5 Discussion

3.5.1 Cytoglobin Positive Cell types

Presented in this study is evidence of CYGB expression within a variety of cell types including bronchiole epithelium, type I pneumocytes, type II pneumocytes, endothelial cells, lymphocytes, macrophages, chondrocytes, fibroblasts and myofibroblasts.

Studies in the literature support these findings. Cytoglobin has been previously reported in human fibroblasts (Halligan *et al.*, 2009) and epithelial cells (Shigematsu *et al.*, 2008). Studies using rodent models have shown CYGB expression in fibroblasts of the lung (Man *et al.*, 2008) as well as in numerous other organs including liver (Nakatani *et al.*, 2004; Schmidt *et al.*, 2004), heart (Man *et al.*, 2008; Schmidt *et al.*, 2004), muscle (Man *et al.*, 2008; Schmidt *et al.*, 2004), colon (Schmidt *et al.*, 2004), kidney (Man *et al.*, 2008; Nakatani *et al.*, 2004; Schmidt *et al.*, 2004), tendon (Schmidt *et al.*, 2004), stomach (Man *et al.*, 2008) and skin (Schmidt *et al.*, 2004). CYGB immunoreactivity has also been observed in bronchiolar, alveolar and vascular interstitial tissue in rats (Nakatani *et al.*, 2004).

In contrast to that reported here, endothelial cells ((Kawada *et al.*, 2001; Man *et al.*, 2008; Nakatani *et al.*, 2004; Schmidt *et al.*, 2004), epithelial cells (Nakatani *et al.*, 2004) and macrophages (Nakatani *et al.*, 2004), have been reported to be negative for CYGB expression in rodent studies. These observations were made in pancreas, liver or kidney of fibrotic or healthy subjects. The contrasting CYGB profile could be due differences between the organs. CYGB may have a role in oxygen homeostasis, and the key role of the lung is in inhalation of oxygen, thus the expression of CYGB in the lung is likely to differ to that elsewhere in the body.

The focus and conclusion of several studies in the literature was the exclusive expression of CYGB in activated stellate cells and fibroblasts (Kawada *et al.*, 2001; Kida *et al.*, 2007; Man *et al.*, 2008; Nakatani *et al.*, 2004). Subsequently, cytoglobin has been presented in the literature as a marker of fibroblasts and, or activated stellate cells. Presented in this study is evidence of CYGB expression in cells other than fibroblasts thus these data would oppose the use of CYGB as a fibroblast marker.

3.5.2 Cell Types which showed Variation in Cytoglobin Expression

The expression profile of CYGB observed in this study was constant is several cell types. Fibroblasts were consistently positive, whilst smooth muscle, neurons, and erythrocytes were constantly negative. Cell types which showed variation in CYGB expression included endothelial cells, HSC, T-Lymphocytes, type I pneumocytes and type II pneumocytes. This variation in expression supports a model in which CYGB expression is not specific to a particular cell type, but all cells have the capacity to express CYGB, in response to stimuli.

3.5.3 Cytoglobin Negative Cell types

3.5.3.1 Cytoglobin Expression is not Observed in Cells which Express Other Globin Proteins

This study, and previous rodent studies have observed negative CYGB expression in smooth muscle cells (Nakatani *et al.*, 2004; Shigematsu *et al.*, 2008), neurons (Burmester *et al.*, 2007; Schmidt *et al.*, 2004) and erythrocytes (Man *et al.*, 2008). Cytoglobin expression has however been documented in a small population of neuronal cells in the rodent brain (Burmester *et al.*, 2007; Schmidt *et al.*, 2004), a predominantly CYGB positive profile was observed in neurons

of the eye (Burmester *et al.*, 2007; Ostojic *et al.*, 2006; Ostojic *et al.*, 2008a; Ostojic *et al.*, 2008b; Schmidt *et al.*, 2005) and CYGB expression has been observed in neuronal cells in culture (Hodges *et al.*, 2008; Li *et al.*, 2007; Schmidt *et al.*, 2004), all of which indicates that neurons are not an exclusively CYGB negative cell population.

The cell types which present with a negative CYGB profile: smooth muscle; erythrocytes; and neurons have each been reported to express the cell specific globins: myoglobin; haemoglobin; and neuroglobin respectively. The presence of cells which are negative for CYGB argues against the model proposed in 3.5.4, that all cells have the capacity to express CYGB. However, suppose these globins compensate for the lack of CYGB expression, induction of CYGB may occur under an environment where CYGB induction stimuli are excessive. This could offer an explanation for the observation of CYGB expression in neurons. CYGB is evolutionarily more ancient than Mb and Hgb (See introduction), so one could speculate that the more specialised Mb and Hgb have evolved from CYGB. The expression of Mb and Hgb in specific cell types would subsequently make the requirement for CYGB expression redundant.

The function of CYGB is likely to relate to those of other members of the globin family and could be expected to fall into one of the common functional niches for the globin family, such as transport and storage of oxygen, oxygen homeostasis, oxidase or peroxidise activity.

3.5.3.2 Cytoglobin Expression is not Observed in Tumour Cells

In the literature CYGB+ promoter methylation, and associated gene silencing has been observed in a variety of human cancers (McRonald *et al.*, 2006; Shaw *et al.*, 2007; Shaw *et*

al., 2009; Shivapurkar *et al.*, 2008; Xinarianos *et al.*, 2006). The absence of CYGB immunoreactivity observed in lung tumour cells in this study supports the observations in the literature, and proposals of CYGB as a tumour suppressor protein.

3.5.4 Localisation of Cell types to Regions of the Fibrotic Lesion

The same cell types localised to the same areas of the lesion in IPF and COPD, with only one exception. Ectopic smooth muscle bundles, which have previously reported in IPF tissue (Ohta *et al.*, 1995) were observed in the fibrosing border of all IPF lesions, but were only occasionally observed in COPD.

The density of other cell types, and the specific phenotypes varied between COPD and IPF. Fibroblasts were the predominant cell type in acellular regions of dense matrix and collagen in both IPF and COPD lesions, although the density of fibroblasts observed in IPF was greater than that in COPD, and phenotypes differed (see 3.5.5 for more details). Fibroblasts, HSC, T-lymphocytes and endothelial cells localised to the fibrosing border in IPF and COPD. T-lymphocytes and Macrophages were more abundant in the fibrosing border of IPF than COPD. Inflammation precedes and drives the fibrosis observed in COPD, whilst abnormal fibroblasts drive fibrosis in IPF. Consequently one may expect to observe a higher level of inflammation in COPD than IPF. IHC captures a snapshot of events within the lesion, and the fibrosis observed in COPD is in response to waves of inflammation. As COPD is self limiting one could assume that inflammation results in a distinct fibrotic event, the fibroblasts of which are not pro-inflammatory, preventing recurrent cycles of inflammation and fibrosis. Subsequently, the sequential events of inflammation followed by fibrosis would result in the co-localisation of inflammation with the fibrotic lesion in an IHC section to be unlikely. The

pathogenesis of IPF however is different, in response to an unknown trigger fibroblasts proliferate uncontrollably, have abnormally low or absent levels of anti-fibrotic PGE production, and release cytokines which initiate an inflammatory response, this is not self limiting but each perpetuates one another and thus events are observed in parallel and foci of fibrosis are associated with inflammation.

The edge and fibrotic borer of IPF tissue regularly showed more staining for CD31, representing the microvasculature, than observed in COPD. Notably, the CD31 staining in IPF was frequently associated with PCNA (See chapter 4 for more details about PCNA staining), a marker of proliferation and could relate to neovascularisation or aberrant angiogenesis, both of which have been reported in IPF. Alterations in the microvascularity in COPD remains inconclusive, with both evidence of both angiogenic and angiostatic events being presented with chronic bronchitis and emphysema respectively. Presented here is evidence of microvasculature heterogeneity between COPD lesions, where some lesions presented with angiogenesis (See chapter 4) and others avascularity.

CD34 expression in endothelial cells of the alveolar wall has been previously reported in healthy lung tissue (Pusztaszeri *et al.*, 2006). The endothelial cells in COPD lesions were predominantly CD34 immunoreactive, however in IPF a CD34+ and CD34- endothelial population was observed in most lesions. The loss of this haematopoietic marker could indicate maturation of endothelium which is not commonly observed in normal tissue. Potentially in healthy tissue endothelial cells may turnover before loss of the CD34 marker. In IPF there are abnormalities in several cell types, such as apoptosis resistant myofibroblasts, and apoptosis sensitive epithelial cells. Potentially, subpopulations of endothelial cells which

are resistant to apoptosis may also be present. These may contribute to fibrosis through synthesis of pro-angiogenesis or pro-fibrotic factors.

Type I pneumocytes were present at the edge of all COPD lesions, but were absent from many IPF lesions. Type II pneumocytes in IPF were large and consistently positive for CK in IPF, which complemented the morphology of IPF type II pneumocytes reported in the literature (Laurent *et al.*, 2008; Selman and Pardo, 2006; Willis and Borok, 2007). Type II pneumocytes observed in COPD were immunoreactive for CK in only a subset of lesions, considerably smaller than IPF type II pneumocytes, and more morphologically similar to those observed in non fibrosed control tissue.

3.5.5 Fibroblast Phenotypes in IPF and COPD

The phenotypes of fibroblasts varied across the lesions. The predominant phenotypes in each area were (MF: Myofibroblast, F: Fibroblast):

	COPD		**IPF**	
AZ	CD34-	MF	CD34-	MF
FBLoV	CD34-	MF		
	CD34+/-	F		
VFB	CD34+	MF		
	CD34+	F	CD34-	F
Edge	CD34+/-	MF	CD34+/-	MF
			CD34+/-	F

The CD34 expression of fibroblasts in the COPD lesion was both positive and negative at the edge, all positive in the VFB, mixed in the FBLoV and all negative in the AZ. Taking CD34 as a marker of haematopoietic origin, it could be speculated from these data that the fibroblasts in the VFB of COPD lesions have originated from circulating mesenchymal progenitor cells. In addition is could be speculated that (CMPC) migrate to the lesions through the capillaries in the vascular fibrosing border of the COPD lesion, from where they migrate either further into the lesion, or towards the edge where maturation and loss of the CD34 expression takes place. Considering the proposed origins of fibroblasts in fibrosis and the structure of the lesion, it would be logical that the localisation of fibroblasts within the lesion correlated to their source, with EMT derived fibroblasts, and resident fibroblasts to migrate to the edge of the lesion whilst CMPC migrate into the fibrosing border. The contribution of fibroblasts from various origins could thus have a significant effect upon the pathogenesis of the lesion.

The CD34 profile of fibroblasts in IPF is distinct to that of COPD lesions, and would argue against this model, as the FB and AZ of the IPF lesion were predominantly CD34-, whilst the edge showed a mixed CD34 profile. One could speculate that CMPC could also migrate to the lesion from the circulation in the parenchyma contributing to the mixed CD34 profile at the edge of the lesion. There is evidence of a CMPC contribution to IPF (Andersson-Sjoland *et al.*, 2008). The fibroblast within the lesion could originate from continued proliferation of fibroblasts localised within the lesion.

All areas of the COPD lesion contained myofibroblasts, but the fibroblast phenotype was predominantly only observed in the fibrosing border. Assuming differentiation of fibroblasts

into a myofibroblast phenotype does not occur until migration into the fibrotic lesion, this would be in-keeping with the above model of fibroblasts migrating into the lesion via the circulation of the VFB.

The AZ of IPF lesions was predominantly myofibroblasts, whilst fibroblasts were predominant in the FB, and a mixed population was observed at the edge. The predominance of αSMA negative fibroblasts within the IPF fibrotic lesion has previously been reported (Kapanci *et al.*, 1995; Yoshinouchi *et al.*, 1999). Several studies using the fibroblasts derived from the BAL of IPF patients have concluded the fibroblasts in IPF are less proliferative, contractile and express αSMA ((Fireman *et al.*, 2001; Kanematsu *et al.*, 1994; Ohta *et al.*, 1995; Ramos *et al.*, 2001; Shahar *et al.*, 1999), which contradicts that observed here, as observed here, the predominant fibroblast phenotype of the lesion were αSMA- fibroblasts. It should be noted that these fibroblasts were derived from the BAL and not the lesion of IPF patients. This study shows that the phenotype of fibroblasts varies across the lesion and thus BAL derived fibroblasts may not be truly representative of those within the lesion.

The origin and phenotype of fibroblasts are evidently different between IPF and COPD lesions. These differences are likely to contribute to the differences observed in the pathology of the fibrotic lesions in IPF and COPD, with particular reference to the self limiting nature of fibrosis in COPD, and self perpetuating nature of fibrosis in IPF.

3.5.6 Cell Type Changes As Markers Of Lesion Severity

This study provides preliminary evidence that with increasing fibrotic severity, smooth muscle and myofibroblasts are more frequently observed in COPD lesions. The increase in

frequency in myofibroblasts agrees with that proposed in the literature, that the myofibroblast is a fundamental cell type in fibrosis.

It was intriguing that the Ashcroft and Sirius red scores did not correlate to changes in the CK phenotype of type II pneumocytes in COPD lesions, as the expression of CK is indicative of differentiation and damage. One could speculate that the damage to pneumocytes at the edge of the COPD lesion may not contribute to the fibrotic progression, and that the events which occur at the edge and within the lesion are independent. The structure of the fibrotic edge is the same as that of the parenchyma, a layer of pneumocytes, associated on occasion in COPD, and always in IPF with endothelial cells via connective tissue. The fibrotic edge is equivalent to the local lung parenchyma and responds to localised damage. In contrast to IPF, the type II pneumocytes are not known to be abnormal. The fibrotic lesion is distinct to the edge, essentially it is a region of wound healing and comprised primarily of fibroblasts, and connective tissue with an absence of pneumocytes. The pathology of the regions are therefore distinct. This supports a model in which the fibrosis of the COPD lesion is driven primarily by the migration of CMPC and other fibrogenic cell types into the fibrosing border (see 3.5.5), and thus the fibrogenesis develops from within the lesion rather from repeated damage to the edge. This is highly speculative based on these data.

The IPF lesions with the highest Sirius red scores, indicative of deposition of larger collagen fibres, had an absence of Type I pneumocytes at the lesion edge. One could speculate that the loss of type I pneumocytes from the lesion may relate to the level of damage of the lesion. The perpetuating fibrosis observed in IPF could support a model in which the edge and the lesion are not independent. Bidirectional signalling between inflammatory cells and

fibroblasts, and epithelial cells and fibroblasts has been observed in pulmonary fibrosis. Potentially damage to type I pneumocytes could initiate pro-fibrotic pathways which perpetuate the fibrosis within the lesion. Additionally the pathogenesis of IPF has been proposed to be related to epithelial cell damage (Willis and Borok, 2007).

Recently it has been speculated that fibrosis can occur independently to inflammation (Willis and Borok, 2007), it was therefore unsurprising that the severity of the lesion was not related to the density of T-lymphocytes in COPD or IPF.

3.5.7 Cytoglobin Expression of the Lesion in IPF and COPD

CYGB was expressed in the AZ of IPF and COPD lesions, and the FBLoV of COPD lesions. The vascular fibrotic borders of IPF and COPD lesions showed some mixed CYGB expression (positive and negative) within HSCs, T-lymphocytes and endothelial cells although predominantly these regions were Cygb+. The edge of IPF and COPD lesions had a more mixed CYGB profile than the fibrotic border, but again a CYGB positive profile was predominant.

The expression of CYGB has been shown to increase at the mRNA and protein level in fibrosed compared to non fibrosed tissue (Kawada *et al.*, 2001; Kida *et al.*, 2007; Man *et al.*, 2008; Nakatani *et al.*, 2004; Tateaki *et al.*, 2004), and in response to fibrotic stimuli both in *vitro* (Gnainsky *et al.*, 2007; Kawada *et al.*, 2001; Nakatani *et al.*, 2004; Zion *et al.*, 2009) and in *vivo* (Gnainsky *et al.*, 2007; Zion *et al.*, 2009). These data presented in this study show that fibroblasts are the predominant cell type within the AZ and fibrosing borders of IPF and COPD lesions, and that fibroblasts are exclusively Cygb+ in both fibrotic and non fibrotic

tissue. This supports a model in which an increase in CYGB expression with fibrosis is a consequence of the migration of fibroblasts, and proliferation of fibroblasts in the region, which express CYGB.

Additionally this study has shown variable CYGB expression within T-lymphocytes, HSCs and endothelial cells, all of which were more frequently Cygb+ within the fibrotic lesion than in normal tissue or at the edge. Variable expression was also observed in pneumocytes, with a Cygb+ profile being observed more frequently at the lesion edge of IPF and COPD tissue than in non fibrosed controls. This would support a model in which CYGB is upregulated in response to local fibrogenic stimuli or as a consequence of fibrosis, as the CYGB profile of these cell types alters in accordance with their localisation in the fibrotic lesion.

There is a relationship between hypoxia and oxidative stress with the fibrosis, as a consequence of the loss of microvascularity, angiogenesis induced reperfusion injury and inflammation. CYGB expression has been reported to increase in response to both hypoxia (Fordel *et al.*, 2004; Fordel *et al.*, 2007a; Fordel *et al.*, 2007b; Guo *et al.*, 2007; Huang *et al.*, 2006; Mammen *et al.*, 2006; Schmidt *et al.*, 2004; Singh *et al.*, 2009) and oxidative stress (Li *et al.*, 2007; Mammen *et al.*, 2006; Powers, 2006), and thus induction of CYGB within the fibrotic lesion could be via hypoxic or redox pathways. The relationship between the CYGB expression of the lesion with hypoxia, and other markers of fibrogenesis were subsequently investigated, and this work is discussed in Chapter 4.

CHAPTER 4: DETERMINING THE SUBCELLULAR ROLE OF CYTOGLOBIN WITHIN THE FIBROTIC LESION.

4.1 Introduction

Several studies have used IHC to determine the tissue, cell and subcellular localisation of CYGB expression. As yet there are no studies which have looked at mechanistic markers to determine the relationship between CYGB distribution and the profile of the fibrotic lesion. Understanding this relationship could shed light on roles of CYGB in fibrosis.

The cells within the fibrotic lesion are assumed to be under hypoxic stress due to a loss of local vascularity, and CYGB has been associated in the literature with hypoxic cytoprotection. CYGB has also been associated with cytoprotection against oxidative stress, which is related to inflammation and repair, processes which are involved in fibrosis. Here we present IHC data from lungs of a severe COPD patient group correlating CYGB expression and markers of the profile of the fibrotic lesion.

4.2 Aim

The overall aim of this chapter was to add to the current understanding of the role of CYGB during fibrosis

The specific objectives were:

- Determine the relationship between CYGB and hypoxia within the fibrotic lesion
- Determine whether CYGB could be a marker of proliferation
- Determine if CYGB is a marker of inflammation
- Determine whether CYGB could be a marker of repair
- Determine if CYGB expression is a marker of fibrotic severity
- Determine the relationship between CYGB expression and vascular remodelling

4.3 Methods

4.3.1 pVHL and CAIX Immunohistochemistry

pVHL and CAIX immunohistochemistry was performed using standard procedures (see M&Ms). For CAIX staining, antigen retrieval was achieved by microwaving to boil in antigen unmasking fluid prior to staining. Staining used 0.5% hydrogen peroxide to quench endogenous peroxides, normal goat serum to block, a rabbit anti human CAIX antibody at 1µg/ml, a biotinylated goat anti rabbit secondary (0.5µg/ml), and the Streptavidin AB/HRP kit for signal amplification. The pVHL protocol was similar, with the following differences, antigen retrieval was achieved using 15lb pressure in antigen unmasking fluid and a biotinylated goat anti mouse secondary was used. The isotype controls used were Rabbit Ig and Mouse IgG1 for CAIX and pVHL respectively.

The lesions interpreted in Chapter 3 were further interrogated to determine the pVHL and CAIX profile of the cells types. The methods used to interpret the sections and analyse these data were the same as those described in chapter 3.

4.3.2 Characterising the Fibrotic Lesions

Markers of collagen deposition, proliferation and inflammation were also used to characterise the fibrotic lesions interpreted in Chapter 3. A score for each was assigned to each region of each lesion

4.3.2.1 The Collagen Deposition Score

The structure and density of collagen I was used as a measure of fibrosis because during fibrogenesis there is an increase in collagen I (Desmouliere *et al.*, 1999; Schwarz and King

1993). The collagen present is characteristically different to that in non-fibrosed tissue, in terms of shape, positioning and thickness. It is also often frayed due to the action of proteases such as collagenase (Schwarz and King 1993). The amount and intensity of the Collagen I staining was graded according to the scoring system as follows: 0: No Staining, 1: weak and sparse, 2: midway, 3: strong and abundant. (See appendix for photographic representation of these grades)

4.3.2.2 The Proliferation Score

PCNA (proliferating cell nuclear antigen), is a co-factor of DNA polymerases which encircle DNA during replication, and can therefore be used to identify the nuclei of proliferating cells. The use of PCNA as a marker for proliferation is limited to detection of cells within the replication, or S phase of the cell cycle (Lodish, 2004; Miura, 1999). Proliferating cell nuclear antigen was used as a marker of proliferation. Proliferation was graded using the scoring system as follows: 0: No staining, 1: sparse, 2: midway, 3: abundant. (See appendix for photographic representation of these grades)

4.3.2.3 Inflammation Score

MAC387 and CD3 were used as markers of inflammation as they identify macrophages and T lymphocytes respectively. Each were graded using the scoring system as follows: 0: No staining, 1: sparse, 2: midway, 3: abundant. (See appendix for photographic representation of these grades)

4.3.3 Data Analysis

Each region of each lesion interpreted in chapter 3 was assigned a score for the each of the following:

	Marker used
Loss of vascularity	Density of CD31
Fibrotic Severity	Ashcroft score, Sirius Red Score, Collagen Score
Proliferation	Density of PCNA
Inflammation	Density of CD3 and MAC387
Pneumocyte mediated repair	Density of CK+ type II pneumocytes
Angiogenesis	Co-localisation of CD31 and PCNA
Stem cell mediated repair	Density of c-kit

The data regarding the CYGB profile of different cell types was grouped according to each of these markers. For example, to determine the relationship between the level of proliferation with CYGB expression in the COPD vascular fibrosing border, the data was segregated into 3 groups: those which were negative for PCNA; those which were positive in less than 50% of the cell population; and those which were positive in more than 50% of the population. The CYGB expression profile of each cell type was compared between the groups, in order to highlight, for example, if a mixed CYGB expression profile in HSCs was exclusively observed in lesions which were negative for PCNA

4.3.4 Grading the Vasculature

The vasculature was graded using an algorithm designed by P Vaughan (Vaughan *et al.*, 2006) For each vessel the sum of the following was calculated:

For each feature of the vasculature in the list below 2 points were assigned if >50% of the vessel was affected, 1 point if <50% of the vessel was affected, and 0 points if absent.

Intima	**Media**
Hypertrophy and or hyperplasia	Hypertrophy and or hyperplasia
Roughened endothelium	Radial smooth muscle cells/re-orientation
Luminal thrombus	Apoptosis
Sclerosis/collagen deposition	Sclerosis/collagen deposition
New internal elastic lamina	Leucocytes in vessel wall
	Indistinct internal elastic lamina
	Indistinct external elastic lamina

The severity of damage to the vessel was also scored using desmin and vimentin as markers of remodelling. The scores assigned were originally identified by G Sirico (Sirico *et al., 2006.*). G Sirico observed that in mildly damaged vessels, desmin and vimentin staining was dense and structured. In moderately damaged vessels there was a re-organisation of vimentin and subsequent loss of signal, and larger regions of negative desmin staining. In severely damaged vessels, there were large regions of negative desmin staining, and immunoreactivity for vimentin was strong, but the structure was disorganised.

4.3.5 Grading Cytoglobin Expression in the Vasculature

Alongside grading the vessels for desmin and vimentin, the CYGB expression profile was also investigated. The CYGB expression profile was vimentin and desmin positive cells was determined using methods described in chapter 3. The intensity of the CYGB signal was noted as follows: 0: negative, 1: weak, 2: midway, 3: strong (See appendix for photographic representation of these grades)

4.4 Results

4.4.1 Cytoglobin as a Marker of Hypoxia

4.4.1.1 Localisation of pVHL staining within the fibrotic lesion

pVHL staining was used as a marker of non hypoxia, where non hypoxia refers to an cellular oxygen tension which is not hypoxic but could be normoxic or hyperoxic. The AZ and FB of IPF lesions were negative for pVHL staining in all cell types, as was the AZ and FBLoV of COPD lesions (see figure 4.1, 4.2, 4.5 and 4.6). The edge of the IPF lesion showed immunoreactivity for pVHL in type II pneumocytes only (see figure 4.7 and 4.9), which was observed in all lesions. In contrast the VFB of the COPD lesion showed some pVHL immunoreactivity in HSCs, and or T-lymphocytes, and or endothelium, and or pneumocytes in a subset of lesions (20% of lesion) (see figure 4.3). pVHL staining was observed in type I and type II pneumocytes at the edge of all COPD lesions (see figure 4.4), 8 lesions had an all pVHL positive population in all pneumocytes whilst in the other lesions pneumocyte populations had a mixed pVHL profile (total number of lesions in which each cell type was observed: 13 for type II, 11 for type II-1, 14 type I). Non-fibrotic controls predominantly presented with a mixed pVHL+/- profile in type II and type I cells (See figure 4.8).

4.4.1.2 Localisation of CAIX Staining within the fibrotic lesion

Carbonic Anhydrase IX is regulated via HIF-1α, and so was used as a marker of HIF-1α activity. CAIX immunoreactivity was observed in all cell types identified (see figures 4.1-4.9), including smooth muscle. The CAIX expression profile was variable across the lesion in all cell types, overall however there was a predominance of positive staining within the cells of the AZ and FBLoV of COPD lesions, and the AZ and FB of IPF lesions (See figures 4.1-

4.9). The VFB and edge of the COPD lesions and edge of IPF lesions predominantly had a mixed CAIX profile (see figures 4.3, 4.4 and 4.7).

The IPF lesions presented with a greater level of CAIX staining than observed in COPD. Control tissue presented primarily with a mixed CAIX+/- profile in pneumocytes, the most abundant cell type present (See figure 4.8). All fibroblast were positive for CAIX in control tissue.

4.4.1.3 Correlating the pVHL, CAIX and Cytoglobin Staining

All cells in the IPF and COPD AZ were positive for CYGB, and the expression of CYGB became more variable through the lesion to the edge (See chapter 3). The pVHL staining had an opposite profile. pVHL staining was absent from the AZ regions, and localised primarily to the edge in type II pneumocytes in IPF and type I and type II pneumocytes in COPD lesions. Pneumocytes, which offered the most variability in CYGB expression were thus the predominant pVHL positive cell type. However, there was no relationship between an all positive pVHL population at the edge and a mixed CYGB profile, or vice versa.

The CAIX staining mirrored that of CYGB, although smooth muscle also presented with CAIX immunoreactivity. CYGB staining was frequently observed in more cells than CAIX in COPD. There was a difference in the pVHL profile of the pneumocytes at the COPD lesion edge between lesion where the CAIX=CYGB and those in which CAIX<CYGB. The pneumocytes at the edge of COPD lesions were all pVHL positive in lesions where CYGB>CAIX signal, but showed a mixed pVHL profile in lesions where CAIX=CYGB.

Figure 4.1 pVHL and CAIX staining in the COPD Acellular Zone

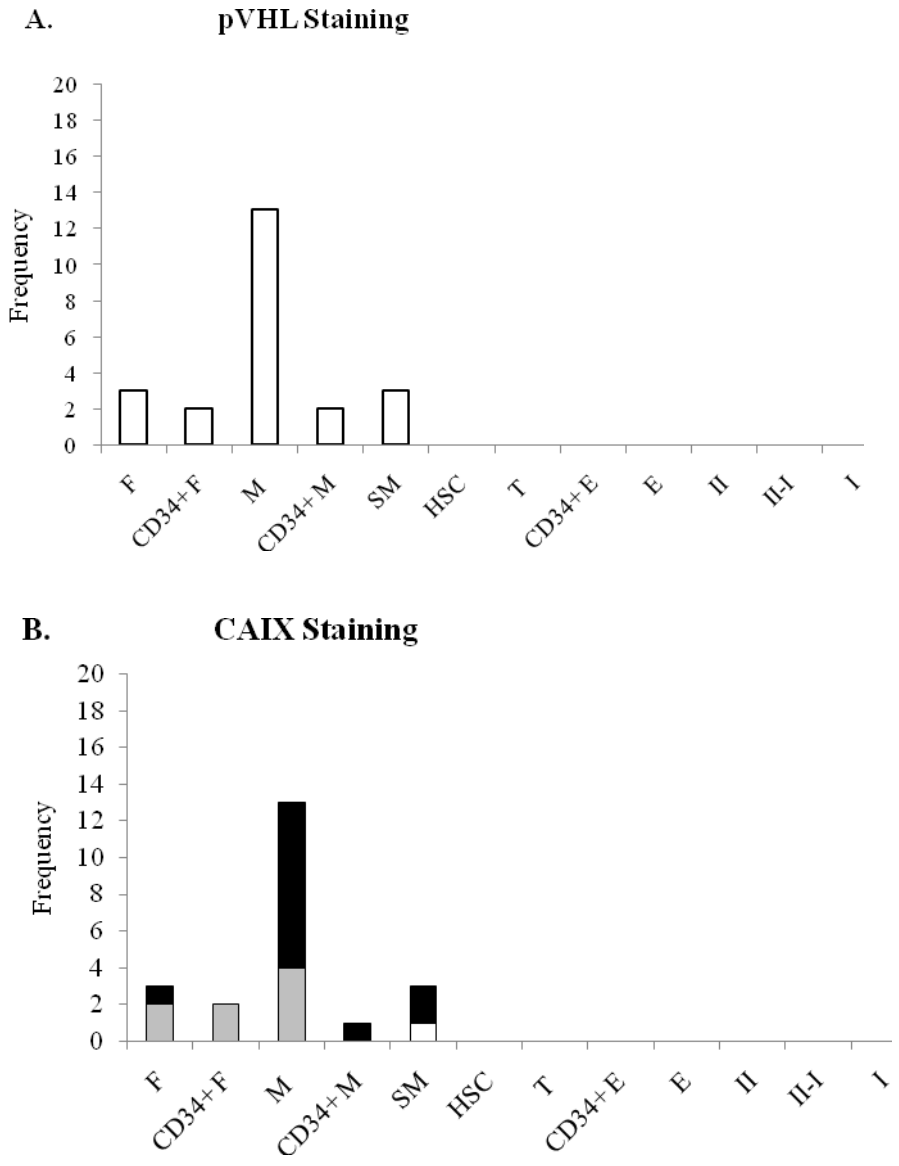

Graphs to show the cell types which stained for pVHL and CAIX in the acellular zone of COPD fibrotic lesions (n=20). Graph A shows the pVHL staining of each cell type within the region. Graph B shows the CAIX profile of each cell type within the region. The size of the bar represents the frequency of lesions in which each cell type was present, and the formats represent the staining profile. White represents all negative, Black all positive and grey mixed (see M&M and appendix for more details). F: Fibroblasts, M: Myofibroblasts, SM: Smooth Muscle, HSC: Haematopoietic stem cells, T: T lymphocytes, E: Endothelium, II: Type II pneumocytes, II-I: Differentiating type II pneumocytes, I: Type I pneumocytes

Figure 4.2 CAIX and pVHL Staining in the FBLoV of COPD Lesions

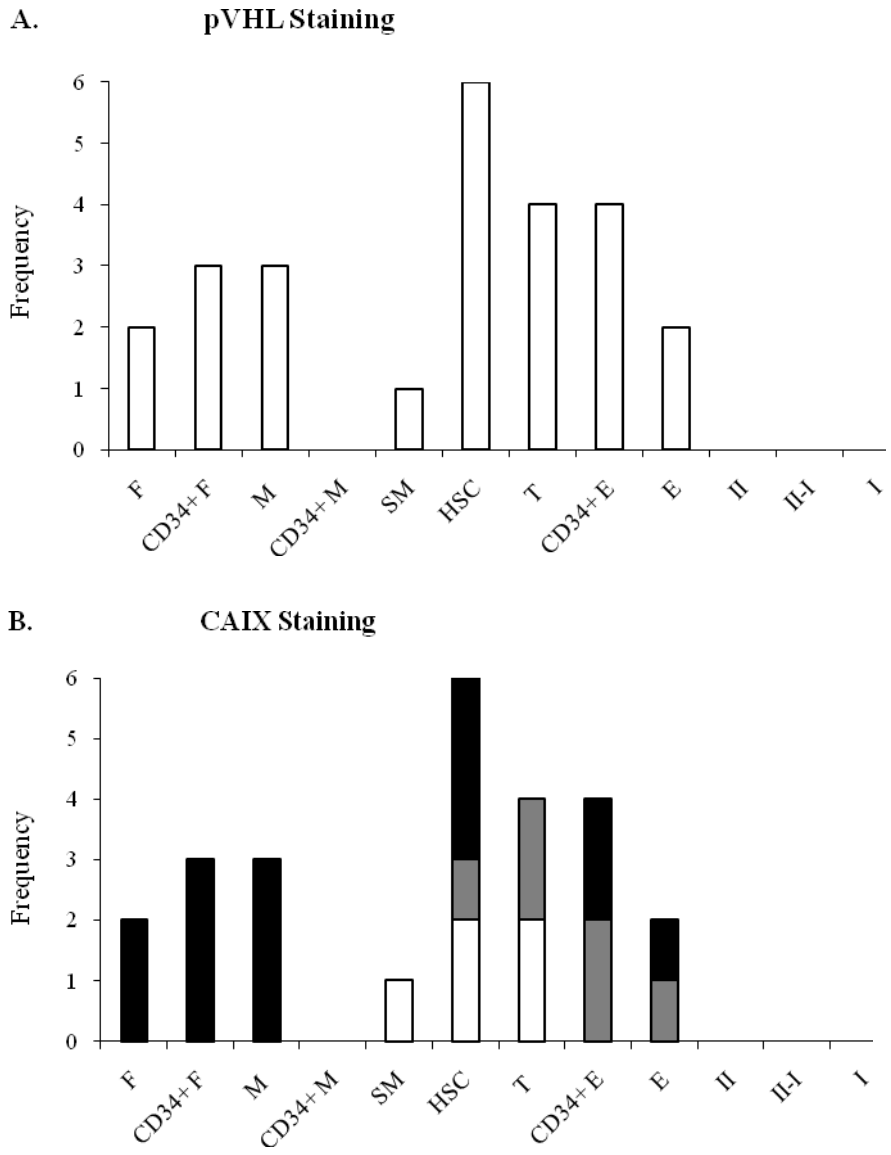

Graphs to show the cell types which stained for pVHL and CAIX in the FBLoV of COPD fibrotic lesions (n=6). Graph A shows the pVHL staining of each cell type within the region. Graph B shows the CAIX profile of each cell type within the region. The size of the bar represents the frequency of lesions in which each cell type was present, and the formats represent the staining profile. White represents all negative, Black all positive and grey mixed (see M&M and appendix for more details). F: Fibroblasts, M: Myofibroblasts, SM: Smooth Muscle, HSC: Haematopoietic stem cells, T: T lymphocytes, E: Endothelium, II: Type II pneumocytes, II-I: Differentiating Type II pneumocytes, I: Type I pneumocytes

Figure 4.3 CAIX and pVHL Staining in the VFB of COPD Lesions

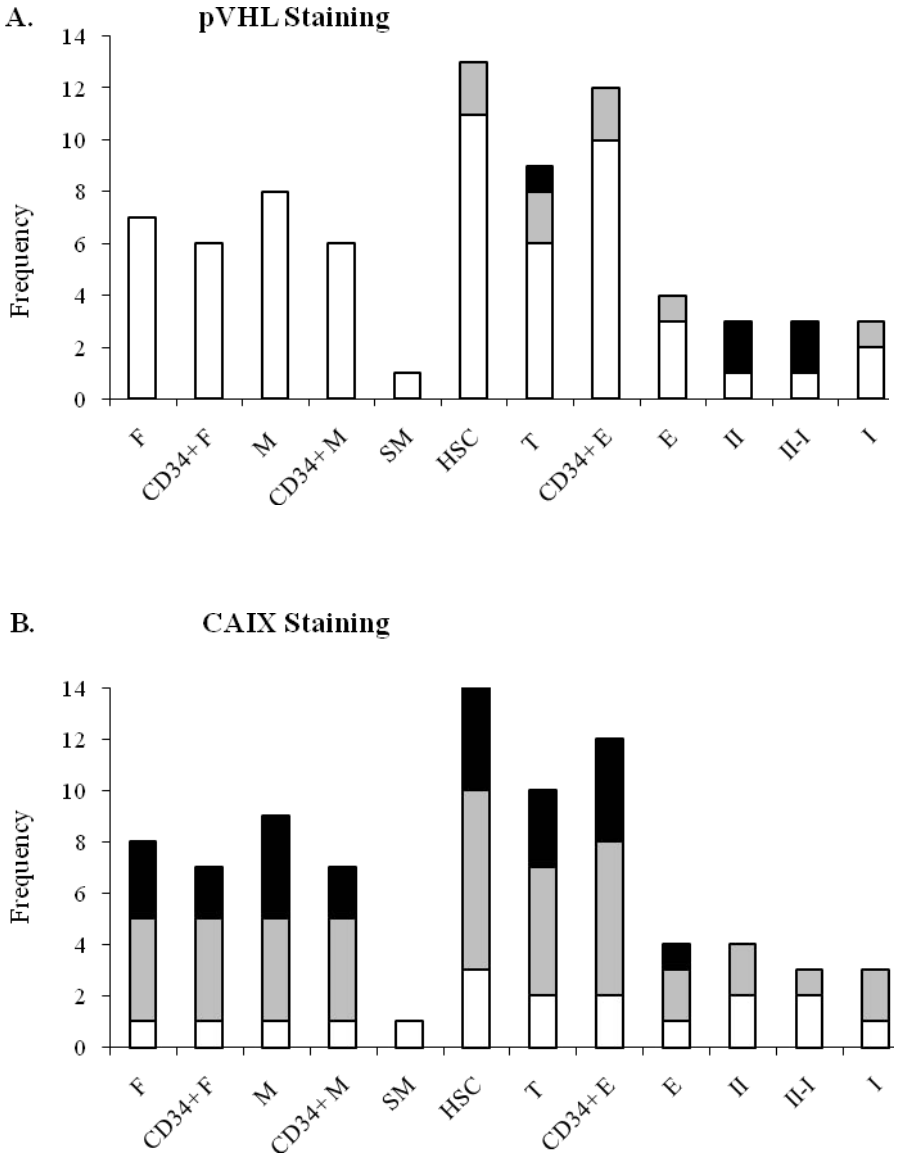

Graphs to show the cell types which stained for pVHL and CAIX in the VFB of COPD fibrotic lesions. Graph A shows the pVHL staining of each cell type within the region (n=13). Graph B shows the CAIX profile of each cell type within the region (n=14). The size of the bar represents the frequency of lesions in which each cell type was present, and the formats represent the staining profile. White represents all negative, Black all positive and grey mixed (see M&M and appendix for more details). F: Fibroblasts, M: Myofibroblasts, SM: Smooth Muscle, HSC: Haematopoietic stem cells, T: T lymphocytes, E: Endothelium, II: Type II pneumocytes, II-I: Differentiating Type II pneumocytes, I: Type I pneumocytes

Figure 4.4 CAIX and pVHL Staining in the Edge of COPD Lesions

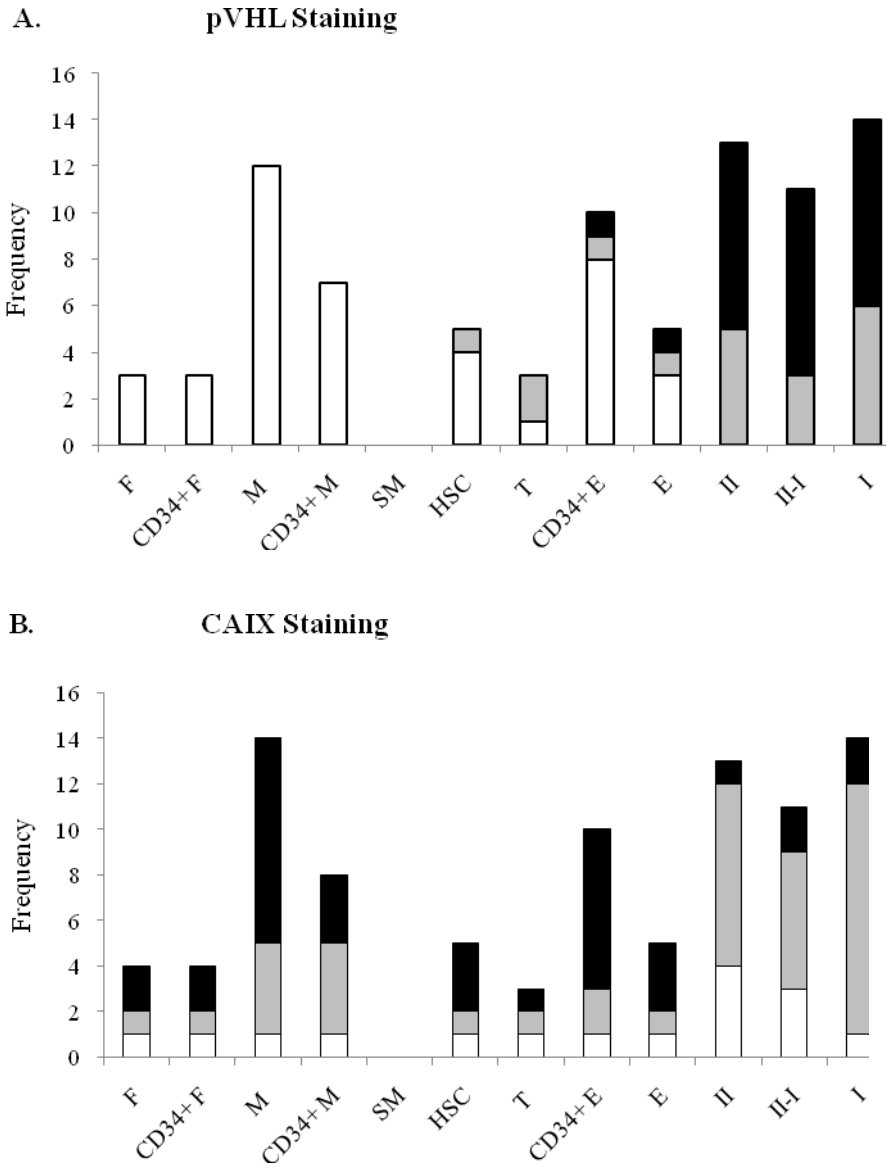

Graphs to show the cell types which stained for pVHL and CAIX in the edge of COPD fibrotic lesions (n=17). Graph A shows the pVHL staining of each cell type within the region. Graph B shows the CAIX profile of each cell type within the region. The size of the bar represents the frequency of lesions in which each cell type was present, and the formats represent the staining profile. White represents all negative, Black all positive and grey mixed (see M&M and appendix for more details). F: Fibroblasts, M: Myofibroblasts, SM: Smooth Muscle, HSC: Haematopoietic stem cells, T: T lymphocytes, E: Endothelium, II: Type II pneumocytes, II-I: Differentiating Type II pneumocytes, I: Type I pneumocytes

Figure 4.5 pVHL Staining in the AZ of IPF Lesions

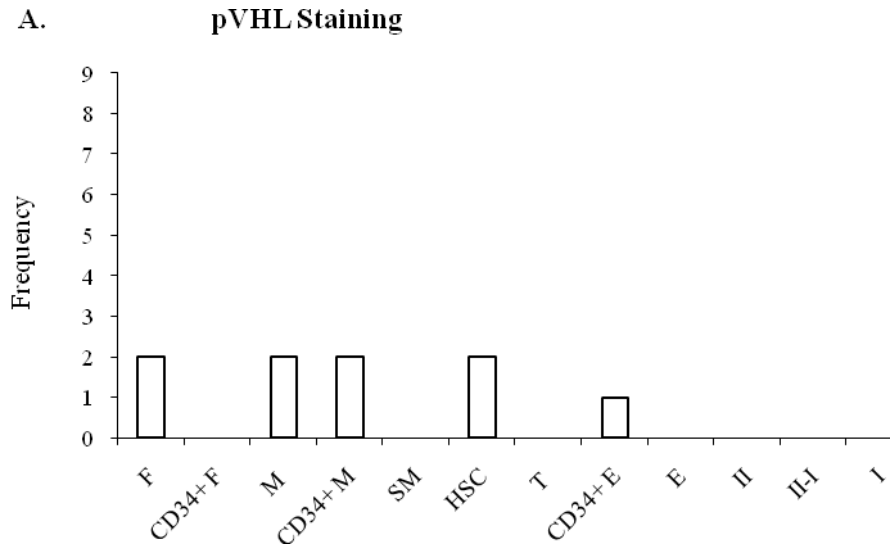

Graphs to show the cell types which stained for pVHL in the AZ of IPF fibrotic lesions (n=9). The graph shows the pVHL staining of each cell type within the region. The size of the bar represents the frequency of lesions in which each cell type was present, and the formats represent the staining profile. White represents all negative, Black all positive and grey mixed (see M&M and appendix for more details). F: Fibroblasts, M: Myofibroblasts, SM: Smooth Muscle, HSC: Haematopoietic stem cells, T: T lymphocytes, E: Endothelium, II: Type II pneumocytes, II-I: Differentiating Type II pneumocytes, I: Type I pneumocytes

Figure 4.6 CAIX and pVHL Staining in the FB of IPF Lesions

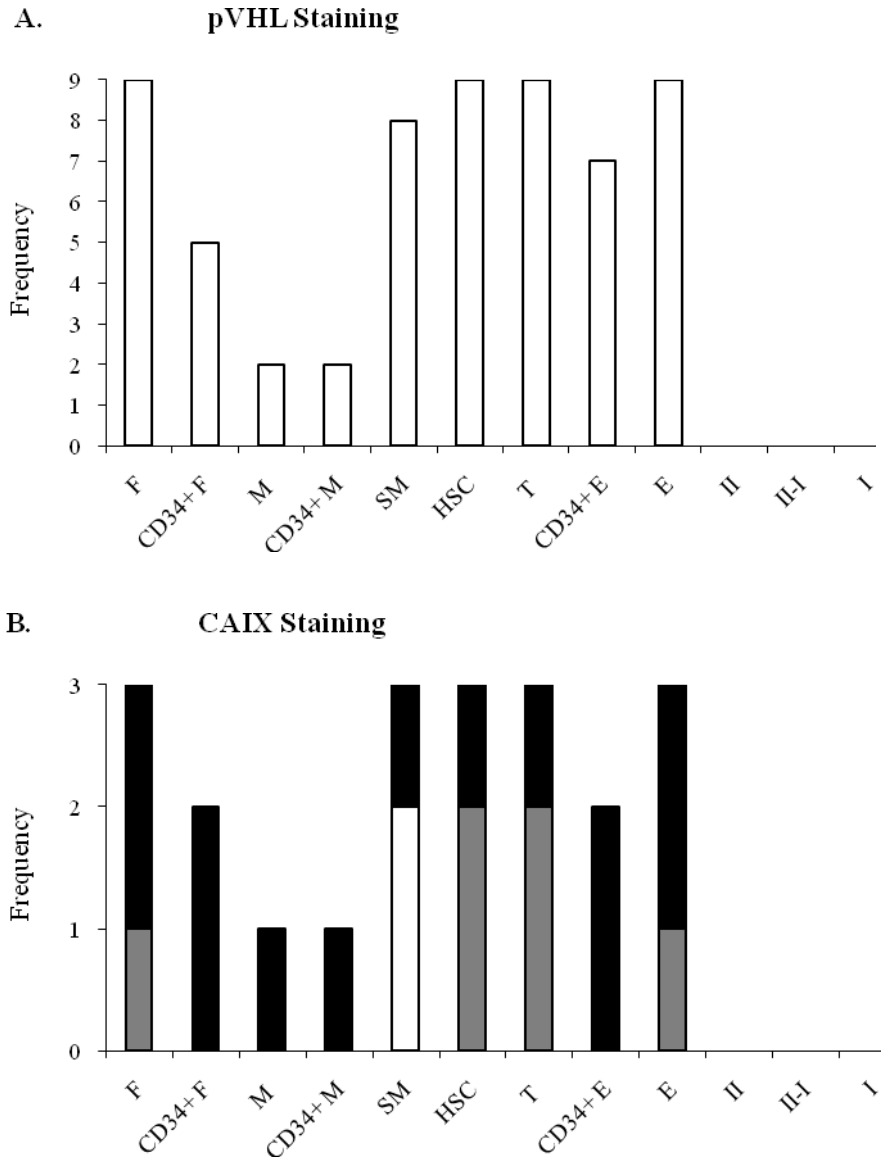

Graphs to show the cell types which stained for pVHL and CAIX in the FB of IPF fibrotic lesions. Graph A shows the pVHL staining of each cell type within the region (n=9). Graph B shows the CAIX profile of each cell type within the region (n=3). The size of the bar represents the frequency of lesions in which each cell type was present, and the formats represent the staining profile. White represents all negative, Black all positive and grey mixed (see M&M and appendix for more details). F: Fibroblasts, M: Myofibroblasts, SM: Smooth Muscle, HSC: Haematopoietic stem cells, T: T lymphocytes, E: Endothelium, II: Type II pneumocytes, II-I: Differentiating Type II pneumocytes, I: Type I pneumocytes

Figure 4.7 CAIX and pVHL Staining in the Edge of IPF Lesions

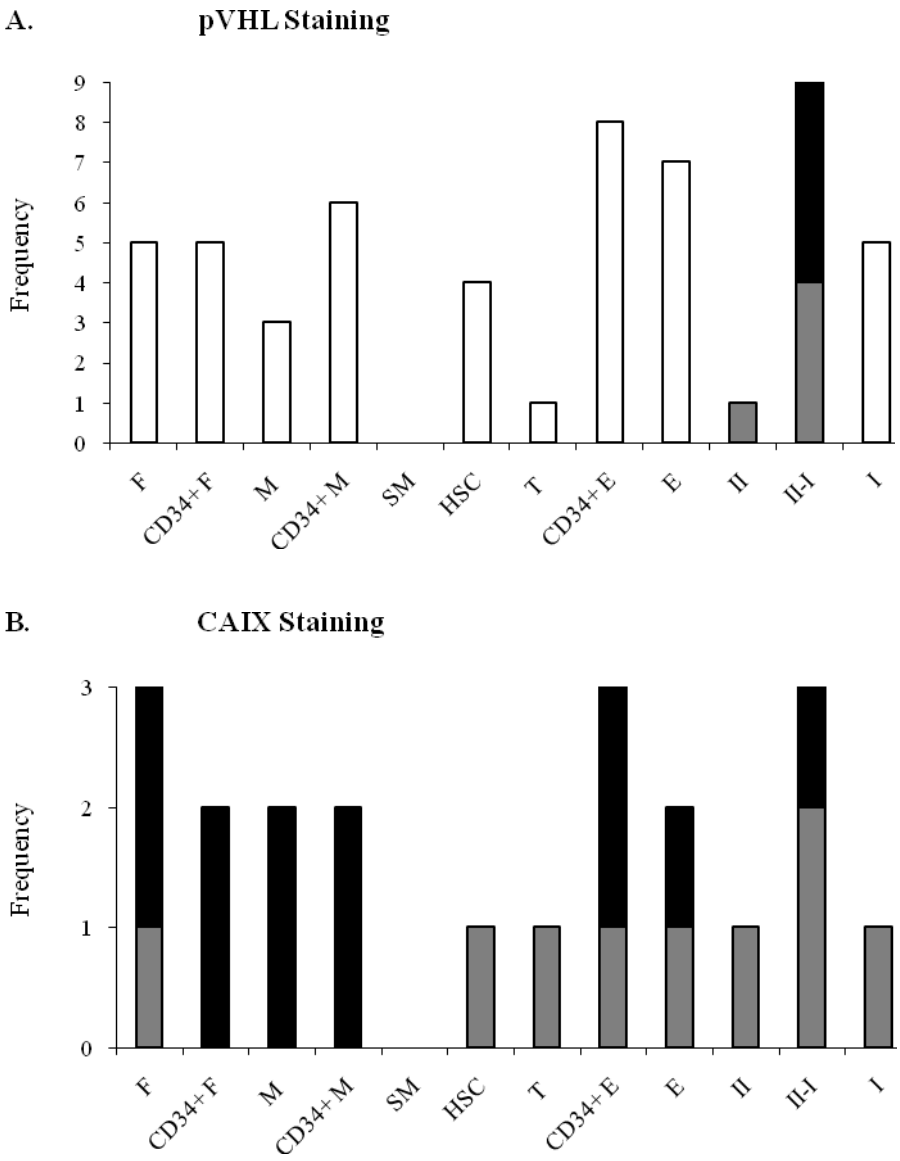

Graphs to show the cell types which stained for pVHL and CAIX in the edge of IPF fibrotic lesions. Graph A shows the pVHL staining of each cell type within the region (n=9). Graph B shows the CAIX profile of each cell type within the region (n=3). The size of the bar represents the frequency of lesions in which each cell type was present, and the formats represent the staining profile. White represents all negative, Black all positive and grey mixed (see M&M and appendix for more details). F: Fibroblasts, M: Myofibroblasts, SM: Smooth Muscle, HSC: Haematopoietic stem cells, T: T lymphocytes, E: Endothelium, II: Type II pneumocytes, II-I: Differentiating Type II pneumocytes, I: Type I pneumocytes

Figure 4.8 CAIX and pVHL Staining in Control Tissue

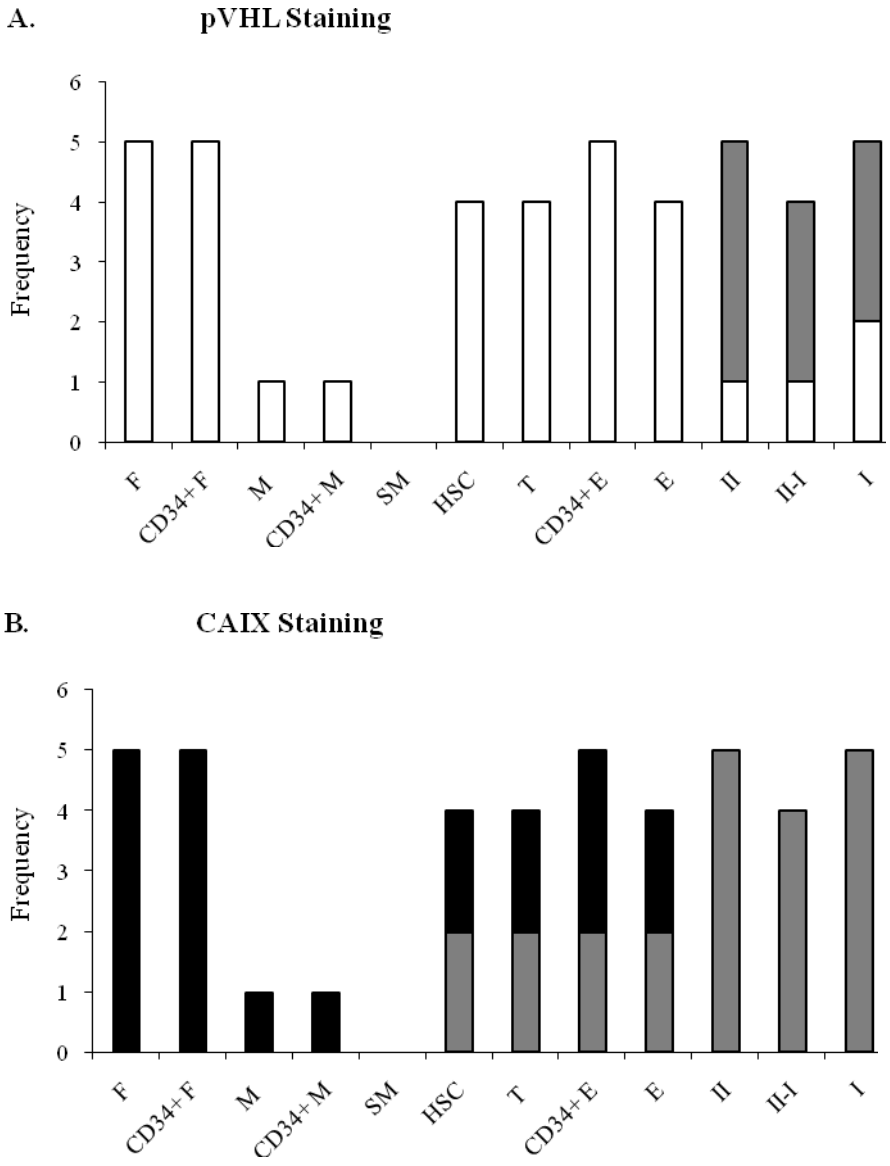

Graphs to show the cell types which stained for pVHL and CAIX in the non fibrosed control tissue. Graph A shows the pVHL staining of each cell type within the region (n=5). Graph B shows the CAIX profile of each cell type within the region (n=5). The size of the bar represents the frequency of lesions in which each cell type was present, and the formats represent the staining profile. White represents all negative, Black all positive and grey mixed (see M&M and appendix for more details). F: Fibroblasts, M: Myofibroblasts, SM: Smooth Muscle, HSC: Haematopoietic stem cells, T: T lymphocytes, E: Endothelium, II: Type II pneumocytes, II-I: Differentiating Type II pneumocytes, I: Type I pneumocytes

Figure 4.9 Cytoglobin, CAIX and pVHL Staining in an IPF Fibrotic Lesion

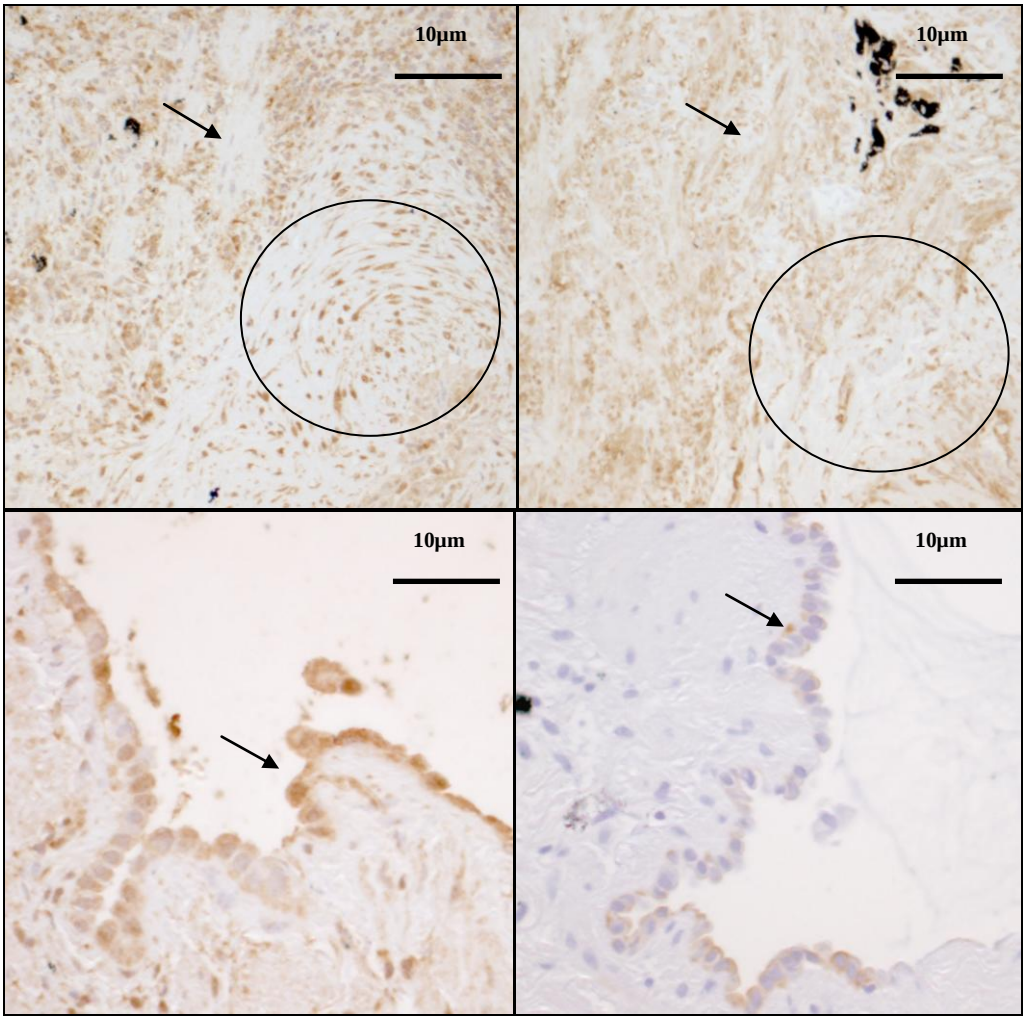

Photographs to show cytoglobin (top and bottom left), CAIX (top right) and pVHL (bottom right) staining in an IPF lesion. The arrows in the top pictures highlight muscle blocks in the fibrosing border, and the circles highlight the AZ region. The arrows in the bottom pictures highlight type II pneumocytes. Pictures are 40% of original size, and were taken at x20 magnification.

4.4.1.4 Correlating Cytoglobin Staining with the Loss of Vascularity

All cells were CYGB positive in regions of avascularity such as the AZ of IPF and COPD lesions. The fibrosing border of COPD lesions were grouped according to vascularity and it was evident that in avascular fibrotic borders (FBLoV) all cells were CYGB+ whilst in fibrotic borders with vascularity a mixed CYGB profile was seen in some cell types (see chapter 3 for more details). At the fibrotic edge of IPF and COPD lesions and in non fibrosed control tissue where the microvascular was intact a mixed CYGB profile was more frequently observed. A mixed CYGB profile correlated to lesions with higher levels of vascularity.

4.4.2 Cytoglobin as a Marker of Fibrosis

During fibrosis there is an increase in proliferation, inflammation, repair, deposition of extracellular matrix and angiogenesis. Makers for each of these were used to characterise each of the fibrotic lesions and or lesion areas analysed in chapter 3. The CYGB expression profile of cells which showed variability in chapter 3 were compared to the profile of these markers to determine whether there was a relationship between the characteristic of the lesion and the CYGB profile.

4.4.3 Correlating Variations in Cytoglobin Expression with Fibrotic Severity of the Lesion in COPD and IPF

The Ashcroft scoring system was used to determine the extent of fibrosis within each lesion and Sirius red and collagen I staining were used as markers of collagen deposition. The CYGB expression data was ordered according to the Ashcroft score for the lesion or grouped according to the lesion score for collagen (grouped according to grade) or Sirius red (3 groups

according to grades: 1-2, 3 or 4-5), to determine whether specific CYGB profiles correlated with fibrotic scores.

In the VFB and edge of COPD lesions the variations observed in the CYGB profile in HSCs, endothelial cells and T-lymphocytes or type II pneumocytes and type I pneumocytes respectively showed no correlation with the Ashcroft, Sirius red or collagen scores. At the edge of IPF lesions there was no definitive correlation between the Ashcroft, Sirius red or collagen scores and CYGB profile in type II pneumocytes. However, all lesions with a score of 4 or higher for Sirius red, corresponding to deposition of large collagen fibres, and acellularity had an all positive CYGB expression profile.

4.4.4 Cytoglobin as a Marker of Pneumocyte-Mediated Alveolar Repair

In response to fibrogenic insult, the lung presents with repair mechanisms including increased density of type II pneumocytes and increased differentiation of type II to type I pneumocytes. Cytokeratin was used as a marker of differentiation of type II pneumocytes.

The type II pneumocytes observed in IPF tissue were larger than those in COPD tissue, and frequently showed co-localisation with CK in all type II pneumocytes at the edge, indicating differentiation into the type I phenotype. Co-localisation of CK was observed in COPD tissue but was never observed in all cells at the lesion edge. COPD lesions which did not present with CK staining in pneumocytes at the edge, had a mixed CYGB profile at the fibrotic edge, in Type I, Type II and differentiating type II pneumocytes (n=8). Where CK+ type II pneumocytes were most abundant at the edge lesion, indicating a high level of repair, type I, type II and differentiating type II pneumocytes were predominantly CYGB+ (n= 5).

Figure 4.10 Cytoglobin Expression in Pneumocytes

A. Cygb Expression in COPD Pneumocytes

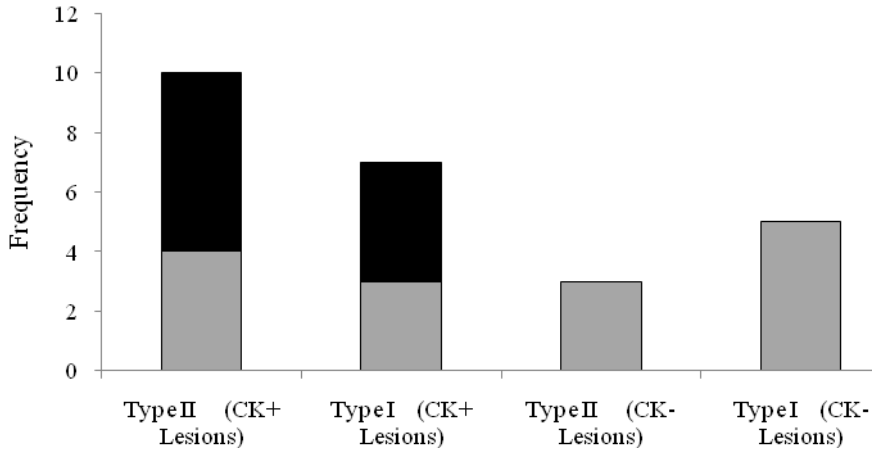

B. Type I pneumocytes in IPF Lesions

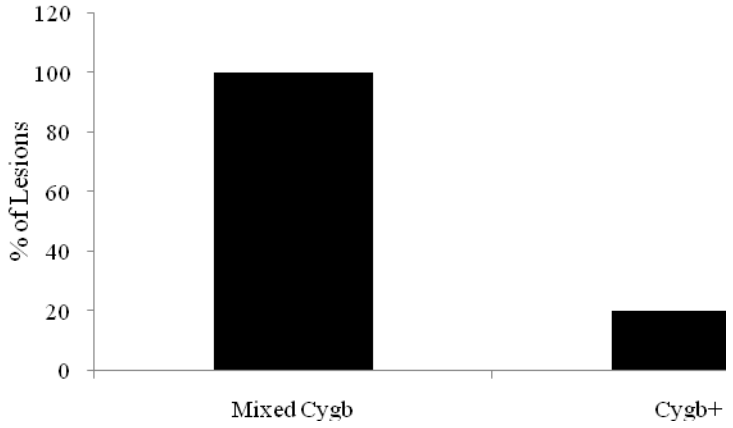

Graph A. The expression profile of CYGB in type I and type II cells at the edge of COPD lesions. Data is grouped according to the CK profile of type II cells at the edge of the lesion. The size of the bar corresponds to the number of lesions in which each cell type was present. The formats represent the CYGB profile. Grey: mixed profile, Black: all cell CYGB+. Graph B shows relationship between the CYGB expression profile of type II pneumocytes and presence of type I pneumocytes at the IPF lesion edge. The bar represents the % of IPF lesions with the relevant CYGB profile which presented with type I pneumocytes at the lesion edge

CK+ type pneumocytes were the predominant cell type at the edge of all IPF lesions. The CYGB profile of these cells varied, either a mixed CYGB profile or CYGB+ profile was observed. It was noted that 80% of the IPF lesions with a CYGB+ profile in type II pneumocytes were lacking in type I pneumocytes (n=5), whilst type I pneumocytes were observed at the edge of lesions with a mixed CYGB+ profile (n=4). Additionally lesions without type I pneumocytes and with a CYGB+ profile in type II pneumocytes had high sirius red scores.

4.4.5 Cytoglobin as a Marker of Proliferation, Inflammation, Angiogenesis and Stem Cell Mediated Repair

PCNA was used a marker of proliferation, CD3 and MAC387 were used as markers of inflammation, cross reactivity of CD31 and PCNA was used as a marker of angiogenesis and co-localisation of c-kit and CD34 were used as markers of stem cells. Each region of every lesion was given a score corresponding to the density of each of these markers (see appendix for scores), as described in chapter 3. As described earlier this was correlated to CYGB expression.

The cell populations which stained for each of these markers were both CYGB positive and negative. There was no correlation between the expression profile of CYGB and distribution of these markers.

4.4.6 Cytoglobin as a Marker of Vascular Remodelling

CYGB expression was observed in the endothelium, media and adventisia of the vasculature. The staining in the media was variable, from weak and sparse to dense and strong. The level of damage to the vessel was assessed and a score assigned. The staining of desmin and vimentin was compared to that of CYGB to determine the source of the CYGB signal, and the relationship with remodelling.

The vimentin positive cells were CYGB positive in all COPD, IPF and control blood vessels. Variations in intensity of the CYGB signal mimicked that of vimentin, in that vessels presented with strong staining for both or neither. The vessels with a high score indicating severe remodelling, presented with stronger CYGB staining than those with lower scores

Figure 4.11 Cytoglobin and Vimentin Staining in Remodelled Vessels

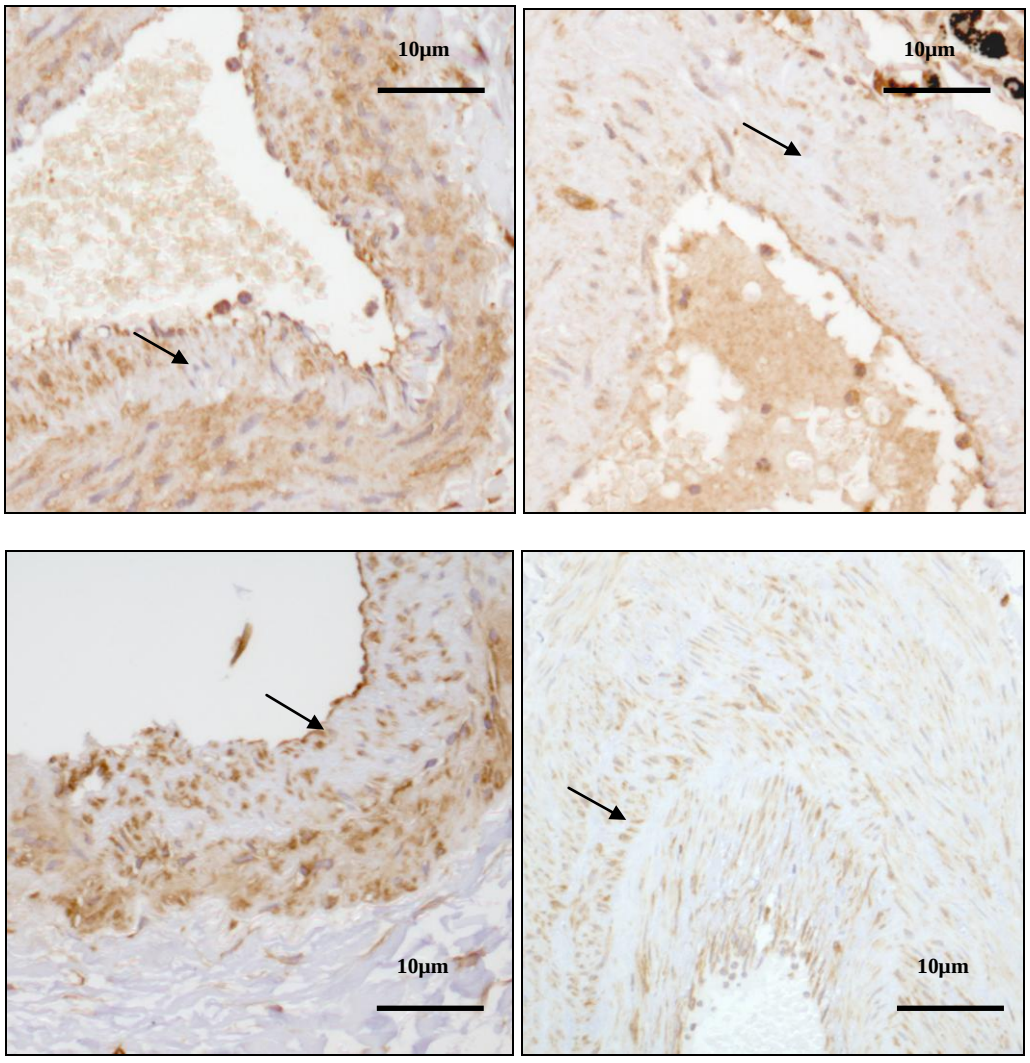

Pictures to show CYGB (Top) and Vimentin (Bottom) staining in severely (left) and moderately (right) damaged COPD vessels. Arrows highlight areas which are negative for these 2 stains but stained positively for desmin. Pictures were taken at x20, and are 40% of the original size.

4.5 Discussion

4.5.1 Hypoxia and the Fibrotic Lesion

Fibrogenesis involves many processes which are activated via hypoxic pathways, such as collagen synthesis, apoptosis, angiogenesis, proliferation and inflammation (Higgins 2008, Jain 2005). Hypoxia is subsequently thought to be related to fibrotic pathogenesis.

pVHL and CAIX were used a markers of non hypoxia, and HIF-1α activity respectively. HIF-1α is the key modulator of the cellular hypoxia response, and its activity is known to increase in response to hypoxia, resulting in an increase in CAIX expression. HIF-1α also responds to non hypoxic stimuli however so detection of HIF-1α activity via CAIX does not exclusively represent hypoxic activation of HIF-1α. Cells with CAIX- and, or pVHL+ phenotypes are subsequently likely to be non-hypoxic. This phenotype was frequently observed at the lesion edge, and thus it is likely that cells in this area are non hypoxic. Within the lesion pVHL immunoreactivity was lost from the fibrotic border and AZ regions. The CAIX- phenotype was observed within the VFB of COPD lesions, but was less frequent in the FBLoV and AZ of COPD lesions, and the FB and AZ of IPF lesions. This non hypoxic phenotype is subsequently lost further into the lesion where the fibrosis becomes more severe. The CAIX and pVHL expression profiles support a model of a non-hypoxic fibrotic border with increasing hypoxia into the centre of the lesion. A loss of vascularity within the lesion was also observed in this study. Avascularity is likely to contribute to the onset of hypoxia, adding further support to this model.

4.5.2 Cytoglobin as a Marker of Hypoxia

Cells at the edge of IPF and COPD lesions presented predominantly with a mixed CYGB profile, and this was the area which was the least immunoreactive with CYGB. The centre of the lesion was CYGB positive in all cells. Assuming, as indicated by the vascularity and pVHL and CAIX expression profile of the lesion, that the edge is non hypoxic, whilst the centre of the lesion is hypoxic, these data support a model in which CYGB is expressed in the lesion in response to hypoxic stimuli, as in regions where non hypoxia is evident, there is less expression than regions where there is no evidence of non hypoxia. In support of this a mixed CYGB expression profile was observed in lesions, and lesion regions, with relatively high vascularity, whilst a CYGB+ phenotype was more readily observed in lesions, or lesion regions which presented with avascularity.

Should CYGB expression be exclusively induced by hypoxia, an increase in the pVHL+ phenotype, representing non hypoxia, would be expected to correlate with a mixed CYGB expression profile, representing a decrease in CYGB expression. In contrast to this model there was no evidence to show a correlation between the pVHL+ profile and a mixed CYGB expression profile. This could indicate that an increase in non hypoxia, or conversely a decrease in hypoxia is not related to CYGB expression. However, CYGB expression is in part controlled by HIF-1α activity (see general introduction), which responds to both hypoxic and non hypoxic stimuli. In regions of pVHL+ phenotypes and thus non-hypoxia, CYGB expression could be as a consequence of non hypoxic stimuli. In support of this, cells which showed CAIX immunoreactivity, which is induced in response to non hypoxic stimuli, were also CYGB positive. CYGB frequently showed a higher level of staining than CAIX, the

lesions in which this was observed all had a pVHL+ edge. One could speculate that an all pVHL+ edge is indicative of a lower level of hypoxia within the lesion, as the edge is assumed to all be non-hypoxic, whereas lesions with a mixed pVHL+ profile where the edge is unlikely to be exclusively non-hypoxia, could be assumed to have a higher level of hypoxia within the lesion. Should this be the case, CYGB expression was shown to exceed than of CAIX in lesions with less hypoxia, thus it could be speculated that CYGB upregulation precedes that of CAIX in response to hypoxia. In *vitro* studies would be required to support this.

Also of note, CAIX expression was observed in smooth muscle cells which were consistently negative for CYGB. The hypoxic response in smooth muscle is likely to differ due to myoglobin expression.

Several papers in the literature present evidence that CYGB protein and mRNA is induced in *vivo* in response to hypoxia (Hankeln *et al.*, 2004; Li *et al.*, 2007; Mammen *et al.*, 2006; Schmidt *et al.*, 2004), a model which is substantiated by this study. Studies into CYGB expression and hypoxia in *vivo* have predominantly subjected rodents to varying degrees of hypoxia and determined the changes in CYGB expression compared to normoxic controls. As yet there are not any reports relating expression of CYGB in response to non hypoxic activation of HIF-1α.

4.5.3 Cytoglobin as a Marker of Fibrosis

These data presented here argue against a role of CYGB as a marker of proliferation, inflammation, angiogenesis or stem cell mediated repair. A slight correlation was observed between the level of ECM deposition and CYGB expression. Whether this is causative or consequential remains to be determined. In the literature, over-expression of CYGB reduced differentiation of fibroblasts into an active myofibroblast phenotype, as characterised by expression of TIMP-1 and TGF-β1 mRNA and a reduction in the levels of collagen production was observed (Xu *et al.*, 2006). It could be interpreted from the study by Xu *et al* that CYGB expression inhibits expression of collagen, which could contradict the observations made in this study. Potentially in the study by Xu *et al*, CYGB offers cytoprotection which prevents the induction of collagen expression, however in vivo, the threshold of this cytoprotection could be surpassed, and thus collagen and CYGB expression are observed simultaneously.

A correlation between an increase in type II pneumocyte to type I pneumocyte differentiation in COPD and CYGB expression was observed in this study. The predominant contributor to COPD is smoking which induces oxidative damage via reactive oxygen species (ROS). Potentially differentiation of type II pneumocytes could be indicative of this oxidative damage. HIF-1α activity and CYGB expression have previously been shown to increase in response to ROS. It could be speculated therefore that type II pneumocytes express CYGB as a cytoprotective response to smoke mediated oxidative damage.

A similar model could be proposed in the IPF lesion where the absence of type I pneumocytes correlated with a CYGB+ expression profile. One could speculate a loss of type I

pneumocytes is representative of excessive injury, in response to which type II pneumocytes express CYGB.

4.5.4 Cytoglobin as a Marker of Vascular Remodelling

Evidence of the absence of CYGB staining in smooth muscle cells was presented in chapter 3, further substantiation of this is presented here as CYGB expression was consistently negative in desmin positive cells of the vessel wall.

CYGB expression paralleled that of vimentin in the vessel wall. Morphologically, these cells are likely to be fibroblasts, which are thought to play a critical role in vascular remodelling. Hypoxia may increase proliferation, ECM deposition, production of mitogenic factors and differentiation of fibroblasts of the vessel wall and adventisia (Pak *et al.*, 2007) subsequently contributing to vascular remodelling. Expression of CYGB within the mesenchymal element of vascular remodelling could be in response to such hypoxic stimuli.

Potentially CYGB expression could increase the capacity of the cell to extract oxygen from the local hypoxic environment to enable efficient cell function and vessel remodelling.

CHAPTER 5: CYTOPROTECTION OF CYTOGLOBIN AGAINST HYDROGEN PEROXIDE INDUCED OXIDATIVE STRESS

5.1 Introduction

There is contradictory evidence surrounding the role of cytoglobin (CYGB) in cytoprotection against oxidative stress (see general introduction), and the function of CYGB during cellular adaptation to this toxic insult remains unclear. Studies have shown CYGB to possess antioxidant enzymatic activity, including peroxidase (Kawada *et al.*, 2001)(Trandafir *et al.*, 2007) whilst others found no evidence to support this (Trandafir *et al* 2007). CYGB expression has been shown to reduce oxidative stress *in vitro* ((Fordel *et al.*, 2006; Hodges *et al.*, 2008; Powers, 2006) and CYGB expression was observed in regions of high oxidative damage *in vitro* (Fordel *et al.*, 2006)

5.2 Aim

The overall aim of this chapter was to add to the current understanding of the possible role of CYGB in cytoprotection against oxidative stress. In particularly we tested the hypothesis that the putative peroxidase activity of CYGB would be protective against H_2O_2 induced oxidative stress

The specific objectives were:

- To determine a concentration range of H_2O_2 which would induce oxidative stress, but not affect cell viability
- To use a CYGB over expressing HEK293 cell line, and a control HEK293 cell line as an *in vitro* model to investigate possible cytoprotection of CYGB over-expression against H_2O_2 induced oxidative stress, using DNA damage and cell death as end points.

5.3 Methods

5.3.1 Preparation of Nuclear and Cytoplasmic Proteins

Cells were cultured in T_{75} flasks, media was aspirated and the cells washed in warm PBS. The cells were scraped into 1ml PBS, and centrifuged at room temperature, 8000 rpm for 3 minutes to collect the cells. The supernatant was aspirated, the pellet re-suspended in 500 µl ice cold buffer A (0.6 % (v/v) NP-40, 150 mM NaCl, 10 mM Tris pH 8, 1 mM Na_2EDTA, 10 µl/ml protease inhibitor), and incubated on ice for 20 minutes, vortexing at 5-minute intervals. The suspension was then centrifuged at 4˚C, 4000 rpm for 10 minutes. The supernatant (100 µl) was aspirated from the pellet and kept on ice, the rest of the supernatant was discarded. The pellet was then washed 3 times by re-suspension in 200 µl ice cold buffer A, centrifugation (4˚C, 4000 rpm, 10 minutes) and removal of the supernatant by aspiration. Following the final wash the pellet was re-suspended in 50 µl buffer B (25 % (v/v) glycerol, 450 mM NaCl, 20 mM Tris pH 8, 0.2 mM Na_2EDTA, 1.5 mM $MgCl_2$, 0.5 mM DTT (Dithiothreitol), 10 µl/ml protease inhibitor) and incubated on ice for 30 minutes, vortexing at 5 minute intervals. Both samples were then centrifuged at 15,000 rpm and 4˚C for 20 minutes. The supernatant of both these samples was then removed and used immediately or stored at -80˚C.

5.3.2 Analysis of Hemoprotein by Spectroscopy

CYGB is a heme protein, and correct incorporation of heme is required for function. Spectroscopy was used to determine the presence of hemoprotein within the CYGB+ cell line compared to the control, HEK293 cell line. Cells were cultured in 75 cm^2 flasks as described previously, media was aspirated and the cells washed with PBS, prior to scraping into 4 ml PBS. Protease inhibitors (10 µl/ml) were then added to the cell suspension, prior to homogenisation on ice. 1ml samples of each cell type were placed into 2 cuvettes with approximately 10 mg of sodium dithionite. Sodium dithionite reduces the iron in the heme

enabling it to bind irreversibly with CO. CO was generated by reacting concentrated HCl and sodium formate and the generated CO was bubbled through one of the 2 cell samples**,** before a difference wavelength scan was taken using a U-3010 Spectrophotometer.

5.3.3 Measuring Oxidative Stress using Fluorescent Dyes

Intracellular dyes cis-PnA (cis-parinaric acid: 9,11,13,15-cis-trans-trans-cis-octodecaeonic acid: Molecular Probes) and DCFH-DA (2',7'-dichlorofluorescin diacetate) were used to assess the level of lipid peroxidation and oxidative stress respectively within HEK293 and CYGB+ cells. Cis-PnA is a fluorescent, 18-carbon poly-unsaturated fatty acid, which once incorporated into cellular membranes irreversibly loses fluorescence upon oxidation. This characteristic enables its use as a probe to evaluate oxidative stress within the cell as the reduction of fluorescence can be used to represent an increase in lipid peroxidation (Gomes *et al.*, 2006). DCFH-DA readily diffuses across the cell membrane into the cell where it is hydrolysed by cellular esterases, to DCFH (2',7'-dichlorofluorescin), which cannot diffuse out of the cell. Oxidation of DCFH by reactive oxygen species, principally H_2O_2, forms the fluorescent product DCF (1,2-dichlorofluororescein), thus an increase in fluorescence represents an increase in oxidative stress (Gomes *et al.*, 2006).

5.3.3.1 cis-Parinaric acid (cis-PnA)

Cells were cultured in 6 well plates, and grown to confluence over 2 days. The media was aspirated and the cells washed with PBS. The cells were incubated with phenol-free DMEM supplemented with the appropriate concentration of H_2O_2 at 37˚C, 5 % CO_2, 95 % air for the

appropriate time period. Following treatment, the media was aspirated off and the cells washed 3 times with PBS, before phenol free DMEM containing 10μM cis-PnA was added to the cells, and cells incubated for 30 minutes at 37˚C, 5 % CO_2, 95 % air. A blank containing no dye was included in all experiments. The cells were then washed, and each sample of cells was resuspended in PBS. The level of fluorescence was measured using a fluorimeter, or fluorimeter plate reader. The excitation and emission were 312nm and 455nm respectively. PBS only blank readings were subtracted from all readings.

5.3.3.2 DCFH-DA

Cells were cultured in 6 well plates, and grown to confluence over 2 days. The media was aspirated and the cells washed with PBS. The cells were incubated with phenol-free DMEM supplemented with 10 μM DCFH-DA for 30 minutes at 37˚C, 5 % CO_2, 95 % air. Following the incubation the media was aspirated off and the cells were washed 3 times with PBS, before phenol free DMEM containing treatments was added to the cells, and they were incubated for the appropriate time period at 37˚C, 5 % CO_2, 95 % air. A blank containing no dye was included in all experiments to control for any endogenous cellular fluorescence. The cells were then washed, and each sample of cells was resuspended in PBS. The level of fluorescence was measured using a fluorimeter, or fluorimeter plate reader. The excitation and emission were 502nm and 520nm respectively. PBS only blank readings were subtracted from all readings.

The Kolmogorov-Smirnov test was used to determine whether the data fitted a normal distribution. As the data didn’t fit a normal distribution the Wilcoxon ranking test, and Mann

Whitney test were used to determine if any effects were significant, for paired and independent data respectively.

5.3.4 The Comet Assay

Cells were cultured and grown to confluence in 6 well plates over 2 days. The media was aspirated and the cells washed with PBS, prior to being replaced with phenol-free media, containing 0-800 µM H_2O_2 and incubated for the 2, 8 or 24 hours.

Following treatment the media was aspirated, the cells washed with PBS, and scraped into 0.5 ml PBS. The cell suspension was centrifuged at 8000 rpm for 5 minutes at room temperature. The supernatant was removed and the pellet re-suspended in 100 µl ice cold phenol free media, 3 µl of the suspension was added to 300 µl LMPA (0.5 % (w/v) low-melting point agarose, dissolved in PBS). Two 150 µl aliquots were taken from each treatment and spread onto two NMPA (0.5% (w/v)) normal-melting point agarose dissolved in PBS) coated microscope slide (BDH, U. K.), and a cover slip was added to each. The microscope slides were prepared 48 hours prior to the assay by cleaning with 70% ethanol before coating with NMPA. Once the LMPA had set, the coverslips were removed and the slides placed into a Coplin jar for 1 hour at 4˚C filled with ice cold complete lysis buffer (2.5 M NaCl, 0.1 M EDTA, 3.33% (v/v) sodium-lauryl-sarcosinate, 10 mM Tris, 0.5 % (v/v) triton-x-100, 5 % (v/v) DMSO pH 10. DMSO and Triton-x100 were added immediately prior to use).

After lysis, the slides were washed, 3 x 5 minutes with FPG enzyme buffer (40 mM HEPES, 0.1 mM KCl, 0.5 mM EDTA, 0.2 mg/µl BSA, pH 8.) 2 slides for each treatment were

prepared and to one of these 1 unit of FPG enzyme in 50 µl FPG enzyme buffer was added, whereas to the other 50 µl FPG enzyme buffer alone was added prior to a coverslip. The slides were incubated in the dark for 1 hour, at 37˚C.

The slides were then incubated in electrophoresis buffer (0.3 M NaOH, 1 mM EDTA) with coverslips removed, for 10 minutes at room temperature, prior electrophoresis for 20 minutes at 25 volts. Following electrophoresis the slides were neutralised by 3 x 5 minute washes with neutralisation buffer (0.4 M Tris pH 7.5). The excess was removed, 50 µl Sybr Gold solution and a coverslip was added to each slide, prior to analysis by inverted fluorescence microscopy (250x magnification, excitation wavelength 515-560 nm, emmision wavelength 590 nm; Zeiss, Germany) using komet image analysis software, version 3 (Kinetic Imaging Ltd. Liverpool, U. K.). 100 cells were counted on each slide. The % tail intensity was used as a relative measurement of DNA breaks. The median from each experiment was taken as the result and the mean of the medians from 5 replicates was used for analysis. The Kolmogorov-Smirnov test was used to determine whether the data fitted a normal distribution. As the data didn't fit a normal distribution the Wilcoxon ranking test, and Mann Whitney test were used to determine if any effects were significant, for paired and independent data respectively.

5.3.5 Assessment of mRNA expression by RT-PCR

The overall principle of RT-PCR is that the RNA within a sample is reverse transcribed to cDNA. Gene specific primers are used to amplify the cDNA through PCR, each cycle of PCR doubles the amount of DNA copies of the gene of interest. This DNA is fluorescently labelled, and so the increase in fluorescence emitted from the sample is proportional to the

amount of cDNA in the reaction, and thus the amount of RNA in the original sample. RNA extraction and quantification methods are summarised in chapter 2.

Data Analysis

An exponential pattern of fluorescence increase is seen due to the principles of PCR. An appropriate threshold level of fluorescence was selected following each PCR run. For each sample the number of cycles (C_T) to reach the threshold, was used for data analysis. The more cycles it takes to reach the threshold, the lower the amount of cDNA within the sample, and vice versa. The C_T Values were used to calculate absolute values. A standard curve with 10 fold increments was made from a cDNA sample known to contain the target cDNA and used to calculate an arbitrary value for the amount of cDNA within each sample. Units 100, 10, 1, 0.1 and so on were used for each concentration on the standard curve. The curve is then used to calculate the 'absolute value' of cDNA within each sample. The amount of target cDNA was divided by the amount of housekeeping cDNA to normalise the data. The normalised values of the treated samples, was then divided by the normalised value of the control sample to determine fold change.

5.3.5.1 One Step RT-PCR

TaqMan® One Step RT-PCR Mix (2.5 µl), CYGB TaqMan (applied biosystems) primers and probes (0.625µl) and DEPC treated water (7.375µl) were pipetted into a TaqMan plate. 5 µl of sample RNA or standard curve RNA was added to each well. A standard curve was made using RNA from a CYGB+ cell line sample and loaded at 100% 10%, 1%, 0.01%, 0.001%, 0.0001%, 0.00001% and 0.000001%. Immediately before use 5 µl TaqMan® RT Enzyme Mix was added. The plate was span at 1000 rpm for 1 minute, and then placed into an Applied Biosystems Real-Time PCR 7500 System.

The programme used was 50^{o}C for 30 minutes; 95^{o}C for 15 minutes; followed by 45 cycles of 94^{o}C for 15 seconds; 57^{o}C for 30 seconds; 76^{o}C for 30 seconds.

The data from the one step RT-PCR was calculated as absolute values. The RNA concentration within each sample was determined using RiboGreen, and used to normalise the data. The data was then presented as % fold change relative to each of the negative control siRNA. In comparing the data to the negative controls this will highlight knockdown which is specific to the presence of TAK-1 positive siRNA. The data did not fit a normal distribution, as determined using the Kolmogorov-Smirnov test and therefore the Wilcoxon's ranking test was used to determine and statistically significant effects

5.4 Results

5.4.1 Characterisation of Cytoglobin Over Expressing HEK293 cells

5.4.1.1 Expression of Functional Cytoglobin in HEK293 cells

AstraZeneca (Charnwood) supplied 4 HEK293 cells lines, one of which was a control cell line, whilst the other 3 had been engineered to over express CYGB. AstraZeneca used retroviral vectors containing cloned human normal brain cDNA to transfect HEK293 cells with the CYGB gene. The CYGB gene was controlled by a CMV promoter and as such was constitutively expressed at high levels. The CYGB over expressing cell lines differed in that they synthesised either an untagged CYGB protein or the CYGB protein with a C or N terminal His Tag.

Whole cell protein was extracted from each of the cell lines, and analysed using western blotting. A polyclonal mouse anti-human CYGB primary antibody (Abnova Taiwan Corporation, Taipei, Taiwan (H00114757-A01)), was used to detect the CYGB protein. An anti- β-actin antibody was used to detect actin, as a positive control.

The western blot (see Figure 5.1(A)), showed a band at the expected size of approximately 20kDa in the untagged cell line, indicating presence of CYGB (Figure 5.1 (A)). The bands on the blot, which correspond to the samples obtained from the cell lines expressing a tagged CYGB protein were at a higher position on the blot than the sample from the cell line expressing the untagged protein, due to the increased the molecular weight caused by the presence of the tag. The western blot showed that in the control cell line CYGB protein expression was not detectable. The actin band was evident within all samples, confirming that protein extraction had been successful. This western blot demonstrates

that the cell lines are expressing the appropriate CYGB protein and that they had not become contaminated.

The purpose of generating His-tagged CYGB protein was that the tag could be used to detect the presence of the CYGB protein, as at the time of engineering a commercial antibody was not available. This western blot however demonstrated that an effective antibody was now available and therefore using the tags would be unnecessary for the purposes of this study. His tagged cell lines were excluded from all further experiments.

CYGB is a heme containing protein, it was therefore essential to confirm that the CYGB present within the CYGB+ cell line was heme bound and not just apoprotein. Heme is known to bind carbon monoxide when reduced by sodium dithionite, producing a diagnostic peak between 400 and 550nm. Analysis by difference spectroscopy revealed a significant peak around 425nm in the CYGB over-expressing cell line (see Figure 5.1 (B)), confirming the presence of heme bound CYGB. This peak was absent in the control cell line, showing that it was specifically derived from the over expressed CYGB protein.

Figure 5.1 Characterisation of the CYGB+ cell line

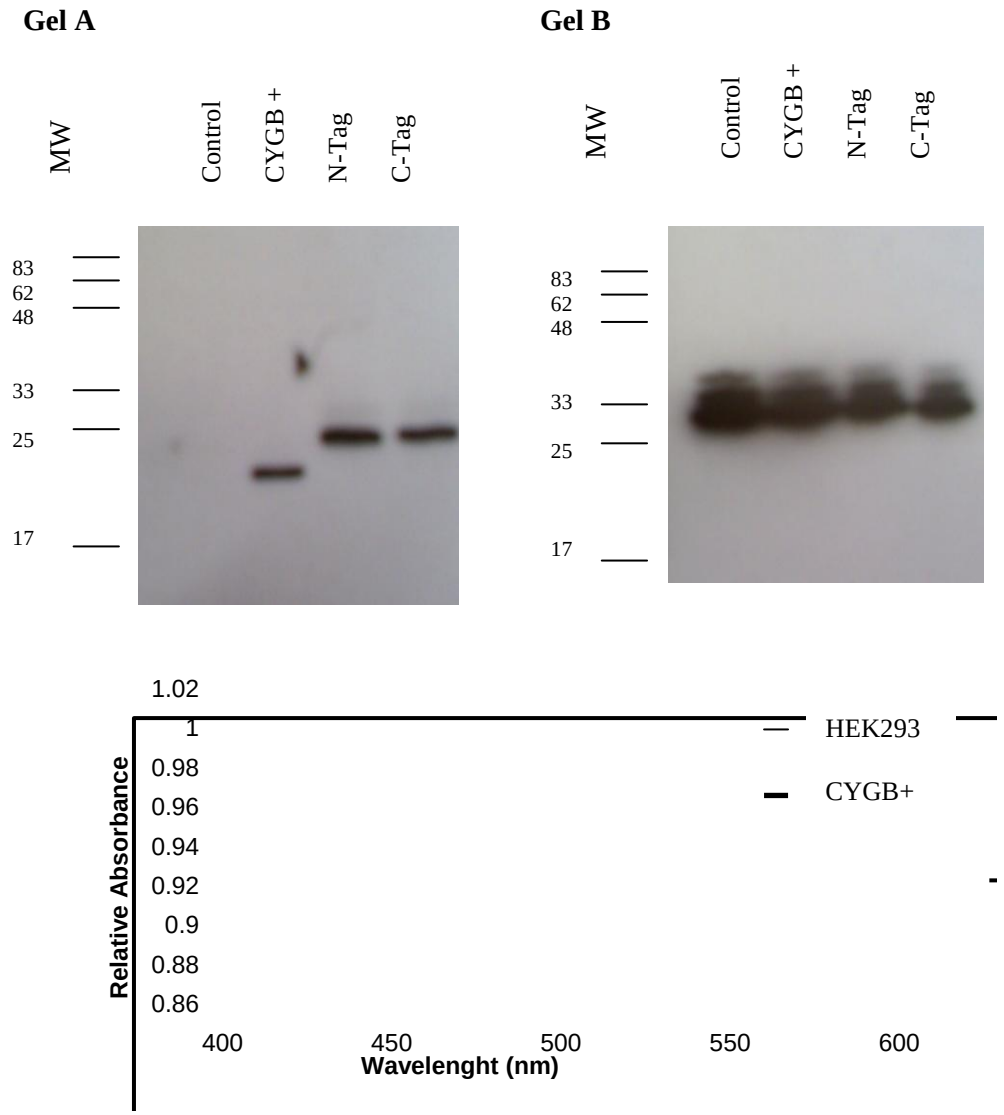

1. Western blot to show which cell lines are expressing CYGB. Gel A shows CYGB antibody binding, at approx 21kDa (0.2mg/ml polyclonal mouse anti-human CYGB primary antibody. Gel B shows An anti- β-actin (Diluted 1:10,000) antibody binding, as a positive control. The lanes on both gels (12% polyacrylamide) contain 20µg of the same samples. A goat anti mouse secondary antibody was used (diluted 1:10, 000) MW: Molecular weight marker Control: Control cell line, CYGB+: CYGB overexpressing cell line, N-Tag: N-terminal tagged CYGB expressing cell line, C-Tag: C-terminal tagged CYGB expressing cell line

2. A graph to show a carbon monoxide difference spectra of HEK293 and CYGB+ cell lines. There is a significant peak in the CYGB+ cell line scan indicating extensive binding of carbon monoxide, and the presence of excessive heme.

5.4.1.2 Subcellular Localisation of Cytoglobin in HEK293 Cells

Cytoplasmic and nuclear extracts from HEK293 and CYGB+ cell lines were analysed in duplicate by western blotting for the presence of CYGB (see Figure 5.2). Lamin was used as a positive control for nuclear material, whilst Actin was used as a positive control for cytoplasmic material.

Western blotting showed bands in the lanes which contained CYGB+ cell cytoplasmic extracts. There was an absence of staining from all other samples. This implies that in this cell line CYGB presence is limited to the cytoplasm. In addition to the western blot, CYGB+ and control HEK293 cells were cultured in 96 well plates. The cells were fixed and stained with an anti CYGB antibody and a fluorescent secondary antibody (see Figure 5.2). The observations made from the fluorescent microscopy supported the western blot data, that CYGB localised exclusively within the cytoplasm and there was no evidence to support nuclear localisation.

Figure 5.2 Subcellular Localisation of Cytoglobin in CYGB+ Cells

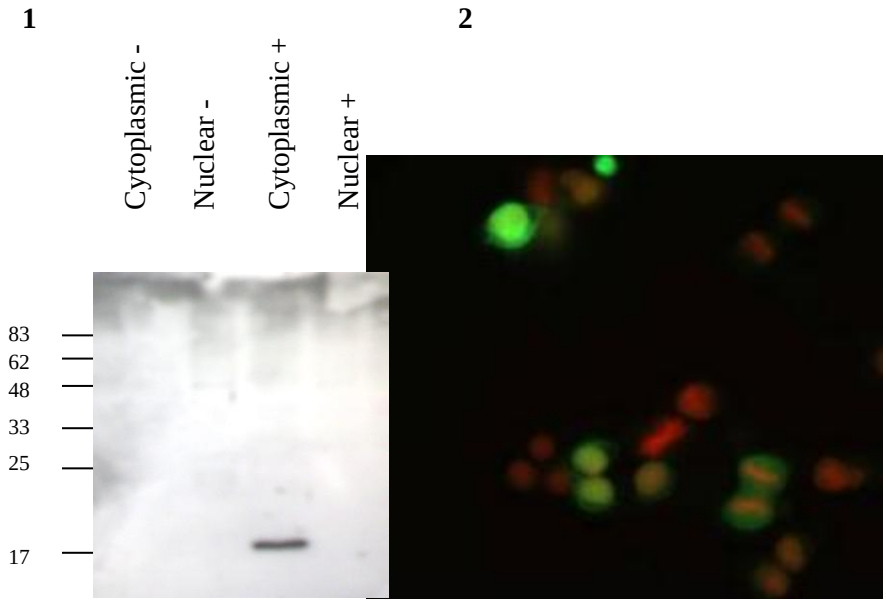

1. A western blot blocked with 20µg/ml polyclonal mouse anti-human CYGB primary antibody. Anti-Lamin A/C (0.4µg/ml) and anti-β-Actin (0.15µg/ml) were used as controls for successful separation of nuclear and cytoplasmic extracts (blot not shown). The labels correspond to the following samples:

Nuclear +	**CYGB+ cell line nuclear extract**
Cytoplasm +	**CYGB+ cell line cytoplasmic extract**
Nuclear -	**HEK293 cell line nuclear extract**
Cytoplasm -	**HEK293 cell line cytoplasmic extract.**

2. A digital photograph of CYGB+ cells. They were lysed before incubating with a mouse anti- human CYGB primary antibody (10µg/ml), followed by an Alexa-488 secondary rabbit and mouse antibody (green). Nuclear staining was achieved using propidium iodide (red).This shows the subcellular localisation of cytoglobin to be cytoplasmic.

5.4.2 Experimental Model Development

The MTT assay was used to determine a hydrogen peroxide concentration range which did not significantly affect cell viability. Fluorescent dyes which detect the levels of reactive oxygen species, and oxidative stress in the form of lipid peroxidation were used to determine the time points for further investigation. From this preliminary data, a range of time points resulting in oxidative stress in the absence cytotoxicity were selected for more detailed analysis

5.4.2.1 Selection of an Appropriate Concentration Range through Assessment of Cell Viability

CYGB+ and HEK293 cells were cultured in 48 well plates and treated with a range of hydrogen peroxide concentrations (0, 200, 400, 600, 800, 1000 µM) for 24 hours and cell viability was assessed using the MTT assay. The MTT assay used followed the optimised protocol described in chapter 5. The data was presented as the relative absorbance (mean % of control).

It can be seen in the Figure 5.3 that there was a concentration dependant decrease in cell viability, however this was not statistically significant. There was a 21.2% (±14.9) and 18.1% (±14.8) decrease between the cell viability of the control and 1000 µM treatment in the HEK293 and CYGB+ cell lines respectively. Although this was not a statistically significant decrease it was indicative of cytotoxicity, so 800 µM was used as the maximum concentration in all further studies.

5.4.2.2 Time Dependant Generation of ROS by Hydrogen Peroxide

CYGB+ and HEK293 cells were cultured in 6 well plates and treated with 0, 200, 400, 600 and 800 µM H_2O_2 for 1, 2, 4, 8, 16 and 24 hours. Prior to treatment DCFH-DA was added as a marker of accumulated intracellular oxidative stress (see 5.3.3 for details). Preliminary data showed that adding cis-PnA resulted in low readings for long time points as the fluorescence was lost over time with oxidative stress. cis-PnA was thus added after treatment to represent the level of lipid peroxidation (see 5.3.3 for details), at that time point. The data of the selected time points is presented in Figure 5.3 as the mean % of control from 3 experimental replicates.

An distinct increase in oxidative stress (not statistically significant) was observed at all time points, as measured by both dyes. 2, 8 and 24 hour treatment times were selected to investigate the potential cytoprotective role of CYGB over expression against H_20_2 induced DNA strand breaks and cell death, using the Comet and MTT assay's respectively.

These data were analysed to determine if CYGB over expression offered any cytoprotection against H_20_2. There was no statistically significant difference between the cell lines in terms of the fluorescence emitted from either dye at any of the time points investigated, representing no difference between the cell lines in the levels lipid peroxidation or accumulation of ROS.

Figure 5.3 Experimental Model Development

A

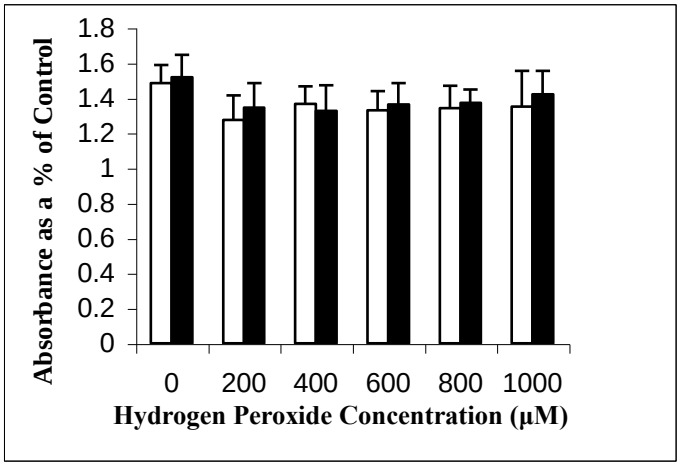

B **DCFH**

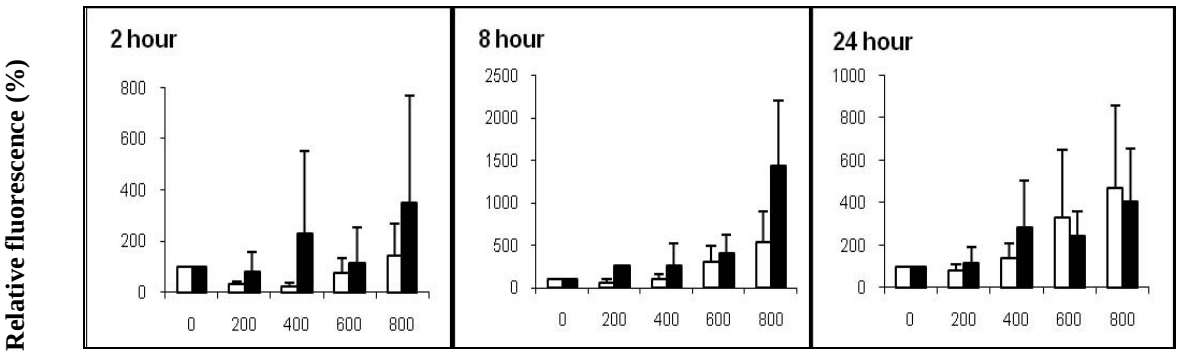

C **Cis PnA**

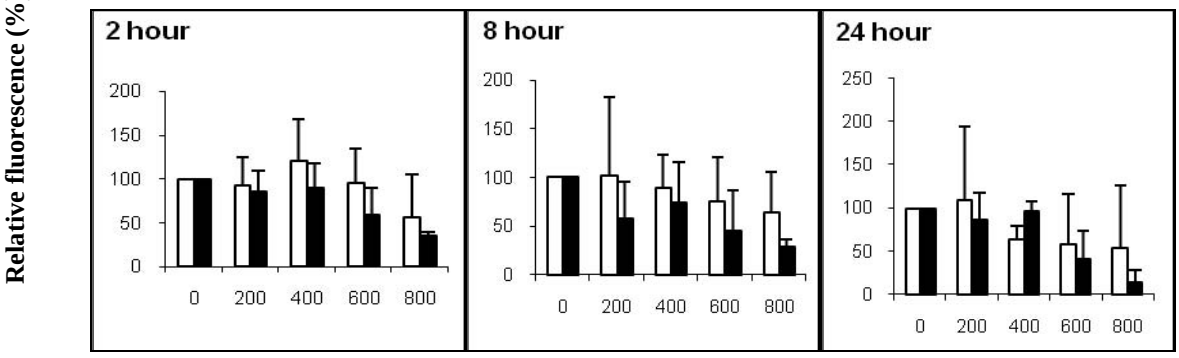

A: A graphical representation of the relative absorbance of HEK293 (white bars) and CYGB+ (black bars) cells treated with hydrogen peroxide for 24 hours and assessed for cell viability using the MTT assay. A mean of 3 repeats is presented. Error bars represent standard deviations. B: Graphical representation of the relative fluorescence from HEK293 (white bars) and CYGB+ (black bars) cell samples which had been treated with H_2O_2 for the time periods stated in the graph titles, and incubated with DCFH. The mean from 3 repeats is presented. Error bars represent standard deviations. C: A graphical representation of relative fluorescence from HEK293 (white bars) and CYGB+ (black bars) cell samples which had been treated with H_2O_2 for the time periods stated in the graph titles, and incubated with cis-PnA. The mean from 3 repeats is presented. Error bars represent standard deviations.

5.4.4 The Effect of Cytoglobin Over Expression in Cytoprotection Against H_2O_2

CYGB+ and HEK293 cell lines were treated with 200, 400, 600 and 800 µM H_20_2 for 2, 8 and 24 hours and assayed using the MTT and comet assay as end points of cytotoxicity and DNA damage respectively.

Figure 5.4 Effect of CYGB Over expression on Cell Viability

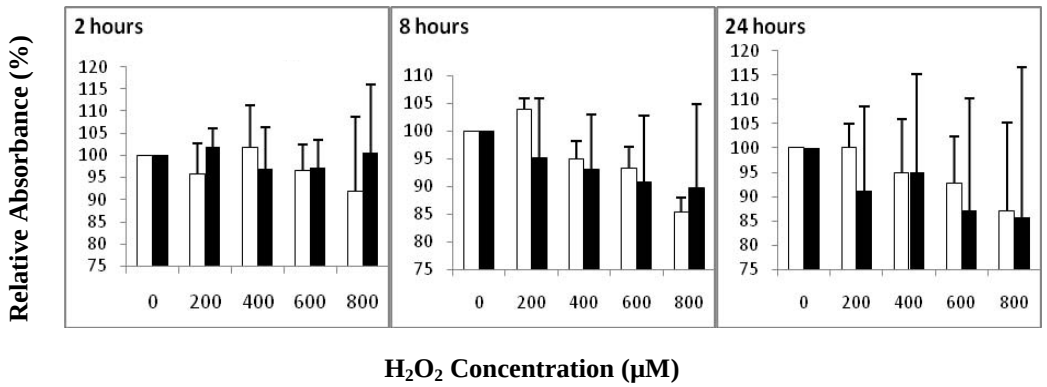

Graphical representation of cell viability, as measured by the MTT assay, of HEK293 (white bars) and CYGB+ (black bars) cells following treatment with H_2O_2, for 2, 8 or 24 hours. Data presented is the mean relative absorbance from 3 repeats. Error bars represent standard deviation.

5.4.4.1 Assessment of Cytoprotection using Cell Viability as an Endpoint.

It is evident from Figure 5.4 that there is a concentration and time dependant response, as there is a decrease in cell viability with increased time and H_2O_2 concentration. However statistically these trends were not significant, and neither was any difference between the cell lines.

5.4.4.2 Assessment of Cytoprotection using DNA Strand Breaks as an Endpoint.

Unmodified Comet Assay

Figure 5.5 shows the results of the comet assay presented as the mean median % tail intensity. Figure 5.5 shows an increase in % tail intensity with dose at 2 and 8 hours in the samples not incubated with FPG in both cells lines, but not at 24 hours. This trend was not statistically significant.

Modified Comet Assay

A concentration response can be seen in Figure 5.5 after 2 and 8 hours treatment, there was an increase in % tail intensity with increasing H_2O_2 concentration. This trend however was not statistically significant and there was no significant difference between the cell lines.

Figure 5.5 Effect of Cytoglobin Over Expression on DNA Damage

A. Comet Assay

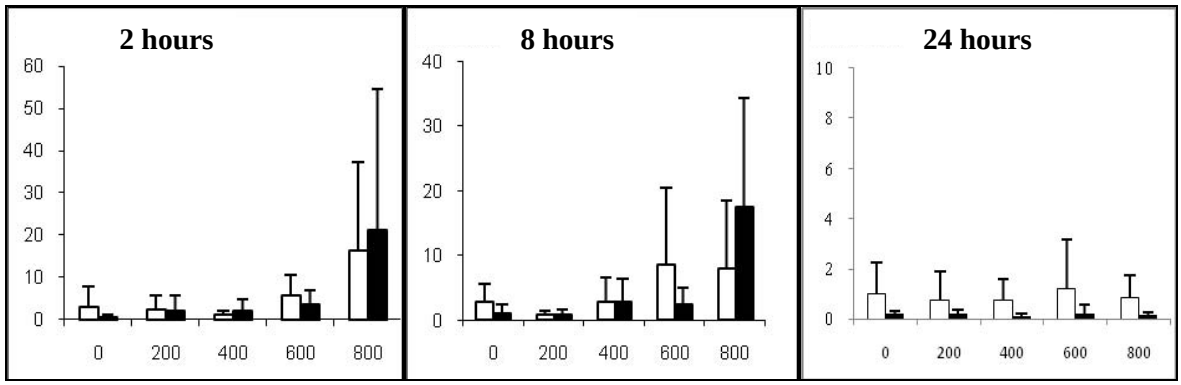

B. Modified Comet Assay

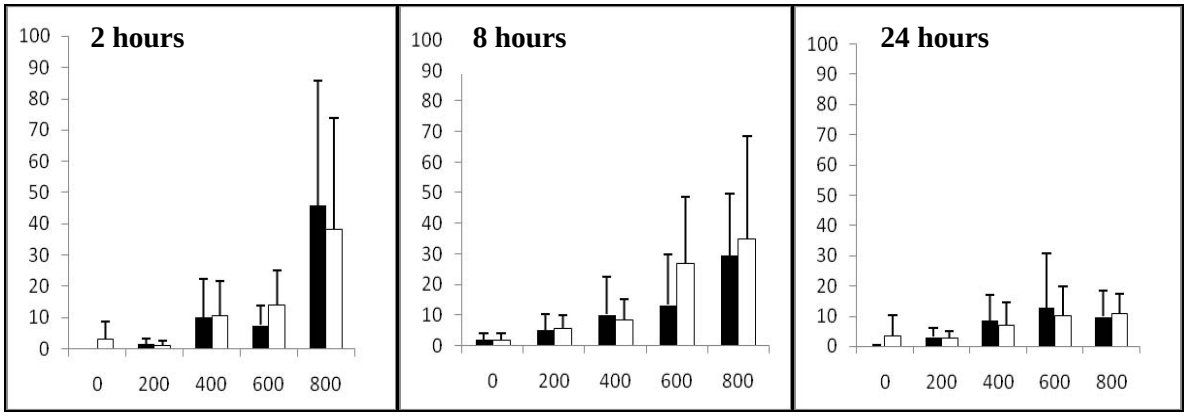

A graphical representation of the mean median % tail intensity calculated following 5 repeats of the comet assay. The % tail intensity represents the relative amount of damaged DNA within the sample. HEK293 (white bars) and CYGB+ (black bars) cells were treated with H_2O_2 for 2, 8 or 24 hours, before analysis with the comet assay. The modified comet data shows the mean median of samples which had been incubated with the FPG enzyme. The error bars represent standard deviation.

5.4.5 Expression of Cytoglobin in Response to H_20_2 Treatment

Subsequent to the previous experiments regarding H_20_2 treatments, a paper was published which stated that CYGB was upregulated through treatment with H_20_2 (Li *et al.*, 2007). In order to ascertain if induction of CYGB was happening in this experimental model, HEK293 cells were cultured in 6 well plates and treated with 200, 400, 600, 800 and 1000 µM H_20_2 for 2, 8 and 24 hours. Following treatment, protein and RNA were extracted from the same samples independently.

5.4.5.1 Expression of Cytoglobin mRNA

Single step RT-PCR was used to assess the CYGB mRNA levels within the RNA samples. The data is presented in Figure 5.6 as the relative expression of CYGB mRNA to the control. The data was normalised to RNA concentration. It can be seen from Figure 5.6 that at 2 and 8 hours there is a concentration dependant induction of CYGB, which peaks at 600 µM. At 24 hours there is no evidence of CYGB mRNA induction. This trend was not statistically significant.

5.4.5.2 Expression of Cytoglobin Protein

Western blotting was used to determine the presence of the CYGB protein within the protein samples. 20 µg of protein was loaded on the gel, the blot was incubated with 0.2 µg/ml of CYGB antibody overnight at 4^{o}C. Figure 5.6 shows the blot, no bands are evident in any of the test samples, indicating that the CYGB protein was undetectable within any of the samples using this method.

Figure 5.6 Induction of Cytoglobin Expression Following Treatment with Hydrogen Peroxide

A

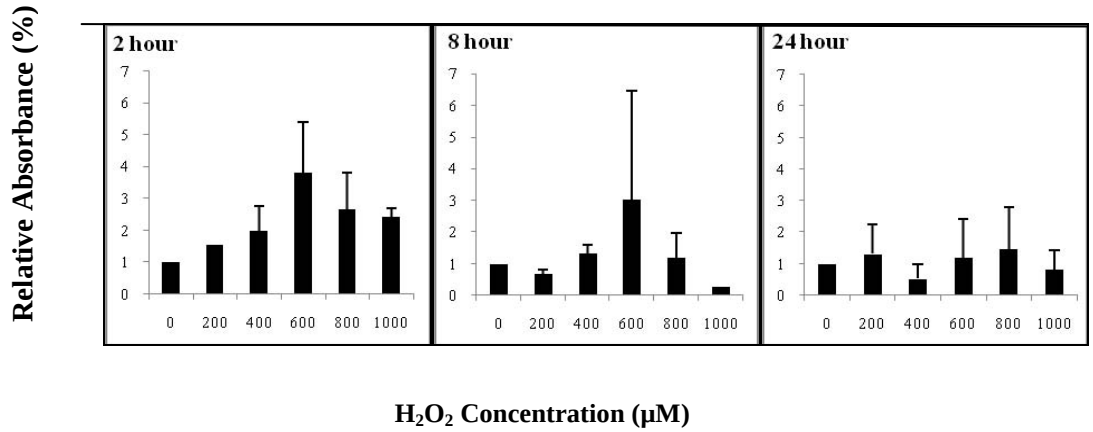

B

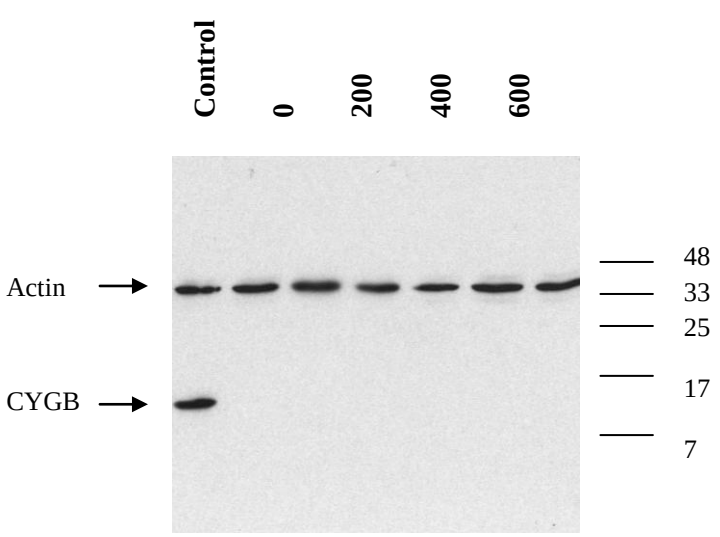

A) A graphical representation of CYGB mRNA levels in HEK293 cells following treatment with H_2O_2 for 2, 8 or 24 hours. Presented is the mean fold induction of CYGB mRNA from 3 repeats. Error bars represent standard deviation. B) A western blot of protein samples taken from HEK293 cells treated with various concentrations (labelled on figure (µM)) of H_2O_2 for 8 hours (Blots for 2 and 24 hours are not shown, but gave the same result). Lane 1 contains a protein sample extracted from CYGB+ cells, used as a positive control. 20µg of protein was loaded into each well, 2µg/ml monoclonal mouse anti-human CYGB primary antibody was used. Anti-β-Actin (0.15µg/ml) primary antibody was used as a positive control for protein. The blot was incubated with primary antibody overnight.

5.5 Discussion

5.5.1 Cytoglobin in Cytoprotection against Oxidative Stress

At the start of this study there was much speculation in the literature regarding a role for CYGB in cytoprotection against oxidative stress, although there was no evidence to support this theory. During the course of this work, evidence has begun to emerge in the literature to support this hypothesis, however in general it has been limited to studies on neuronal cell lines (Fordel *et al.*, 2006; Hodges *et al.*, 2008; Li *et al.*, 2007; Xu *et al.*, 2006). Here we investigated a potential role for CYGB in cytoprotection against oxidative stress in a non neuronal cell line, HEK293. In contrast to data presented in the literature this study found no evidence to support cytoprotective role of CYGB against hydrogen peroxide induced oxidative stress. There was no difference in DNA damage, cell viability, lipid peroxidation or intracellular ROS of cells over expressing CYGB compared to a control cell line, which expressed only endogenous CYGB. Of note this is the first study to look at HEK293 cells.

Xu *et al* (Xu *et al.*, 2006) investigated cytoprotection of CYGB against 50 μM Ferric nitrolotriacetate and 20 μM arachidonic acid induced oxidative stress, using a rat hepatic stellate cell line which had been transfected with a CYGB, or GFP (control) over expressing plasmid (Bondarenko *et al.*, 2006). Over expression of CYGB reduced the level of oxidative stress within the cells, as measured using markers of lipid peroxidation. Evidence was also provided to support the hypothesis that this was through increased levels of oxyradical scavenging (Bondarenko *et al.*, 2006).

All other studies have used neuronal cell lines, in which (see chapter 5) CYGB has been shown to localise to the nuclei and cytoplasm, in contrast to non-neuronal cells in which most evidence suggests a strictly cytoplasmic localisation (see chapter 5). The differences in the subcellular localisation patterns of the cell types indicates that the role of CYGB within the different cell lines may vary, so although these studies are of interest, the difference between the cell lines used could explain the contradictions in the data generated.

Hodges *et al* (Hodges *et al.*, 2008) presented evidence of cytoprotection of over expressed CYGB against oxidative stress in a neuronal cell line TE671 (Ostojic *et al.*, 2008). Following exposure to Ro19-8022, which causes oxidative DNA damage, the cells showed an increase in intracellular ROS and oxidative DNA damage (8-oxo-dG), which was reduced by overexpression of CYGB. 8-oxo-dG is formed from oxidation of the DNA sugar Guanine, which occurs readily under oxidative stress. Of note, over expression of CYGB did not confer protection against DNA damage which was not specifically 8-oxo-dG (Ostojic *et al.*, 2008). The levels of damage observed in this study with and without FPG incubation were comparable for the CYGB overexpressing cell line, whereas the control cell line exhibited distinctly more damage following FPG incubation. This implies that the protection offered by CYGB was specific to oxidative stress induced DNA damage.

There are 2 studies in the literature which present evidence of CYGB mediated cytoprotection against H_2O_2 induced oxidative stress, however both studies used neuronal cells lines. The first used N2a (mouse) neuroblastoma cells (Hodges *et al.*, 2008), and the second in SH-SY5Y (human) neuroblastoma cells ((Kida *et al.*, 2007). The study in N2a cells used a siRNA

vector to reduce CYGB expression (Li *et al.*, 2007), and observed that following treatment with 500 μM H_2O_2 for 4 hours, the cells with reduced CYGB protein expression suffered a significantly greater loss in cell viability than the cells with endogenous CYGB expression(Hodges *et al.*, 2008). The study in SH-SY5Y cells took a different approach and looked at over expression of CYGB (Kida *et al.*, 2007). Exposure of CYGB over expressing cells, GFP (control) over expressing cells, and non-transfected controls to 300 μM for 24 hours, showed 70% (significant) less cell death, in those cells with CYGB over expression compared to the non-transfected controls. Of note, transfection with a GFP plasmid offered 28% less cell death, thus one can assume that 40% of the reduction in cell death was due to the presence of excessive CYGB (Kida *et al.*, 2007).

Further studies by Fordel *et al* in SH-SY5Y cells investigated the effect of anoxia on the generation of H_2O_2 (Shigematsu *et al.*, 2008). Cells containing antisense CYGB, which effectively reduced the production of CYGB mRNA by 47%, showed a significant increase in H_2O_2 generation following 16 and 24 hours anoxia, whilst over expression of CYGB (verified at the mRNA and protein level) led to a decrease in H_2O_2 generation (not significant) (Shigematsu *et al.*, 2008).

This study did not find any evidence of CYGB cytoprotection against H_2O_2 induced oxidative stress in HEK293 cells, and as yet there is nothing in the literature to specifically contradict this observation. In rat HSC cells, using a different method of inducing of oxidative stress, over expression of CYGB appears to offer some cytoprotection (Bondarenko *et al.*, 2006). There is mounting evidence that in neuronal cells CYGB overexpression, or inhibition offers

cytoprotection, or increased stress respectively against oxidative stress. It remains elusive whether this role is replicated in non neuronal human cells (Burmester *et al.*, 2007; Hodges *et al.*, 2008; Kida *et al.*, 2007; Ostojic *et al.*, 2008; Shigematsu *et al.*, 2008).

5.5.2 Induction of Cytoglobin Expression in Response to Hydrogen Peroxide

Presented here is evidence of a trend in induction of CYGB mRNA in response to, 400, 600, 800 and 1000 μM hydrogen peroxide after 2 and 8 hours, in HEK293 cells. Although this isn't significant the trend shows a peak (3-4fold) at 600 μM at both time points. This is in a similar range to that which Li *et al* observed in N2a neuroblastoma cells, following treatment with 250 μM H_2O_2 for 3, 6, 12, 24 hours (Hodges *et al.*, 2008). A significant increase in mRNA of 2-4 fold was observed. In addition an increase in CYGB mRNA expression was observed *in vitro*, in the regions of rat brain which have previously been reported to respond to oxidative stress, following hypoxic treatment (Trandafir *et al.*, 2007).

The evidence in the literature with respect to induction of CYGB mRNA in response to oxidative stress is somewhat limited, and further studies are required to make sound conclusions. This study hints towards a model in which oxidative stress induces expression of CYGB. Further studies in the mechanism of induction are required, especially as there is no evidence of an Antioxidant Response Element (ARE) within the CYGB promoter region. In absence of an ARE, it could be speculated that an increase in CYGB mRNA could be a downstream consequence, or side effect of oxidative stress rather than a direct response. Another potential source of CYGB up-regulation in response to oxidative stress is via HIF-1α.

Several papers in the literature suggest that HIF-1α can regulate oxidative stress response genes (Kietzmann and Gorlach, 2005), and that ROS may have a level of control over HIF-1α activity (Siddiq *et al.*, 2007). A review by Kietzmann and Gorlach (Kietzmann and Gorlach, 2005)concluded that under non hypoxic conditions an increase in the levels of ROS lead to an increase in HIF-1α expression. Taking this onto account, and the observations made in this study, it could be speculated that CYGB upregulation in response to ROS is mediated via HIF-1α.

5.5.3 The Subcellular Localisation of Cytoglobin

The CYGB literature provides contradictory evidence regarding the subcellular localisation of CYGB. Geuens *et al* were the first group to present evidence of CYGB within the nucleus (Geuens *et al.*, 2003). In 2003 they showed using IHC that CYGB was found exclusively in the nucleus of cells of mouse tissue. In addition CYGB was isolated from nuclear extracts of mouse liver, using affinity chromatography and western blotting.

In *vitro* studies have presented evidence of CYGB expression solely within the cytoplasm of A549 cells (Hodges *et al.*, 2008; Huang *et al.*, 2006), F9 cells (Nakatani *et al.*, 2004), HEpG2, MCP13, HeLa and mouse embryonic fibroblasts (Hodges *et al.*, 2008). In contrary, HeLa and Vero cells were shown to express CYGB within the nucleus (Schmidt *et al.*, 2004) however this was investigated using a Cygb-GFP construct, which was potentially small enough to diffuse into the nucleus, as such this study argues against active nuclear transport of CYGB in HeLa and Vero cells, rather than for a nuclear subcellular localisation of CYGB.

In *vitro* analysis of neuronal cells, SKHSH, TE671 shows a nuclear and cytoplasmic localisation of CYGB (Hodges *et al.*, 2008), which has been supported by in *vivo* studies in dogs, (Ostojic *et al.*, 2006), mice (Geuens *et al.*, 2003), (Man *et al.*, 2008) (Schmidt *et al.*, 2005)) and rats (Li *et al.*, 2007). In addition, CYGB was found absent from mitochondrial and membrane fractions of rat brain (Li *et al.*, 2007).

Nuclear and cytoplasmic expression of CYGB has been presented in mouse liver haematopoietic stem cells, and on occasion in fibroblasts (Man *et al.*, 2008). All other cell types investigated have shown cytoplasmic localisation of CYGB, including fibroblasts of the mouse heart, lung, kidney and thigh muscle (Man *et al.*, 2008), rat kidney fibroblasts (Nakatani *et al.*, 2004). In contradiction of the study by Man *et al*, Schmidt *et al* presented evidence of CYGB expression being exclusive to the cytoplasm in HSCs, fibroblasts, chondrocytes, oesteoblasts and osteocytes (Schmidt *et al.*, 2004) using IHC on mice tissue.

The relationship between hypoxia and CYGB subcellular localisation was investigated by Li *et al* who observed no change in localisation after 1, 3, 7 or 14 days at 10% O_2 in rat brain.

Presented here is evidence of a cytoplasmic localisation of CYGB in HEK293 cells in *vitro* and in numerous cell types in *vivo* (see Chapter 3). It is evident from the literature and this study, that the predominant subcellular localisation of CYGB is cytoplasmic in all non

neuronal cells, but in neuronal cells nuclear localisation is also evident. This leads to the speculation that the role of CYGB in neuronal and non neuronal cells differs.

5.5.4 Physiological Considerations

This study has hinted towards induction of CYGB in response to H_2O_2 induced oxidative stress, but showed no evidence that over expression of CYGB offers cytoprotection against this insult. Notably, a trend of CYGB mRNA induction was observed which peaked at 600 μM. Lipid peroxidation, endogenous ROS, and DNA damage, in general presented a clear increase at 800 μM compared to 600 μM doses. It could be speculated that there was no difference between the cell lines in terms of these endpoints at doses of 600 μM and lower, because induction of endogenous CYGB offered comparable cytoprotection to that afforded through over expression. After this dose the induction of CYGB is reduced, and it could be speculated that as a consequence an increase in cellular damage is observed. The cell viability data shows there is reduction in cell viability with 800 μM H_2O_2, it would add weight to this argument to determine whether this was due to an increase in cell death or a reduction in cell proliferation, and whether there is a significant switch from reduced proliferation to cell death at 800 μM.

The manner in which CYGB could offer cytoprotection to ROS is unclear, there has been evidence presented in the literature that CYGB can act to catabolise H_2O_2 (Kawada *et al.*, 2001). Another study showed however that the catalase activity of CYGB was negligible compared to true enzymes (Trandafir *et al.*, 2007). It remains elusive whether CYGB could

act to directly detoxify ROS, however these studies have demonstrated that CYGB can bind ROS. Several studies have shown that an increase in CYGB expression results in lower levels of ROS ((Bondarenko *et al.*, 2006; Ostojic *et al.*, 2008; Shigematsu *et al.*, 2008). It could be speculated from this that the mechanism of cytoprotection relates directly to managing levels of ROS, possibly through savaging ROS, through enzymatic activity to stabilise ROS, or potentially the binding of ROS to CYGB could initiate a pathway of ROS degradation, or in complexing ROS, CYGB could be signalled for degradation resulting in a simultaneous reduction of CYGB and ROS levels. All of these hypothesises are highly speculative as the literature on the subject is somewhat limited.

CHAPTER 6: GENERAL DISCUSSION

The *cygb* gene has been shown to be evolutionarily ancient, arising prior to the development of the circulatory system (Sugimoto *et al.*, 2004). It is also well conserved (Pesce *et al.*, 2004; Trent and Hargrove, 2002), indicating the role of cytoglobin to be fundamental to an ancient biological function.

6.1 Cytoglobin in the Transport of Oxygen to the Mitochondria.

A role for CYGB in the transport of oxygen to the mitochondria has been both proposed and refuted in the literature. The main objection against this role for CYGB concerned the absence of CYGB expression in several cell types. Reported here however is evidence that CYGB expression was observed in the majority of cell types. The exception to the rule being the observation of negative expression in cells which express other members of the globin family, potentially however due to other globins compensating for the absence of CYGB. The levels of CYGB in the cell have been reported to be low (Fago *et al.*, 2004). One cannot therefore assume that cells which appear to offer negative CYGB expression are in fact negative for CYGB, as the basal level of expression may just be undetectable via IHC and western blotting, the techniques used. Therefore what may have been observed in this study, and others, is that cells which are positive for CYGB are presenting with increased expression whilst those which appear negative are offering a basal level of expression. Therefore the conclusion in the literature that CYGB is not involved in the transport of oxygen to the mitochondria, because it is not expressed by all cell types, may not be valid. However, should CYGB have a role in transport of the oxygen to the mitochondria, it would be unlikely that in a hypoxic scenario upregulation would be observed. In response to hypoxia there is a

reduction in transcription and translation of unessential proteins (Wenger, 2002). It would appear unlikely that if the primarily role of CYGB was transport of oxygen to the mitochondria, where there was little oxygen, and therefore a reduction in the requirement for CYGB, that the cell would respond to increase CYGB expression. Additionally the low cellular levels of CYGB, would argue against a role in transport of oxygen to the mitochondria (Fago *et al.*, 2004). A role of CYGB in transport of oxygen to the mitochondria is plausible, should a basal level of expression be observed in all cell types, however overall the available evidence suggests that this in unlikely to be the primary role of CYGB.

6.2 Cytoglobin in Oxygen Transport, Storage and Sensing

There is substantial evidence in the literature to support CYGB binding to oxygen in a manner which enables oxygen transport (Sawai *et al.*, 2003; Trent and Hargrove, 2002). CYGB expression has previously been shown to increase in response to low oxygen levels (Fordel *et al.*, 2004a; Fordel *et al.*, 2004b; Fordel *et al.*, 2007a; Fordel *et al.*, 2007b; Guo *et al.*, 2007; Huang *et al.*, 2006; Mammen *et al.*, 2006; Schmidt *et al.*, 2004; Singh *et al.*, 2009), and preliminary work done alongside this study showed an increase in CYGB expression, although not statistically significant, in BEAS-2B and HEK293 cells after incubation with 1% oxygen for 1,3,6 and 9 hours. This study has further substantiated this by showing an increase in the CYGB positive phenotype of cells within hypoxic fibrotic lesions. These observations support speculated roles of CYGB in O_2 storage, transport and sensing. It has been suggested that CYGB could be involved in the supply of oxygen to particular cellular processes, such as contraction of myofibroblasts (Kawada *et al.*, 2001) or collagen synthesis (Fago *et al.*, 2004; Man *et al.*, 2008; Nakatani *et al.*, 2004; Schmidt *et al.*, 2004). Although

this is plausible, it seems more likely that the primary function of CYGB is more fundamental, and essential to a wider array of cell types.

CYGB may have a role in extracting O_2 from the local environment, in a similar manner to myoglobin, facilitating diffusion of oxygen into the cell and then to the mitochondria. The immediate upregulation of CYGB in response to hypoxic stimuli, reported in the literature and supported by observations in this study, would support this role. CYGB bound oxygen would not contribute to the partial pressure of oxygen (PO_2) in the region, thus by increasing expression of CYGB, and 'mopping up' free oxygen within the cell, the partial pressure of oxygen within the cell may fall lower than that externally, thus driving diffusion of oxygen into the cell. The level of cellular CYGB would therefore correlate to the PO_2 within the cell, in that higher levels of CYGB would drive down the internal PO_2, enabling diffusion of oxygen into the cell at lower oxygen tensions. In this model CYGB could also act as an O_2 reservoir, as the release of oxygen from CYGB would relate to the subcellular PO_2, and would only be released where and when needed. This would enable the release of O_2 by CYGB to cellular reactions as previously proposed, such as contraction of myofibroblasts and collagen synthesis.

In the current study, CYGB expression was consistently positive throughout the fibroblast population, but no other cell type. The relative levels of expression within fibroblasts compared to other cell types however, has not yet been investigated. Fibroblasts migrate to regions of damage, which are frequently related to vascular damage and subsequent hypoxia. As observed in this study, as the predominant cell type within the lesion, and in regions of avascularity were fibroblasts. Potentially fibroblasts may present with a higher level of CYGB

expression than other cell types, offering an oxygen storage role under normal conditions, and in response to damage, a role in transporting oxygen to regions of damage induced hypoxia.

A putative model was proposed at the start of this study which considered that expansion of the fibrotic lesion was limited by expression of CYGB at the fibrotic border, which may create a hyperoxic environment, protecting the normoxic parenchyma from the hypoxic lesion. The data presented here argues against this, as expression of CYGB was variable at the edge, but consistent within the lesion.

A role of CYGB in oxygen sensing is plausible. As previously discussed, up-regulation of CYGB in response to hypoxia could facilitate diffusion of O_2 into anoxic cells, restoring normoxia. The expression level of CYGB may subsequently return to basal levels, as observed in in *vitro* studies looking at reoxygenation (Fordel *et al.*, 2007a), proving a feedback loop. The level of CYGB within the cell would therefore be related to the PO_2, supporting an oxygen sensing role.

6.3 Cytoglobin as a Redox Sensor and in ROS Scavenging

As previously discussed, one potential role of CYGB could be to increase the capacity of the cell to extract oxygen from the local environment. Molecular oxygen is a pre-requisite of ROS, and there is a long-standing debate regarding the relationship between ROS and oxygen homeostasis. It has previously been proposed that ROS produced from the mitochondrial respiratory chain could contribute to oxygen sensing (Kietzmann and Gorlach, 2005). This model however assumes under hypoxic condition the levels of ROS decrease. This has been shown in several studies, however numerous studies have also presented contradictory

evidence (Kietzmann and Gorlach, 2005). The majority of the studies which reported an increase in ROS in response to hypoxia, used DFCH to measure the levels of ROS. Although DCFH is oxidised by ROS, principally H_2O_2, to form a fluorescent product, DCF, there is also evidence however that heme can also oxidise DFCH to DCF directly (Ohashi *et al.,* 2002). These studies could thus have been detecting an increase in heme, potentially due to CYGB induction, rather than an increase in ROS. It seems more likely that a decrease in ROS is observed with hypoxia.

A model associating oxygen tension and ROS may also involve CYGB. Under hypoxic conditions, CYGB expression increases, which may result in normalisation of oxygen levels, and subsequently a reduction in CYGB expression back to basal levels, as discussed earlier. Under hyperoxic conditions however, leading to the generation of ROS, or in response to other causes of oxidative stress, induction of CYGB could also occur, as observed in the current study. This may be followed by binding to ROS. CYGB binding could potentially stabilise ROS, or target it for degradation, or the degradation of a ROS-CYGB complex. There is some evidence that CYGB may have peroxidase activity (Asahina *et al.*, 2002; Kawada *et al.,* 2001), and can detoxify reactive nitrogen species (Halligan *et al.*, 2009; Smagghe *et al.*, 2008), although as yet a cytoglobin reductase has not been identified to enable catalytic cycles of detoxification. Although no evidence has been provided to support this, the reduction in ROS levels due to CYGB activity may feedback to reduce the CYGB expression back to basal levels. There may also be competitive binding between O_2 and ROS, with CYGB offering a higher affinity for ROS, thus enabling stabilisation of ROS, and or degradation at high oxygen tensions, and under low oxygen tensions where ROS are not

generated CYGB could readily bind O_2. Cytoglobin may thus be involved at maintaining oxygen homeostasis by responding to both hyperoxic and hypoxic insults.

There was evidence provided in this study of similar patterns of expression of CAIX and CYGB, it could therefore be speculated that like CAIX, CYGB is regulated by HIF-1α in response to hypoxic and non hypoxic stimuli. Non hypoxic regulation of HIF-1α includes stimulation by ROS (Kietzmann and Gorlach, 2005), and thus regulation of CYGB in response to hyperoxia and hypoxia may be via HIF-1α.

6.4 Other Potential Roles of Cytoglobin

CYGB is a putative tumour suppressor, which has been proposed due to the loss of CYGB expression within several tumours as a result of promoter methylation (McRonald *et al.*, 2006; Shaw *et al.*, 2006; Shaw *et al.*, 2009; Shivapurkar *et al.*, 2008; Xinarianos *et al.*, 2006). The loss of any of the functions previously discussed could lead to a loss of redox balance, or hypoxia which could act as a causative agent, or more likely contribute to tumour progression. It appears unlikely that CYGB has a direct role in the cell cycle, especially as CYGB expression does not appear to be associated with proliferation. Additionally a yeast 2 hybrid study showed no associated between CYGB and cell cycle proteins (Hodges, NJ. personal communication). Loss of CYGB expression however could result in aberrant expression of cell cycle mediating proteins via a loss of redox homeostasis.

It is evident from observations presented here that the role of CYGB is not directly, or specifically related to inflammation, angiogenesis or stem cell mediated repair. The results of

this study would also argue against the use of CYGB as a marker of activated fibroblasts and stellate cells

6.5 Summary of Findings

CYGB expression was observed in a range of cell types indicating a fundamental role, of no cell type specificity. This study also provides evidence of CYGB upregulation in response to oxidative stress in *vitro*. CYGB expression was most prevalent within a fibrotic lesion and more variable at the edge, and was shown to be associated with fibroblast infiltration, avascularity and potentially hypoxia. The expression of CYGB within the lesion paralleled that of CAIX indicating related regulation of expression. These findings support a role for CYGB in cellular redox and oxygen homeostasis, regulated via HIF-1α in response to both hypoxic and non hypoxic stimuli.

6.6 Future Work

Despite extensive work, 10 years after its identification, the subcellular role of CYGB remains elusive. However, extensive in *vivo* and in *vitro* studies are required to determine the subcellular role of CYGB. It would of interest to ascertain the following:

- Direct evidence of a role in detoxification of ROS, using purified proteins or over expressing systems in *vitro.*
- The affinity with which CYGB binds ROS and whether this is competitive O_2.
- Whether CYGB expression increases the capacity of the cell to take up oxygen.
- Determine whether all cell types have a basal level of CYGB expression.
- Whether fibroblasts have a higher level of CYGB expression than other cell types
- Whether CYGB is induced in response to non hypoxic induction of HIF-1α activity.

REFERENCES

Andersson-Sjoland, A., de Alba, C.G., Nihlberg, K., et al. (2008) Fibrocytes are a potential source of lung fibroblasts in idiopathic pulmonary fibrosis. **The international journal of biochemistry & cell biology,** 40 (10): 2129-2140.

Asahina, K., Kawada, N., Kristensen, D.B., et al. (2002) Characterization of human stellate cell activation-associated protein and its expression in human liver. **Biochimica et biophysica acta,** 1577 (3): 471-475.

Ashcroft, T., Simpson, J.M. and Timbrell, V. (1988) Simple method of estimating severity of pulmonary fibrosis on a numerical scale. **Journal of clinical pathology,** 41 (4): 467-470.

Bancroft, J.D. and Stevens, A. (1990) **Theory and practice of histological techniques.** 3rd ed. Edinburgh: Churchill Livingstone.

Barkhordari, A., Stoddart, R.W., McClure, S.F., et al. (2004) Lectin histochemistry of normal human lung. **Journal of molecular histology,** 35 (2): 147-156.

Barnes, P.J. (2004) Mediators of chronic obstructive pulmonary disease. **Pharmacological reviews,** 56 (4): 515-548.

Berra, E., Ginouves, A. and Pouyssegur, J. (2006) The hypoxia-inducible-factor hydroxylases bring fresh air into hypoxia signalling. **EMBO reports,** 7 (1): 41-45.

Bondarenko, V., Dewilde, S., Moens, L., et al. (2006) Solution 1H NMR characterization of the axial bonding of the two His in oxidized human cytoglobin. **Journal of the American Chemical Society,** 128 (39): 12988-12999.

Bradford, M.M. (1976) A rapid and sensitive method for the quantitation of microgram quantities of protein utilizing the principle of protein-dye binding. **Analytical Biochemistry,** 72 248-254.

Brahimi-Horn, M.C. and Pouyssegur, J. (2009) HIF at a glance. **Journal of cell science,** 122 (Pt 8): 1055-1057.

Breeze, R. and Turk, M. (1984) Cellular structure, function and organization in the lower respiratory tract. **Environmental health perspectives,** 55 3-24.

Britton, M. (2003) The burden of COPD in the U.K.: results from the Confronting COPD survey. **Respiratory medicine,** 97 Suppl C S71-9.

Buckingham, S., Heinemann, H.O., Sommers, S.C., et al. (1966) Phospholipid synthesis in the large pulmonary alveolar cell. Its relation to lung surfactants. **The American journal of pathology,** 48 (6): 1027-1041.

Burmester, T., Ebner, B., Weich, B., et al. (2002) Cytoglobin: a novel globin type ubiquitously expressed in vertebrate tissues. **Molecular biology and evolution,** 19 (4): 416-421.

Burmester, T., Gerlach, F. and Hankeln, T. (2007) Regulation and role of neuroglobin and cytoglobin under hypoxia. **Advances in Experimental Medicine and Biology,** 618 169-180.

Burmester, T., Haberkamp, M., Mitz, S., et al. (2004) Neuroglobin and cytoglobin: genes, proteins and evolution. **IUBMB life,** 56 (11-12): 703-707.

Chung, K.F. and Adcock, I.M. (2008) Multifaceted mechanisms in COPD: inflammation, immunity, and tissue repair and destruction. **The European respiratory journal : official journal of the European Society for Clinical Respiratory Physiology,** 31 (6): 1334-1356.

Cruz-Gervis, R., Stecenko, A.A., Dworski, R., et al. (2002) Altered prostanoid production by fibroblasts cultured from the lungs of human subjects with idiopathic pulmonary fibrosis. **Respiratory research,** 3 17.

Darby, I.A. and Hewitson, T.D. (2007) Fibroblast differentiation in wound healing and fibrosis. **International review of cytology,** 257 143-179.

de Sanctis, D., Dewilde, S., Pesce, A., et al. (2003) New insight into the haemoglobin superfamily: preliminary crystallographic characterization of human cytoglobin. **Acta crystallographica.Section D, Biological crystallography,** 59 (Pt 7): 1285-1287.

de Sanctis, D., Dewilde, S., Pesce, A., et al. (2004a) Crystal structure of cytoglobin: the fourth globin type discovered in man displays heme hexa-coordination. **Journal of Molecular Biology,** 336 (4): 917-927.

de Sanctis, D., Dewilde, S., Pesce, A., et al. (2004b) Mapping protein matrix cavities in human cytoglobin through Xe atom binding. **Biochemical and biophysical research communications,** 316 (4): 1217-1221.

Desmouliere, A. Tuchweber, B. and Arora, P.D. (1999) **Tissue repair and fibrosis : the role of the myofibroblast.** Vol. 93 Berlin ; London: Springer.

Diaz, A., Chepenik, K.P., Korn, J.H., et al. (1998) Differential regulation of cyclooxygenases 1 and 2 by interleukin-1 beta, tumor necrosis factor-alpha, and transforming growth factor-beta 1 in human lung fibroblasts. **Experimental cell research,** 241 (1): 222-229.

Droge, W. (2002) Free radicals in the physiological control of cell function. **Physiological Reviews,** 82 (1): 47-95.

Fago, A., Hundahl, C., Dewilde, S., et al. (2004a) Allosteric regulation and temperature dependence of oxygen binding in human neuroglobin and cytoglobin. Molecular mechanisms and physiological significance. **The Journal of biological chemistry,** 279 (43): 44417-44426.

Fago, A., Hundahl, C., Malte, H., et al. (2004b) Functional properties of neuroglobin and cytoglobin. Insights into the ancestral physiological roles of globins. **IUBMB life,** 56 (11-12): 689-696.

Fireman, E., Shahar, I., Shoval, S., et al. (2001) Morphological and biochemical properties of alveolar fibroblasts in interstitial lung diseases. **Lung,** 179 (2): 105-117.

Fordel, E., Geuens, E., Dewilde, S., et al. (2004a) Hypoxia/ischemia and the regulation of neuroglobin and cytoglobin expression. **IUBMB life,** 56 (11-12): 681-687.

Fordel, E., Geuens, E., Dewilde, S., et al. (2004b) Cytoglobin expression is upregulated in all tissues upon hypoxia: an in vitro and in vivo study by quantitative real-time PCR. **Biochemical and biophysical research communications,** 319 (2): 342-348.

Fordel, E., Thijs, L., Martinet, W., et al. (2006) Neuroglobin and cytoglobin overexpression protects human SH-SY5Y neuroblastoma cells against oxidative stress-induced cell death. **Neuroscience letters,** 410 (2): 146-151.

Fordel, E., Thijs, L., Martinet, W., et al. (2007a) Anoxia or oxygen and glucose deprivation in SH-SY5Y cells: a step closer to the unraveling of neuroglobin and cytoglobin functions. **Gene,** 398 (1-2): 114-122.

Fordel, E., Thijs, L., Moens, L., et al. (2007b) Neuroglobin and cytoglobin expression in mice. Evidence for a correlation with reactive oxygen species scavenging. **The FEBS journal,** 274 (5): 1312-1317.

Fries, K.M., Blieden, T., Looney, R.J., et al. (1994) Evidence of fibroblast heterogeneity and the role of fibroblast subpopulations in fibrosis. **Clinical immunology and immunopathology,** 72 (3): 283-292.

Fuchs, C., Burmester, T. and Hankeln, T. (2006) The amphibian globin gene repertoire as revealed by the Xenopus genome. **Cytogenetic and genome research,** 112 (3-4): 296-306.

Fuchs, C., Luckhardt, A., Gerlach, F., et al. (2005) Duplicated cytoglobin genes in teleost fishes. **Biochemical and biophysical research communications,** 337 (1): 216-223.

Gabbiani, G., Ryan, G.B. and Majne, G. (1971) Presence of modified fibroblasts in granulation tissue and their possible role in wound contraction. **Experientia,** 27 (5): 549-550.

Gadgil, A. and Duncan, S.R. (2008) Role of T-lymphocytes and pro-inflammatory mediators in the pathogenesis of chronic obstructive pulmonary disease. **International journal of chronic obstructive pulmonary disease,** 3 (4): 531-541.

Garneau-Tsodikova, S. and Thannickal, V.J. (2008) Protein kinase inhibitors in the treatment of pulmonary fibrosis. **Current medicinal chemistry,** 15 (25): 2632-2640.

Genin, O., Rechavi, G., Nagler, A., et al. (2008) Myofibroblasts in pulmonary and brain metastases of alveolar soft-part sarcoma: a novel target for treatment? **Neoplasia (New York, N.Y.),** 10 (9): 940-948.

Geuens, E., Brouns, I., Flamez, D., et al. (2003) A globin in the nucleus! **The Journal of biological chemistry,** 278 (33): 30417-30420.

Gnainsky, Y., Kushnirsky, Z., Bilu, G., et al. (2007) Gene expression during chemically induced liver fibrosis: effect of halofuginone on TGF-beta signaling. **Cell and tissue research,** 328 (1): 153-166.

Gomes, A., Fernandes, E. and Lima, J.L. (2006) Use of fluorescence probes for detection of reactive nitrogen species: a review. **Journal of Fluorescence,** 16 (1): 119-139.

Gomperts, B.N. and Strieter, R.M. (2007) Fibrocytes in lung disease. **Journal of leukocyte biology,** 82 (3): 449-456.

Green, F.H. (2002) Overview of pulmonary fibrosis. **Chest,** 122 (6 Suppl): 334S-339S.

Gribbin, J., Hubbard, R.B., Le Jeune, I., et al. (2006) Incidence and mortality of idiopathic pulmonary fibrosis and sarcoidosis in the UK. **Thorax,** 61 (11): 980-985.

Guo, X., Philipsen, S. and Tan-Un, K.C. (2007) Study of the hypoxia-dependent regulation of human CYGB+ gene. **Biochemical and biophysical research communications,** 364 (1): 145-150.

Guo, X., Philipsen, S. and Tan-Un, K.C. (2006) Characterization of human cytoglobin gene promoter region. **Biochimica et biophysica acta,** 1759 (5): 208-215.

Halligan, K.E., Jourd'heuil, F.L. and Jourd'heuil, D. (2009) Cytoglobin Is Expressed in the Vasculature and Regulates Cell Respiration and Proliferation via Nitric Oxide Dioxygenation. **The Journal of biological chemistry,** 284 (13): 8539-8547.

Hamdane, D., Kiger, L., Dewilde, S., et al. (2003) The redox state of the cell regulates the ligand binding affinity of human neuroglobin and cytoglobin. **The Journal of biological chemistry,** 278 (51): 51713-51721.

Hankeln, T., Wystub, S., Laufs, T., et al. (2004) The cellular and subcellular localization of neuroglobin and cytoglobin -- a clue to their function? **IUBMB life,** 56 (11-12): 671-679.

Henson, P.M., Vandivier, R.W. and Douglas, I.S. (2006) Cell death, remodeling, and repair in chronic obstructive pulmonary disease? **Proceedings of the American Thoracic Society,** 3 (8): 713-717.

Hetzel, M., Bachem, M., Anders, D., et al. (2005) Different effects of growth factors on proliferation and matrix production of normal and fibrotic human lung fibroblasts. **Lung,** 183 (4): 225-237.

Higgins, D.F., Kimura, K., Bernhardt, W.M., et al. (2007) Hypoxia promotes fibrogenesis in vivo via HIF-1 stimulation of epithelial-to-mesenchymal transition. **The Journal of clinical investigation,** 117 (12): 3810-3820.

Higgins, D.F., Kimura, K., Iwano, M., et al. (2008) Hypoxia-inducible factor signaling in the development of tissue fibrosis. **Cell cycle (Georgetown, Tex.),** 7 (9): 1128-1132.

Hinata, N., Takemura, T., Ikushima, S., et al. (2003) Phenotype of regenerative epithelium in idiopathic interstitial pneumonias. **Journal of medical and dental sciences,** 50 (3): 213-224.

Hodges, N.J., Innocent, N., Dhanda, S., et al. (2008) Cellular protection from oxidative DNA damage by over-expression of the novel globin cytoglobin in vitro. **Mutagenesis,** 23 (4): 293-298.

Hodges, R.J., Jenkins, R.G., Wheeler-Jones, C.P., et al. (2004) Severity of lung injury in cyclooxygenase-2-deficient mice is dependent on reduced prostaglandin E(2) production. **The American journal of pathology,** 165 (5): 1663-1676.

Hogg, J.C. (2008) Lung structure and function in COPD. **The international journal of tuberculosis and lung disease : the official journal of the International Union against Tuberculosis and Lung Disease,** 12 (5): 467-479.

Hostettler, K.E., Roth, M., Burgess, J.K., et al. (2008) Airway epithelium-derived transforming growth factor-beta is a regulator of fibroblast proliferation in both fibrotic and normal subjects. **Clinical and experimental allergy : journal of the British Society for Allergy and Clinical Immunology,** 38 (8): 1309-1317.

Huang, J., Gao, W.X., Gao, Y.Q., et al. (2006) Hypoxia upregulates the expression of cytoglobin in lung cancer cells. **Zhonghua yi xue za zhi,** 86 (5): 321-324.

Jain, M. and Sznajder, J.I. (2005) Effects of hypoxia on the alveolar epithelium. **Proceedings of the American Thoracic Society,** 2 (3): 202-205.

Jeffery, P.K. (2004) Remodeling and inflammation of bronchi in asthma and chronic obstructive pulmonary disease. **Proceedings of the American Thoracic Society,** 1 (3): 176-183.

Jeffery, P.K. (2001) Remodeling in asthma and chronic obstructive lung disease. **American journal of respiratory and critical care medicine,** 164 (10 Pt 2): S28-38.

Kaluz, S., Kaluzova, M., Liao, S.Y., et al. (2009) Transcriptional control of the tumor- and hypoxia-marker carbonic anhydrase 9: A one transcription factor (HIF-1) show? **Biochimica et biophysica acta,** 1795 (2): 162-172.

Kanematsu, T., Kitaichi, M., Nishimura, K., et al. (1994) Clubbing of the fingers and smooth-muscle proliferation in fibrotic changes in the lung in patients with idiopathic pulmonary fibrosis. **Chest,** 105 (2): 339-342.

Kapanci, Y., Desmouliere, A., Pache, J.C., et al. (1995) Cytoskeletal protein modulation in pulmonary alveolar myofibroblasts during idiopathic pulmonary fibrosis. Possible role of transforming growth factor beta and tumor necrosis factor alpha. **American journal of respiratory and critical care medicine,** 152 (6 Pt 1): 2163-2169.

Kawada, N., Kristensen, D.B., Asahina, K., et al. (2001) Characterization of a stellate cell activation-associated protein (STAP) with peroxidase activity found in rat hepatic stellate cells. **The Journal of biological chemistry,** 276 (27): 25318-25323.

Keane, M.P., Arenberg, D.A., Lynch, J.P.,3rd, et al. (1997) The CXC chemokines, IL-8 and IP-10, regulate angiogenic activity in idiopathic pulmonary fibrosis. **Journal of immunology (Baltimore, Md.: 1950),** 159 (3): 1437-1443.

Keane, M.P., Belperio, J.A., Burdick, M.D., et al. (2001) ENA-78 is an important angiogenic factor in idiopathic pulmonary fibrosis. **American journal of respiratory and critical care medicine,** 164 (12): 2239-2242.

Keerthisingam, C.B., Jenkins, R.G., Harrison, N.K., et al. (2001) Cyclooxygenase-2 deficiency results in a loss of the anti-proliferative response to transforming growth factor-beta in human fibrotic lung fibroblasts and promotes bleomycin-induced pulmonary fibrosis in mice. **The American journal of pathology,** 158 (4): 1411-1422.

Kida, Y., Asahina, K., Inoue, K., et al. (2007) Characterization of vitamin A-storing cells in mouse fibrous kidneys using CYGB/STAP as a marker of activated stellate cells. **Archives of Histology and Cytology,** 70 (2): 95-106.

Kietzmann, T. and Gorlach, A. (2005a) Reactive oxygen species in the control of hypoxia-inducible factor-mediated gene expression. **Seminars in cell & developmental biology,** 16 (4-5): 474-486.

Kietzmann, T. and Gorlach, A. (2005b) Reactive oxygen species in the control of hypoxia-inducible factor-mediated gene expression. **Seminars in cell & developmental biology,** 16 (4-5): 474-486.

Kim, K.M., Park, S.H., Kim, J.S., et al. (2008) Polymorphisms in the type IV collagen alpha3 gene and the risk of COPD. **The European respiratory journal : official journal of the European Society for Clinical Respiratory Physiology,** 32 (1): 35-41.

Kinnula, V.L. and Myllarniemi, M. (2008) Oxidant-antioxidant imbalance as a potential contributor to the progression of human pulmonary fibrosis. **Antioxidants & redox signaling,** 10 (4): 727-738.

Koh, M.Y. and Powis, G. (2009) HAF : the new player in oxygen-independent HIF-1alpha degradation. **Cell cycle (Georgetown, Tex.),** 8 (9): 1359-1366.

Kugelstadt, D., Haberkamp, M., Hankeln, T., et al. (2004) Neuroglobin, cytoglobin, and a novel, eye-specific globin from chicken. **Biochemical and biophysical research communications,** 325 (3): 719-725.

Laurent, G.J., McAnulty, R.J., Hill, M., et al. (2008) Escape from the matrix: multiple mechanisms for fibroblast activation in pulmonary fibrosis. **Proceedings of the American Thoracic Society,** 5 (3): 311-315.

Li, D., Chen, X.Q., Li, W.J., et al. (2007) Cytoglobin up-regulated by hydrogen peroxide plays a protective role in oxidative stress. **Neurochemical research,** 32 (8): 1375-1380.

Li, R.C., Lee, S.K., Pouranfar, F., et al. (2006) Hypoxia differentially regulates the expression of neuroglobin and cytoglobin in rat brain. **Brain research,** 1096 (1): 173-179.

Lodish, H. (2004) **Molecular cell biology.** 5th ed. New York, New York: W. H. Freeman.

Luzina, I.G., Todd, N.W., Iacono, A.T., et al. (2008) Roles of T lymphocytes in pulmonary fibrosis. **Journal of leukocyte biology,** 83 (2): 237-244.

Lv, Y., Wang, Q., Diao, Y., et al. (2008) Cytoglobin: a novel potential gene medicine for fibrosis and cancer therapy. **Current gene therapy,** 8 (4): 287-294.

Macdonald, J., Galley, H.F. and Webster, N.R. (2003) Oxidative stress and gene expression in sepsis. **British journal of anaesthesia,** 90 (2): 221-232.

Makino, M., Sugimoto, H., Sawai, H., et al. (2006) High-resolution structure of human cytoglobin: identification of extra N- and C-termini and a new dimerization mode. **Acta crystallographica.Section D, Biological crystallography,** 62 (Pt 6): 671-677.

Mammen, P.P., Shelton, J.M., Ye, Q., et al. (2006) Cytoglobin is a stress-responsive hemoprotein expressed in the developing and adult brain. **The journal of histochemistry and cytochemistry : official journal of the Histochemistry Society,** 54 (12): 1349-1361.

Man, K.N., Philipsen, S. and Tan-Un, K.C. (2008) Localization and expression pattern of cytoglobin in carbon tetrachloride-induced liver fibrosis. **Toxicology letters,** 183 (1-3): 36-44.

Martey, C.A., Pollock, S.J., Turner, C.K., et al. (2004) Cigarette smoke induces cyclooxygenase-2 and microsomal prostaglandin E2 synthase in human lung fibroblasts: implications for lung inflammation and cancer. **American journal of physiology.Lung cellular and molecular physiology,** 287 (5): L981-91.

Mason, R.J. and Williams, M.C. (1977) Type II alveolar cell. Defender of the alveolus. **The American Review of Respiratory Disease,** 115 (6 Pt 2): 81-91.

McRonald, F.E., Liloglou, T., Xinarianos, G., et al. (2006) Down-regulation of the cytoglobin gene, located on 17q25, in tylosis with oesophageal cancer (TOC): evidence for trans-allele repression. **Human molecular genetics,** 15 (8): 1271-1277.

Meltzer, E.B. and Noble, P.W. (2008) Idiopathic pulmonary fibrosis. **Orphanet journal of rare diseases,** 3 8.

Miura, M. (1999) Detection of chromatin-bound PCNA in mammalian cells and its use to study DNA excision repair. **Journal of radiation research,** 40 (1): 1-12.

Montes, G.S. and Junqueira, L.C. (1991) The use of the Picrosirius-polarization method for the study of the biopathology of collagen. **Memorias do Instituto Oswaldo Cruz,** 86 Suppl 3 1-11.

Mosmann, T. (1983) Rapid colorimetric assay for cellular growth and survival: application to proliferation and cytotoxicity assays. **Journal of immunological methods,** 65 (1-2): 55-63.

Mutsaers, S.E., Foster, M.L., Chambers, R.C., et al. (1998) Increased endothelin-1 and its localization during the development of bleomycin-induced pulmonary fibrosis in rats. **American journal of respiratory cell and molecular biology,** 18 (5): 611-619.

Nakatani, K., Okuyama, H., Shimahara, Y., et al. (2004) Cytoglobin/STAP, its unique localization in splanchnic fibroblast-like cells and function in organ fibrogenesis. **Laboratory investigation; a journal of technical methods and pathology,** 84 (1): 91-101.

Numazawa, S. and Yoshida, T. (2004) Nrf2-dependent gene expressions: a molecular toxicological aspect. **The Journal of toxicological sciences,** 29 (2): 81-89.

Ohashi, T., Mizutani, A., Murakami, A., et al. (2002) Rapid oxidation of dichlorodihydrofluorescin with heme and hemoproteins: formation of the fluorescein is independent of the generation of reactive oxygen species. **FEBS letters,** 511 (1-3): 21-27.

Ohta, K., Mortenson, R.L., Clark, R.A., et al. (1995) Immunohistochemical identification and characterization of smooth muscle-like cells in idiopathic pulmonary fibrosis. **American journal of respiratory and critical care medicine,** 152 (5 Pt 1): 1659-1665.

Orihara, K. and Matsuda, A. (2008) Pathophysiological roles of microvascular alterations in pulmonary inflammatory diseases: possible implications of tumor necrosis factor-alpha and CXC chemokines. **International journal of chronic obstructive pulmonary disease,** 3 (4): 619-627.

Ostojic, J., Grozdanic, S., Syed, N.A., et al. (2008a) Neuroglobin and cytoglobin distribution in the anterior eye segment: a comparative immunohistochemical study. **The journal of histochemistry and cytochemistry : official journal of the Histochemistry Society,** 56 (9): 863-872.

Ostojic, J., Grozdanic, S.D., Syed, N.A., et al. (2008b) Patterns of distribution of oxygen-binding globins, neuroglobin and cytoglobin in human retina. **Archives of Ophthalmology,** 126 (11): 1530-1536.

Ostojic, J., Sakaguchi, D.S., de Lathouder, Y., et al. (2006) Neuroglobin and cytoglobin: oxygen-binding proteins in retinal neurons. **Investigative ophthalmology & visual science,** 47 (3): 1016-1023.

Pak, O., Aldashev, A., Welsh, D., et al. (2007) The effects of hypoxia on the cells of the pulmonary vasculature. **The European respiratory journal : official journal of the European Society for Clinical Respiratory Physiology,** 30 (2): 364-372.

Pan, L.H., Yamauchi, K., Uzuki, M., et al. (2001) Type II alveolar epithelial cells and interstitial fibroblasts express connective tissue growth factor in IPF. **The European respiratory journal : official journal of the European Society for Clinical Respiratory Physiology,** 17 (6): 1220-1227.

Park, G.Y. and Christman, J.W. (2006) Involvement of cyclooxygenase-2 and prostaglandins in the molecular pathogenesis of inflammatory lung diseases. **American journal of physiology.Lung cellular and molecular physiology,** 290 (5): L797-805.

Patel, V.S., Cooper, S.J., Deakin, J.E., et al. (2008) Platypus globin genes and flanking loci suggest a new insertional model for beta-globin evolution in birds and mammals. **BMC biology,** 6 34.

Pesce, A., Bolognesi, M., Bocedi, A., et al. (2002) Neuroglobin and cytoglobin. Fresh blood for the vertebrate globin family. **EMBO reports,** 3 (12): 1146-1151.

Pesce, A., De Sanctis, D., Nardini, M., et al. (2004) Reversible hexa- to penta-coordination of the heme Fe atom modulates ligand binding properties of neuroglobin and cytoglobin. **IUBMB life,** 56 (11-12): 657-664.

Powers, J.M. (2006) P53-Mediated Apoptosis, Neuroglobin Overexpression, and Globin Deposits in a Patient with Hereditary Ferritinopathy. **Journal of neuropathology and experimental neurology,** 65 (7): 716-721.

Pusztaszeri, M.P., Seelentag, W. and Bosman, F.T. (2006) Immunohistochemical expression of endothelial markers CD31, CD34, von Willebrand factor, and Fli-1 in normal human tissues. **The journal of histochemistry and cytochemistry : official journal of the Histochemistry Society,** 54 (4): 385-395.

Ramos, C., Montano, M., Garcia-Alvarez, J., et al. (2001) Fibroblasts from idiopathic pulmonary fibrosis and normal lungs differ in growth rate, apoptosis, and tissue inhibitor of metalloproteinases expression. **American journal of respiratory cell and molecular biology,** 24 (5): 591-598.

Rennard, S.I. (2001) Epithelial cells and fibroblasts. **Novartis Foundation symposium,** 234 104-12; discussion 112-9.

Roesner, A., Fuchs, C., Hankeln, T., et al. (2005) A globin gene of ancient evolutionary origin in lower vertebrates: evidence for two distinct globin families in animals. **Molecular biology and evolution,** 22 (1): 12-20.

Santos, S., Peinado, V.I., Ramirez, J., et al. (2002) Characterization of pulmonary vascular remodelling in smokers and patients with mild COPD. **The European respiratory journal :**

official journal of the European Society for Clinical Respiratory Physiology, 19 (4): 632-638.

Sawai, H., Kawada, N., Yoshizato, K., et al. (2003) Characterization of the heme environmental structure of cytoglobin, a fourth globin in humans. **Biochemistry,** 42 (17): 5133-5142.

Scandalios, J.G. (2005) Oxidative stress: molecular perception and transduction of signals triggering antioxidant gene defenses. **Brazilian journal of medical and biological research = Revista brasileira de pesquisas medicas e biologicas / Sociedade Brasileira de Biofisica ...[et al.],** 38 (7): 995-1014.

Schmidt, M., Gerlach, F., Avivi, A., et al. (2004) Cytoglobin is a respiratory protein in connective tissue and neurons, which is up-regulated by hypoxia. **The Journal of biological chemistry,** 279 (9): 8063-8069.

Schmidt, M., Laufs, T., Reuss, S., et al. (2005) Divergent distribution of cytoglobin and neuroglobin in the murine eye. **Neuroscience letters,** 374 (3): 207-211.

Schwarz, M.I. and King, T.E. (1993) **Interstitial lung disease.** 2nd ed. St. Louis, Mo. ; London: Mosby-Year Book.

Selman, M. and Pardo, A. (2006) Role of epithelial cells in idiopathic pulmonary fibrosis: from innocent targets to serial killers. **Proceedings of the American Thoracic Society,** 3 (4): 364-372.

Sethi, S. and Murphy, T.F. (2008) Infection in the pathogenesis and course of chronic obstructive pulmonary disease. **The New England journal of medicine,** 359 (22): 2355-2365.

Shahar, I., Fireman, E., Topilsky, M., et al. (1999) Effect of endothelin-1 on alpha-smooth muscle actin expression and on alveolar fibroblasts proliferation in interstitial lung diseases. **International journal of immunopharmacology,** 21 (11): 759-775.

Shaw, R.J., Hall, G.L., Woolgar, J.A., et al. (2007) Quantitative methylation analysis of resection margins and lymph nodes in oral squamous cell carcinoma. **The British journal of oral & maxillofacial surgery,** 45 (8): 617-622.

Shaw, R.J., Liloglou, T., Rogers, S.N., et al. (2006) Promoter methylation of P16, RARbeta, E-cadherin, cyclin A1 and cytoglobin in oral cancer: quantitative evaluation using pyrosequencing. **British journal of cancer,** 94 (4): 561-568.

Shaw, R.J., Omar, M.M., Rokadiya, S., et al. (2009) Cytoglobin is upregulated by tumour hypoxia and silenced by promoter hypermethylation in head and neck cancer. **British journal of cancer,** 101 (1): 139-144.

Sheffer, Y., Leon, O., Pinthus, J.H., et al. (2007) Inhibition of fibroblast to myofibroblast transition by halofuginone contributes to the chemotherapy-mediated antitumoral effect. **Molecular cancer therapeutics,** 6 (2): 570-577.

Shigematsu, A., Adachi, Y., Matsubara, J., et al. (2008) Analyses of expression of cytoglobin by immunohistochemical studies in human tissues. **Hemoglobin,** 32 (3): 287-296.

Shivapurkar, N., Stastny, V., Okumura, N., et al. (2008) Cytoglobin, the newest member of the globin family, functions as a tumor suppressor gene. **Cancer research,** 68 (18): 7448-7456.

Siafakas, N.M., Antoniou, K.M. and Tzortzaki, E.G. (2007) Role of angiogenesis and vascular remodeling in chronic obstructive pulmonary disease. **International journal of chronic obstructive pulmonary disease,** 2 (4): 453-462.

Siddiq, A., Aminova, L.R. and Ratan, R.R. (2007) Hypoxia inducible factor prolyl 4-hydroxylase enzymes: center stage in the battle against hypoxia, metabolic compromise and oxidative stress. **Neurochemical research,** 32 (4-5): 931-946.

Singh, S., Manda, S.M., Sikder, D., et al. (2009) Calcineurin activates cytoglobin transcription in hypoxic myocytes. **The Journal of biological chemistry,** 284 (16): 10409-10421.

Sirico, G., Vaughan, P., Pinnion, K., Waller, D. & Foster, M.L. "Histology of Arteriole Wall Remodelling in a Lung Volume Reduction Surgery (LVRS) Patient Cohort", *British Thoracic Society Winter Meeting*.

Smagghe, B.J., Sarath, G., Ross, E., et al. (2006) Slow ligand binding kinetics dominate ferrous hexacoordinate hemoglobin reactivities and reveal differences between plants and other species. **Biochemistry,** 45 (2): 561-570.

Smagghe, B.J., Trent, J.T.,3rd and Hargrove, M.S. (2008) NO dioxygenase activity in hemoglobins is ubiquitous in vitro, but limited by reduction in vivo. **PloS one,** 3 (4): e2039.

Stagner, J.I., Parthasarathy, S.N., Wyler, K., et al. (2005) Protection from ischemic cell death by the induction of cytoglobin. **Transplantation proceedings,** 37 (8): 3452-3453.

Stenmark, K.R., Gerasimovskaya, E., Nemenoff, R.A., et al. (2002) Hypoxic activation of adventitial fibroblasts: role in vascular remodeling. **Chest,** 122 (6 Suppl): 326S-334S.

Stroka, D.M., Burkhardt, T., Desbaillets, I., et al. (2001) HIF-1 is expressed in normoxic tissue and displays an organ-specific regulation under systemic hypoxia. **The FASEB journal : official publication of the Federation of American Societies for Experimental Biology,** 15 (13): 2445-2453.

Stryer, L. (1995) **Biochemistry.** 4th ed. New York: Freeman.

Sugimoto, H., Makino, M., Sawai, H., et al. (2004) Structural basis of human cytoglobin for ligand binding. **Journal of Molecular Biology,** 339 (4): 873-885.

Szilasi, M., Dolinay, T., Nemes, Z., et al. (2006) Pathology of chronic obstructive pulmonary disease. **Pathology oncology research : POR,** 12 (1): 52-60.

Tateaki, Y., Ogawa, T., Kawada, N., et al. (2004) Typing of hepatic nonparenchymal cells using fibulin-2 and cytoglobin/STAP as liver fibrogenesis-related markers. **Histochemistry and cell biology,** 122 (1): 41-49.

Trandafir, F., Hoogewijs, D., Altieri, F., et al. (2007) Neuroglobin and cytoglobin as potential enzyme or substrate. **Gene,** 398 (1-2): 103-113.

Trent, J.T.,3rd and Hargrove, M.S. (2002) A ubiquitously expressed human hexacoordinate hemoglobin. **The Journal of biological chemistry,** 277 (22): 19538-19545.

Tzouvelekis, A., Anevlavis, S. and Bouros, D. (2006) Angiogenesis in interstitial lung diseases: a pathogenetic hallmark or a bystander? **Respiratory research,** 7 82.

Uhal, B.D., Ramos, C., Joshi, I., et al. (1998) Cell size, cell cycle, and alpha-smooth muscle actin expression by primary human lung fibroblasts. **The American Journal of Physiology,** 275 (5 Pt 1): L998-L1005.

Valko, M., Leibfritz, D., Moncol, J., et al. (2007) Free radicals and antioxidants in normal physiological functions and human disease. **The international journal of biochemistry & cell biology,** 39 (1): 44-84.

Vaughan, P., Pinnion, K., Waller, D. et al. (2006) **A robust Grading System for Vascular Remodelling in Severe COPD Lung Resections.**

Vinck, E., Van Doorslaer, S., Dewilde, S., et al. (2004) Structural change of the heme pocket due to disulfide bridge formation is significantly larger for neuroglobin than for cytoglobin. **Journal of the American Chemical Society,** 126 (14): 4516-4517.

Voelkel, N.F., Douglas, I.S. and Nicolls, M. (2007) Angiogenesis in chronic lung disease. **Chest,** 131 (3): 874-879.

Weber, R.E. and Fago, A. (2004) Functional adaptation and its molecular basis in vertebrate hemoglobins, neuroglobins and cytoglobins. **Respiratory physiology & neurobiology,** 144 (2-3): 141-159.

Weiland, T.R., Kundu, S., Trent, J.T.,3rd, et al. (2004) Bis-histidyl hexacoordination in hemoglobins facilitates heme reduction kinetics. **Journal of the American Chemical Society,** 126 (38): 11930-11935.

Wenger, R.H. (2002) Cellular adaptation to hypoxia: O2-sensing protein hydroxylases, hypoxia-inducible transcription factors, and O2-regulated gene expression. **The FASEB**

journal : official publication of the Federation of American Societies for Experimental Biology, 16 (10): 1151-1162.

Wilborn, J., Crofford, L.J., Burdick, M.D., et al. (1995) Cultured lung fibroblasts isolated from patients with idiopathic pulmonary fibrosis have a diminished capacity to synthesize prostaglandin E2 and to express cyclooxygenase-2. **The Journal of clinical investigation,** 95 (4): 1861-1868.

Willis, B.C. and Borok, Z. (2007) TGF-beta-induced EMT: mechanisms and implications for fibrotic lung disease. **American journal of physiology.Lung cellular and molecular physiology,** 293 (3): L525-34.

Wynn, T.A. (2008) Cellular and molecular mechanisms of fibrosis. **The Journal of pathology,** 214 (2): 199-210.

Wystub, S., Ebner, B., Fuchs, C., et al. (2004) Interspecies comparison of neuroglobin, cytoglobin and myoglobin: sequence evolution and candidate regulatory elements. **Cytogenetic and genome research,** 105 (1): 65-78.

Xaubet, A., Roca-Ferrer, J., Pujols, L., et al. (2004) Cyclooxygenase-2 is up-regulated in lung parenchyma of chronic obstructive pulmonary disease and down-regulated in idiopathic pulmonary fibrosis. **Sarcoidosis, vasculitis, and diffuse lung diseases : official journal of WASOG / World Association of Sarcoidosis and Other Granulomatous Disorders,** 21 (1): 35-42.

Xi, Y., Obara, M., Ishida, Y., et al. (2007) Gene expression and tissue distribution of cytoglobin and myoglobin in the Amphibia and Reptilia: possible compensation of myoglobin with cytoglobin in skeletal muscle cells of anurans that lack the myoglobin gene. **Gene,** 398 (1-2): 94-102.

Xinarianos, G., McRonald, F.E., Risk, J.M., et al. (2006) Frequent genetic and epigenetic abnormalities contribute to the deregulation of cytoglobin in non-small cell lung cancer. **Human molecular genetics,** 15 (13): 2038-2044.

Xu, R., Harrison, P.M., Chen, M., et al. (2006) Cytoglobin overexpression protects against damage-induced fibrosis. **Molecular therapy : the journal of the American Society of Gene Therapy,** 13 (6): 1093-1100.

Yoshinouchi, T., Ohtsuki, Y., Ueda, R., et al. (1999) Myofibroblasts and S-100 protein positive cells in idiopathic pulmonary fibrosis and rheumatoid arthritis-associated interstitial pneumonia. **The European respiratory journal : official journal of the European Society for Clinical Respiratory Physiology,** 14 (3): 579-584.

Zhong, H. and Simons, J.W. (1999) Direct comparison of GAPDH, beta-actin, cyclophilin, and 28S rRNA as internal standards for quantifying RNA levels under hypoxia. **Biochemical and biophysical research communications,** 259 (3): 523-526.

Zion, O., Genin, O., Kawada, N., et al. (2009) Inhibition of transforming growth factor beta signaling by halofuginone as a modality for pancreas fibrosis prevention. **Pancreas,** 38 (4): 427-435.

APPENDIX

A1. Table of Materials

Generic Chemicals	**Source**	**Catalogue number**
Acrylamide	GeneFlow Ltd	
Ethanol	Fischer Scientific	
Formalin	VWR International Poole (BDH)	
Hydrogen Peroxide	BDH, UK	
Methanol	Fischer Scientific	
Generic Lab Equipment		
Cell Scraper	Corning Inc	
Centrifuge tubes	Falcon, Becton Dickinson Labware	
Eppendorfs	Greiner bio-one	
Cell Culture-Cells		
HEK298 Cells	AstraZeneca	
Cygb+ HEK298 Cells	AstraZeneca	
Cell Culture-Media and supplements		
LHC-9 Medium	GIBCO, Invitrogen	
Fetal Bovine Serum	Gibco, Invitrogen	
Fibronectin	Invitrogen	
Cell Culture- Plates		
Collagen/Poly-D-Lysine coated plates	Becton Dickinson	
Flasks 25cm^2	Falcon, Becton Dickinson Labware	
Flasks 75cm^2	Falcon, Becton Dickinson Labware	
Lab-Tek II Chamber slides	Nalge Nunc. International	
Cell Culture Plates	Cellstar	

Cell Culture- Equipment		
Cryovials	Naglene, New york	
Disposable haemocytometer	Immune Systems	
Haemocytometer	Weber scientific international ltd	
Protein Analysis- Quantification		
BCA Protein Assay Kit	Pierce	23225
Bradford Dye	BioRad, Germany	500-0006
Filter (0.45µm)	Pall Corporation	4654
Protein Analysis- Concentration		
Centrifugal filter units	Millipore	42407
Western Blotting-Generic Materials		
Chemiluminescence detection agents	GeneFlow Ltd	
Gels, 12%, 15 wells	BioRad, Germany	161-1120EDU
Glass plates and supports	BioRad, Germany	
Hyperfilm	Amersham Biosciences, UK	
Kaleisdoscope protein marker	BioRad, Germany	
Laemmili buffer	BioRad, Germany	
Low fat powdered milk	Marvel, UK	
Nitrocellulose membrane	Amersham, Biosciences, UK	
Pre-stained protein marker	BioLabs, England	
Pre-stained protein marker	Pierce	
Tris/Glycine buffer	BioRad, Germany	
Tris/Glycine/SDS buffer	BioRad, Germany	
Western blotting equipment	BioRad, Germany	3342
Fluorescence Microscopy and IHC		
Vectashield Mounting Medium	Vector Laboratories	H00114757-A01
Immunohistochemistry-Generic Materials		

Wash Buffer (PBS)	Sigma	P3813-10PAK
Diluent (0.1%BSA in PBS)	Sigma	P3688-10PAK
10% Buffered Formalin	Pioneer Research Chemicals Ltd, Colchester	
Parafin	Pfizer Scientific	
Xylene	Fisher Scientific	X/0100/PB17
Ethanol	Fisher Scientific	E/0650DF/P17
Industrial methylated spirits	Fisher Scientific	M/4450/PB17
Immunohistochemistry-H&E		
Gill II haemotoxylin	Pioneer Research Chemicals Ltd, Colchester	
Eoisin Y	Acros Organics, Fisher Scientific	
Immunohistochemistry-Antigen Retrieval		
Antigen Unmasking Fluid	Vector Laboratories	H-3300
High pH Antigen retrieval Solution	Dako	DM812
Low pH Antigen retrieval Solution	Dako	DM809
Boric Acid	Fisher Scientific	B/3800/53
Immunohistochemistry-Serum		
Normal Goat Serum	Dako	X0907
Normal Swine Serum	Dako	X0901
Normal Horse Serum	Vector Laboratories	S-2000
Immunohistochemistry-Amplification Kits		
Tryamide Signal Amplification Kit	PerkinElmer	NEL700
Streptavidin AB/HRP Kit	Dako	K0377
Envision Flex (anti-Mouse)	Dako	K4000
Envision Flex (anti-Rabbit)	Dako	K4003
Immunohistochemistry-Chromogens		
DAB	Dako	
NovaRED	Vector Laboratories	SK-4800

Peroxidase Subatrate Kit (Nickle DAB)	Vector Laboratories	SK-4700
Immunohistochemistry-Pico-Sirius Red		
Sirius Red	Sigma	365548
Primary Antibodies		
CYGB Monoclonal primary antibody	Abnova	H00114757-M02
CYGB polyclonal primary antibody	Abnova	H00114757-A01
Lamin Antibody	Santa Cruz	
Monoclonal Anti-β-Actin Antibody	Sigma	A1978
α Smooth Muscle Actin	Dako	M0851
CD3	Dako	A 0452
CD31 (PECAM-1)	Abcam	Ab9498
CD34 Class II	Dako	M7165
CD68	Dako	M0814
Carbonic Anhydrase IX	BD Biosciences	15086
C-Kit	Dako	A4502
Collagen I	Abcam	COL_1
Cytokeratin	Dako	M0821
Desmin	Dako	M0760
MAC 387	Serotec	MCA 874G
Proliferative Cell Nuclear Antigen	Novocastra	NCL-PCNA
S100A4	Dako	A5114
Surfactant A	DakoCytomation	M4501
Tubulin Antibody	Calbiochem	
Vimentin	Dako	M0725
Von Hippel Lindou	BD Biosciences	556347
Wheat Germ Agglutinin	Vector Laboratories	B-0125
Primary Antibodies-Isotype Controls		

Mouse IgG1	Dako	X0931
Mouse IgG2a Kappa	BD Pharmingen	550339
Rabbit Ig	Serotec	PRAB101
Rabbit Ig	Dako	X0936
Mouse IgG2a	Dako	X0943
Mouse IgG2b	Serotec	PMP50
Acetylglucoasamine Sugar	Vector Laboratories	S-9002
Secondary Antibodies		
Goat anti mouse HRP secondary	Dako	P0447
Biotinylated Goat anti Mouse	Dako	E0433
Biotinylated Goat anti Rabbit	Dako	E0432
Biotinylated Swine anti Rabbit	Dako	E0353
Biotinylated Horse anti Mouse	Vector Laboratories	BA-2001
Alexa 488-labelled Rabbit anti Mouse	Molecular Probes, Invitrogen	A11059
RNA Extraction		
RNAqueous-4 PCR Kit	Ambion, Applied Biosytems	AM1914
RNeasy 96	Qiagen Ltd	74181
RNeasy mini kit	Qiagen Ltd	74106
RNA Quantification		
RiboGreen Kit	Invitrogen	R11490
Agilent RNA 6000 Nano Kit	Agilent Technologies	5067-1511
DNase I Treatment of RNA Samples		
DNase I	Ambion, Applied Biosytems	AM2222
Intracellular Fluorescent Dyes		
2,7-dichlorodihydrofluorescein diacetate	Molecular Probes, Invitrogen	
cis-parinaric acid	Molecular Probes, Invitrogen	
The Comet Assay		

FPG Enzyme	Trevigen	4040-100-01
Sybr Gold	Invitrogen	
Microscope slides	BDH, UK	
Coverslips glass 22mmX64mm	BDH, UK	
DNase I Treatment of RNA Samples		
DNase I	Ambion, Applied Biosytems	AM2222
RT PCR		
18s rRNA primers and probes		
Agilent RNA 6000 Nano Kit	Agilent Technologies	
Cytoglobin primers and probes		
DNase I	Ambion, Applied Biosytems	
OliGreen Kit		
RiboGreen Kit		
RNAqueous-4 PCR Kit	Ambion, Applied Biosytems	AM1914
RNeasy 96	Qiagen Ltd	
RNeasy mini kit	Qiagen Ltd	
Superscript II kit		
TAK-1 Primers and probes		
TaqMan Machine		
TaqMan mastermix (one step)		
TaqMan mastermix (two step)		
siRNA transfection		
CYGB siRNA	Dharmacon	LQ-016960-01
Transfection Lipid	Silence therapeutics	Autofect01 #0336
Luciferase 1 siRNA	Dharmacon	CLIAA-0047
Luciferase 2 siRNA	Dharmacon	CLIAA-0049

Negative siRNA #1	Dharmacon	D-001810-01-05
Negative siRNA #2	Dharmacon	D-001810-02-05
OptiMem + Glutamax-1	Gibco	51985-026 #0435
TAK-1 siRNA (pool 2)	Dharmacon	BODKA-00009

A2. Example Ethical Consent Form

13.6.2007: Version 1

Subject Information Leaflet and Consent Form

Study Title: Use of Tissue from Lung Resections to Investigate the Molecular and Functional Mechanisms of Human Lung Disease

Principle Investigator: Professor Andrew Wardlaw

Study Funded by: Astra-Zeneca

You are being invited to take part in a research study. Before you decide it is important for you to understand why the research is being done and what it will involve. Please take time to read the following information carefully and discuss it with others if you wish. Ask us if there is anything that is not clear or if you would like more information. Take time to decide whether or not you wish to take part.

Introduction

Lung disease causes pain, discomfort and can prevent sufferers from carrying out everyday activities. Whilst available treatments including steroids and other drugs may relieve symptoms, none provide a cure. Operations may help some people. More research is needed to find new treatments that can cure lung disease.

What is the purpose of the study?

In order to find the causes of lung disease such as COPD and lung cancer and to find new ways of treating these diseases we have to do more research. It is ideal to do the research on tissue from human lungs because we are investigating a human disease. The lung research teams at Glenfield Hospital, Leicester Birmingham Heartlands Hospital, Walsgrave Hospital, Coventry and AstraZeneca (a pharmaceutical company) have joined together in order to collaborate on studies into lung disease using human lung tissue. A numbers of diseases will be studied and the lung tissue will be used in a number of different laboratory studies. AstraZeneca will use the lung tissue in the understanding of lung disease and development of

new treatments for lung disease. These experiments will be done on lung tissue that has been removed from patients as part of their medical treatment, which would otherwise be destroyed. In some cases we may also wish to take a blood sample to compare the findings in the lung tissue and blood.

Why have I been chosen?

You have been chosen because your doctor has said that you may need to have some of your lung removed to treat your disease.

Do I have to take part?

It is up to you to decide whether or not to take part. If you do decide to take part you will be given this information sheet to keep and be asked to sign a consent form. If you decide to take part you are still free to withdraw at any time and without giving a reason. A decision to withdraw at any time, or a decision not to take part, will not affect the standard of care you receive.

What will happen to me if I take part?

You are about to undergo an operation for your current condition. We would like to retain some of the spare lung tissue that will be removed as part of your operation, which would otherwise be destroyed. If you are willing to take part in this research, we will pass the surplus lung tissue to the collaborating hospitals and AstraZeneca.. The surgeon will not remove any extra lung tissue for this research. We will also record some information about your recent medical history, medicines taken and reason for the operation from your medical records. In terms of your operation, stay in hospital and subsequent follow up there will be no difference to what will happen to you whether you take part in the study or not except that in a few cases we may wish to take an extra blood sample of approximately 15mL (about three tablespoons full) before your operation.

What happens if I don't want to take part?

Nothing, you simply don't sign this form. This will not affect your medical care or your legal rights in any way.

What rights do I have to the results of the research?

You are being asked to donate your tissue as a gift to the researchers in the hospitals involved and AstraZeneca. Any information derived directly or indirectly from this research by the collaborating hospitals or by AstraZeneca, as well as any patents, diagnostic tests, drugs, or biological products developed directly or indirectly as a result, are the sole property of the company (or their successors, licensees, and assigns) and may be used for commercial purposes. You have no right to this property or to any share of the profits that may be earned directly or indirectly as a result of this research.

However, in signing this form and donating a blood sample, you do not give up any rights that you would otherwise have as a participant in research.

What do I have to do?
There is nothing extra to do as a result of being part of this study

What are the possible disadvantages and risks of taking part?
There are no disadvantages or risks to taking part in the study over and above the normal risks associated with this surgery, which you require as part of your care. If you are asked to donate an additional blood sample there may be some discomfort of the needle being inserted into a vein in your arm and the possibility of bruising developing afterwards around the area that the needle was inserted. This should disappear in a few days

What are the possible benefits of taking part in the study?
There are no direct benefits. Taking part in this study means that you may possibly help suffers of lung disease in the future, as information about the changes that occur in the lung may be used to develop new treatments.

What if something goes wrong?
We do not think there is any significant risk of any harm occurring as a result of participating in this study. However if you are harmed by taking part in this research project, there are no special compensation arrangements. If you are harmed due to someone's negligence, then you may have grounds for a legal action but you may have to pay for it. Regardless of this, if you wish to complain, or have any concerns about any aspect of the way you have been approached or treated during the course of this study, the normal National Health Service complaints mechanisms would be available to you.'

Will my taking part in this study be kept confidential?
All information resulting from you taking part in the study will be stored and analysed in a computer and will be treated confidentially. You will be identified in the computer by a number and only your doctor will be able to identify the number as belonging to you. The study records will not be made available in any form to anyone other than authorised representatives of the health authorities and AstraZeneca. In all instances, your confidentiality will be maintained, in accordance with the Data Protection Act or as local laws permit.

AstraZeneca and Regulatory authorities may wish to check that this research has been done properly, they may have access to your files and know your identity, but they are under a duty of confidentiality not to disclose details to others.

What will happen to the samples that I have donated?

The samples will be processed by the research team and used in a range of experiments into the causes of lung disease. Samples may be transported to AstraZeneca or other hospitals in the collaborating group to do further experiments including tests to develop new drugs. Those samples that are not fully used up in experiments may be stored by the research team or by AstraZeneca, for use in future experiments, for up to 20 years.

Who is organising and funding the research?

The research is a collaboration between the lung research teams at the hospitals in Leicester, Coventry, Birmingham and AstraZeneca. The study is organised and operated by the individual hospitals involved and the overall collaboration has been funded by AstraZeneca. The income obtained from AstraZeneca will only be used to support the work carried out as pat of this project.

Can I Withdraw my consent?

You may withdraw your consent to the use of your data and samples at any time. If you withdraw your permission consent before your donated tissue and data are used, we will not use the data and the samples will be destroyed. If you withdraw your consent after your tissue sample has been sent for analysis we will ensure that your sample(s) are destroyed. However, if analysis has already been performed neither AstraZeneca nor ourselves are obliged to destroy results of this research.

Who has reviewed the study?

The study has been reviewed by the research teams within the consortium and by the members of the Department of Respiratory Medicine, Allergy and Thoracic Surgery. Individual research projects where we use the lung tissue have been reviewed by a variety of charities and funding organisations

If you have any further questions about this study please do discuss them with:

Professor Wardlaw or Mr Waller (0116 2563841)

This document must be kept in the investigator's study file and retained for a minimum period of 20 years after completion of the study.

Study Title: **Use of Tissue from Lung Resections to Investigate the Molecular** and Functional Mechanisms of Human Lung Disease

	Initials
1. I confirm that I have read and understood the patient information form on the above project and have been given a copy to keep. I have had the opportunity to ask questions about the project and understand why the research is being done and any foreseeable risks involved.	☐
2. I agree to donate as a gift a sample of tissue for research in the above project. I understand how the sample will be collected and that giving the sample is voluntary. I am free to withdraw my approval for use of the sample at any time without giving any reason and without my medical treatment or legal rights being affected.	☐
3. I give permission for my medical records to be looked at and Information taken from them to be treated in strict confidence by responsible people from Glenfield Hospital and AstraZeneca.	☐
4. I understand that my doctor will be informed if any of the results of the tests done as part of the research are important for my health.	☐
5. I understand that I will not benefit financially if this research leads to a new treatment or medical test.	☐
6. I do know where to contact Professor Wardlaw, if I need further information.	☐

	YES	NO
7. Do you agree to take part in this study?		

Signed**: ……** Date**: ……..**

Name (Block capitals) ……..

I, **(Name of investigator, block letters)** ……

have explained the nature and purpose of the study to …….

and believe that he/she understands what the study involves.

Signed: …….. **Date**: ……..

A.3 Density Grading

All pictures were taken at x20

	1	3
CD3	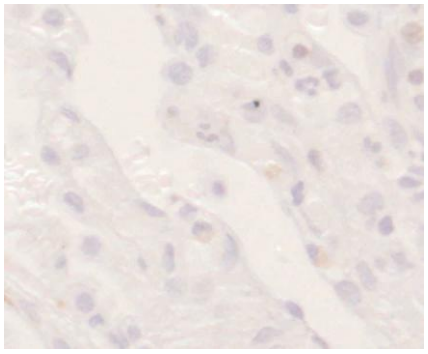	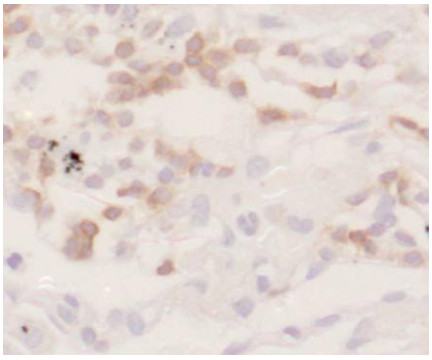
CD31	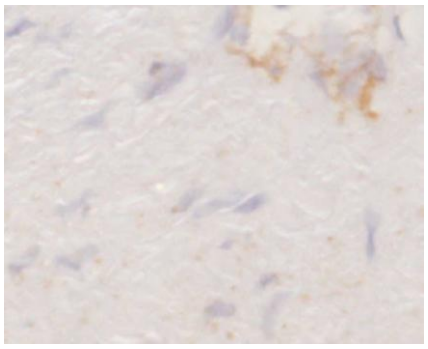	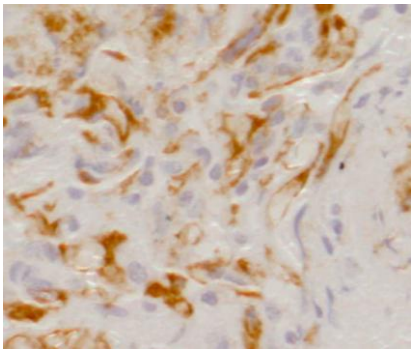

	1	3
C-kit	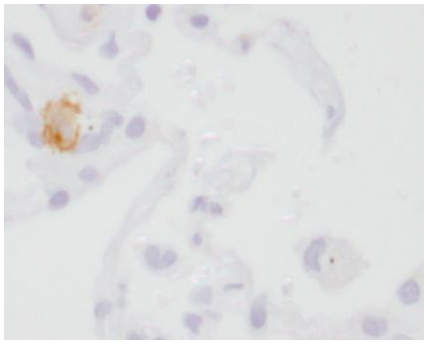	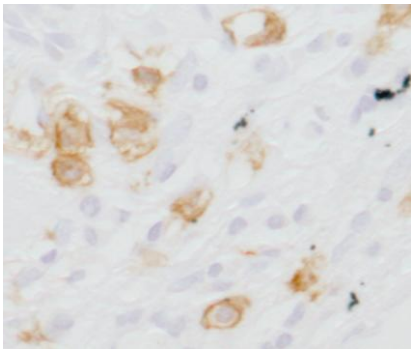
Collagen	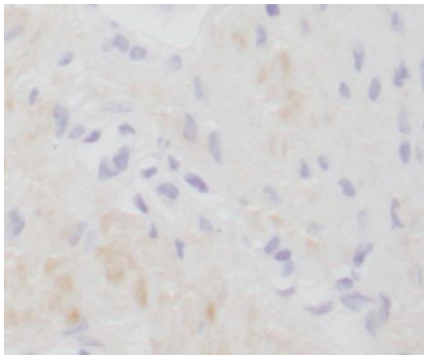	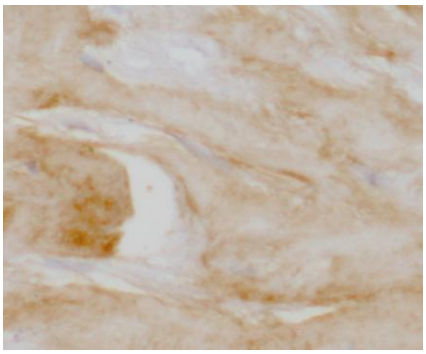
Cytokeratin	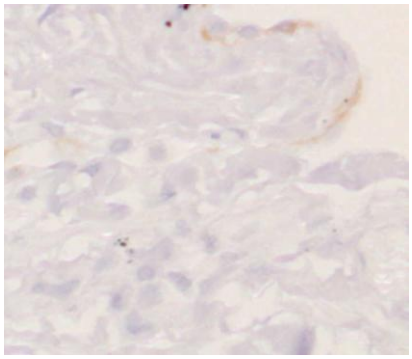	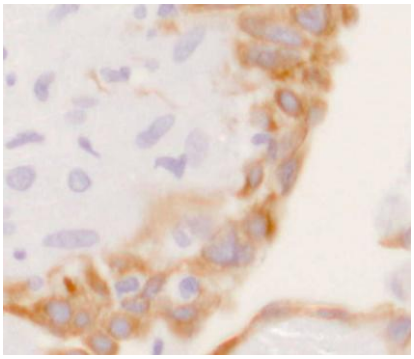

	1	3
MAC387	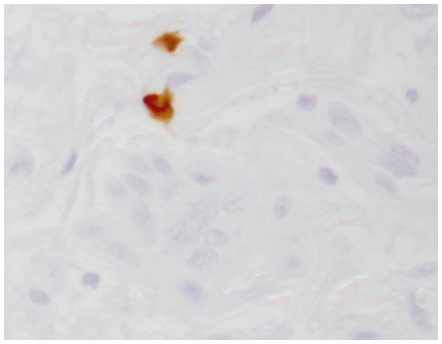	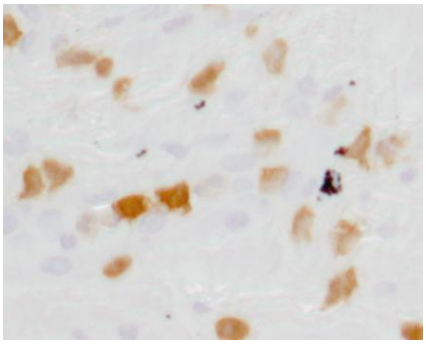
PCNA	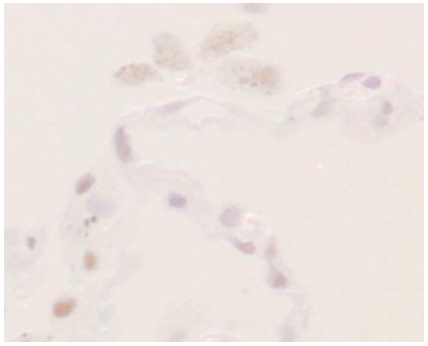	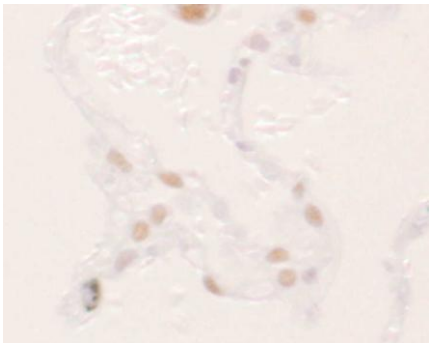
Surfactant	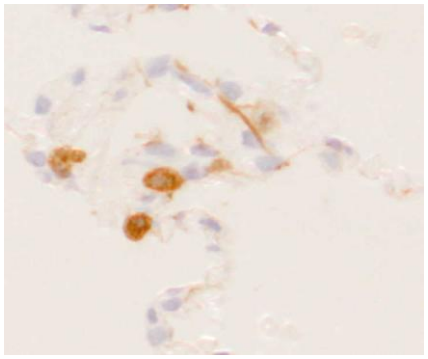	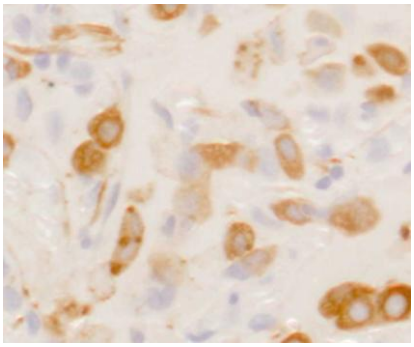

1 **3**

Vimentin

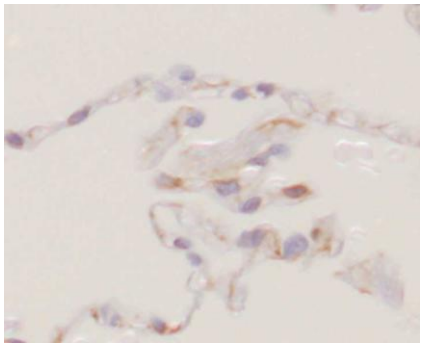
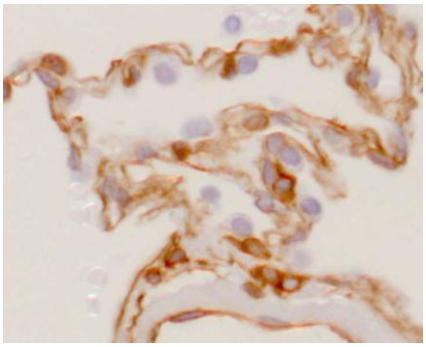

Wheat Germ Agglutinin

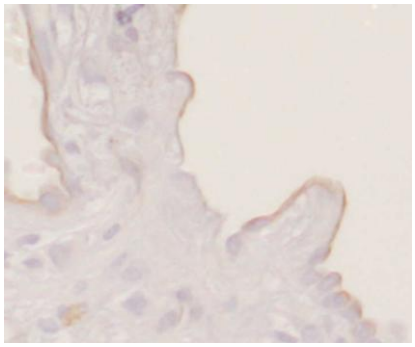
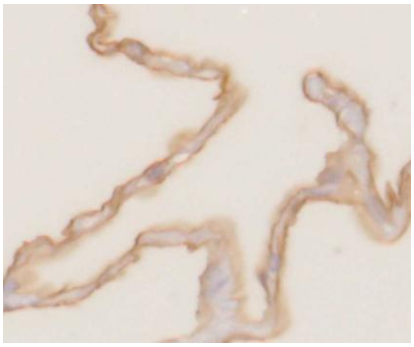

Cytoglobin Staining in the Vasculature

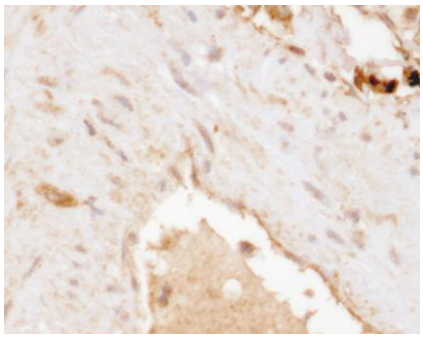
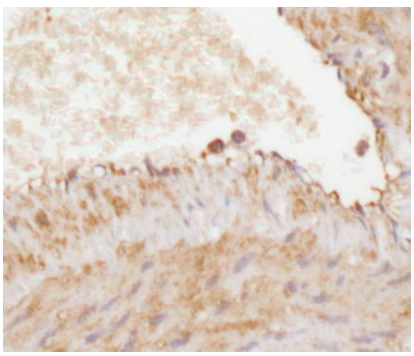

A.4 Isotype Controls

Pictures are all 20% of original taken at x20.

αSMA CAIX CD3

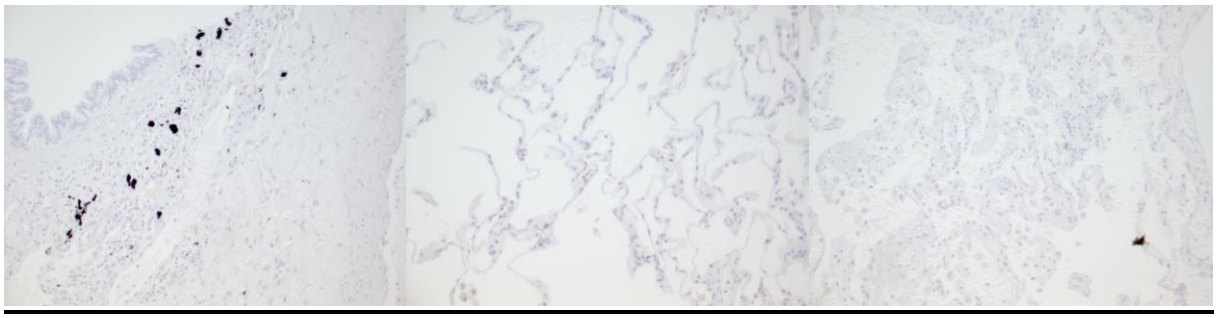

CD31 CD34 CK

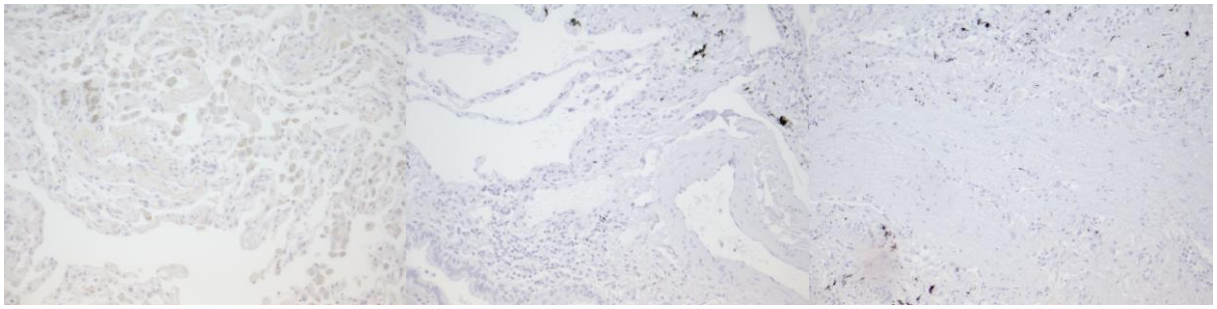

C-kit Collagen CYGB

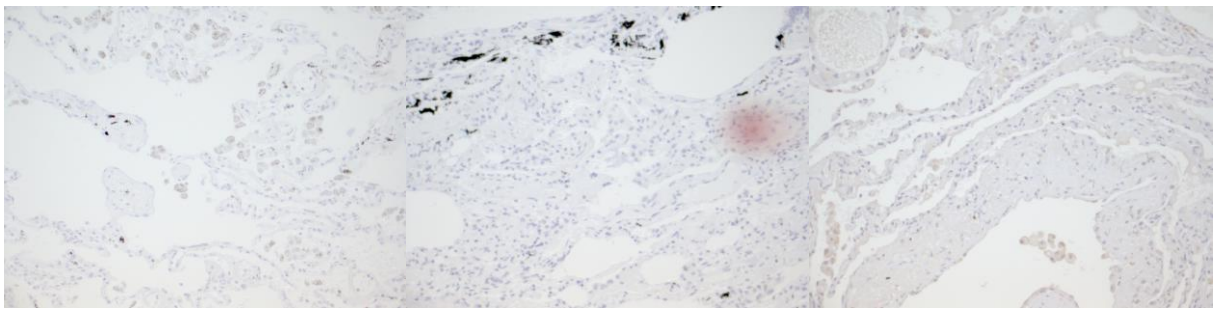

Desmin WGA MAC387

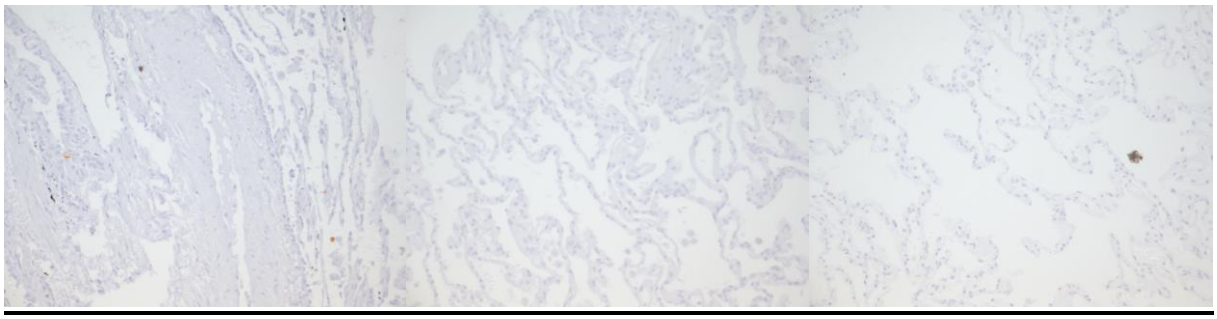

PCNA pVHL S100A4

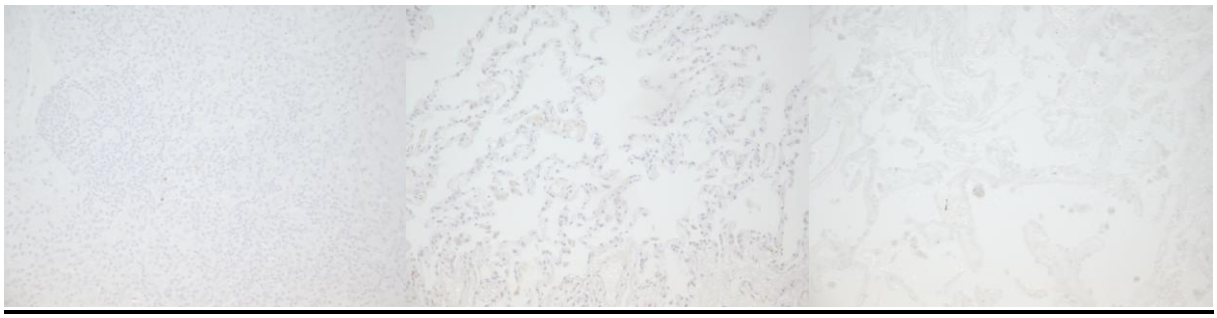

Surfactant Vimentin